Understanding intestinal and pancreatic hormone secretion in health and type 2 diabetes: (pre-)clinical studies and technical innovations



A thesis by

Weikun Huang

B. Agr. (Veterinary Medicine), M. Phil. (Physics)

For the degree of

Doctor of Philosophy (Medicine)

Adelaide Medical School

November 2023

TABLE OF CONTENTS

TABLE OF CONTENTS	I
THESIS ABSTRACT	VII
DECLARATION	X
ACKNOWLEDGEMENTS	XI
PUBLICATIONS ARISING FROM PHD	XIII
CONFERENCE PRESENTATIONS	XVI
CHAPTER 1: DEVELOPMENT OF INNOVATIVE TOOLS FOR INVESTIGATION NUTRIENT-GUT INTERACTION	
Statement of Authorship	2
1.1 Abstract	4
1.2 Introduction	4
1.3 Cellular Models	5
1.4 Tissue-based Gut Hormone Release ex vivo	9
1.5 Intestinal Organoids	10
1.6 Intestinal Perfusion in vivo	11
1.7 Novel Techniques to Study Gut Hormone Secretion	14
1.8 Conclusions	16
1.9 References	17
CHAPTER 2: SENSING INTRA- AND EXTRA-CELLULAR CALCIUM IN THE IS LANGERHANS	
Statement of Authorship	29
2.1 Abstract	31
2.2 Ca ²⁺ Homeostasis and Signalling	31
2.3 Insulin Secretion and Ca ²⁺ Signalling	33
2.3.1 Pancreatic islets and pulsatile secretion of insulin	
2.3.2 Intracellular Ca ²⁺ signalling: a trigger for insulin secretion	
2.3.3 Intracellular Ca ²⁺ signalling: an integrator for insulin secretion?	
2.4 Conventions of Sensing Cellular Ca ²⁺ in Islets	
2.4.1 Chemically synthesised fluorescent indicators for [Ca ²⁺] _c	40

2.4.2 Genetically encoded Ca ²⁺ indicators for [Ca ²⁺] _c	45
2.4.3 Ca ²⁺ -selective microelectrode (CSM) for [Ca ²⁺] _{ex}	50
2.5 The State-of-the-Art Sensors for [Ca ²⁺] _{ex}	52
2.5.1 Low-affinity synthetic Ca ²⁺ indicators	53
2.5.2 Nano-structured sensors for [Ca ²⁺] _{ex}	55
2.5.3 Microfluidics-based multiplexed sensing platforms	60
2.6 Conclusions and Outlook	66
2.7 References	70
CHAPTER 3: DISPARITIES IN THE GLYCAEMIC AND INCRETIN RESPONSES T INTRADUODENAL GLUCOSE INFUSION BETWEEN HEALTHY YOUNG MEN A WOMEN	ND
Statement of Authorship	
3.1 Abstract	
3.2 Introduction	
3.3 Methods	
3.3.1 Participants	
3.3.2 Protocol	
3.3.3 Measurement of blood glucose and plasma insulin, total GIP and GLP-1	
3.3.4 Statistical analysis	
3.4 Results	
3.4.1 Blood glucose	
3.4.2 Plasma insulin	
3.4.3 Plasma total GIP	
3.4.4 Plasma total GLP-1	100
3.5 Discussion	100
3.6 References	103
CHAPTER 4: SERUM ALANINE TRANSAMINASE IS PREDICTIVE OF FASTING POSTPRANDIAL INSULIN AND GLUCAGON CONCENTRATIONS IN TYPE 2	AND
DIABETES	
Statement of Authorship	109
4.1 Abstract	112
4.2 Introduction	112
4.3 Methods	114

4.3.1 Participants	114
4.3.2 Protocol	114
4.3.3 Measurements	115
4.3.4 Statistical Analysis	116
4.4 Results	117
4.4.1 Relationships between metabolic parameters and liver enzymes in fasting and aft oral glucose load and before and after a mixed meal	
4.4.2 Blood glucose and plasma insulin, C-peptide and glucagon in T2D subjects class according to ALT	
4.5 Discussion	124
4.6 References	127
4.7 Supplementary Information	131
CHAPTER 5: THE 'EARLY' POSTPRANDIAL GLUCAGON RESPONSE IS RELATED THE RATE OF GASTRIC EMPTYING IN PATIENTS WITH TYPE 2 DIABETES	
Statement of Authorship	135
5.1 Abstract	137
5.2 Introduction	137
5.3 Research Design and Methods	139
5.3.1 Subjects	139
5.3.2 Study protocol	139
5.3.3 Measurement of blood glucose, plasma glucagon and GE	140
5.3.4 Statistical analysis	140
5.4 Results	141
5.3.1 Blood glucose, plasma glucagon and GE	141
5.4.2 Relationships between blood glucose and GE	141
5.4.3 Relationships between plasma glucagon and GE	143
5.4.4 Relationships between blood glucose and plasma glucagon	143
5.4.5 Blood glucose and plasma glucagon levels in subgroups with fast, medium and sl	
5.5 Discussion	144
5.6 References	148
CHAPTER 6: EFFECTS OF A BITTER SUBSTANCE, DENATONIUM BENZOATE, ON PANCREATIC HORMONE SECRETION: AN <i>EX VIVO</i> EVALUATION USING BOTH RODET B-CELL LINE AND ISOLATED MOUSE ISLETS	

	Statement of Authorship	. 154
	6.1 Abstract	. 156
	6.2 Introduction	. 156
	6.3 Methods	. 158
	6.3.1 Culture of INS-1 832/13 cells	. 158
	6.3.2 Isolation of mouse pancreatic islets	. 158
	6.3.3 Hormone secretion study	. 159
	6.3.4 Hormone measurements	. 160
	6.3.5 Analysis of RNA-sequencing datasets	. 160
	6.3.6 Assessment of cell apoptosis and viability	. 160
	6.3.7 Statistical analysis	. 161
	6.4 Results	. 161
	6.4.1 DB potentiates insulin secretion at both low and high glucose concentrations in IN 832/13 cells and mouse pancreatic islets	
	6.4.2 A high concentration of DB induces cell apoptosis	. 162
	6.4.3 Potentiation of insulin secretion by DB is dependent on the closure of the K_{ATP} channel and BTR signalling in β -cells	. 163
	6.4.4 Intra-islet GLP-1 may play a role in mediating the effects of DB on insulin secretic from isolated islets.	
	6.4.5 Effect of DB on somatostatin and glucagon secretion from mouse pancreatic islets	166
	6.5 Discussion	. 166
	6.6 References	. 169
	6.7 Supplementary Information	. 173
C	HAPTER 7: DEVELOPMENT OF A GUT-ON-A-CHIP PLATFORM TO MONITOR GL	P-1
S	ECRETION FROM PRIMARY INTESTINAL TISSUE	. 176
	Statement of Authorship	. 177
	7.1 Abstract	. 179
	7.2 Introduction	. 179
	7.3 Methods	. 181
	7.3.1 Preparation of mouse small intestinal tissues	. 181
	7.3.2 Design, fluidic simulation and fabrication of the microfluidic device	. 182
	7.3.3 Optical examination of the dimensions of the microfluidic channels	. 182
	7.3.4 Experimental characterisation of on-chip fluidic dynamics	. 183

7.3.5 On-chip study of GLP-1 secretion from small intestinal tissue	183
7.3.6 Measurement of GLP-1 concentrations	183
7.3.7 Hematoxylin and eosin (H&E) staining of intestinal tissues	184
7.3.8 Statistical analysis	184
7.4 Results and Discussion	184
7.4.1 Off-chip characterisation of GLP-1 release from mouse small intestine	. 184
7.4.2 Design, fabrication and characterisation of the GOC device	187
7.4.3 Characterisation of fluidic dynamics and on-chip GLP-1 secretion from primary intestinal tissue	189
7.4.4 Assessment of tissue morphology after static incubation and dynamic perfusion	192
7.5 Conclusions	193
7.6 References	193
7.7 Supplementary Information	197
CHAPTER 8: A MULTIPLEXED MICROFLUIDIC PLATFORM TOWARDS INTERROGATING ENDOCRINE FUNCTION: SIMULTANEOUS SENSING OF EXTRACELLULAR CA ²⁺ AND HORMONE	201
Statement of Authorship	202
8.1 Abstract	204
8.2 Introduction	204
8.3 Experimental Sections	206
8.3.1 Determination of dissociation constant (K _d)	206
8.3.2 Fluidic dynamics simulation	207
8.3.3 Microfluidic chip fabrication	207
8.3.4 Dual-sensing of oscillating Ca ²⁺ and insulin	208
8.4 Results and Discussion	208
8.4.1 Fluorometric characterisations of Rhod-5N	208
8.4.2 Design principle and fluidic dynamics	212
8.4.3 Flow velocity profile	213
8.4.4 U-shape cups for trapping	214
8.4.5 Optical window for fluorescence readout	216
8.4.6 Generation of a dynamic microenvironment	216
8.4.7 Biomedical applications	218
8.5 Conclusions	222

	8.6 References	223
	8.7 Supplementary Information	227
	8.7.1 Chemicals and reagents	. 227
	8.7.2 Fluorescence detection by plate reader (off-chip measurement)	. 228
	8.7.3 Calibration of effective Ca^{2+} concentration ($[Ca^{2+}]_e$)	. 228
	8.7.4 Surface characterisations of the microfluidic chip	229
	8.7.5 On-chip imaging and fluorescence detection	. 230
	8.7.6 Analysis of diffusion and flow rate in the channel	231
	8.7.7 Preparation and loading of Polyethylene (PE) microspheres suspension	232
	8.7.8 Calibration curve of Ca ²⁺ -induced fluorescence of Rhod-5N (on-chip)	233
	8.7.9 Temporal characterisation of the on-chip perfusion	233
	8.7.10 Measurement of Ca ²⁺ -induced fluorescence of Rhod-5N in serum or cell culture medium with FBS	234
	8.7.11 Supporting references	. 244
C	HAPTER 9: CONCLUSIONS AND PERSPECTIVES	. 245

THESIS ABSTRACT

The gastrointestinal (GI) tract and pancreatic islets are key components of the endocrine system, responsible for the release of an array of peptide hormones, which orchestrate metabolic homeostasis through regulation of energy intake, nutrient digestion, absorption and metabolism. Of numerous hormones released from the gut, the incretin hormones, glucagon-like peptide-1 (GLP-1) and glucose-dependent insulinotropic polypeptide (GIP), govern the secretion of both insulin and glucagon from pancreatic islets. Together, these hormones play a critical role in maintaining glucose homeostasis. Disrupted secretion and/or action of the incretins and pancreatic hormones underpins the development of type 2 diabetes (T2D) - a global epidemic characterised by elevated blood glucose concentrations and associated with devastating micro- and macro-vascular complications. Accordingly, an improved understanding of the physiology and pathophysiology of GI and pancreatic hormones in health and T2D is of major relevance to the development of effective strategies to both prevent and better manage T2D. This thesis comprises a series of clinical and preclinical evaluations that provide novel insights into the determinants of GI and islet hormone secretion (Chapters 3-6). In addition, it details the cross-disciplinary collaborative development of two 'organ-on-a-chip' platforms for dissecting the secretory function of both intestinal tissues and pancreatic islets (Chapters 7-8).

Chapter 1 provides an overview of the secretion and action of GI hormones arising from the complex interaction between luminal nutrients/bioactive compounds and the gut mucosa, and details conventional and innovative research tools/platforms that are indispensable for the investigation of GI hormone secretion. **Chapter 2** summarises the molecular mechanisms underlying insulin secretion from pancreatic islets, with a focus on the role of Ca²⁺ signalling, and systematically reviews the development of diverse research platforms that are fundamental to progressing islet research.

Given the substantial sex-related differences in glucose metabolism and risk of T2D, the study described in **Chapter 3** explores the sex disparity in incretin hormone secretion, and compares the incretin and glycaemic responses to standardised intraduodenal glucose infusions within the physiological range of gastric emptying between healthy young men and women.

While insulin resistance and consequently a relative deficiency in insulin secretion are recognised as key metabolic derangements in T2D, there is accumulating evidence indicating that excessive glucagon secretion also underpins the development of dysglycaemia during both the fasting and postprandial phases. In the liver, insulin and glucagon signalling pose counter-regulatory effects on hepatic glucose production. Alterations in hepatic function have the potential to disrupt hepatic insulin and glucagon signalling, leading to pathological changes in insulin and glucagon secretion. The study reported in **Chapter 4** evaluates the relationships of blood glucose, plasma insulin, C-peptide and glucagon, both during fasting and after 75g oral glucose, with serum liver enzymes in healthy and T2D subjects, and in T2D subjects before and after a mixed meal. Given the major role of the rate of gastric emptying (GE) in determining nutrient digestion and absorption, GE may influence the glucagon and glycaemic responses in T2D. Therefore, **Chapter 5** further examines the relationships of plasma glucagon and blood glucose with the rate of gastric emptying (GE) of a standardised mashed potato meal in individuals with well-controlled T2D.

Strategies that are effective for modulating GI and pancreatic hormone secretion have the potential to improve glycaemic control in T2D. The recent recognition that the GI tract can detect a range of physiological and pharmacological bitter substances via a family of type 2 monomeric G-protein-coupled receptors, namely bitter taste receptors (BTRs), to release GI hormones has led to growing interest in the administration of bitter tastants to stimulate GI hormone secretion for the management of metabolic disorders, including T2D. However, the effects of bitter substances beyond the GI tract have received little attention. **Chapter 6** reports the effect of a bitter substance, denatonium benzoate (DB), on insulin secretion in a series of *in vitro* and *ex vivo* experiments using a rodent pancreatic β -cell line, INS-1 832/13 cells, and isolated mouse pancreatic islets. In the latter, the effects of DB on the secretion of other islet hormones, including glucagon, GLP-1 and somatostatin, were also characterised.

While the currently available cell/tissue models and *in vivo* tools have substantially advanced the knowledge on the physiology and pathophysiology of incretins and islet hormones, there is rising demand for sophisticated biomimetic platforms to address the increasingly complicated

biological challenges and improve the translational success from benchtop to bedside. To this end, the development of a gut-on-a-chip (GOC) system is described in **Chapter 7** which facilitates continuous monitoring of dynamic GLP-1 secretion from primary mouse intestinal tissue. Similarly, the development and customisation of a microfluidic sensing platform is described in **Chapter 8**, allowing quantification of the dynamic changes of Ca²⁺ and insulin concurrently, enabling investigation of the secretory function of isolated islets.

DECLARATION

I certify that this work contains no material which has been accepted for the award of any other

degree or diploma in my name, in any university or other tertiary institution except for Chapter 8,

which involved (i) the establishment of a microfluidic biosensor for measurements of Ca²⁺

originated from my thesis submitted for Master of Philosophy degree at the University of

Adelaide, and (ii) proof-of-concept demonstration of the device in biomedical applications

performed as part of my PhD study.

To the best of my knowledge and belief, this work contains no material previously published or

written by another person, except where due reference has been made in the text. In addition, I

certify that no part of this work will, in the future, be used in a submission in my name, for any

other degree or diploma in any university or other tertiary institution without the prior approval

of the University of Adelaide and where applicable, any partner institution responsible for the

joint award of this degree.

The author acknowledges that copyright of published works contained within the thesis resides

with the copyright holder(s) of those works.

I give permission for the digital version of my thesis to be made available on the web, via the

University's digital research repository, the Library Search and also through web search engines,

unless permission has been granted by the University to restrict access for a period of time.

Weikun Huang

24th of November 2023

X

ACKNOWLEDGEMENTS

Commencing in August 2019, my PhD journey has witnessed a series of historical moments in the fight against COVID-19, the fifth documented pandemic since the 1918 flu, which impacted almost every intended milestone of my candidature. But time waits for no man. Only by sparing no effort in making progress in each project and having the support from many people was I able to achieve a timely completion of this thesis with a satisfying quality.

My first thanks go to my supervisors Associate Professor Tongzhi Wu, Professor Christopher K. Rayner, Professor Heike Ebendorff-Heidepriem and Dr. Jiangbo Zhao. They have guided me into the world of interdisciplinary research and provided a wealth of advice that paved the way for the establishment of my unique skillsets and knowledge. A special 'thank you' goes to my Principal Supervisor, Tongzhi, who always inspires me with prolific research ideas and is willing to assist me in stepping into unexplored but crucial areas, and in developing my research leadership skills. This support has enabled me to develop an outstanding number of publications, awards and even successful grant applications. I am extremely fortunate to have been guided by such a team who provided excellent role models, and it would be a great pleasure to enjoy their ongoing mentorship in my future research career.

I was lucky enough to have opportunities to collaborate with several outstanding senior investigators around the world. Their knowledge and research experience have greatly enriched the diversity and quality of my PhD work. I would like to express my appreciation to Professor Michael Horowitz, Professor Karen Jones, Associate Professor Richard L. Young, Dr. Lisa M. Nicholas, Associate Professor Nicolai J. Wewer Albrechtsen, Professor Zilin Sun, and Associate Professor Craig Priest. I look forward to further fruitful collaborations with them in my future career.

To the members of the Rayner and Wu research group, including Dr. Cong Xie, Mrs. Michelle Bound, Ms. Jacqueline Grivell, Ms. Chunjie Xiang and Ms. Tingting Li, thank you for offering your invaluable friendship and support through my candidature. A particular thank you goes to Cong, who has created a number of superb figures and slides that have greatly enhanced several

of my papers and presentations. My gratitude also goes to many staff and students at the Adelaide Medical School and the School of Physics, who have supported me along the way. These include Dr Yunle Wei, Dr. Xuanzhao Pan, Mr. Mingze Yang, Mr. Feng Tang, Ms. Stephanie E. O'Hara, Ms. Kelly M. Gembus, Dr. Fidelma McCorry, Mr. Scott Standfield, and Dr. Yasmyn E. Winstanley. Many of them are now lifelong friends.

Words cannot express my gratitude to my family. Although I have not been able to see my mum Yanfang Zhang, my sister Jing Huang and her husband Lu Qi in person for more than three years, their love and care have never stopped. In my Master's thesis, I wrote that it has been my greatest fortune to have them in my life, and this is certainly unchanged. Finally, a big thank you to my partner Chiwei Feng, who has been there for the entire journey, giving me unending support and comfort that have held me up and carried me through difficult times. Thank you.

PUBLICATIONS ARISING FROM PHD

Publications included in this thesis:

- 1. **Huang, W.,** Xie, C., Young, R. L., Zhao, J., Ebendorff-Heidepriem, H., Jones, K. L., Rayner C. K., Wu, T. (2020). Development of innovative tools for investigation of nutrient-gut interaction. *World Journal of Gastroenterology*, 26(25), 3562. doi: 10.3748/wjg.v26.i25.3562
- 2. **Huang, W.,** Wu, T., Xie, C., Rayner, C. K., Priest, C., Ebendorff-Heidepriem, H., & Zhao, J. (2022). Sensing intra- and extra-cellular Ca²⁺ in the islet of Langerhans. *Advanced Functional Materials*, 32(3), 2106020. doi: 10.1002/adfm.202106020
- 3. Xie, C., **Huang, W.,** Sun, Y., Xiang, C., Trahair, L., Jones, K. L., Horowitz, M., Rayner C. K., Wu, T. (2023). Disparities in the glycemic and incretin responses to intraduodenal glucose infusion between healthy young men and women. *The Journal of Clinical Endocrinology & Metabolism*, dgad176. doi: 10.1210/clinem/dgad176
- Huang, W., Xie, C., Albrechtsen, N. J. W., Sang, M., Sun, Z., Jones, K. L., Horowitz, M., Rayner C. K., Wu, T. (2023). Serum alanine transaminase is predictive of fasting and postprandial insulin and glucagon concentrations in type 2 diabetes. *Peptides*, 171092. doi: 10.1016/j.peptides.2023.171092
- 5. **Huang, W.,** Xie, C., Albrechtsen, N. J. W., Jones, K. L., Horowitz, M., Rayner, C. K., Wu, T. (2023). The 'early' postprandial glucagon response is related to the rate of gastric emptying in type 2 diabetes. *Peptides*, 161, 170941. doi: 10.1016/j.peptides.2023.170941
- 6. **Huang, W.,** O'Hara, S. E., Xie, C., Liu, N., Rayner, C. K., Nicholas, L. M., Wu, T. (2023). Effects of bitter substance, denatonium benzoate, on pancreatic hormone secretion: an *ex vivo* evaluation using both a rodent β-cell line and isolated mouse islets. To be submitted for publication

- 7. **Huang, W.,** Zhao, J., Xie, C., Ebendorff-Heidepriem, H., Priest, C., Young, R. L., Rayner, C. K., Wu, T. (2023). Development of a gut-on-a-chip platform to monitor GLP-1 secretion from primary intestinal tissue. To be submitted for publication. To be submitted for publication
- 8. **Huang, W.,** Wu, T., Shallan, A., Kostecki, R., Rayner, C. K., Priest, C., Ebendorff-Heidepriem, H., Zhao, J., (2020). A multiplexed microfluidic platform towards interrogating endocrine function: simultaneous sensing of extracellular Ca²⁺ and hormone, *ACS Sensors*, 5(2):490-499. doi: 10.1021/acssensors.9b02308

Publications not included in the thesis

- Xie, C., Jalleh, R. J., Watson, L. E., Huang, W., Sun, Y., Jones, K. L Horowitz, M., Rayner C. K., Wu, T. (2023). Determinants of blood glucose concentrations following a high carbohydrate meal in type 2 diabetes: A multiple linear regression analysis. *Diabetes Research and Clinical Practice*, 198, 110606. doi: 10.1016/j.diabres.2023.110606
- Wang, X., Chen, C., Xie, C., Huang, W., Young, R. L., Jones, K. L., Horowitz, M., Rayner, C. K., Sun, Z., Wu, T. (2022). Serum bile acid response to oral glucose is attenuated in patients with early type 2 diabetes and correlates with 2-hour plasma glucose in individuals without diabetes. *Diabetes, Obesity and Metabolism*, 24(6), 1132-1142. doi: 10.1111/dom.14683
- 11. Xie, C., Huang, W., Watson, L. E., Soenen, S., Young, R. L., Jones, K. L., Horowitz, M., Rayner, C. K., Sun, Z., Wu, T. (2022). Plasma GLP-1 response to oral and intraduodenal nutrients in health and type 2 diabetes—impact on gastric emptying. *The Journal of Clinical Endocrinology & Metabolism*, 107(4), e1643-e1652. doi: 10.1210/clinem/dgab828
- 12. Palasis, K. A., Lokman, N. A., Quirk, B. C., Adwal, A., Scolaro, L., **Huang, W.,** Ricciardelli, C., Oehler, M. K., McLaughlin, R. A., Abell, A. D. (2021). Optical fibre-enabled photoswitching for localised activation of an anti-cancer therapeutic

- drug. International Journal of Molecular Sciences, 22(19), 10844. doi: 10.3390/ijms221910844
- 13. Xie, C., **Huang, W.,** Wang, X., Trahair, L. G., Pham, H. T., Marathe, C. S., Young, R. L., Jones, K. L., Horowitz, M., Rayner, C. K., Wu, T. (2021) Gastric emptying in health and type 2 diabetes: An evaluation using a 75 g oral glucose drink. *Diabetes Research and Clinical Practice* 2021;171:108610. doi: 10.1016/j.diabres.2020.108610.
- 14. Xie, C*, **Huang, W***, Young, R. L, Jones, K. L, Horowitz, M, Rayner, C. K, & Wu, T. Role of bile acids in the regulation of food intake, and their dysregulation in metabolic disease. *Nutrients* 2021;13(4):1104. doi: 10.3390/nu13041104. (* joint first authorship) doi: 10.3390/nu13041104

CONFERENCE PRESENTATIONS

- 1. Effect of a bitter tasting substance, denatonium benzoate, on pancreatic hormone secretion (*Pincus Taft Young Investigator Award Finalist*). Oral presentation at Australian Diabetes Congress (ADC), Adelaide, Australia, Aug. 2023.
- 2. Serum alanine transaminase is predictive of fasting postprandial insulin and glucagon concentrations in type 2 diabetes (*Clinical Poster Award Finalist*). Poster presentation at ADC, Adelaide, Australia, Aug. 2023.
- 3. Determinants of blood glucose concentrations after a high carbohydrate meal in type 2 diabetes: a multi-liner regression analysis. Oral presentation at the 58th Annual Meeting of the European Association for the Study of Diabetes (EASD), Stockholm, Sweden, Sept. 2022.
- 4. The 'early' postprandial glucagon response to a mixed meal is dependent on the rate of gastric emptying in type 2 diabetes. Oral presentation at the 58th Annual Meeting of EASD, Stockholm, Sweden, Sept. 2022.
- 5. SGLT2 inhibition prevents high fat diet-induced glucose intolerance, but not weigh gain, in C57BL/6 male mice. Short oral discussion at the 58th Annual Meeting of EASD, Stockholm, Sweden, Sept. 2022.
- 6. The 'early' postprandial glucagon response to a mixed meal is dependent on the rate of gastric emptying in type 2 diabetes. Oral presentation at ADC, Brisbane, Australia, Aug. 2022.
- 7. SGLT2 inhibition prevents high fat diet-induced glucose intolerance, but not weigh gain, in C57BL/6 male mice (*Poster Award Finalist*). Poster presentation at ADC, Brisbane, Australia, Aug. 2022.

- 8. An integrated microfluidic sensing system platform for dissecting insulin secretion and extracellular Ca²⁺ dynamics of pancreatic islets. Short oral discussion at The 57th Annual Meeting of EASD, Virtual, Sept. 2021.
- 9. Serum bile acids after an oral glucose load in Chinese healthy individuals and patients with type 2 diabetes relationship with glycaemia. Poster presentation at ADC, Virtual, Aug. 2021.
- 10. A novel microfluidic sensing platform for dissecting insulin secretion and extracellular Ca²⁺ dynamics of pancreatic islets (*Pincus Taft Young Investigator Award Finalist*). Oral presentation at ADC, Virtual, Nov. 2020.
- 11. Dissecting insulin secretion and extracellular Ca²⁺ of pancreatic islets via a novel microfluidic platform. Poster presentation at the Florey Postgraduate Research Conference, The University of Adelaide (virtual, Sept. 2020)
- 12. A novel sensing platform for extracellular Ca(II) and insulin. Oral poster presentation at the International Diabetes Federation Congress 2019, Busan, Korea, Dec. 2019.

CHAPTER 1: DEVELOPMENT OF INNOVATIVE
TOOLS FOR INVESTIGATION OF
NUTRIENT-GUT INTERACTION

Statement of Authorship

Title of the paper	Development of innovative tools for investigation of nutrient-gut interaction		
Publication status	Published		
	Huang, W., Xie, C., Young, RL., Zhao, J., Ebendorff-Heidepriem, H., Jones, KL.,		
Publication details	Rayner, CK., Wu, T., (2020). "Development of innovative tools for investigation of		
	nutrient-gut interaction", World Journal of Gastroenterology, 26(25), 3562.		

Principal Author

Candidate	Weikun Huang		
Contribution	Conception, design and drafting and revision of the manuscript.		
Overall percentage	80%		
Certification	This paper reports on original research I conducted during the period of my Higher Degree by Research candidature and is not subject to any obligations or contractual agreements with a third party that would constrain its inclusion in this thesis. I am the primary author of this paper		
Signature		Date	September 2023

Co-Author Contributions

By signing the Statement of Authorship, each author certifies that: i) the candidate's stated contribution to the publication is accurate (as detailed above); ii) permission is granted for the candidate to include the publication in the thesis; and iii) the sum of all co-author contributions is equal to 100% less the candidate's stated contribution.

Name of Co-Author	Cong Xie		
Contribution	Conception and review of the manuscript		
Signature		Date	September 2023

Name of Co-Author	Richard L. Young		
Contribution	Conception and review of the manuscript		
Signature	Date September 2023		
Name of Co-Author	Jiangbo Zhao		
Contribution	Conception and review of the manu	script	
Signature	Date September 2023		
Name of Co-Author	Heike Ebendorff-Heidepriem		
Contribution	Conception and review of the manuscript		
Signature		Date	September 2023
Name of Co-Author	Karen L. Jones		
Contribution	Conception and review of the manuscript		
Signature	Date September 2023		September 2023
Name of Co-Author	Christopher K. Rayner		
Contribution	Conception and review of the manuscript		
Signature	Date September 2023		
Name of Co-Author	Tongzhi Wu		
Contribution	Conception, design and drafting of the manuscript and guarantor of the paper		
Signature		Date	September 2023

1.1 Abstract

The gastrointestinal tract is the key interface between the ingesta and the human body. There is wide recognition that the gastrointestinal response to nutrients or bioactive compounds, particularly the secretion of numerous hormones, is critical to the regulation of appetite, body weight and blood glucose. This concept has led to an increasing focus on "gut-based" strategies for the management of metabolic disorders, including type 2 diabetes and obesity. Understanding the underlying mechanisms and downstream effects of nutrient-gut interactions is fundamental to effective translation of this knowledge to clinical practice. To this end, an array of research tools and platforms have been developed to better understand the mechanisms of gut hormone secretion from enteroendocrine cells. This review discusses the evolution of *in vitro* and *in vivo* models and the integration of innovative techniques that will ultimately enable the development of novel therapies for metabolic diseases.

Key words: Nutrient-gut interaction, Metabolic disorders, Incretin hormones, Enteroendocrine cells, Enteroids, Intestinal intubation, Intestine-on-a-chip

1.2 Introduction

It is now widely appreciated that the gastrointestinal (GI) tract not only serves to process food, but also represents the largest endocrine organ in the body, releasing a wide array of peptide hormones to orchestrate metabolic homeostasis [1]. Ghrelin, for example, is released from gastric Gr-cells into the circulation during fasting or periods of negative energy balance and triggers hunger to drive food intake [2]; ghrelin levels in circulation are subsequently suppressed upon feeding [3]. The interaction of nutrients and digestive juices with the intestinal mucosa triggers the secretion of a number of postprandial hormones, including cholecystokinin (CCK) from enteroendocrine (EE) I-cells [4] and glucose-dependent insulinotropic polypeptide (GIP) from K-cells in the upper small intestine, and glucagon-like peptide-1 (GLP-1) and peptide YY (PYY) from L-cells located predominantly in the distal small and large intestine [5,6]. A subset of EE cells in the proximal small intestine has also been shown to secrete both GLP-1 and GIP [7]. GLP-1 and GIP are known as the incretin hormones; both stimulate insulin secretion in a glucose-dependent manner [8,9]. GLP-1 also suppresses glucagon and acts with CCK and PYY to inhibit appetite, slow the delivery of nutrients from the stomach into the small intestine and

retard their subsequent absorption [10]. Accordingly, the integrated responses of GI hormones to meal ingestion are critical determinants of energy balance and postprandial glycaemia.

That plasma concentrations of GI hormones are typically increased after enteral, but not intravenous, nutrient administration attests to the importance of nutrient-gut interactions to the release of these hormones [11]. Accordingly, an improved understanding of the sensor and actuator mechanisms through which nutrients or bioactive compounds interact with EE cells, has the potential to yield novel "gut-based" approaches for the management of metabolic diseases. In the last few decades, a broad range of preclinical and clinical models have been developed to study nutrient-gut interactions, with increasing efforts to achieve clinically relevant outcomes. To this end, *ex vivo* studies have extended from the use of EE cell lines towards primary intestinal tissues and organoids, and have increasingly incorporated sophisticated culture conditions to mimic normal physiology. Clinical studies employing customised intestinal perfusion catheters for targeted delivery of nutrients or therapeutic compounds, or novel ingestible sensors, have attempted to better characterise the regional specificity of GI responses. In this review, we summarise the research tools and models used to investigate nutrient-gut interactions, and discuss their advantages and limitations for clinical translation of findings (Table 1).

1.3 Cellular Models

The GI mucosa incorporates a monolayer of columnar epithelium with region-specific architecture and EE cell composition that is uniquely tuned to secrete specific gut hormones and absorb nutrients to fulfil specific metabolic functions. EE cells account for less than 1% of all epithelial cells, and their distribution varies substantially along the GI tract (Figure 1) [12]. Immortalised cell lines derived from murine and human intestinal tumours have been developed for *in vitro* studies, and retain the capacity to secrete GI hormones in response to nutrient stimuli (Table 2).

 Table 1 Available tools used for investigation of nutrient-gut interactions

Tools		Advantages	Disadvantages/Challenges	
Cellular models	EE cell lines	established secretion profiles;	limited resemblance to native L-cells;	
Centulal inodels		genetically modifiable;	lack of inter-organ interaction;	
		readily accessible	limited success in clinical translation	
	intestinal organoids	preserved native architecture;	undefined secretion profiles;	
		region-specific functions;	lack of integrated nervous or immune systems;	
Tissue-based		high plasticity for oriented differentiation	inconsistent culture outcomes	
approaches	isolated intestine	preserved native intestinal structure;	short viable period;	
		access to luminal and basolateral surface	lack of inter-organ interaction;	
		high physiological relevance	limited access to human tissue;	
			low EE cell density	
Intestinal in vivo infusion in region-speci		region-specific delivery;	technically demanding;	
		direct insights into human (patho-)physiology	restricted to specialised research centre	
	3D culture	enhanced anatomical complexity;	limited cellular variety;	
		compatibility with co-culture system	static culture environment	
N1	intestine-on-a-chip	dynamic culture environment;	sophisticated validation of the system;	
Novel		recapitulation of luminal events	partial resemblance to luminal physiology	
techniques	ingestible sensors	a broad range of applications;	difficulty in signal interpretation;	
		high potential for multi-purposed in vivo investigation	lack of stability;	
			high cost	

Note: EE cell: enteroendocrine cell

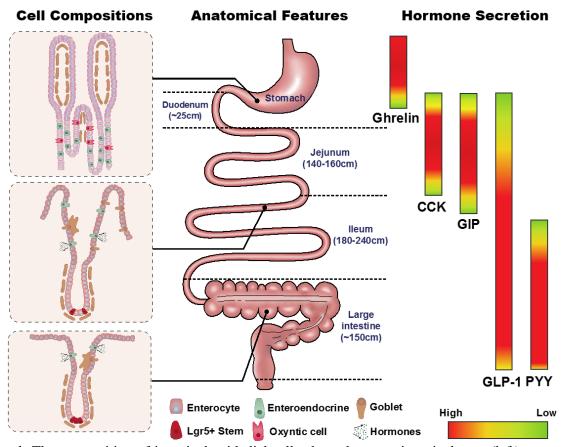


Figure 1. The composition of intestinal epithelial cells along the gastrointestinal tract (left); anatomical features and typical length of different sections of the gastrointestinal tract (middle); regionally specific secretion profile of different gut hormones, including ghrelin, cholecystokinin (CCK), glucose-dependent insulinotropic polypeptide (GIP), glucagon-like peptide 1 (GLP-1) and peptide YY (PYY) (right).

STC-1 cells are a heterogeneous and poorly differentiated EE cell line derived from intestinal secretin-producing tumours in mice. They have a high immunoreactivity to anti-proglucagon sera and are capable of releasing glucagon-like immuno-reactants [13]. STC-1 cells were subsequently shown to secrete multiple gut hormones, including CCK [14], GLP-1 [15,16], GIP [17], and PYY [18,19], in a similar manner to native murine EE cells, when stimulated by glucose [20], amino acids and fatty acids. As a result, STC-1 cells have been a popular model to screen for gut hormone-releasing stimuli. However, the clinical relevance of this model has been frequently questioned. For example, treatment with potato protease inhibitor concentrate (PPIC) or whey protein does not induce CCK secretion from STC-1 cells [21,22]. By contrast, oral administration of PPIC (100 mg/kg per day) stimulates CCK secretion in rodents [21], while ingestion of whey protein (55 g) increases plasma CCK levels in humans [23].

Table 2 Enteroendocrine cell models

Species	Model	Origin	Hormones	Features
Mouse	STC-1	Duodenal	GLP-1,	Heterogeneous cell population; responds to
		secretin	GLP-2, CCK,	glucose, amino acids, fatty acids and neural
		tumour cells	GIP, PYY,	stimuli; poor expression of CaSR
	GLUTag	Colonic	GLP-1,	Subcloned homogenous cells; respond to
		tumour	GLP-2, CCK	glucose, bile acids, fatty acids, amino acids
Human	NCI-H716	Colorectal	GLP-1, GLP-2	Heterogeneous cell population; poorly
		carcinoma		differentiated; responds to glucose, fatty acids,
				protein hydrolysates
	HuTu-80	Duodenal	GLP-1, PYY,	Respond to antioxidant compounds, sweet and
		carcinoma	GIP, CCK	bitter substances

Note: CCK: cholecystokinin; GLP-1: glucagon-like peptide 1; GIP: glucose-dependent insulinotropic polypeptide; PYY: peptide YY; CaSR: Ca²⁺-sensing receptor

GLUTag cell line is a subcloned homogeneous EE cell model developed by the Drucker group from an endocrine carcinoma of the large bowel in transgenic mice [24]. These cells express both proglucagon and CCK genes [25] but produce primarily GLP1(7-36)-amide. GLUTag cells are equipped with a wide repertoire of nutrient sensors and transporters, including G-protein coupled receptors (GPCRs) [26], glucokinase [27] and the sodium-glucose linked transporter 1 (SGLT1) [28] involved in nutrient-induced GLP-1 secretion. In agreement with *in vivo* findings, GLUTag cells exhibit robust release of GLP-1 in response to glucose [29], bile acids [30], fatty acids [31] and amino acids [32]. These observations have promoted GLUTag cells as a frontline model of L cells, leading to a wide application for studying the mechanisms underlying GLP-1 secretion and for screening potential GLP-1 secretagogues. However, clinical studies are still required to validate *in vitro* findings. For example, the treatment of glutamine (10 mmol/L) was shown to markedly increase GLP-1 secretion (7-fold) from GLUTag cells [32]. However, oral administration of encapsulated ileal-release glutamine (6 g) or intra-duodenal glutamine infusion (7.5-15 g) evoked only modest increases in plasma GLP-1 levels in healthy subjects and patients with type 2 diabetes (T2D) [33,34].

The human cell lines NCI-H716 and HuTu-80 have also been used widely to characterise nutrient-evoked GLP-1 release. The NCI-H716 cell line was first reported by Park *et al* [35] from human colorectal carcinoma. It contains dense-core granules, expresses chromogranin A, and secretes GLP-1 in response to glucose, fatty acids and protein hydrolysates [36]. Studies incorporating the NCI-H716 cell line have revealed critical roles of amino acid transporters [37], type 1 taste receptors [38] and monoacylglycerol-sensing GPCR [31] in GLP-1 secretion.

However, the secretory profile of NCI-H716 cells is more limited compared to murine STC-1 or GLUTag cells. For example, NCI-H716 cells secrete GLP-1 and GLP-2 but not GIP, PYY or CCK in response to 50 mmol/L KCl, or combined glucose (10 mmol/L), forskolin and phosphodiesterase inhibitor (10 μ mol/L) [39]. That NCI-H716 cells do not secrete PYY reflects their limited resemblance to native L-cells.

The HuTu-80 cell line is an alternative EE cell model of human origin that secretes GLP-1, GIP, PYY and CCK [40] and was developed initially to study the biology of GI cancers [41]. Sweet and bitter taste receptors are abundantly expressed in HuTo-80 cells as in native human L-cells, making them a potential model to investigate tastant-induced gut hormone secretion [42,43]. However, unlike native L-cells, bitter tastants, including quinine, denatonium benzoate and phenylthiocarbamide fail to trigger GLP-1 secretion from HuTu-80 cells[44]. Relative to the three aforementioned cell lines, HuTu-80 cells have been less frequently employed to study nutrient-gut interactions.

1.4 Tissue-based Gut Hormone Release ex vivo

The major functional differences between immortalised intestinal cell lines and primary EE cells have led to an increased research focus on primary intestinal models to study the endocrine function of the gut. These have included the isolation and use of primary EE cells [45-47] and the use of *ex vivo* intestinal tissue preparations from animals [48-51] and humans [52,53]. These tissue-based approaches maintain native cell-cell connections and polarity, and have hitherto yielded a deep understanding of the mechanisms governing nutrient and drug-evoked 5-hydroxytryptamine and GLP-1 release [54,55]. However, clinical access to gut endoscopic, colonoscopic or surgical tissues, tissue viability and potentially low EE cell density can limit these primary models. The purification of primary EE cells is also technically demanding. The recent development of intestinal organoids holds the promise to overcome some of these limitations.

1.5 Intestinal Organoids

Intestinal organoids, also known as "mini-guts", are miniaturised intestinal units that display many features of gut tissue architecture and function. In 2007, Barker and colleagues identified leucine-rich repeat-containing GPCRG-5 (Lgr5) -positive cells as stem cells in the small intestine and colon via genetic lineage tracing experiments [56]. Subsequently, a single Lgr5-positive stem cell was shown to differentiate into crypt-villus organoids, namely enteroids, that are inclusive of all cell types present in the native intestinal epithelium [57]. Of note, enteroids can be developed from Lgr5-positive cells originating from any section of the gut. *Ex vivo* characterisation has shown that these enteroids display the basal-apical polarity of mature epithelial cells [58,59]. Moreover, they retain many region-specific functions of the original location from which the stem cells were taken [60].

Intestinal organoids can also be developed from human pluripotent stem cells, which are referred to as human intestinal organoids (HIOs) [61,62]. HIOs have a similar morphology as enteroids and display crypt-villus structures inclusive of all intestinal cell types. By contrast, HIOs contain a mesenchyme layer that is composed of myofibroblasts, endothelial cells and smooth muscle [63]. Moreover, HIOs do not show region-specific features and eventually grow into an unselective population of EE cells [61]. The differentiation process has been shown to be enhanced by the Happy Cell Advanced Suspension Medium[64] and by activation of the bone morphogenetic protein signalling pathway [65].

In contrast to primary intestinal epithelium, intestinal organoids remain viable for over 1-year *ex vivo* and show plasticity in cellular composition in response to changes in the culture environment or modified gene expression. Accumulating evidence suggests that the density of EE cells in organoids is subject to the expression of several translational factors, including Neurogenin 3 and *Aristaless*-related homobox [61,66,67], raising the prospect that EE cells can be customised in an organoid. Indeed, exposure of mouse or human enteroids to short-chained fatty acids (SCFAs) increases the number of L cells, and hence GLP-1 secretion, over 48 hours of SCFA treatment [68]. Similar trends in differentiation have also been observed with enteroids treated with dibenzazepine or bile acids [69,70]. However, the secretory profile of intestinal organoids in response to nutrients or non-nutritive compounds has not been well characterised. It

should also be noted that delivery of stimuli to the lumen of the organoids requires individual microinjection, which is both labour-intensive and technically demanding due to their small size [71]. Moreover, the culture of organoids in conventional platforms makes it difficult to mimic the continuous movement of luminal contents and the constantly changing nature of the extracellular fluid. Finally, it is not yet possible to recreate the architectural complexity of the GI tract, including its vascular, nervous, immune, mucous elements and the microbiome, in any organoid preparation.

1.6 Intestinal Perfusion in vivo

The development of intestinal perfusion techniques and analytic methods capable of measuring GI hormones released into the peripheral circulation has allowed the evaluation of nutrient-gut interactions *in vivo*. In rodents, dietary effects on gut hormone secretion have been investigated in models of isolated intestinal perfusion [72,73]. In humans, it is also possible to characterise the responses of various regions of the gut to intraluminal stimuli, and to examine the underlying mechanisms.

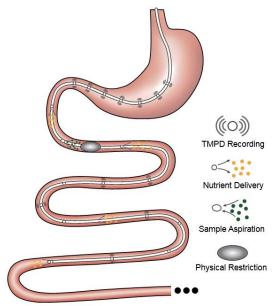


Figure 2. Schematic of a multichannel intestinal catheter to study regional specificity of nutrient-gut interactions. Multiple channels are opened on the catheter to record the transmucosal potential difference (TMPD) and monitor its position. These channels can also deliver investigational compounds of aspirate luminal samples in a specific region of the intestine. The balloon is generally designed to create physical restriction to prevent the fluid flow or the movement of the catheter.

A rubber feeding tube was initially designed to deliver medication to the intestine and to examine luminal contents in paediatric patients [74]. This early design incorporated 1-2 cm wide lateral window(s) for infusion/aspiration of liquids and a weighted terminal bulb to facilitate passage of the catheter by peristalsis. Subsequently, intestinal catheters have been increasingly customised to study gut function. For example, the integration of an inflatable balloon at the distal end of the catheter was employed to evaluate the perception of distension or control the position of the catheter [75]. The use of a multi-lumen catheter has allowed for multiple inflatable balloons, making it possible to isolate segments of the lumen [76], within which nutrient absorption can be carefully characterised [77-79]. Incorporation of manometry and impedance sensors into the catheter design has further facilitated concurrent recording of gut motility [34] and flow events [80]. Positioning these catheters has relied on fluoroscopy, for which radiation exposure represents a major limitation. To overcome this, Andersson and Grossman established an alternative method of monitoring catheter position by measuring transmucosal potential difference (TMPD) between skin or blood and the intestinal lumen [81]. Corresponding to the differences in pH between the stomach and the duodenum, TMPD in the distal antral channel and the proximal duodenal channel record around -40 mV and 0 mV, respectively [82,83]. Accordingly, a change of TMPD from -40 mV to 0 mV reflects the passage of channels through the transpyloric area (Figure 2).

Relative to oral administration, intestinal perfusion of nutrients or investigational compounds circumvents the impact of inter-individual variations in the rate of gastric emptying – which can be substantial [84-86] – such that the exposure of the small intestine to nutrients can be standardised. Studies employing intraduodenal infusion of nutrients spanning the normal range of gastric emptying (1-4 kcal/min) have established that the stimulation of gut hormones, including CCK, GIP, GLP-1 and PYY, is dependent on the rate of nutrient entry into the small intestine. In line with the biological distribution of respective EE cells, the secretion of CCK and GIP appears to be proportional to the load of glucose, lipid or protein, whereas GLP-1 and PPY responses are non-linear, being modest at 1-2 kcal/min and substantially greater at 3-4 kcal/min [87]. Moreover, when glucose and fat are infused intraduodenally at an identical rate of 2 kcal/min, it is observed that fat is significantly more potent than glucose at stimulating GLP-1 and GIP secretion [88].

A multi-lumen catheter of adequate length can also be positioned over a long length of small intestine to allow targeted delivery of nutrients or investigational compounds into proximal or distal sites, to determine the regional specificity of nutrient-gut interactions. In this way, infusion of glucose (2 kcal/min) into the jejunum (50 cm distal to pylorus) was shown to elicit more GLP-1 and GIP release compared to equivalent duodenal infusion (12 cm distal to pylorus) in healthy men [89]. Furthermore, ileal glucose infusion (2 kcal/min, 190 cm distal to pylorus) resulted in markedly greater GLP-1 and lower (but more sustained) GIP responses compared to intraduodenal infusion, and was associated with a greater incretin effect and GI-mediated glucose disposal in both healthy subjects and patients with T2D (Figure 3) [90]. Administration of compounds into the rectum can similarly be undertaken using a soft tube with minimal discomfort [91,92]. Characterisation of the region-specific profile of gut hormone release has shed light on the mechanisms by which Roux-en-Y gastric bypass surgery improves blood glucose control in T2D [93]. In addition, this knowledge has directed the precise delivery of stimuli to optimise gut hormone response for therapeutic gain. For example, enteric coating of a small dose of lauric acid to allow targeted release in the ileum and colon was shown to be effective at stimulating GLP-1 secretion and lowering blood glucose in patients with T2D [94].

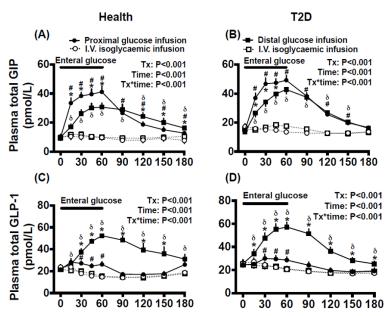


Figure 3. Comparison of the effect of enteral (proximal or distal) and intravenous (i. v.) isoglycaemic glucose administrations on plasma incretin hormone, glucose-dependent insulinotropic polypeptide (GIP) and glucagon-like peptide-1 (GLP-1) secretions in healthy subjects and subjects with type 2 diabetes (T2D).

Access to the intestines via endoscopy and colonoscopy has provided an additional means for targeting intestinal perfusion to a specific region, while also allowing for the collection of mucosal biopsies to study anatomical and molecular mechanisms underlying nutrient-gut interactions (discussed in earlier section). In this way, sweet taste receptors (STRs) (heterodimeric T1R2 and T1R3) were found to be involved in intestinal glucose sensing and linked to the regulation of glucose absorption in both health and T2D; in patients with T2D, a defect in the downregulation of STRs in the face of hyperglycaemia was shown to contribute to excessive postprandial glycaemic excursions [95]. Moreover, *ex vivo* studies using human intestinal biopsies have revealed a critical role for both SGLT1 and the facilitative glucose transporter 2 in mediating glucose-induced GLP-1 secretion [55].

1.7 Novel Techniques to Study Gut Hormone Secretion

Several novel techniques are emerging to evaluate nutrient-gut interactions with improved physiological or therapeutic relevance, while overcoming limitations of clinical studies.

Recent development of culture engineering techniques has allowed the integration of advanced culture interfaces into the conventional 2D culture platforms of intestinal organoids and primary epithelial cells. This has enabled the provision of culture frameworks that support the growth of intestinal cells and facilitate the assessment of tissue function in a more physiologically relevant environment [96,97]. For example, culturing intestinal cells on a porous polyester membrane provides access to both basolateral and apical sides of the polarised epithelial cells, which is of particular importance for the investigation of intestinal function in response to luminal stimuli (Figure 4A). In addition, the membrane can be coated with an extracellular matrix containing growth factors to induce growth and differentiation of organoids. This experimental platform is being increasingly used to study intestinal barrier function [98,99], immune responses [100], and drug metabolism [101,102], with a handful of studies focusing on nutrient-gut interactions. Kozuka *et al* [103] developed an intestinal monolayer culture platform utilising Transwell (a culture plate with an inserted membrane) with a 0.4 μ m or 1 μ m pore membrane and successfully cultured murine and human intestinal enteroids. Treatment with forskolin (100 μ M) in the apical chamber stimulated GLP-1 release into the basolateral chamber, consistent with the

presence of functional L-cells and GLP-1 deployment mechanisms. With this compartmental culture system, it is possible to model the interaction between the intestinal epithelium and luminal content and monitor the hormonal response in the downstream chamber.

More advanced and complex intestine models have been achieved by applying microfluidic devices in gut function studies, also known as "intestine-on-a-chip". These microfluidic devices have the capacity to provide a dynamic culture environment, including continuously refreshed culture media and biomimetic mechanical strain, to more accurately resemble physiological conditions (Figure 4B). Current in vitro gut models on microfluidic devices have mainly been used to investigate drug metabolism [104] and gut-liver interactions [105]. The application of the "intestine-on-a-chip" model for gut hormone secretion study is in its infancy. In 2016, Hsiao et al [106] developed a high-throughput automated microfluidic platform to assess the response of NCL-H716 cells to sweet and bitter stimuli. Although gut hormones were not measured in the study, the microfluidic system recorded dynamic changes in intracellular Ca²⁺ in over 500 single NCI-H716 cells trapped in each micro-well. In another study, Park and his colleagues established a co-culture of GLUTag cells and the β -cell line INS-1 to screen compounds of anti-diabetic potential [107]. Relative to the use of intestinal cancer cell line, intestinal organoids cultured on a microfluidic device display a high resemblance to the native intestine transcriptome, including the expression of genes related to cell proliferation, digestion and responses to nutrients [108], and may prove to be a useful ex vivo model for studying GI hormone secretion.

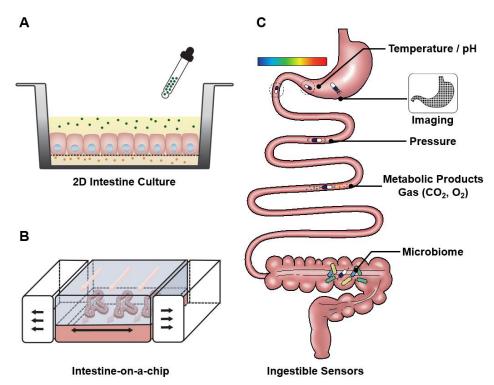


Figure 4. Emerging advanced techniques to study nutrient-gut interaction. (A) 2D culture of intestinal epithelium on a porous membrane. (B) An intestine-on-a-chip model with intestinal organoids cultured in a microfluidic device, where constant perfusion and periodic mechanical strain can be applied to the system. (C) Ingestible sensors for measuring various parameters relevant to gut functions.

Ingestible sensors are under rapid development in clinical settings. These are typically capsule devices of up to 11 mm in diameter and 28 mm in length, to allow easy transit through the gut while measuring biomedical parameters (Figure 4C). To date, ingestible sensors have been developed for imaging [109-112] and measurements of gases [113], pH, temperature [114-117], pressure [118] and luminal contents [119-121]. The pH sensors have been used to assess gastric emptying and small intestinal transit, marked by abrupt pH changes between the stomach and duodenum (> 3 units) and between the ileum and colon (> 1 unit) [122,123]. The wide applications of ingestible sensors will require further technical development to improve stability, signal interpretation and reduce costs, but offer an exciting glimpse into the future of GI surveillance.

1.8 Conclusions

A better understanding of the mechanisms underlying nutrient-gut interactions is fundamental to the development of gut-based therapies for major metabolic disorders. For this purpose, the development of *in vitro* EE cell models, and techniques suitable for *in vivo* studies, particularly in humans, is of critical importance. EE cell lines of both murine (STC-1 and GLUTag) and human (NCI-H716 and HuTo-80) origin are useful for early studies on gut hormone secretion, but have had limited translational success. This necessitates the development of more physiologically relevant *in vitro* gut models. The emergence of intestinal organoids and novel co-culture systems represents a major advance in this area. In particular, the combination of intestinal organoids and microfluidics will provide an unprecedented opportunity to study the dynamic hormonal response to stimuli under various conditions. *In vivo* validation of research outcomes derived from these models remains critical. In clinical studies, intestinal intubation and the application of novel ingestible sensors, have provided deep knowledge of the region-specific nature of nutrient-gut interactions, and ensuing hormonal and metabolic responses. Further development of non-invasive techniques suitable for use in humans will expand opportunities to translate research findings from the bench to bedside.

1.9 References

- 1. Steinert, R.E., *et al.* Ghrelin, CCK, GLP-1, and PYY (3–36): secretory controls and physiological roles in eating and glycemia in health, obesity, and after RYGB. *Physiological Reviews* **97**, 411-463 (2017).
- 2. Shiiya, T., *et al.* Plasma ghrelin levels in lean and obese humans and the effect of glucose on ghrelin secretion. *The Journal of Clinical Endocrinology & Metabolism* **87**, 240-244 (2002).
- 3. Spiegel, K., Tasali, E., Leproult, R., Scherberg, N. & Van Cauter, E. Twenty-four-hour profiles of acylated and total ghrelin: relationship with glucose levels and impact of time of day and sleep. *The Journal of Clinical Endocrinology & Metabolism* **96**, 486-493 (2011).
- 4. Polak, J.M., *et al.* Identification of cholecystokinin-secreting cells. *The Lancet* **306**, 1016-1018 (1975).
- 5. Buffa, R., Capella, C., Fontana, P., Usellini, L. & Solcia, E. Types of endocrine cells in the human colon and rectum. *Cell and Tissue Research* **192**, 227-240 (1978).
- 6. Svendsen, B., *et al.* An analysis of cosecretion and coexpression of gut hormones from male rat proximal and distal small intestine. *Endocrinology* **156**, 847-857 (2015).

- 7. Theodorakis, M.J., *et al.* Human duodenal enteroendocrine cells: source of both incretin peptides, GLP-1 and GIP. *American Journal of Physiology-Endocrinology and Metabolism* **290**, E550-E559 (2006).
- 8. Mojsov, S., Weir, G. & Habener, J. Insulinotropin: glucagon-like peptide I (7-37) co-encoded in the glucagon gene is a potent stimulator of insulin release in the perfused rat pancreas. *The Journal of Clinical Investigation* **79**, 616-619 (1987).
- 9. Kreymann, B., Ghatei, M., Williams, G. & Bloom, S. Glucagon-like peptide-1 7-36: a physiological incretin in man. *The Lancet* **330**, 1300-1304 (1987).
- 10. Näslund, E., *et al.* Energy intake and appetite are suppressed by glucagon-like peptide-1 (GLP-1) in obese men. *International Journal of Obesity* **23**, 304-311 (1999).
- 11. Perley, M.J. & Kipnis, D.M. Plasma insulin responses to oral and intravenous glucose: studies in normal and diabetic subjects. *The Journal of Clinical Investigation* **46**, 1954-1962 (1967).
- 12. McLaughlin, J., *et al.* Fatty acids stimulate cholecystokinin secretion via an acyl chain length-specific, Ca²⁺-dependent mechanism in the enteroendocrine cell line STC-1. *The Journal of Physiology* **513**, 11-18 (1998).
- 13. Rindi, G., *et al.* Development of neuroendocrine tumors in the gastrointestinal tract of transgenic mice. Heterogeneity of hormone expression. *The American Journal of Pathology* **136**, 1349 (1990).
- 14. Wang, Y., Prpic, V., Green, G.M., Reeve Jr, J.R. & Liddle, R.A. Luminal CCK-releasing factor stimulates CCK release from human intestinal endocrine and STC-1 cells. *American Journal of Physiology-Gastrointestinal and Liver Physiology* **282**, G16-G22 (2002).
- 15. Cordier-Bussat, M., *et al.* Peptones stimulate both the secretion of the incretin hormone glucagon-like peptide 1 and the transcription of the proglucagon gene. *Diabetes* **47**, 1038-1045 (1998).
- 16. Hirasawa, A., *et al.* Free fatty acids regulate gut incretin glucagon-like peptide-1 secretion through GPR120. *Nature Medicine* **11**, 90 (2005).
- 17. Hand, K.V., Giblin, L. & Green, B.D. Hormone profiling in a novel enteroendocrine cell line pGIP/neo: STC-1. *Metabolism* **61**, 1683-1686 (2012).

- 18. Geraedts, M.C., Troost, F.J. & Saris, W.H. Peptide-YY is released by the intestinal cell line STC-1. *Journal of Food Science* **74**, H79-H82 (2009).
- 19. Hand, K.V., *et al.* Examining acute and chronic effects of short- and long-chain fatty acids on peptide YY (PYY) gene expression, cellular storage and secretion in STC-1 cells. *European Journal of Nutrition* **52**, 1303-1313 (2013).
- 20. Mangel, A.W., Prpic, V., Scott, L. & Liddle, R.A. Inhibitors of ATP-sensitive potassium channels stimulate intestinal cholecystokinin secretion. *Peptides* **15**, 1565-1566 (1994).
- 21. Komarnytsky, S., Cook, A. & Raskin, I. Potato protease inhibitors inhibit food intake and increase circulating cholecystokinin levels by a trypsin-dependent mechanism. *International Journal of Obesity* **35**, 236 (2011).
- 22. Foltz, M., *et al.* Protein hydrolysates induce CCK release from enteroendocrine cells and act as partial agonists of the CCK1 receptor. *Journal of Agricultural and Food Chemistry* **56**, 837-843 (2008).
- 23. Komarnytsky, S., Cook, A. & Raskin, I. Potato protease inhibitors inhibit food intake and increase circulating cholecystokinin levels by a trypsin-dependent mechanism. *International Journal of Obesity* **35**, 236-243 (2011).
- 24. Ma, J., *et al.* Effects of a protein preload on gastric emptying, glycemia, and gut hormones after a carbohydrate meal in diet-controlled type 2 diabetes. *Diabetes Care* **32**, 1600-1602 (2009).
- 25. Lee, Y.C., Asa, S.L. & Drucker, D.J. Glucagon gene 5'-flanking sequences direct expression of simian virus 40 large T antigen to the intestine, producing carcinoma of the large bowel in transgenic mice. *Journal of Biological Chemistry* **267**, 10705-10708 (1992).
- 26. Drucker, D.J., Jin, T., Asa, S.L., Young, T.A. & Brubaker, P.L. Activation of proglucagon gene transcription by protein kinase-A in a novel mouse enteroendocrine cell line. *Molecular Endocrinology* **8**, 1646-1655 (1994).
- Oya, M., *et al.* The G protein-coupled receptor family C group 6 subtype A (GPRC6A) receptor is involved in amino acid-induced glucagon-like peptide-1 secretion from GLUTag cells. *Journal of Biological Chemistry* **288**, 4513-4521 (2013).
- 28. Parker, H., *et al.* Predominant role of active versus facilitative glucose transport for glucagon-like peptide-1 secretion. *Diabetologia* **55**, 2445-2455 (2012).

- 29. Gribble, F.M., Williams, L., Simpson, A.K. & Reimann, F. A novel glucose-sensing mechanism contributing to glucagon-like peptide-1 secretion from the GLUTag cell line. *Diabetes* **52**, 1147-1154 (2003).
- 30. Reimann, F. & Gribble, F.M. Glucose-sensing in glucagon-like peptide-1-secreting cells. *Diabetes* **51**, 2757-2763 (2002).
- 31. Parker, H., *et al.* Molecular mechanisms underlying bile acid-stimulated glucagon-like peptide-1 secretion. *British Journal of Pharmacology* **165**, 414-423 (2012).
- 32. Lauffer, L.M., Iakoubov, R. & Brubaker, P.L. GPR119 is essential for oleoylethanolamide-induced glucagon-like peptide-1 secretion from the intestinal enteroendocrine L-cell. *Diabetes* **58**, 1058-1066 (2009).
- 33. Reimann, F., Williams, L., da Silva Xavier, G., Rutter, G. & Gribble, F. Glutamine potently stimulates glucagon-like peptide-1 secretion from GLUTag cells. *Diabetologia* **47**, 1592-1601 (2004).
- 34. Meek, C.L., *et al.* The effect of encapsulated glutamine on gut peptide secretion in human volunteers. *Peptides* **77**, 38-46 (2016).
- 35. Chang, J., et al. Effects of Intraduodenal Glutamine on Incretin Hormone and Insulin Release, the Glycemic Response to an Intraduodenal Glucose Infusion, and Antropyloroduodenal Motility in Health and Type 2 Diabetes. *Diabetes Care* **36**, 2262 (2013).
- 36. Park, J.-G., *et al.* Characteristics of cell lines established from human colorectal carcinoma. *Cancer Research* **47**, 6710-6718 (1987).
- 37. Reimer, R.A., *et al.* A human cellular model for studying the regulation of glucagon-like peptide-1 secretion. *Endocrinology* **142**, 4522-4528 (2001).
- 38. Reimer, R.A. Meat hydrolysate and essential amino acid-induced glucagon-like peptide-1 secretion, in the human NCI-H716 enteroendocrine cell line, is regulated by extracellular signal-regulated kinase1/2 and p38 mitogen-activated protein kinases. *Journal of Endocrinology* **191**, 159-170 (2006).
- 39. Jang, H.-J., *et al.* Gut-expressed gustducin and taste receptors regulate secretion of glucagon-like peptide-1. *Proceedings of the National Academy of Sciences* **104**, 15069-15074 (2007).

- 40. Kuhre, R.E., *et al.* Peptide production and secretion in GLUTag, NCI-H716, and STC-1 cells: a comparison to native L-cells. *Journal of Molecular Endocrinology* **56**, 201-211 (2016).
- 41. Rozengurt, N., *et al.* Colocalization of the α-subunit of gustducin with PYY and GLP-1 in L cells of human colon. *American Journal of Physiology-Gastrointestinal and Liver Physiology* **291**, G792-G802 (2006).
- 42. Schmidt, M., Deschner, E.E., Thaler, H.T., Clements, L. & Good, R.A. Gastrointestinal cancer studies in the human to nude mouse heterotransplant system. *Gastroenterology* **72**, 829-837 (1977).
- 43. Ohtsu, Y., *et al.* Diverse signaling systems activated by the sweet taste receptor in human GLP-1-secreting cells. *Molecular and Cellular Endocrinology* **394**, 70-79 (2014).
- 44. Pham, H., *et al.* A bitter pill for type 2 diabetes? The activation of bitter taste receptor TAS2R38 can stimulate GLP-1 release from enteroendocrine L-cells. *Biochemical and Biophysical Research Communications* **475**, 295-300 (2016).
- 45. Le Nevé, B., Foltz, M., Daniel, H. & Gouka, R. The steroid glycoside Hg-12 from Hoodia gordonii activates the human bitter receptor TAS2R14 and induces CCK release from HuTu-80 cells. *American Journal of Physiology-Gastrointestinal and Liver Physiology* **299**, G1368-G1375 (2010).
- 46. Buchan, A., Barber, D., Gregor, M. & Soll, A. Morphologic and physiologic studies of canine ileal enteroglucagon-containing cells in short-term culture. *Gastroenterology* **93**, 791-800 (1987).
- 47. Koop, I. & Buchan, A.M. Cholecystokinin release from isolated canine epithelial cells in short-term culture. *Gastroenterology* **102**, 28-34 (1992).
- 48. BRUBAKER, P.L. & VRANIC, M. Fetal rat intestinal cells in monolayer culture: a new *in vitro* system to study the glucagon-like immunoreactive peptides. *Endocrinology* **120**, 1976-1985 (1987).
- 49. Drucker, D.J. & Brubaker, P.L. Proglucagon gene expression is regulated by a cyclic AMP-dependent pathway in rat intestine. *Proceedings of the National Academy of Sciences* **86**, 3953-3957 (1989).

- 50. Shima, K., Suda, T., Nishimoto, K. & Yoshimoto, S. Relationship between molecular structures of sugars and their ability to stimulate the release of glucagon-like peptide-1 from canine ileal loops. *European Journal of Endocrinology* **123**, 464-470 (1990).
- 51. ØRSKOV, C., *et al.* Glucagon-like peptides GLP-1 and GLP-2, predicted products of the glucagon gene, are secreted separately from pig small intestine but not pancreas. *Endocrinology* **119**, 1467-1475 (1986).
- 52. Dumoulin, V.r., Moro, F.d.r., Barcelo, A., Dakka, T. & Cuber, J.-C. Peptide YY, glucagon-like peptide-1, and neurotensin responses to luminal factors in the isolated vascularly perfused rat ileum. *Endocrinology* **139**, 3780-3786 (1998).
- 53. Sun, E.W., *et al.* Metformin triggers PYY secretion in human gut mucosa. *The Journal of Clinical Endocrinology & Metabolism* **104**, 2668-2674 (2019).
- 54. Young, R.L., *et al.* Expression of taste molecules in the upper gastrointestinal tract in humans with and without type 2 diabetes. *Gut* **58**, 337-346 (2009).
- 55. Lumsden, A.L., *et al.* Sugar responses of human enterochromaffin cells depend on gut region, sex, and body mass. *Nutrients* **11**, 234 (2019).
- 56. Sun, E.W., *et al.* Mechanisms controlling glucose-induced GLP-1 secretion in human small intestine. *Diabetes* **66**, 2144 (2017).
- 57. Barker, N., *et al.* Identification of stem cells in small intestine and colon by marker gene Lgr5. *Nature* **449**, 1003-1007 (2007).
- 58. Sato, T., *et al.* Single Lgr5 stem cells build crypt-villus structures *in vitro* without a mesenchymal niche. *Nature* **459**, 262-265 (2009).
- 59. Matano, M., *et al.* Modeling colorectal cancer using CRISPR-Cas9–mediated engineering of human intestinal organoids. *Nature Medicine* **21**, 256 (2015).
- 60. Sugimoto, S. & Sato, T. Establishment of 3D intestinal organoid cultures from intestinal stem cells. in *3D Cell Culture* 97-105 (Springer, 2017).
- 61. Middendorp, S., *et al.* Adult stem cells in the small intestine are intrinsically programmed with their location-specific function. *Stem Cells* **32**, 1083-1091 (2014).
- 62. Spence, J.R., *et al.* Directed differentiation of human pluripotent stem cells into intestinal tissue *in vitro*. *Nature* **470**, 105-109 (2011).
- 63. McCracken, K.W., Howell, J.C., Wells, J.M. & Spence, J.R. Generating human intestinal tissue from pluripotent stem cells *in vitro*. *Nature Protocols* **6**, 1920 (2011).

- 64. Watson, C.L., *et al.* An *in vivo* model of human small intestine using pluripotent stem cells. *Nature Medicine* **20**, 1310 (2014).
- 65. Takahashi, Y., *et al.* A refined culture system for human induced pluripotent stem cell-derived intestinal epithelial organoids. *Stem Cell Reports* **10**, 314-328 (2018).
- 66. Múnera, J.O., *et al.* Differentiation of human pluripotent stem cells into colonic organoids via transient activation of BMP signaling. *Cell Stem Cell* **21**, 51-64. e56 (2017).
- 67. Chang-Graham, A.L., *et al.* Human intestinal enteroids with inducible neurogenin-3 expression as a novel model of gut hormone secretion. *Cellular and Molecular Gastroenterology and Hepatology* **8**, 209-229 (2019).
- 68. Du, A., *et al.* Arx is required for normal enteroendocrine cell development in mice and humans. *Developmental Biology* **365**, 175-188 (2012).
- 69. Petersen, N., *et al.* Generation of L cells in mouse and human small intestine organoids. *Diabetes* **63**, 410-420 (2014).
- 70. Petersen, N., *et al.* Targeting development of incretin-producing cells increases insulin secretion. *The Journal of Clinical Investigation* **125**, 379-385 (2015).
- 71. Lund, M.L., *et al.* L-Cell differentiation is induced by bile acids through GPBAR1 and paracrine GLP-1 and serotonin signaling. *Diabetes* (2020).
- 72. Bartfeld, S., *et al. In vitro* expansion of human gastric epithelial stem cells and their responses to bacterial infection. *Gastroenterology* **148**, 126-136. e126 (2015).
- 73. Svendsen, B. & Holst, J.J. Regulation of gut hormone secretion. Studies using isolated perfused intestines. *Peptides* **77**, 47-53 (2016).
- 74. Cheung, G.W.C., Kokorovic, A., Lam, C.K.L., Chari, M. & Lam, T.K.T. Intestinal cholecystokinin controls glucose production through a neuronal network. *Cell Metabolism* **10**, 99-109 (2009).
- 75. Scheltema, G. Permeation in the examination and treatment of the stomach and intestines. *Archives of the Roentgen Ray* **13**, 144-149 (1908).
- 76. Jones, C. & Pierce, F. The mechanism and reference of pain from the lower intestinal tract. *Tr. A. Am. Physicians* **46**, 311 (1931).
- 77. MILLER, G. & Abbott, W. Intestinal intubation: a practical technique. *The American Journal of the Medical Sciences* **187**, 595-598 (1934).

- 78. Abbott, W.O. & Miller, T.G. Intubation studies of the small intestine: III. A technic for the collection of pure intestinal secretion and for the study for intestinal absorption. *Journal of the American Medical Association* **106**, 16-18 (1936).
- 79. Abbott, W.O., Karr, W.G. & Miller, T.G. Intubation studies of the human small intestine: VII. Factors concerned in absorption of glucose from the jejunum and ileum. *The American Journal of Digestive Diseases* **4**, 742-752 (1937).
- 80. Groen, J. The absorption of hexoses from the upper part of the small intestine in man. *The Journal of Clinical Investigation* **16**, 245-255 (1937).
- 81. Shay, H., Gershon-Cohen, J., Fels, S.S., Munro, F.L. & Siplet, H. The absorption and dilution of glucose solutions in the human stomach and duodenum. *The American Journal of Digestive Diseases* **6**, 535-544 (1939).
- 82. Silny, J. Intraluminal multiple electric impedance procedure for measurement of gastrointestinal motility. *Neurogastroenterology & Motility* **3**, 151-162 (1991).
- 83. Andersson, S. & Grossman, M.I. Profile of pH, pressure, and potential difference at gastroduodenal junction in man. *Gastroenterology* **49**, 364-371 (1965).
- 84. Veedfald, S., *et al.* Hyperosmolar duodenal saline infusion lowers circulating ghrelin and stimulates intestinal hormone release in young men. *The Journal of Clinical Endocrinology & Metabolism* **103**, 4409-4418 (2018).
- 85. Wu, T., *et al.* Effects of vildagliptin and metformin on blood pressure and heart rate responses to small intestinal glucose in type 2 diabetes. *Diabetes care* **40**, 702-705 (2017).
- 86. Hutson, W.R., Roehrkasse, R.L. & Wald, A. Influence of gender and menopause on gastric emptying and motility. *Gastroenterology* **96**, 11-17 (1989).
- 87. Watson, L.E., *et al.* Gastric emptying in patients with well-controlled type 2 diabetes compared with young and older control subjects without diabetes. *The Journal of Clinical Endocrinology & Metabolism* **104**, 3311-3319 (2019).
- 88. Cecil, J., Francis, J. & Read, N. Comparison of the effects of a high-fat and high-carbohydrate soup delivered orally and intragastrically on gastric emptying, appetite, and eating behaviour. *Physiology & Behavior* **67**, 299-306 (1999).
- 89. Wu, T., Rayner, C.K., Young, R.L. & Horowitz, M. Gut motility and enteroendocrine secretion. *Current Opinion in Pharmacology* **13**, 928-934 (2013).

- 90. Wu, T., *et al.* Comparative effects of intraduodenal fat and glucose on the gut-incretin axis in healthy males. *Peptides* **95**, 124-127 (2017).
- 91. Wu, T., *et al.* Comparative effect of intraduodenal and intrajejunal glucose infusion on the gut–incretin axis response in healthy males. *Nutrition & Diabetes* **5**, e156-e156 (2015).
- 92. Zhang, X., *et al.* Comparative effects of proximal and distal small intestinal glucose exposure on glycemia, incretin hormone secretion, and the incretin effect in health and type 2 diabetes. *Diabetes Care* **42**, 520-528 (2019).
- 93. Wu, T., *et al.* Effects of rectal administration of taurocholic acid on glucagon-like peptide-1 and peptide YY secretion in healthy humans. *Diabetes, Obesity and Metabolism* **15**, 474-477 (2013).
- 94. Lennernäs, H., Fagerholm, U., Raab, Y., Gerdin, B. & Hällgren, R. Regional rectal perfusion: a new *in vivo* approach to study rectal drug absorption in man. *Pharmaceutical Research* **12**, 426-432 (1995).
- 95. Laferrère, B., *et al.* Incretin levels and effect are markedly enhanced 1 month after Roux-en-Y gastric bypass surgery in obese patients with type 2 diabetes. *Diabetes Care* **30**, 1709-1716 (2007).
- 96. Ma, J., *et al.* A randomised trial of enteric-coated nutrient pellets to stimulate gastrointestinal peptide release and lower glycaemia in type 2 diabetes. *Diabetologia* **56**, 1236-1242 (2013).
- 97. Young, R.L., *et al.* Disordered control of intestinal sweet taste receptor expression and glucose absorption in type 2 diabetes. *Diabetes* **62**, 3532 (2013).
- 98. Wang, Y., *et al.* A microengineered collagen scaffold for generating a polarized crypt-villus architecture of human small intestinal epithelium. *Biomaterials* **128**, 44-55 (2017).
- 99. Chen, Y., Zhou, W., Roh, T., Estes, M.K. & Kaplan, D.L. *In vitro* enteroid-derived three-dimensional tissue model of human small intestinal epithelium with innate immune responses. *PloS One* **12**(2017).
- 100. Eaton, A., Zimmermann, C., Delaney, B. & Hurley, B. Primary human polarized small intestinal epithelial barriers respond differently to a hazardous and an innocuous protein. *Food and Chemical Toxicology* **106**, 70-77 (2017).

- 101. Bhatt, A.P., *et al.* Nonsteroidal anti-inflammatory drug-induced leaky gut modeled using polarized monolayers of primary human intestinal epithelial cells. *ACS Infectious Diseases* **4**, 46-52 (2018).
- 102. Graves, C.L., *et al.* A method for high purity intestinal epithelial cell culture from adult human and murine tissues for the investigation of innate immune function. *Journal of Immunological Methods* **414**, 20-31 (2014).
- 103. Speer, J.E., Wang, Y., Fallon, J.K., Smith, P.C. & Allbritton, N.L. Evaluation of human primary intestinal monolayers for drug metabolizing capabilities. *Journal of Biological Engineering* **13**, 1-15 (2019).
- 104. Takayama, K., *et al.* Generation of human iPSC-derived intestinal epithelial cell monolayers by CDX2 transduction. *Cellular and Molecular Gastroenterology and Hepatology* **8**, 513-526 (2019).
- 105. Kozuka, K., *et al.* Development and characterization of a human and mouse intestinal epithelial cell monolayer platform. *Stem Cell Reports* **9**, 1976-1990 (2017).
- 106. Kimura, H., Sakai, Y. & Fujii, T. Organ/body-on-a-chip based on microfluidic technology for drug discovery. *Drug Metabolism and Pharmacokinetics* **33**, 43-48 (2018).
- 107. Choe, A., Ha, S.K., Choi, I., Choi, N. & Sung, J.H. Microfluidic Gut-liver chip for reproducing the first pass metabolism. *Biomedical Microdevices* **19**, 4 (2017).
- 108. Hsiao, Y.-H., Hsu, C.-H. & Chen, C. A High-throughput automated microfluidic platform for calcium imaging of taste sensing. *Molecules* **21**, 896 (2016).
- 109. Nguyen, D.T.T., van Noort, D., Jeong, I.-K. & Park, S. Endocrine system on chip for a diabetes treatment model. *Biofabrication* **9**, 015021 (2017).
- 110. Kasendra, M., *et al.* Development of a primary human small Intestine-on-a-Chip using biopsy-derived organoids. *Scientific Reports* **8**, 2871 (2018).
- 111. Kalantar-zadeh, K., Ha, N., Ou, J.Z. & Berean, K.J. Ingestible sensors. *ACS Sensors* 2, 468-483 (2017).
- 112. van der Schaar, P.J., *et al.* A novel ingestible electronic drug delivery and monitoring device. *Gastrointestinal Endoscopy* **78**, 520-528 (2013).
- 113. Steiger, C., *et al.* Ingestible electronics for diagnostics and therapy. *Nature Reviews Materials* **4**, 83-98 (2019).

- 114. Byrne, C. & Lim, C.L. The ingestible telemetric body core temperature sensor: a review of validity and exercise applications. *British Journal of Sports Medicine* **41**, 126-133 (2007).
- 115. Kalantar-Zadeh, K., *et al.* A human pilot trial of ingestible electronic capsules capable of sensing different gases in the gut. *Nature Electronics* **1**, 79-87 (2018).
- 116. Gora, M.J., *et al.* Tethered capsule endomicroscopy enables less invasive imaging of gastrointestinal tract microstructure. *Nature Medicine* **19**, 238-240 (2013).
- 117. Kuo, B., *et al.* Generalized transit delay on wireless motility capsule testing in patients with clinical suspicion of gastroparesis, small intestinal dysmotility, or slow transit constipation. *Digestive Diseases and Sciences* **56**, 2928-2938 (2011).
- 118. Rao, S.S., *et al.* Investigation of colonic and whole-gut transit with wireless motility capsule and radiopaque markers in constipation. *Clinical Gastroenterology and Hepatology* **7**, 537-544 (2009).
- 119. Maqbool, S., Parkman, H.P. & Friedenberg, F.K. Wireless capsule motility: comparison of the SmartPill® GI monitoring system with scintigraphy for measuring whole gut transit. *Digestive Diseases and Sciences* **54**, 2167-2174 (2009).

CHAPTER 2: SENSING INTRA- AND EXTRA-CELLULAR CALCIUM IN THE ISLET OF LANGERHANS

Statement of Authorship

Zhao,				
J. (2022). "Sensing intra- and extra-cellular Ca ²⁺ in the islet of Langerhans", Advanced				

Principal Author

Candidate	Weikun Huang				
Contribution	Conception, design and drafting and revision of the manuscript.				
Overall percentage	80%				
Certification	This paper reports on original research I conducted during the period of my Higher Degree by Research candidature and is not subject to any obligations or contractual agreements with a third party that would constrain its inclusion in this thesis. I am the primary author of this paper				
Signature		Date	September 2023		

Co-Author Contributions

By signing the Statement of Authorship, each author certifies that: i) the candidate's stated contribution to the publication is accurate (as detailed above); ii) permission is granted for the candidate to include the publication in the thesis; and iii) the sum of all co-author contributions is equal to 100% less the candidate's stated contribution.

Name of Co-Author	Tongzhi Wu				
Contribution	Conception, design and drafting of the manuscript and guarantor of the paper				
Signature		Date	September 2023		

Name of Co-Author	Cong Xie				
Contribution	Conception and review of the manuscript				
Signature	Date September 2023				
Name of Co-Author	Christopher K. Rayner				
Contribution	Conception and review of the manuscript				
Signature		Date	September 2023		
Name of Co-Author	Craig Priest				
Contribution	Conception and review of the manuscript				
Signature		Date	September 2023		
Name of Co-Author	Heike Ebendorff-Heidepriem				
Contribution	Conception and review of the manuscript				
Signature		Date	September 2023		
Name of Co-Author	Jiangbo Zhao				
Contribution	Conception, design and drafting of the manuscript and guarantor of the paper				
Signature		Date	September 2023		

2.1 Abstract

Calcium ions (Ca²⁺) take part in intra- and intercellular signalling to mediate cellular functions. Sensing this ubiquitous messenger is instrumental in disentangling the specific functions of cellular sub-compartments and/or intercellular communications. In this review, we first describe intra- and intercellular Ca²⁺ signalling in relation to insulin secretion from the pancreatic islets, and then outline the development of diverse sensors, e.g., chemically synthesised indicators, genetically encoded proteins and ion-selective microelectrodes, for intra- and extracellular sensing of Ca²⁺. Particular emphasis is placed on emerging approaches in this field, such as low-affinity Ca²⁺ indicators and unique Ca²⁺-responsive composite materials. We conclude by remarking on the challenges and opportunities for further developments in this field, which may facilitate a more comprehensive understanding of Ca²⁺ signalling within and outside the islets, and its relevance in health and disease.

2.2 Ca²⁺ Homeostasis and Signalling

The homeostasis of calcium ions (Ca²⁺, free ionic form unless specified) is critical to a range of cellular functions [1-3], including endocrine and exocrine secretions [4] gene expression [5], muscle contraction [6], fertilisation [7], and neuronal activity [8]. As a ubiquitous messenger, Ca²⁺ is pivotal to transmitting cascade signalling within and between cells, thus coordinating complex cellular activities in response to internal and/or external stimuli. During these processes, there are coordinated exchanges of Ca²⁺ between cellular sub-compartments or among cells, leading to dynamic changes in Ca²⁺ concentration ([Ca²⁺]) in varying domains. As shown in Figure 1a, in the resting state, cytoplasmic concentration of $Ca^{2+}([Ca^{2+}]_c)$ is maintained at about 50~100 nM via plasma membrane Ca²⁺ transport ATPase (PMCA) [9] and Na⁺/Ca²⁺ exchanger (NCX) [10]; both export Ca²⁺ from the cytoplasm to the extracellular domain. Ca²⁺ concentrations in the mitochondria ([Ca²⁺]_{mito}) and nucleus ([Ca²⁺]_n) are comparable (0.1-100 μM). Ca²⁺ in the endoplasmic reticulum (ER) ([Ca²⁺]_{ER}) (or sarcoplasmic reticulum (SR) in the case of muscle cells), approximates up to ~500 µM, reflecting its reservoir role for Ca²⁺ inside cells [11]. The concentration of extracellular Ca²⁺ ([Ca²⁺]_{ex}) can reach around 1 mM, i.e. four orders of magnitude higher than [Ca²⁺]_c [12]. Upon stimulation, influx of extracellular Ca²⁺ into cytoplasm, via plasma membrane Ca²⁺ channels and release of Ca²⁺ from the ER (or SR) via the

1, 4, 5-triphosphate receptor (IP3R) [13] and ryanodine receptor (RyR) [14], leads to temporary rises of $[Ca^{2+}]_c$ up to 1 μ m. The elevated $[Ca^{2+}]_c$, in turn, re-establishes a concentration equilibrium, by extruding Ca^{2+} back into the extracellular domain or refilling the ER (or SR) and mitochondria via Sacro/Endoplasmic Reticulum Ca^{2+} -ATPase (SERCA) [15] and the mitochondrial Ca^{2+} uniporter (MCU) [16], respectively.

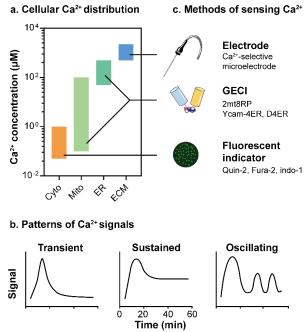


Figure 1. Cellular Ca^{2+} concentrations, signal patterns and sensors commonly used in islet studies. (a) Overview of typical $[Ca^{2+}]$ in intra- and extracellular domains, including Ca^{2+} in the cytoplasm (Cyto, 50-1000 nM), mitochondria (Mito) and nucleus (N, 0.1-100 μM), endoplasmic reticulum (ER, 50–500 μM), and extracellular matrix (ECM, 1 mM) [17]. (b) Schematics of three representative types of cytoplasmic Ca^{2+} signals: transient (left), sustained (middle) and oscillating (right) patterns. (c) Sensing tools commonly used for measuring Ca^{2+} in islet studies, including Ca^{2+} -selective microelectrodes for extracellular Ca^{2+} , genetically encoded Ca^{2+} indicator (GECI) protein-based indicators (e.g. 2mt8RP for mitochondrial Ca^{2+} , Ycam-4ER and D4ER) for endoplasmic reticulum Ca^{2+} , and fluorescent Ca^{2+} indicators (e.g. Quin-2, Fura-2 and Indo-1) for cytoplasmic Ca^{2+} .

Within the cytoplasm, variations in Ca²⁺ signals appear in transient, sustained or oscillatory patterns (Figure 1b), in the context of physiological or pathological processes [18]. The transient increase in [Ca²⁺]_c reflects a rapid influx of extracellular Ca²⁺ through Ca²⁺-permeable channels in response to cellular depolarisation, followed by prompt and effective Ca²⁺ transport into other intra- or extracellular compartments (described in the preceding paragraph). The latter drives [Ca²⁺]_c to return to its original level in a short timeframe to avoid overloading of Ca²⁺ [19-21]. Accordingly, any impairment in this process may result in prolonged elevation of [Ca²⁺]_c, leading to programmed cell death or necrosis [22, 23]. Physiological cellular responses to

continued stimulation are therefore associated with oscillatory changes in $[Ca^{2+}]_c$, as well as $[Ca^{2+}]$ in other intra- and extracellular domains, although the pattern may be atypical in many instances [24-29].

Following the discovery that skeletal muscle contraction is linked to coordinated, and repeated, changes in $[Ca^{2+}]_c$ [30], Ca^{2+} oscillations have since been recognised as a universal mechanism underlying many biological events, such as egg fertilisation [31], insulin secretion from pancreatic β -cells [32], and interleukin production from macrophages [33]. In this review, we first discuss the relevance of intra- and intercellular Ca^{2+} signalling based on the function of pancreatic islets, particularly the phenomenon of a pulsatile insulin response to glucose. We then outline the chronological development of Ca^{2+} sensing methodologies (Figure 1c) that are critical to the in-depth understanding of these physiological processes in the islets, where we remark on the rationale (pros and cons) for the selection of prevalent and emerging indicators, as well as the analytical techniques/platforms in the context of various applications. We finally provide an outlook on the prospects of Ca^{2+} sensing in the study of islets and in broader biomedical research, highlighting the challenges and opportunities.

This review is not intended to be exhaustive, but instead emphasises the sensing techniques for detection/monitoring of dynamic cellular Ca²⁺ concentrations and associated secretory activity. Accordingly, measurement of non-labile calcium (i.e. calcium tightly incorporated within cellular structures) is beyond the scope of this work. The extensive range of chemical and protein-based Ca²⁺ sensors and corresponding sensing mechanisms has been summarised elsewhere [34-38], and will not be specifically discussed. We anticipate that knowledge relevant to the development and selection of Ca²⁺ sensors in islet studies will be applicable to a broad range of research interests, such as monitoring of neuronal activity, cardiovascular functions and cancer development [39-41].

2.3 Insulin Secretion and Ca²⁺ Signalling

2.3.1 Pancreatic islets and pulsatile secretion of insulin

The pancreatic islet is a miniaturised endocrine organ that comprises α -, β - and δ -cells, responsible for the secretion of glucagon, insulin and somatostatin, respectively. As illustrated in

Figure 2a, these three endocrine cells are distributed in a scattered fashion in the human islet, but exhibit region-specific distribution in the mouse islet (with β -cells condensed in the core and surrounded by other cells) [42, 43].

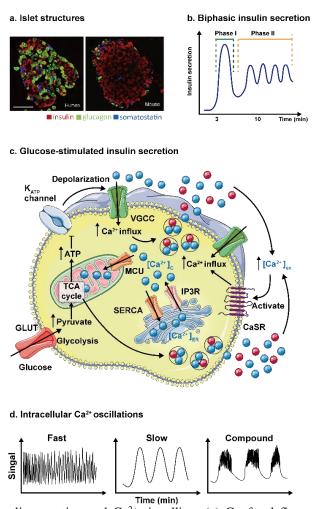


Figure 2. Physiology of insulin secretion and Ca²⁺ signalling. (a) Confocal fluorescence microscopy images of human and mouse pancreatic islets with immunostaining of insulin (red), glucagon (green) and somatostatin (blue). Scale bar, 50 µm. Reproduced with permission [43]. Copyright 2013, Elsevier. (b) Representative of biphasic insulin secretion of pancreatic islets, where a transient peak of insulin secretion is followed by a trail of oscillatory insulin release of smaller amplitude compared with the preceding phase. (c) Schematics of Ca²⁺ signalling in the course of glucose-stimulated insulin secretion (GSIS). Subsequent to the rise of blood glucose and increased production of ATP in β-cells, the closure of K_{ATP} channel reduces the hyperpolarising K_{ATP} current and induces a depolarising current, which leads to the opening of voltage-gated Ca²⁺ channel (VGCC) and the consequent influx of Ca²⁺. The latter triggers the firing of action potential and the fusion of pre-existing insulin-containing granules with the membrane to release insulin, i.e. the phase I secretion. Meanwhile, the production of ATP promotes the synthesis of insulin in endoplasmic reticulum, which sustains the slow, oscillatory insulin release, i.e. the phase II secretion. During this biphasic secretion process, mitochondria and endoplasmic reticulum (ER) participate in the regulation of cytoplasmic Ca²⁺ concentration by storing (via MCU and SERCA) or discharging (via IP₃R) Ca²⁺. Exocytosis of the secretory granules containing insulin and Ca²⁺ means that insulin and Ca²⁺ are co-released into the extracellular domain (exocytosis of granules containing other molecules is not discussed). The presence of Ca²⁺ in the extracellular domain may in turn activate the Ca²⁺-sensing receptor to signal VGCC for the Ca²⁺ influx. (d) Three typical patterns of Ca²⁺ oscillation in cytoplasm during insulin secretion.

In both humans and rodents, the secretion of insulin is maintained at a low basal level during the fasting state, when blood glucose concentrations usually fluctuate between 3.9-5.6 mM in humans [44] and 3.4-7.2 mM in mice [45, 46]. In response to elevated glucose levels (e.g. following intravenous glucose administration), insulin is released in a highly coordinated manner, comprising an early, rapid release (Phase I) and a later, slower, but sustained oscillatory release (Phase II) to facilitate glucose metabolism (Figure 2b).

In 1967, Anderson *et al* observed a pulsatile pattern of insulin concentrations in the portal vein of a dog 14 hours after meal ingestion [47]. Subsequent studies have revealed that insulin is secreted in an oscillatory manner from the islets [48-50]. The pulsatility of insulin secretory cycles has been reported to vary from 2 to 13 minutes, probably due to the differences in blood sampling sites (e.g., portal vs. peripheral vein) and frequencies between studies. However, the majority of studies reported 5-10 minutes per cycle [51]. That the oscillatory patterns of insulin secretion between the pancreas *in vivo* and individual islets *ex vivo* are almost identical, suggests that the secretion of insulin is synchronised between β -cells both within an individual islet and across all stimulated islets in the pancreas [52].

The amplitude of insulin pulses is diminished in patients with type 2 diabetes (T2D), although the overall release of insulin may be augmented in the face of insulin resistance. In healthy individuals administered somatostatin-14 (which suppresses endogenous insulin secretion), administration of exogenous insulin in a pulsatile manner (a 2-minute infusion pulse every 11 minutes), compared to a constant infusion, was shown to be more effective at lowering blood glucose (mean blood glucose nadir 4.66 ± 0.08 mM versus 5.53 ± 0.06 mM) [53]. In patients with type 1 diabetes (T1D), the insulin requirement for suppressing hepatic glucose production is ~40% less when given in a pulsatile manner compared to continuous insulin administration [54]. Accordingly, exposure to insulin in a pulsatile pattern appears critical to its glucose-lowering efficacy. The attenuated amplitude of insulin pulses observed in first-degree relatives of patients with T2D may therefore represent an important deficit, predisposing them to T2D [55-58].

2.3.2 Intracellular Ca²⁺ signalling: a trigger for insulin secretion

Intracellular Ca²⁺ is an integral messenger that signals a cascade of intracellular activities of major relevance to the secretion of insulin. As depicted in Figure 2c, in response to elevated glucose, glycolysis driven by the enzyme phosphofructokinase-1 (PFK1) increases adenosine triphosphate (ATP), which gives rise to the closure of ATP-sensitive potassium channels (K_{ATP} channel) and hence cellular depolarisation [59, 60]. The latter is also accompanied by the opening of voltage-gated Ca²⁺ channels (VGCCs, also known as voltage-dependent Ca²⁺ channels) [61, 62]. Due to the stark contrast in concentrations between [Ca²⁺]_{ex} (~1 mM) and [Ca²⁺]_c (100 nM), a burst of Ca²⁺ influx temporarily drives [Ca²⁺]_c up to 1 μM, triggering an action potential and fusion of insulin-containing granules with the cytoplasmic membrane to release insulin and other small molecules including Ca²⁺ [63], i.e. the exocytosis of insulin. This process is known as first-phase insulin secretion, associated with an abrupt peak during the first 10 minutes after stimulation (Figure 2b, Phase I). Elevated cytoplasmic Ca²⁺ (up to ~1 µM) is swiftly transported into the mitochondria (~100 μ M [Ca²⁺]_{mito}) and ER (~500 μ M [Ca²⁺]_{ER}) via the aforementioned transporters to allow [Ca²⁺]_c to return to the basal level. Concurrently, [Ca²⁺]_{mito} signals an enhanced synthesis of ATP to ensure energy supply for subsequent insulin synthesis [64, 65]. As an intracellular reservoir of Ca²⁺, the ER buffers intracellular Ca²⁺ and shapes the pattern of [Ca²⁺]_c oscillation during insulin release. The ER also accommodates the conversion of preproinsulin to proinsulin, which is subsequently folded and packaged into secretory granules, together with proinsulin converting proteases and small molecules such as Ca²⁺ and Zn²⁺ [66]. Consequently, exocytosis of insulin granules is anticipated to result in an increase of [Ca²⁺]_{ex} [67]. As long as the energy supply from glycolysis continues, synthesis, assembly and exocytosis of insulin can be sustained, forming the second phase of insulin secretion (Figure 2b, Phase II). These processes highlight (i) the intimate involvement of intracellular Ca²⁺ and (ii) the important role of Ca²⁺ oscillation in the respective domains [68].

Several lines of observation support the importance of Ca^{2+} signalling pathways in glucose-stimulated insulin secretion (GSIS). Within the cytoplasm, oscillations of $[Ca^{2+}]_c$, with a typical periodicity of 5-10 minutes in both dispersed β -cells [69] and coordinated β -cells in intact islets [70, 71], coincide with those of insulin secretion, both of which are markedly suppressed once VGCC is blocked [72, 73]. Oscillations of $[Ca^{2+}]_{mito}$ are in line with those of $[Ca^{2+}]_c$ [74,

75]. Silencing MCU [76] or retarding the change of $[Ca^{2+}]_{mito}$ [77], has therefore been found to attenuate the synthesis of ATP and second-phase insulin secretion. Similarly, $[Ca^{2+}]_{ER}$ increases following the rising $[Ca^{2+}]_c$ due to the influx of Ca^{2+} via SERCAs (including SERCA2b and SERCA3), and decreases in phase with the downstroke of $[Ca^{2+}]_c$ oscillation [78]. Manipulation of the activity of SERCAs thus affects the buffering effect of ER on $[Ca^{2+}]_c$. Indeed, the amplitude of glucose-induced $[Ca^{2+}]_c$ is augmented in SERCA3 knock-out β -cells and by thapsigargin, which blocks all SERCAs [79-81]. Along with an enhanced amplitude of $[Ca^{2+}]_c$ oscillation, insulin secretion is also amplified [81, 82].

Hitherto, three patterns of $[Ca^{2+}]_c$ oscillation have been observed in β -cells, including fast oscillation (small amplitude with periodicity at tens of seconds), slow oscillation (large amplitude with a cyclical pulse every 5-10 minutes) and compound oscillations (a hybrid pattern of fast superimposed on slow oscillations) (Figure 2d) [18]. Given the match of the fast and slow frequency between insulin and $[Ca^{2+}]_c$, it is tempting to attribute the pulsatility of insulin secretion to the oscillation of $[Ca^{2+}]_c$. However, the role of other metabolic processes in affecting the rate of insulin secretion should not be underestimated. For example, the M-type isoform of the glycolytic enzyme phosphofructokinase (PFK-M) is known to exhibit oscillatory activity with a similar periodicity as that of insulin [83]. In addition, the amplitude of pulsatile insulin release in the fasting state is impaired in humans with PFK-M deficiency [84]. Moreover, insulin secretion from pancreatic β -cells can be decoupled from changes of $[Ca^{2+}]_c$ in MIN6 cells that are depolarised by 40 mM KCl [85].

2.3.3 Intracellular Ca²⁺ signalling: an integrator for insulin secretion?

The coherent insulin secretory patterns between β -cells within an individual islet, or stimulated islets within the pancreas, suggest that a fast signalling factor(s) instantaneously coordinates the activities within and between islets. Relative to neurotransmitters, intra-islet hormones and gut-derived incretin hormones, extracellular Ca²⁺ appears to be a dominant factor for synchronising insulin secretion, via the Ca²⁺-sensing receptor (CaSR), a G-protein-coupled receptor expressed abundantly on β -cells [12, 86].

As the name suggests, CaSR was initially discovered as a sensor for variations in $[Ca^{2+}]_{ex}$ in order to regulate the release of parathyroid hormone [87]. The following extensive investigations

have revealed that CaSR signalling is essential to a variety of cellular processes, including differentiation [88] and apoptosis [89]. A study performed by De Luisi and Hofer has uncovered an important role of CaSR signalling in mediating intercellular communication. In that work, non-CaSR-expressing BHK-21 cells (donor cells) and CaSR-expressing HEK293 cells (HEK-CaSR, sensor cells) were co-cultured. Treatment with the Ca²⁺-mobilising agonist histamine (selective to BHK-21 cells) increased the [Ca²⁺]_c of BHK-21 cells and induced active extrusion of Ca²⁺ into the extracellular space. An increase in [Ca²⁺]_c was also observed in adjacent HEK-CaSR cells (<10 µm away) with a delay of fewer than 10 seconds, suggesting an activated intracellular signalling cascade in the HEK-CaSR. By contrast, the stimulated BHK-21 cells failed to elicit the same change of [Ca²⁺]_c in wild type HEK293 cells. These observations provide strong support for the role of CaSR in intercellular communication [90].

In the context of β -cells (e.g. MIN6 cells), activation of CaSR over 48 hours using the calcimimetic R568 was reported to double the expression of epithelial-cadherin, indicating an increased cell proliferation. Moreover, CaSR activation increased L-type VGCC expression by 70% compared to control, leading to augmentation of the basal-to-peak amplitude of $[Ca^{2+}]_c$ in response to ATP and tolbutamide (both of which close potassium channels) [91], and increased insulin secretion, particularly in the presence of sufficient $[Ca^{2+}]_{ex}$ in the culturing medium [92]. Conversely, down-regulation of CaSR expression on MIN6 cells, even when cultured in an islet-like three-dimensional architecture, was associated with a marked reduction in GSIS [93].

Box 1 Intercellular communication via gap junctions or Ca²⁺?

Gap junctions (Gjs) comprise specialised proteins/channels that physically connect adjacent cells and mediate rapid exchange of small molecules between them. Within the islets, Gjs are spatially restricted to adjacent β -cells. However, the cellular network of the endocrine cells differs substantially between humans and rodents (Figure 2). Such a distinction in architecture argues against the role of Gjs as a universal integrator of coordinated insulin secretion.

Nevertheless, in mouse islets, Gjs facilitate the spreading of membrane depolarisation and transmission of stimulatory signals between neighbouring β -cells by selectively transporting cations and small molecules [42]. Disruption of Gjs, to some extent, impairs $[Ca^{2+}]_c$ oscillation and normal GSIS. These observations suggest that the communication between β -cells in mice relies, at least in part, on Gjs [94].

2.4 Conventions of Sensing Cellular Ca²⁺ in Islets

Over the last six decades, the development of sensing methodologies has underpinned major knowledge gains in relation to cell biology. The invention of Ca^{2+} sensors and associated techniques/platforms has, in particular, played an indispensable role in the understanding of the secretory function of pancreatic β -cells and islets, as illustrated in Figure 3.

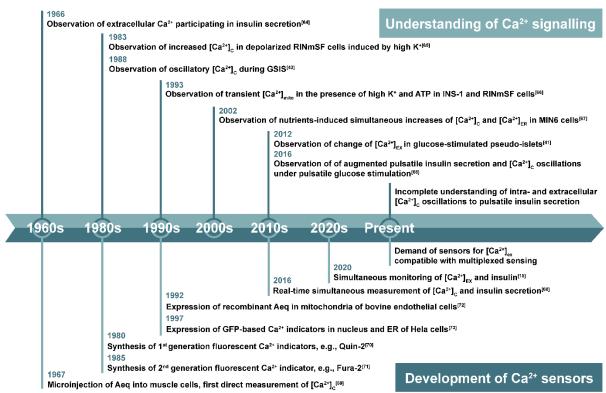


Figure 3. Development of understanding of the role of Ca^{2+} in insulin secretion in relation to the evolution of Ca^{2+} sensing methods. While Quin-2 and Fura-2 have been prominent, there are serial relevant indicators invented over this timeframe. Our illustration focuses on concurrent measurements of Ca^{2+} and insulin, but there are many other key developments, e.g. the multiplexed sensing of $[Ca^{2+}]_c$ and the surrogate markers for insulin exocytosis (such as Zn^{2+} , which is co-released with insulin [85], or phosphatidylinositol-3,4,5-trisphosphate (PIP3, which is coupled to the autocrine effect of insulin) [105]. RINmSF: an insulin-releasing clonal cell.

In 1966, the omission of Ca^{2+} but not Mg^{2+} in the perfusate was found to inhibit insulin secretion from isolated rat pancreas *in vitro*, highlighting that extracellular Ca^{2+} is a prerequisite for insulin secretion [95]. In the next year, the discovery and application of the luminescent protein, aequorin (Aeq), isolated from the *Aequorea* jellyfish, made it possible to record intracellular Ca^{2+} (i.e., $[Ca^{2+}]_c$) for the first time in living cells [100]. Aeq and its derivatives were popular

tools for Ca²⁺ sensing over the subsequent 20 years, but failed to enrich understanding of physiology substantially due to their intrinsic limitations, including low fluorescence and the need for continuous replacement of oxidised components. This stagnation emphasises the importance and urgency of developing Ca2+ indicators with bright fluorescence and high sensitivity to changes of [Ca²⁺]. Moreover, the upcoming indicators should be introduced into cells in a manner less invasive than microinjection, which was used for Aeq. In the 1980s, the synthetic Ca²⁺ indicators (e.g. Quin-2 [101] and Fura-2 [102] of stronger fluorescence than Aeq) were developed, and their applications in β -cells revealed the oscillations of $[Ca^{2+}]_c$ during the GSIS [69, 106]. Conjugation of the membrane-permeable acetoxymethyl (AM) ester with the synthetic indicators also enabled non-invasive loading of the Ca²⁺ indicators into cytoplasm [107]. Between 1990-2000s, with the advent and maturation of genetic editing and transcriptional regulation techniques, the expression of genetically encoded Ca²⁺ indicators (GECIs), including recombinant Aeq [104] and fluorescent proteins (FPs)-based Ca²⁺ indicator [104], into a specific subcellular compartment of living cells was established. The applications of these GECIs in monitoring Ca²⁺ dynamics in the organelles of β-cells have revealed links between insulin secretion and Ca2+ oscillations in the mitochondria (in 1993) [97] and ER (in 2002) [98]. Complementary to the measurement of intracellular Ca²⁺, Ca²⁺-selective microelectrodes (CSMs) have advanced the monitoring of $[Ca^{2+}]_{ex}$ in the vicinity of β -cells [108] and in the extracellular cavity within a pseudo-islet, such as that formed by INS-1E cells [67]. In these models, elevation of glucose levels is found to induce substantial fluctuations of [Ca²⁺]_{ex} in the interstitial space around β-cells, providing the basis for an autocrine/paracrine cell-to-cell communication via [Ca²⁺]_{ex}. However, the point-of-care measurement by CSMs is insufficient to elucidate whether and how such an intercellular communication functions in the scale of intact islets. Therefore, novel Ca2+ sensors are needed to comprehend the roles of [Ca2+]ex in modulating and synchronising insulin secretion.

2.4.1 Chemically synthesised fluorescent indicators for [Ca²⁺]_c

The jellyfish-sourced luminescent protein Aeq, emitting blue luminescence spontaneously after binding to Ca²⁺, was once a spearhead for sensing Ca²⁺. Its weak fluorescence, however, has become a major obstacle to its utility for tracing Ca²⁺ in biological studies. Therefore, many other indicators have been developed; some examples are listed in Table 1. Unless otherwise

specified, Ca²⁺ indicators discussed in this section predominantly refer to those used in islet studies.

Chemically synthesised fluorescent indicators are the most widely used cellular Ca^{2+} sensors. They usually consist of a fluorophore, Ca^{2+} chelator (such as 1,2-bis(o-aminophenoxy)-ethane-N, N, N', N'-tetraacetic acid (BAPTA)), and a linker. The binding affinity of such an indicator to Ca^{2+} depends on the property of the Ca^{2+} chelator and its intramolecular electronic state after conjugation with the fluorophore and linker. The K_d describes the propensity of an indicator to bind Ca^{2+} and, hence, defines the effective sensing range. Accordingly, K_d should be the first key consideration when assessing the suitability of a synthetic Ca^{2+} indicator (Box 2). Another consideration relates to the alternations of the optical property of the indicator upon binding to Ca^{2+} , including the variation in the intensity of fluorescence and the shift in the peak of excitation/emission wavelengths (Box 2). Moreover, the fluorescence signals may vary substantially because of the specific experimental setup for Ca^{2+} imaging/sensing, including the use of excitation light and filters as well as the configuration of the photodetector.

There are three principal mechanisms underlying Ca²⁺-induced optical changes for chemically synthesised fluorescent Ca²⁺ indicators and GECIs, including photo-induced electron transfer (PiET), internal charge transfer (ICT) and Förster resonance energy transfer (FRET) [112].

As shown in Figure 4a, i (left), for a PiET-based indicator, the electrons of the fluorophore on the highest occupied molecular orbital (HOMO) are re-populated to its lowest unoccupied molecular orbital (LUMO) upon light excitation [125]. The consequent electron vacancies are inclined to be re-filled by their intrinsic electrons on LUMO via radiative de-excitation. At the same time, the electrons on the HOMO of the chelator compete to fill the vacancies, which prohibits the relaxation of the fluorophore and the subsequent fluorescence emission. In the case of binding between chelator and Ca²⁺ (Figure 4a, i (right)), the chelator experiences an increase in redox potential, pulling its HOMO energy level below the HOMO of the fluorophore, so that electron transfer from chelator to fluorophore is effectively suppressed. As a result, radiative relaxation of excited electrons on the fluorophore LUMO becomes dominant, producing an emission of an unquenched fluorescence. Such a fluorescence response in the absence/presence of Ca²⁺ is depicted in Figure 4a, ii. Since the degree of impedance of the competitive de-excitation channel

is sensitive to the availability of Ca^{2+} to the indicators (i.e., the concentration of Ca^{2+}), its fluorescence behaviour is $[Ca^{2+}]$ -dependent (Figure 4a, iii) [38]. The indicator maintains its sensitivity to the changes of $[Ca^{2+}]$ as long as the Ca^{2+} -binding sites of the chelators are not saturated.

Box 2 Considerations of choosing Ca²⁺ indicators in practice

Dissociation constant (K_d)

 K_d is a fundamental parameter of an indicator, which is used to measure the propensity of its binding to the target (i.e., Ca^{2+} in the current context) [109]. At the equilibrium, K_d , in relation to the binding kinetics between Ca^{2+} , the indicator (noted as N), and their complex molecule (noted as CaN), is expressed as follow:

$$K_d = \frac{[Ca^{2+}] \times [N]}{[CaN]}$$

The equilibrium concentration of Ca²⁺ can be calculated by:

$$[Ca^{2+}] = K_d \left(\frac{F - \dot{F}_{min}}{F_{max} - F} \right)$$

where F is the fluorescence of Ca^{2+} -bound indicator, F_{min} is the background fluorescence in the absence of Ca^{2+} and F_{max} is the fluorescence when all indicator molecules are bound to Ca^{2+} .

Based on the law of mass action, $0.1-10 \times K_d$ defines the indicator's effective sensing range, representing the scope of approximately 20–80% of the indicators bound to Ca^{2+} , over which fluorescence intensity changes linearly as a function of $[Ca^{2+}]$ on a logarithmic scale [34]. To accurately quantify $[Ca^{2+}]$ and its variations at different cellular compartments, the K_d of an indicator needs to be taken into account in the search for the most appropriate indicator(s). For instance, Fura-2, with K_d at 224 nM, is suitable to track intracellular $[Ca^{2+}]$, but not extracellular $[Ca^{2+}]$, since the latter approximates 1 mM (exceeding 10 times of its K_d). Similarly, it is suboptimal to use Quin-2 (K_d , 60 nM) to monitor glucose-induced oscillations of $[Ca^{2+}]_c$ with amplitudes as high as 1000 nM (Figure 1a), beyond the upper limit of the indicator (600 nM) [110].

Intensity-based or ratiometric indicator?

In general, it is challenging to employ an intensity-based indicator for quantitative analysis of Ca^{2+} , partly because the signal of an indicator is prone to self-shifting as a function of its concentration, thereby interfering with precise quantification of $[Ca^{2+}]$ [111]. Other factors, including its heterogeneous distribution, leakage and photobleaching as well as non-uniform excitation conditions, further confound efforts to evaluate $[Ca^{2+}]$ quantitatively.

In contrast, a ratiometric indicator has the potential to circumvent the aforementioned limitations since, by definition, it relies on ratios of the signal at different wavelengths, i.e. relative intensity, so is intrinsically self-calibrated.

ICT-based indicators are constructed by a pair of so-called donor and accepter molecules that occupy each end of a fluorophore via a direct conjugation (Figure 4b, i). Both the donor and

accepter possess Ca²⁺-binding sites (without a linker). Upon light excitation, the electron transfer from the donor to the acceptor is accompanied by an instantaneous change in the dipole moment of the fluorophore. The relaxation of the dipole leads to a Stoke-shifted fluorescence of the fluorophore. The flexibility of anchoring the chelator onto either the donor (D) or acceptor (A) side allows ICT-based indicators to exhibit blue- or red-shift fluorescence (Figure 4b, ii) [126]. A blue shift occurs when both the electron-donating property and conjugation strength of the donor are restrained by the chelator; conversely, a red shift appears when the electron-withdrawing property of accepter is enhanced by the adjacent chelator [127]. Fura-2 is a representative ICT-based fluorescent indicator. As shown in Figure 4b, iii, the excitation spectrum peak of Fura-2 shifts from ~380 to ~340 nm with increasing fluorescence intensity in response to the increased binding of Ca²⁺ to its donor side. In addition, the ratiometric feature of Fura-2 at 340/380 nm offers self-calibrated fluorescence signals and hence minimises the potential interference from the sensing environment. In this context, a ratiometric indicator may be preferable to an intensity-based indicator for quantification of [Ca²⁺] (Box 2).

Despite tremendous successes in probing intracellular Ca²⁺, the advent and development of chemically synthesised fluorescent Ca²⁺ indicators have faced several issues. First, photobleaching, a notorious problem with almost all these indicators, interferes with precise quantification of [Ca²⁺] during long-term tracking, resulting in a limited observation window [128]. Second, exposure to UV light is associated with phototoxicity, which impairs cellular function. Substitution for the visible light-excitable indicators seems to be a rational option to circumvent photobleaching and reduce phototoxicity. However, only a few Ca²⁺ indicators that are excitable by visible light have been developed, providing a limited range of K_d and optical performance. In light of these limitations, the use of ratiometric indicators appears preferable in principle [129]. However, interferences caused by compartmentalisation, leakage and incomplete hydrolysis may still disrupt the recording or interpretation of results [34].

Table 1. Chemically synthesised indicators for sensing [Ca²⁺]_c

			tation nm		ission 1m	D (D			
Indicators	K _d (пм)	Ca ²⁺ free	Ca ²⁺ bound	Ca ²⁺ free	Ca ²⁺ bound	F_{max}/F_{min} (R_{max}/R_{min})	Subjects	Note	Ref.
Quin-2	60	355	330	495	495	5-8	1, 6	a	[96, 113]
Fura-2	224	380	340	510	505	(13-25)	1, 2, 3, 4	b	[114-119]
Indo-1	230	346	330	475	400	(20-80)	2	c	[70]
Fura-PE3	250	364	334	508	500	(18)	2	d	[81, 120]
Fluo-3	390	503	506	525	525	40-100	4	e	[71]
Fura-red	140	470	435	660	660	(5-12)	2, 4, 5	f	[105, 121, 122]

Note: $F_{\text{max}}/F_{\text{min}}$, the ratio of maximum to minimum fluorescence of indicator; $R_{\text{max}}/R_{\text{min}}$ contrast of ratios of maximum fluorescence to minimum fluorescence between Ca^{2+} -free and Ca^{2+} bound states of the indicator. Besides the listed references, we also refer to *The Handbook: A Guide to Fluorescent Probes and Labelling Technologies* (11 ed.) [123]. $F_{\text{max}}/F_{\text{min}}$ or $R_{\text{max}}/R_{\text{min}}$ is provided depending on which is available. Subjects:

- 1. Isolated mouse β -cells
- 2. Intact mouse islet
- 3. Isolated human β -cells
- 4. Intact human islet
- 5. MIN6 β -cells (highly differentiated and glucose-responsive murine β -cell line) [124]
- 6. Clonal insulin-releasing cell line RINm5F

Note:

- a. The first-generation indicator, whose absorption and quantum efficiency are lower than fluorescent indicators developed subsequently [34].
- b. A ratiometric indicator featuring high compartmentalisation and strong protein binding characteristics.
- c. A ratiometric indicator with dual emissions [70].
- d. A Fura-2 derivative developed for monitoring leakage resistance of cytoplasmic Ca²⁺ (i.e., the efflux process). The absorption peak of Fura-PE3 undergoes a significant blue shift upon binding Ca²⁺.
- e. An indicator featuring enhanced fluorescence and visible excitation light (thus, reduced photodamage).
- f. A ratiometric indicator, characteristic of a long-wavelength emission, such as red, and used for multiplexing sensing in conjunction with other ion-sensitive indicators.

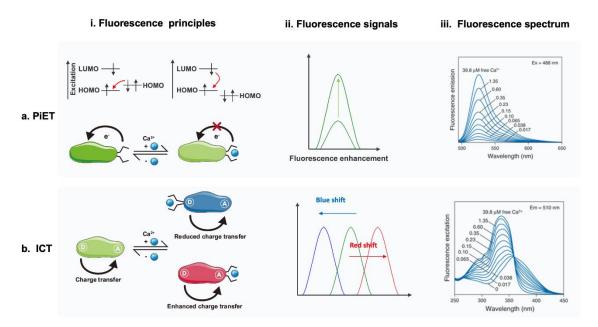


Figure 4. Schematic of fluorescent principles and optical responses of synthetic fluorescent indicators upon binding Ca²⁺. (a) Photo-induced electron transfer (PiET)-based fluorescent indicator: (i) Energy scheme and reversible process of binding/unbinding Ca²⁺ in the regulation of the optical responses; (ii) Fluorescence enhancement of PiET-based indicator in the presence of Ca²⁺, where a spectral shift is usually negligible even if it occurs; (iii) Fluorescence enhancement of PiET-based Fluo-3 proportional to increase in [Ca²⁺] (excitation 488nm, emission ~525 nm). (b) Internal charge transfer (ICT)-based fluorescent indicators: (i) Schematic of Ca²⁺-modulated ICT process. In the absence of Ca²⁺, ICT occurs as the charge transfer from the electron donor (denoted by D, e.g. dialkylamino-) to the electron acceptor (denoted by A, e.g. carbonyl). When a Ca²⁺ chelator is linked to D (negatively charged), binding of Ca²⁺ suppresses the electron transfer from D to A (blue); on the contrary, Ca²⁺-binding with the chelator linked to A enhances the ICT (red); (ii) A reduced ICT leads to a blue shift of the emission band, while an enhanced ICT undergoes a red shift; (iii) Shift of excitation spectra of Fura-2 (an ICT-based fluorescent indicator) in response to Ca²⁺.

2.4.2 Genetically encoded Ca²⁺ indicators for [Ca²⁺]_c

GECIs, also known as fluorescent Ca^{2+} indicator proteins (FCIPs), are another mainstay optical toolkit for sensing $[Ca^{2+}]_c$. As described in Figure 5a, the nucleic acid sequence of the indicator is tagged with a selected promoter sequence from the target organelle. The fused cDNA is then transfected into the target cells, mostly via lipofection [103] or viral transduction [130]. Under the guidance of a promoter gene, GECIs can be precisely expressed in the target subcellular compartment, e.g. mitochondria, ER, nucleus, Golgi and plasma membrane. Similar to chemically synthesised indicators, the optical property (mostly the fluorescence intensity) of GECIs is altered upon binding Ca^{2+} . For the selection of a suitable GECI, both K_d and the optical property remain key considerations.

As shown in Figure 5b, four types of GECIs are widely used:

- (i) Recombinant Aeq, is a type of protein that is produced by reconstructing the native Aeq sequence using genetic engineering techniques. This can be achieved by transfecting cells with Aeq cDNA fused with a tag sequence for targeted expression [131]. Similar to the native Aeq, the recombinant Aeq expressed in cells exhibits spontaneous fluorescence at 470 nm when binding to Ca²⁺ [103]. The emission of fluorescence is accompanied by the oxidation of coelenterazine to colenteramide in the recombinant Aeq molecule (Figure 5b). Recombinant Aeq used in islet studies has allowed recording of the [Ca²⁺]_{mito}, showing that [Ca²⁺]_{mito} increased and oscillated in MIN6 cells treated by KCl (22 mM) or glucose (30 mM) with a higher peak concentration than that of [Ca²⁺]_c (2 μM [Ca²⁺]_{mito} vs. 900 nM [Ca²⁺]_c) [132]; KCl-evoked elevation in [Ca²⁺]_{mito} induced an immediate increase in cytosolic and mitochondrial free ATP, suggesting that the [Ca²⁺]_{mito} is essential for mitochondrial metabolism, i.e., the production of ATP [75].
- (ii) Bioluminescence resonance energy transfer (BRET)-based GECI, also called hybrid recombinant Aeq, is composed of a recombinant Aeq and a fluorescent protein, in which the excitation spectrum of the fluorescent protein is overlapped with the emission of Aeq, hence leading to BRET. As shown in Figure 5b, ii, as Ca²⁺ binding induces a conformational change to the indicator, the distance between Aeq and the fluorescent protein reduces, and then the BRET takes place and is stoked. As a result, the fluorescent protein is excited by the luminescence of Aeq without the need for an external light source [133]. While BRET-based GECIs have improved the intensity of fluorescence signal compared with pure Aeq, their application in islet studies is limited by the demand for constant replacement of the oxidised component, i.e., the coelenterazine.

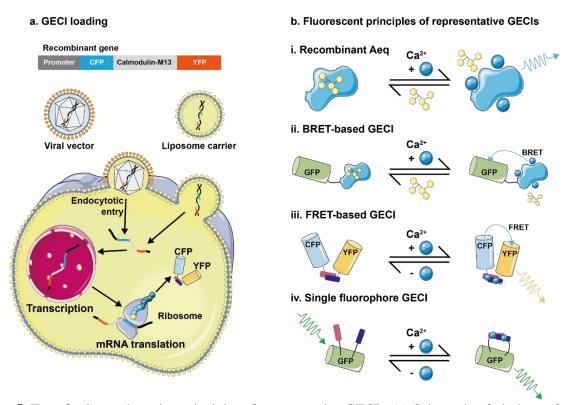


Figure 5. Transfection and sensing principles of representative GECIs. (a) Schematic of viral transfection or lipofection loading of GECIs into a target cell. The viral vector or liposome carrier embedded with the fusion recombinant gene transfects the host cell by releasing the fused DNA. The indicator DNA is added into the host gene by integrase and subsequently expressed in the target compartment after DNA transcription and mRNA translation. (b) Fluorescence principles of representative GECIs: (i) In the presence of Ca²⁺, recombinant Aeq, undergoing internal oxidation of coelenterazine to coelenteramide, releases a coelenteramide and gives emission at 470 nm. Its reversible pathway - refunctionalisation of Aeq - proceeds with the provision of coelenterazine; (ii) Bioluminescence resonance energy transfer (BRET)-based GECI comprises a single green fluorescent protein (GFP) and its conjugated Aeq, showing GFP's fluorescence once Ca²⁺ binding switches on the emission of Aeq since the latter overlaps with the absorption of Aeq; (iii) A representative of Förster resonance energy transfer (FRET)-based GECI, typically consisting of a cyan fluorescent protein (CFP), a yellow fluorescent protein (YFP), a Ca²⁺-binding peptide calmodulin (CaM, linker in black) and a CaM-binding peptide M13 (linker in red). Conformational changes of CaM and M13 induced by binding Ca²⁺ lead to a reduced distance between CFP and YFP. Under external light excitation, the shortened distance between CFP and YFP accelerates the FRET, i.e., a portion of fluorescence of CFP will be absorbed by YFP for its own emission; (iv) Single fluorophore-based GECI, for example, a GFP conjugated with CaM and M13. The binding of Ca²⁺ induces conformational changes to both CaM and M13, hence modulating the optical properties of the GFP.

(iii) FRET-based GECI, is constructed by connecting two FPs with a linker, e.g., Ca²⁺-binding protein calmodulin and calmodulin-binding protein M13. The most frequently used FPs belong to the chameleon family. As shown in Figure 5b, iii, an exemplified FRET-based GECI is constituted by the cyan fluorescent protein (CFP) and the yellow fluorescent protein (YFP). In the absence of Ca²⁺, the emission of CFP at 480 nm dominates. Upon binding to Ca²⁺, an

intramolecular conformational change occurs and pulls the two FPs closer, causing an enhanced FRET. Therefore, YFP is switched on by the emission of CFP and emits fluorescence at around 530 nm [104]. In islet studies, for example, its use (e.g. Ycam-4ER, K_d = 100-1000 μ M, and D4ER, K_d = 65 μ M) [104, 134] has enabled the direct measurement of [Ca²+]_{ER} in response to varying stimuli and provided insights into the roles of Ca²+ transporters in the organelles of β -cells. In particular, [Ca²+]_{ER} imaging using Ycam-4ER showed that [Ca²+]_{ER} increased in MIN6 cells with 20 mM glucose treatment. In addition, resting [Ca²+]_{ER} was markedly reduced after the suppression of SERCA2b but not SERCA3, suggesting that SERCA2b is the principal ER Ca²+-ATPase in MIN6 cells [98]. Simultaneous monitoring of [Ca²+]_C and [Ca²+]_{ER}, using Fura-PE3 and D4ER, respectively, revealed that [Ca²+]_{ER} oscillated concurrently with [Ca²+]_C under glucose stimulation. This study also demonstrated that the increase in [Ca²+]_{ER} was not abolished but only slightly decreased when SERCA3 was knocked out, reflecting the predominant role of SERCA2a in the regulation of [Ca²+]_{ER} within β -cells [82, 98].

(iv) Single fluorophore GECI, as a GCaMP family member, can be represented by indicators containing a circularly permuted GFP, conjugated with the Ca^{2+} -binding protein calmodulin on one side and M13 on the other side [135]. Conformational changes in calmodulin induced by the presence of Ca^{2+} increase the interaction between calmodulin and M13, which in turn impacts the intramolecular protonation state of the fluorophore GFP. As such GFP fluorophore gives rise to enhanced emissions in proportion to the concentration of Ca^{2+} (Figure 5b, iv) [136]. One selected example is the derivative of Pericam, 2mt8PR ($K_d = 1.7 \mu M$), which was invented for targeted expression in the mitochondria of living cells [137]. The application of 2mt8PR in mouse β-cells showed that the increase in $[Ca^{2+}]_{mito}$ induced by 17 mM glucose followed the elevated $[Ca^{2+}]_c$ with a temporal delay for around 80 seconds. In the same study, the increase in $[Ca^{2+}]_{mito}$ was substantially impaired when the expression of mitochondrial Ca^{2+} uniporter (MCU) was suppressed using shRNA. However, the fact that the increase in $[Ca^{2+}]_c$ was not affected by MCU silencing suggested an alternative pathway for clearing increased $[Ca^{2+}]_c$ in mouse β-cells [74].

Clarifying the complex interaction of multiple bio-factors that constitute the signalling network underlying insulin secretion is critical to the understanding of islet biology. For this purpose, multiplexed sensing, deploying multiple sensors for concurrent monitoring of [Ca²⁺]_c and other

regulatory factors, is of importance. For example, cyclic adenosine monophosphate (cAMP) is an intermediate regulator that has been considered to enhance intracellular Ca2+ signal and exocytosis via protein kinase A (PKA)-dependent and -independent pathways. While cAMP signalling is pivotal to the insulinotropic effect of gut hormones, the correlation between intracellular cAMP and [Ca²⁺]_c was unclear. Simultaneous monitoring of [Ca²⁺]_c and cAMP has identified that cytoplasmic cAMP oscillates in β-cells or MIN6 cells with the provision of 11 mM glucose. The pattern of cAMP oscillation resembled [Ca²]_c and partially relied on [Ca²⁺]_c oscillation, as inhibition of the [Ca²⁺]_c change using the VGCC blocker methoxyverapamil (50 μM) did not abolish cAMP oscillation. Therefore, the multiplexed sensing of [Ca²⁺]_c and cAMP has clarified that cAMP, while oscillating with [Ca²⁺]_c, is not directly driven by the latter [105]. This enlightening work has stimulated further studies, which, for example, found that the suppression of cAMP formation by inhibiting adenylyl cyclase (the enzyme that converts ATP to cAMP) reduced GSIS from β-cells, and that the effect of cAMP on modulating pulsatile insulin secretion could be mediated by a cAMP-dependent guanine nucleotide exchange factor, Epac2. Together, these observations have provided a novel understanding of the formation of pulsatile insulin secretion (Figure 6a) [105, 138].

Knowledge about the interaction between $[Ca^{2+}]_c$ and mitochondrial activity in β -cells has also been advanced with the aid of multiplexed sensing methodology. Simultaneous measurements of NADH (by autofluorescence), $[Ca^{2+}]_c$ (by Fura-red) and mitochondrial membrane potential (by Rh123) in mouse β -cells under 10 mM glucose have shown that: (i) NADH oscillates around every 5 minutes; (ii) these oscillations are almost coherent with those of $[Ca^{2+}]_c$; (iii) $[Ca^{2+}]_c$ and NAD(P)H oscillations are both abolished with inhibition of L-type VGCC by nifedipine; and (iv) the effect of $[Ca^{2+}]_c$ is dependent on glucose, as elevated $[Ca^{2+}]_c$ augmented NADH autofluorescence of β -cells at 3 mM glucose but lowered NADH autofluorescence at 10 mM glucose. These observations suggest that slow oscillations of NADH within intact islets are modulated by $[Ca^{2+}]_c$, such that intracellular Ca^{2+} represents a key element of feedback regulation of the respiratory activity in mitochondria (Figure 6b) [121]. Another illustration of multiplexed sensing relates to the simultaneous recording of $[Ca^{2+}]_c$ (by Fura-red) and cytoplasmic ATP concentrations (by Perceval, a protein-based ATP indicator) (Figure 6c), which has revealed that glucose induces pronounced oscillations of intracellular ATP, whose

concentration is negatively correlated with $[Ca^{2+}]_c$. Of note, ATP oscillations were abolished once L-type Ca^{2+} channels were blocked by methoxyverapamil.

2.4.3 Ca²⁺-selective microelectrode (CSM) for [Ca²⁺]_{ex}

A CSM, generally comprising an amplifier, a voltmeter and sensing and reference electrodes, is made by combining an ion-selective functionality with a microelectrode (capable of measuring cell membrane potential, resistance and net ion transport). CSMs have been developed to trace concentration changes of a specific ion, such as Ca²⁺, Na⁺, K⁺, H⁺ and Cl⁻ [139].

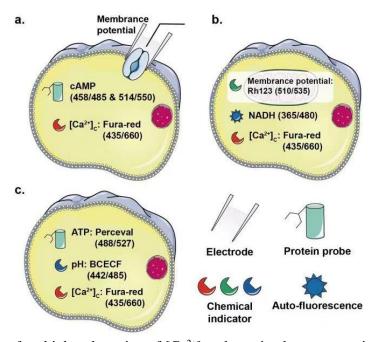


Figure 6. Illustration of multiplexed sensing of $[Ca^{2+}]_c$, where simultaneous sensing is enabled by using long-wavelength emission of Fura-red ($\lambda_{ex}/\lambda_{ex}=435/660$ nm) in combination with sensors for other concerned intracellular molecules, including: (a) Sensing of $[Ca^{2+}]_c$ by Fura-red, cyclic adenosine monophosphate (cAMP) by a cAMP biosensor ($\lambda_{ex}/\lambda_{ex}=485/535$ nm) and cytoplasmic membrane potential by patch-clamp [105, 138]. (b) Sensing of $[Ca^{2+}]_c$ by Fura-red, NADH by autofluorescence ($\lambda_{ex}/\lambda_{ex}=365/480$ nm) and mitochondrial membrane potential by Rh123 ($\lambda_{ex}/\lambda_{ex}=510/535$ nm) [121]. (c) Sensing of $[Ca^{2+}]_c$ by Fura-red, ATP by Perceval ($\lambda_{ex}/\lambda_{ex}=488/527$ nm) and pH by BCECF ($\lambda_{ex}/\lambda_{ex}=442/485$ nm) [122].

Figure 7a is a schematic of a typical Ca^{2+} sensing electrode, which consists of a Ca^{2+} -selective ionophore cocktail (lipophilic liquid phase with ion-exchange properties), electrolyte (usually concentrated KCl solution containing Ca^{2+}), and a reference electrode (containing Ca^{2+} -free electrolyte) [140]. Once there is a $[Ca^{2+}]$ difference between the sample and internal electrolyte, Ca^{2+} -selective ionophores specifically bind Ca^{2+} and transport Ca^{2+} between the sample and

electrolyte, towards a concentration equilibrium. Alongside the transportation of Ca^{2+} , changes in the electric potential are induced between the microelectrode and the reference electrode, and the corresponding voltage is recorded by the voltmeter. Since the varying potential is proportional to the logarithm of $[Ca^{2+}]$ (based on the Nernst equation), CSMs will extract the dynamic changes of $[Ca^{2+}]$ accordingly [141].

Perez-Armendariz and Atwater have made a pioneering contribution by exploiting CSMs to probe [Ca²⁺]_{ex} in the intercellular space of β-cells [142]. They observed that, in a measurement lasting for ~1 minute, there is an instant depletion of 0.5 mM [Ca²⁺]_{ex} under glucose stimulation (11 mM), before reverting to the basal level. This observation has clarified that there is a correlation between the fast oscillatory [Ca²⁺]_{ex} and stimulation of the islet by glucose. Moura combined CSM (placed in the vicinity of the cell) with a potential-sensitive microelectrode (impaled within the β -cell) for multiplexed sensing of $[Ca^{2+}]_{ex}$ and membrane electrical activity. This work showed that the addition of glucose (11 mM) depolarised the β-cells and induced biphasic electrical activity accompanied by small oscillations of [Ca²⁺]_{ex} in an islet (Figure 7b). The respective waveforms of [Ca²⁺]_{ex} and membrane potential were essentially concomitant, with a delay of only 1 minute between the oscillatory behaviour of [Ca²⁺]_{ex} and the membrane potential. These outcomes are in good agreement with the Ca2+ signalling process, i.e., membrane depolarisation first induces Ca²⁺ influx from the extracellular space, followed by the transport of Ca²⁺ into the extracellular space during repolarisation [108]. Gerbino et al. measured [Ca²⁺]_{ex} in the intercellular cavity by placing a CSM close to an INS-1E pseudo-islet (Figure 7c). They found that exposure of the pseudo-islet to both high glucose (20 mM) and non-nutrient insulinotropic compounds raised [Ca²⁺]_{ex}, which increased with exocytosis of Ca²⁺-rich granules (Figure 7d) [67].

The characteristics of a variety of prevailing optical-based Ca²⁺ indicators and CSM techniques are summarised in Table 2. In brief, CSMs are capable of probing [Ca²⁺] in a range of nM to mM [143]. Their sensing principle avoids the issues of photobleaching and diffusion that affect fluorescence-based indicators. CSMs thus permit a stable, long-term tracking of [Ca²⁺]_{ex}. In view of the large tip size and possible mechanical damage to cells, the CSM-based sensing technique is preferable for measurements in the interstitial space [144]. The measurements mainly relate to the vicinity of the tip, so they do tend to be spatially limited.

2.5 The State-of-the-Art Sensors for [Ca²⁺]_{ex}

The potential for [Ca²⁺]_{ex} to coordinate intercellular signalling has given rise to the demand for sensors for *in situ* real-time tracking of [Ca²⁺]_{ex}. An ideal sensor for this purpose should: (i) accurately quantify [Ca²⁺]_{ex} in the order of mm i.e., with a high-value K_d (or low affinity to Ca²⁺); (ii) faithfully discern small fluctuations of [Ca²⁺]_{ex} from the high basal level, e.g., up to hundreds of μm changes over around 1.2 mM extracellular Ca²⁺; (iii) selectively and instantaneously respond to Ca²⁺; and (iv) track [Ca²⁺]_{ex} over a protracted period. In addition, the increasing demands for multiplexed sensing require high compatibility of indicators for both [Ca²⁺]_{ex} and other related bioactive molecules. In this section, we review the sensors that meet these criteria despite their applications may not be prevailing in islet studies.

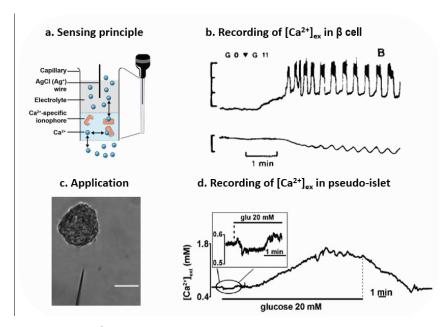


Figure 7. Applications of a Ca²⁺-selective microelectrode (CSM) in islet studies. (a) Schematic of a CSM tip in measuring Ca²⁺, where Ca²⁺-selective ionophores can transport Ca²⁺ reversibly between the sample and the inner electrolyte. (b) CSM measuring [Ca²⁺]_{ex} in combination with potential electrode measuring plasma membrane potential. Upper panel: Variations in β-cell membrane potential upon increasing glucose from 0 to 11 mM; lower panel: corresponding changes of [Ca²⁺]_{ex} during this process. Reproduced with permission [108]. Copyright 1995, Elsevier. (c) Microscope image illustrates the placement of a double-barrelled selective microelectrode in proximity to an INS-1E pseudo-islet. Scale bar, 100 μm. Reproduced with permission [67]. Copyright 2012, Elsevier. (d) Response of extracellular [Ca²⁺] of the pseudo-islet under stimulation with 20 mM glucose, measured by CSM inserted in the intercellular space. Reproduced with permission [67]. Copyright 2012, Elsevier.

2.5.1 Low-affinity synthetic Ca²⁺ indicators

A simple way to develop low-affinity indicators is to engineer conventional chemically synthesised indicators by reducing the ratio of Ca²⁺ binding sites (e.g., the carboxylic group) to its fluorophore molecules. A typical example is to truncate the carboxylic groups of the BAPTA-based indicators, which usually comprise four carboxylic groups for binding Ca²⁺ [123, 156]. The truncated indicator developed by He *et al.* exhibits increased fluorescence intensity by ~34% per 1 mM Ca²⁺ in the range of 0.3-2.2 mM (Figure 8a, i left), and also maintains the high selectivity for Ca²⁺ over Mg²⁺ [151]. An alternative method is to increase the ratio of fluorophores to the binding sites. For example, conjugation of an increased amount of fluorophore, BODIPY (4,4-difluoro-4-bora-3a,4a-diaza-s-indacene) with the truncated BAPTA resulted in an indicator with K_d up to ~0.92 mM and high selectivity for Ca²⁺ (about 9 times over other metal ions under physiological conditions) (Figure 8a, ii right) [152].

Other than modifying the BAPTA-based Ca²⁺ indicators, the renaissance of chemically synthesised indicators for extracellular Ca²⁺ also deserves attention. Of a list of commercial Ca²⁺ indicators, Rhod-5N emerges as a promising low-affinity Ca²⁺ indicator (K_d ~0.32 mM, as specified by the manufacturer) for sensing [Ca²⁺]_{ex}. The apparent K_d of Rhod-5N was increased to 3.29 mM in the cell culture medium (Dulbecco's Modified Eagle Medium, DMEM) where the high selectivity to Ca²⁺ was not compromised (Figure 8b, i). This suggests that Rhod-5N is suitable for measuring Ca²⁺ between 0.33-33 mM, a range covering both physiological and pathophysiological variations in [Ca²⁺]_{ex}. Moreover, the sensing profile of Rhod-5N for Ca²⁺ was retained in both raw and filtered human serum samples (Figure 8b, ii left). In DMEM or DMEM+10% FBS mixture (Figure 8b, ii right), the fluorescence enhancement of Rhod-5N exhibited a linear dependence on logarithmic [Ca²⁺] [17]. The work by Rusakov and Fine demonstrated that the fluorescence of Rhod-5N responded to 0-2 mM [Ca²⁺] in an almost linear pattern, with a ~2% increase per 100 µM [153]. This was realised by encapsulating Rhod-5N (dispersed in a Ca²⁺-free buffer) into a concentric shell attached to a micropipette with tip size 2-3 µm (Figure 8b, iii left). A constant pressure was applied to the pipette to hold the Rhod-5N buffer at the tip. Upon contact with Ca²⁺-containing aqueous solvent, fluorescence at the tip area increased in response to the diffusion of Ca²⁺ into the shell (Figure 8b, iii right).

Table 2. Summary of conventional Ca²⁺ sensors for islet studies

		GEO		
	Synthetic indicators	Recombinant Aeq	Fluorescent proteins	CSMs
[Ca ²⁺] sensing (µM)	0.04 – 1 [69, 114, 145]	50 – 500 or 0	500 – 1500 [67]	
$K_{d}(\mu M)$	$0.06 - 0.39^{[123,146,147]}$	$0.2-50^{\ [146,\ 147]}$	1.7 - 1000 [34, 148]	$10^{-4} - 10^{2} {}^{[149, 150]}$
Signal strengths	••••	•	•••	••••
Advantages	high signal-noise ratiogood localisationinstantaneousresponse	free from excitation lightprecise localisationlow photobleaching	preciselocalisationlowphotobleachinghighly selective	- stable signal reading - good selectivity
Limitations	photobleachingprone to aggregatenon-specific binding	-non-ratiometric - very poor signal	pH-sensitiverelatively weaksignal	 low spatial resolution concern of mechanical damages slow response to Ca²⁺

Aggregation-induced emission (AIE) fluorogens-based Ca2+ indicators are another emerging sensor for measuring [Ca²⁺]. When embedded into Ca²⁺-chelating ligands, AIE fluorogens emit fluorescence upon aggregation of fluorogens induced by Ca²⁺. As illustrated in Figure 8c, i, one such sensor can be synthesised from chelator-conjugated polyacrylic acid (PAA) and AIE fluorogen tetraphenylethene (TPE) into a polymer gel form. In the presence of Ca²⁺, the conformational changes of PAA pull the TPE appendants closer to trigger fluorescence [157]. Subject to the relative amount of TPE content (x), K_d of PAA-TPE_x varies from 0.43 to 2.8 mM. For example, g-PAA-TPE_{0.02} exhibits 10% and 3% changes in fluorescence intensity when [Ca²⁺] oscillates between 0.1-1.1 mM or 1.1-1.3 mM, respectively. Of note, the optical signal strength drops by ~ 20% after 5 cycles (about 25 minutes) [154]. SA-4CO₂Na represents another AIE-based Ca²⁺ indicator, which is similarly generated by incorporating the AIE fluorogen salicyladazine (SA) into the negatively charged iminodiacetate groups (Ca²⁺ chelator). Upon exposure to Ca²⁺, SA-4CO₂Na forms highly emissive fibrillary aggregates, leading to a linear increase in fluorescence over 11 folds in response to increasing [Ca²⁺] from 0.6 to 3 mM (Figure 8c, ii left). SA-4CO₂Na also shows a high selectivity to Ca²⁺ over other metal ions and biomolecules (Figure 8c, ii right). Furthermore, SA-4CO₂Na remains viable for sensing Ca²⁺ in

solid analytes, including psammomatous meningioma slices, microcracks on bovine bone surface and micro-defects on a hydroxyapatite-based scaffold [155].

The sensors that have been developed to probe serum/blood Ca^{2+} represent a less explored group for tracing $[Ca^{2+}]_{ex}$. Moirangthem *et al* showed that a cholesteric liquid crystalline (CLC) polymer film could sense $[Ca^{2+}]$ in the range of 0.1-10 mM. The polymer film utilised benzoic acids as metal-binding sites, and the emission of the film exhibited a blue shift in response to Ca^{2+} as the wavelength changed from green to blue $(\Delta\lambda = 70 \text{ nm})$. The Ca^{2+} -induced wavelength corresponded to distinct colour changes, making the application of this film suited for rapid detection of blood Ca^{2+} , e.g. diagnosis of hypocalcemia or hypercalcemia [158]. Ding *et al* utilised 3-aminopropyltriethoxysilane-coupled carboxylic acid (APS-CCA) to sense Ca^{2+} in the blood, and observed that the fluorescence of APS-CCA increased over 2 folds in response to 2 mM Ca^{2+} . The fluorescence response to other metal ions was negligible even at supraphysiological levels (2 mM). Incorporation of APS-CCA with a hydrophobic substrate-based microarray results in a high-throughput fluorimetric microarray, which facilitates high-throughput screening of blood Ca^{2+} (0.01-2 mM, over 20 blood samples in one measurement), with a sensitivity of 0.005 mM [159].

2.5.2 Nano-structured sensors for [Ca²⁺]_{ex}

Nano-structured Ca^{2+} sensors are an array of hybrid materials that can convert the change of $[Ca^{2+}]$ into discernible optical, electrical or magnetic signals. The signal type and detection range of these sensors depend on the modality of the nanomaterials and the binding affinity of the chelators. There is a growing list of nano-structured sensors that meet the requirement for measuring $[Ca^{2+}]_{ex}$ [160]. In this sub-section, we focus on the nano-structured Ca^{2+} sensors of low binding affinity.

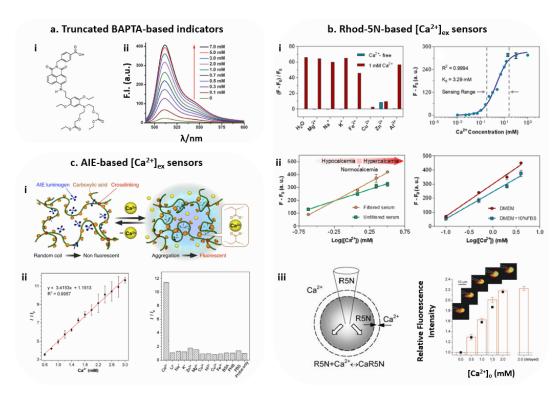


Figure 8. Emerging low-affinity Ca²⁺ indicators for measuring high concentrations of Ca²⁺. (a) (i) A truncated BAPTA-based low-affinity Ca²⁺ indicator. As illustrated, the molecular structure (left) consists of Ca²⁺ recognition units and a fluorophore (4-amino-1,8-naphthalimide). Reproduced with permission [151]. Copyright 2008, Elsevier; (ii) The optical responses ($\lambda_{ex} = 477$ nm) of truncated BAPTA in HEPES buffer (pH 7.4) upon addition of a series of Ca²⁺ stimuli. Reproduced with permission [152]. Copyright 2016, Wiley. (b) (i) Ion-selectivity investigation of Rhod-5N to Ca²⁺ in the presence of common extracellular cations, the concentrations of which were set to mimic the extracellular environment, including Mg²⁺ (1 mM), Na⁺ (150 mM), K⁺ (5 mM), Fe²⁺ (50 μ M), Cu²⁺ (50 μ M), Zn²⁺ (50 μ M), and Al³⁺ (50 μ M). The data represent relative fluorescence changes (F – F₀)/F₀ of 50 μ M Rhod-5N with (red bars) and without (blue bars) addition of Ca^{2+} ($\lambda_{ex}/\lambda_{em} = 530/580$ nm), where F and F₀ are the fluorescence of Rhod-5N in the presence and absence of the respective metal ions (left). The titration curve of 50 µM Rhod-5N, obtained by fitting its fluorescence at 580 nm (with Ca²⁺ from 1 μM to 1 M in the cell culture medium at 37 °C) via Hill's equation, where Hill's coefficient (n_h) was determined as 0.94 ± 0.06 , and K_d as 3.29 ± 0.41 mM, with an R^2 of 0.9994 (right); (ii) Sensing $[Ca^{2+}]_{ex}$ in biomedical scenarios: fluorescence of Rhod-5N increases linearly in response to a wide range of [Ca²⁺] in unfiltered and filtered human serum samples (left). [Ca²⁺]-dependent fluorescence enhancement of Rhod-5N in Dulbecco's Modified Eagle Medium (DMEM) with and without fetal bovine serum (FBS, 10%) (right). Reproduced with permission [17]. Copyright 2020, American Chemical Society. (iii) A micro-pipette probe filled with 3 mm Rhod-5N for sensing extracellular Ca²⁺ (left). The probe displays a linear fluorescence signal change in response to [Ca²⁺] from 0 to 2 mM (right). Reproduced with permission [153]. Copyright 2008. Elsevier. (c) (i) Schematic illustration of one aggregation-induced emission (AIE)-based fluorescent indicator (g-PAA-TPE) for Ca²⁺ sensing. Reproduced with permission [154]. Copyright 2016, Springer Nature. (ii) Relative fluorescence intensity changes of SA-4CO₂Na at 560 nm as a function of different [Ca²⁺] (left); Relative fluorescence of SA-4CO₂Na in response to various metal ions and biological molecules in phosphate-buffered saline (PBS) (right): Ca²⁺ (3.0 mM), Li⁺ (1.0 mM), Na⁺ (150 mM), K⁺ (150 mM), Zn^{2+} (50 μ M), Mg^{2+} (2.0 mM), Co^{2+} (50 μ M), Cu^{2+} (50 μ M), Fe^{3+} (50 μ M), [Bovine serum albumin, BSA] = [Porcine haemoglobin, PHB] = [FBS] = 0.05 mg/mL, [SA-4CO2Na] = 1.0 mM; $\lambda_{ex}/\lambda_{em}$ = 351/560 nm. Reproduced with permission [155]. Copyright 2018, American Chemical Society.

For gold nanoparticles (AuNPs), the specific electromagnetic fields (e.g., incident light) acting on the particles can drive resonant oscillations of electrons of the conductor at the NP interface, namely surface plasmon resonance (SPR) characteristic, which has been utilised for sensing provided that there are analyte-induced changes at the NP-environment boundary (e.g., variations in the size and shape of AuNPs and absorption of molecules onto the surface) [165]. In general, SPR wavelength shift reflects such variations. As exemplified in Figure 9a, i, Russell *et al.* functionalised AuNPs with carbohydrate moieties (lactose), and showed that the degree of AuNP clustering and associated colourimetric changes were dependent on [Ca²⁺] in the range of 0.8-2.2 mM (overlapping part of physiological [Ca²⁺]_{ex}) and 10-35 mM. The authors suggested that the sensing range is closely related to the length of the linker that bridges AuNPs and the chelator, such as ethylene glycol [166]. As shown in Figure 9a, ii and iii, calsequestrin (CSQ)-AuNPs aggregate in the presence of Ca²⁺ (but not other metal ions) and undergo a linear colourimetric shift when serum Ca²⁺ changes from 2.4 to 3.5 mM [161].

Another development of nano-structured Ca²⁺ sensors is largely driven by their capacity for assembling or encapsulating fluorescent Ca²⁺ indicators into a nanoscale matrix [167]. Its salient feature includes protection of the indicators from unwanted interferences of the surroundings and acting as new carriers for delivery [168]. Compared to native indicators, the nanoscale capsule may mitigate the photobleaching issue (e.g., negligible impairment over a 40-minute exposure to UV light) and reduce the leaking rate (<3% leakage over 24 hours) [169]. One construction is to encapsulate the probes with biologically localised embedding (PEBBLE) (Figure 9b, i), where polyacrylamide or poly-(decylmelacrylate) works as the matrix to accommodate different Ca²⁺ indicators, such as Rhod-2 [162], Calcium Green [170] or Fluo-4 [171]. PEBBLE nanosensors with dimensions of 20 to 600 nm, have been generated for the detection of various bioactive molecules, including cellular Ca²⁺ (Figure 9b, ii). As shown in Figure 9b, iii, a PEBBLE nanosensor incorporating Rhod-5N exhibits a K_d of ~1.25 \pm 0.006 mM, which is suitable for measuring high [Ca²⁺] [162]. Such nano-structured Ca²⁺ sensors are also generated by utilising silica NPs as the host matrix. Conjugation of dextran-encapsulated silica NPs with both the Fluo-4 and a reference dye can generate a ratiometric sensor that responds to Ca²⁺ up to 50 µM [172]. Its sensing range can be enlarged by replacing Fluo-4 with a low-affinity Ca²⁺ indicator, e.g. calcein.

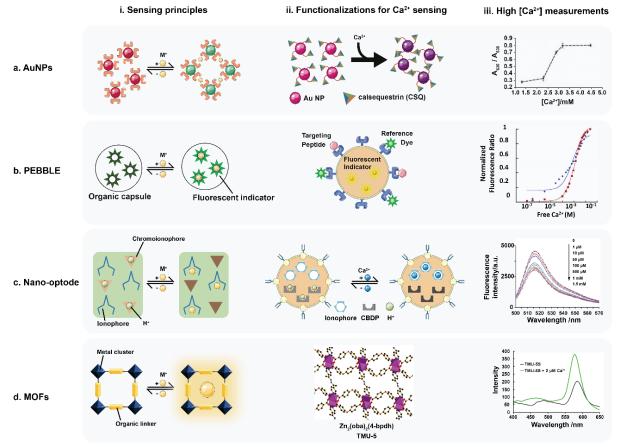


Figure 9. Nano-structured Ca²⁺ biosensors. (a) (i) Sensing mechanism of Ca²⁺ chelator-functionalised gold nanoparticles (AuNPs). The presence of Ca²⁺ induces aggregation of NPs, leading to the SPR peak shift and colour change; (ii) Illustration of the process that calsequestrin (CSQ)-functionalised AuNPs undergo aggregation and exhibit colourimetric responses in the presence of Ca²⁺; (iii) Correlation of the ratio change of absorbance at 630 and 530 nm (A₆₃₀/A₅₃₀) as a function of [Ca²⁺]. Reproduced with permission [161]. Copyright 2009, Wiley. (b) (i) Sensing mechanism of Ca²⁺ probes encapsulated by biologically localised embedding (PEBBLE), in which the fluorescence of the indicator increases upon binding to Ca²⁺; (ii) A representative PEBBLE sensor constructed by anchoring a reference dye, such as Hilyte, onto the surface of the polymer matrix, for ratiometric sensing capacity for Ca²⁺; (iii) Fluorescent responses of Rhod-dextran/Hilyte (blue) and Rhod-5N/Hilyte (red) PEBBLEs as a function of [Ca²⁺]. Reproduced with permission [162]. Copyright 2012, American Chemical Society. (c) (i) Sensing mechanism of a nano-optode constructed by Ca²⁺-selective ionophore and pH-sensitive chromoionophore; (ii) Ion-exchange process in a polymeric lipophilic nanospheres embedded with Ca²⁺-selective ionophore (ETH 129) and chromoionophores (calix[4]arene-functionalised bodipy, CBDP). The ionophore selectively transports Ca2+ into the nanosphere in exchange with H+, leading to a change in the fluorescence of CBDP; (iii) The emission spectra of CBDP-encapsulated nanospheres as a function of [Ca²⁺] from 1 μ M to 1.5 mM in PBS solution, pH 7.4 ($\lambda_{ex}/\lambda_{em} = 480/516$ nm). Reproduced with permission [163]. Copyright 2016, American Chemical Society. (d) (i) Sensing mechanism of metal-organic frameworks (MOFs). The optical property of MOFs is susceptible to the conformational changes induced by the guest metal ions; (ii) Structure of Zn₂(oba)₂(4-bdph) TMU-5, a Ca²⁺-responsive MOFs: 6-coordinated Zn₂(-COO)₄(-PY)₂ paddlewheel secondary building units are linked via oba and 4-bpdh ligands resulting in three-dimensional azine-functionalised interconnected pores; (iii) Emission spectra of TMU-5S dispersed in distilled water with and without 2×10^{-6} M Ca²⁺ ($\lambda_{ex} = 355$ nm). Reproduced with permission [164]. Copyright 2020, American Chemical Society.

More recently, nano-structured optical Ca²⁺ sensors have also emerged from ion-selective nano-optodes, which are composed of Ca²⁺-responsive ionophores (that are often used in CSM), ion-exchanger and lipophilic-sensing components (chromoionophore), such as a pH indicator, in a polymeric lipophilic matrix [173]. As depicted in Figure 9c, i, the ionophores selectively transport Ca²⁺ into the optode, driven by the concentration gradient. Subsequently, H⁺ is released to maintain the electroneutral state inside. As a consequence, the internal pH of the sensor changes, which further influences the optical properties of the embedded lipophilic-sensing components (e.g. chromoionophore). Figure 9c, ii illustrates a representative of Ca²⁺-responsive nano-optode, which consists of Ca²⁺ ionophore II (ETH 129) and chromoionophore calix[4]arene-functionalised bodipy (CBDP). In response to [Ca²⁺] from 1 µM to 1 mM, this sensor shows a gradual decrease in fluorescence intensity (Figure 9c, iii). Similar to PEBBLE sensors, the encapsulation of nano-optode in a polymer also prevents disturbance from the environment, which is advantageous for tracing [Ca²⁺] over a prolonged time. The other nanooptode containing either **CBDP** sensors, 9-(diethylamino)-5-[(2-octyldecyl)imino]benzo[a]phenoxazine (ETH 5350) as chromoionophore, exhibit stable fluorescence in the first 3 hours after being loaded into Hela cells (an immortal cell line derived from human cervical cancer), followed by around 40% decrease over 24 hours [163]. The sensing range of nano-optodes appears to depend on the binding affinity of the Ca²⁺selective ionophore. Therefore, the effective sensing range is flexible to be tuned for different sensing purposes, including measurement of [Ca²⁺]_{ex} by adopting low-affinity ionophores. In comparison to CSM, the response time of nano-optode is improved by orders of magnitude, as short as ~1 second to date, but this remains barely competitive with the temporal resolution of chemically synthetic or protein-based Ca²⁺ indicators. Such a temporal resolution may result in the distortion or dismissal when extracting transient Ca²⁺ signals.

An emerging high-performance sensor is based on metal-organic frameworks (MOFs), a type of crystalline solid constructed by connecting metal cations or groups of cations (nodes) via organic ligands (linkers that have multiple binding sites) to form single- or multi-dimensional extended coordination networks [174-176]. Of note, MOFs fluoresce upon either irradiated metal components or organic ligands. In addition, the optical characteristics of MOFs are dependent on

node-to-ligand or ligand-to-ligand interaction, or the interaction between MOFs and the surrounding environment [177]. With different pore sizes and combinations of metal ions and ligands, it is feasible to customise MOFs to sense various molecules that are smaller than the pore of MOFs (Figure 9d, i) [178]. For example, Ca²⁺-responsive MOFs have been developed from three-dimensional lanthanide anionic structure based $\{K_5[Tb_5-(IDC)_4(ox)_4]\}_n \cdot n_3(20H_2O)_n$. K⁺ in its one-dimensional channel can exchange with Ca^{2+} to induce a remarkable increase in fluorescence at ~480 and 550 nm. However, these MOFs also respond to other metal ions, such as Fe²⁺ and Cu²⁺ [179]. The poor selectivity towards Ca²⁺ thus restricts their biological application. Figure 9d, ii shows the spectra of a MOF-based ratiometric Ca^{2+} sensor, TMU-5S, $[Zn(C_{14}O_5H_8 (C_{14}H_{14}N_4)_{0.5}]\cdot (C_3NOH_7)_{1.5}(RhB)_{0.002}$, which was synthesised by integrating rhodamine B with the MOF. Upon addition of 2 µM Ca2+ (in a cell-free experimental setup), fluorescence of of TMU-5S is increased, in association with a blue shift (from 485 nm to 465 nm, and from 585 nm to 575 nm, respectively) (Figure 9d, iii). The results also showed that TMU-5S preferentially binds to Ca²⁺ over other metal cations at physiological concentrations, and exhibits a 5-second response (the time required to obtain the 90% real value) and 40-second recovery (the time for releasing up to 90% from a specific target) [164]. The temporal responsiveness is sufficient for tracing slow Ca²⁺ changes, but may be too protracted for fast-tracking or instantaneous reading of [Ca²⁺] changes.

2.5.3 Microfluidics-based multiplexed sensing platforms

A microfluidic sensing platform typically comprises three core modules: perfusion controller(s), customised microfluidic chip and (multi-) analytical station(s) [180]. The perfusion system customises the perfusion rate, in the micro- or nano-liter range per minute, via peristaltic pumps (for long-term perfusion) or syringe pumps (for short-term perfusion). The second component, a microfluidic chip, is central in the system. It incorporates the mechanism to immobilise biological samples and provide them with a biomimetic environment, while the channel structures in the microchip regulate the shear stress that the trapped tissues are exposed to, which impacts the viability of the tissues to be studied. Moreover, the microfluidic chip features the flexibility and compatibility required for simultaneous multiplexed tracing of bioactive molecules. Subject to the specific research question, analytical modules such as optical microscope and on-chip immunoassay based on antigen-antibody reactions can be incorporated,

allowing for tracking small molecules (e.g., ions and ATP) or large biomolecules (e.g., peptide and protein).

For the first module, the selection of the perfusion controller is based on the perfusion requirements as mentioned in the preceding paragraph. The major variation between microfluidic chips lies in the design of the microchannels and trapping structures, which should ensure effective capturing and immobilisation of the samples of interest, e.g. the primary pancreatic islets and islet spheroids.

Figure 10 illustrates four types of frequently adopted tissue-trapping structures in microfluidic sensing platforms. Under hydrodynamic force, the U-cup tissue array is able to sequentially immobilise individual primary pancreatic islets in each cup while reducing the shear stress imposed on the trapped tissue via directing the branch of the perfusion flow into the cup (Figure 10a) [17, 184]. The U-cups are selective for islets with a specific range of dimensions, as the smaller islets would either escape the capture of the cup via the neck or stack within the cup, while the larger ones drift downstream along the channel and are not directed into the cup. Regarding the other chambers, a dam-wall-like tissue chamber is preferable to load tissue of different sizes, despite that the flow imposed on the trapped islets has been shown to dampen the glucose-stimulated Ca²⁺ response of the periphery of the islet where fluid shear stress is greatest (Figure 10b) [185].

In addition to acting as trapping sites for primary tissues, the chambers are adaptable to enable the on-chip formation of islet organoids/spheroids. As shown in Figure 10c, the microwell chambers have been used to host islet organoids that grow from stem cells captured from the perfused medium by gravity [182]. It has been suggested that the capturing function of wells is consistent when the flow rates are less than 2 μ L/min, which however may be too slow to grow healthy organoids [186]. Though the fabrication of the microwell is relatively simple, the challenge lies in the uneven provision of nutrients in the well, because the fluid exchange at the bottom is much slower than on its surface [187]. To mitigate these issues, a microchamber with 15 microtraps based on 7 circularly patterned micropillars is developed, allowing for efficient exchange of interstitial fluid and capturing of the suspended cells in a perfused medium (e.g., 2×10^6 cells/mL) (Figure 10d). The fluidic dynamic simulation has suggested there is a stable,

uniform flow with negligible shear stress in these microtraps. This may account for good-differentiation and high survival rates of islet organoids in the micropillar trap – over 72-hour culturing, 85% of cells are viable in the micropillar trap in contrast to 45% in the microwell trap) [183].

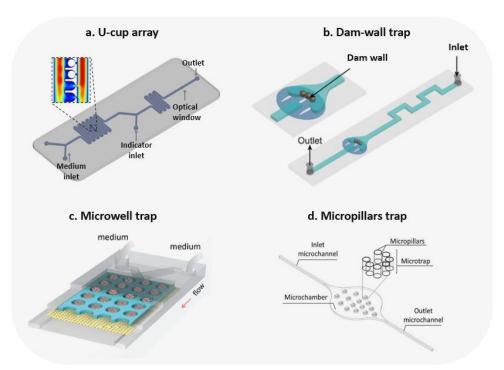


Figure 10. Illustration of selected microfluidic chips. (a) Layout of a U-cup-based microfluidic chip, with two Y-shape inlets, two sections of serpentine channel, a column of U-cups, an optical window and an outlet. Reproduced with permission [17]. Copyright 2020, American Chemical Society. (b) A schematic of a microfluidic device that utilises a dam-wall design to capture pancreatic islets. Islets and media are delivered into the device by flow from the inlet to outlet ports with tubing. This two-layer device contains a 125 µm tall main channel and a 25 µm tall dam wall. The schematic of the zoomed-in holding area shows that islets in this channel are prevented from moving down the channel by the drop in height. This design maintains the islets stationary with flow directed at the islets. Reproduced with permission [181]. Copyright 2013, Royal Society of Chemistry. (c) Schematic diagram of organoids on the chip with well traps. The device consists of four parts: top and bottom PDMS layers separated by a through-hole PDMS membrane and a polycarbonate porous membrane. The microwell array of the upper layer allows a three-dimensional culture of islet organoids under dynamic medium perfusion. A polycarbonate porous membrane is applied to separate the media flow of the upper channel from the lower. Reproduced with permission [182]. Copyright 2019, Royal Society of Chemistry. (d) Layout of a microfluidic system with microchambers for the collection and culture of multiple islet cells. The culture chamber consists of 15 round microtraps (280 μm × 280 μm) and 7 micropillars each (145 μm × 145 μm × 200 μm), which support the construction of islet-like tissue (islet diameter ~185 µm). Reproduced with permission [183]. Copyright 2019, Elsevier.

As introduced in Section 2, insulin secretion is initiated by multi-step intracellular Ca²⁺ signalling and synchronised by intercellular communication. Multiplexed sensing is in great

demand, to provide a comprehensive understanding of the steps involved, since it carries the following advantages: (i) it provides biologically relevant perfusion and enables organ-crosstalk that mimics *in vivo* conditions; (ii) it is compatible with different sensing agents and modules, allowing for simultaneous monitoring of multiple bioactive molecules that are involved in insulin secretion; and (iii) it has the flexibility to include temporal and spatial sensing modalities that are needed for precise comprehension of a signalling network.

Provision of dynamic and bio-mimicking environments for the immobilised islets in a microfluidic chip is advantageous for maintaining the viability and bioactivity of islets in response to stimuli. In contrast to conventional culture in a petri dish, the application of a microfluidic setup was shown to preserve the GSIS from around 72 hours to over 240 hours [188]. However, the disruption of the capillary vascular system of isolated islets is unlikely to be compensated solely by providing a biomimetic perfusion environment [189, 190]. As such, there is growing research into incubating islet-like tissues in the microfluidic chip, such as islet micro-tissues and islet spheroids (organoids) from dispersed primary islet cells and pluripotent stem cells, which retain the biological features of primary islets, including islet morphology, cellular composition and secretory profiles [191]. Consequently, the observation window for the evaluation of islet function can be extended to 28 days for the islet micro-tissue [191] and 45 days for islet spheroids [182]. Based on a dam-wall islet trap, a microfluidic chip system has been developed to provide glucose at either a constant or pulsatile rate with varying amplitudes (0.5, 1, 1.5 on the basis of 11 mM mean glucose level) and periodicities (spanning from 20 to 2 minutes). Upon these varied waveforms, [Ca²⁺]_c resonates and reaches the apex of its oscillation only when glucose is perfused with a periodicity resembling in vivo glucose oscillation (around 5-10 minutes per cycle) [50, 192]. The improved responsiveness to glucose is further supported by the amplified insulin release at the second phase of GSIS under the same pattern of glucose stimulation [99].

The microfluidic chip is also a unique sensing platform for the investigation of organ crosstalk that may participate in the regulation of insulin secretion. In the body, adipocytes secrete nonesterified fatty acids (NEFAs) that have been shown to exert a bimodal effect on insulin secretion, i.e., short-term exposure (less than several hours) to NEFAs enhances insulin secretion [195, 196] while chronic exposure (over 1-2 days) suppresses it [197]. It is difficult to gain

in-depth knowledge of the dynamic interaction between adipocytes and pancreatic islets based on the conventional static incubation method. As shown in Figure 11a, adipocytes (3T3-L1, a mouse adipose cell line) and primary mouse islets can be co-cultured in a microfluidic sensing platform. In this setup, Lu *et al* demonstrated that signals derived from adipocytes in the upper stream of the perfusion augmented glucose-induced (11 mM) insulin secretion from the downstream islets substantially [193].

Likewise, the gut-derived incretin hormone, glucagon-like peptide 1 (GLP-1), stimulates insulin secretion in a glucose-dependent manner. GLP-1 mimetics are now a mainstay in the management of T2D [198]. Screening for effective stimuli for GLP-1 secretion represents an approach to identifying new therapies for T2D [199]. To this end, a microfluidic chip system was developed to co-culture GLUTag cells (GLP-1 secreting cells) and INS-1 cells (β-cell line) (Figure 11b). The functionality of the cultured cells in the two chambers was evaluated independently by measuring insulin and GLP-1 secretion when the glucose concentration was increased from 3 to 20 mM. The results showed that insulin secretion was increased by around 5 ng/10⁶ cells in the INS-1 chamber and GLP-1 secretion by 0.6 ng/10⁶ from the GLUTag chamber. In addition to glucose concentration, the flow rate also influenced the secretion of both hormones, as insulin and GLP-1 increased from 21 to 32 ng/10⁶ cells and from 0.6 to 4.8 ng/10⁶ cells, respectively, when the perfusion rate was increased from 2 µL/min to 10 µL/min. This study further demonstrated that the co-culture with GLUTag cells improved the insulin output by around 1 ng/10⁶ cells/minute compared with the culture of the INS-1 cells alone [194]. It should be noted that both of the cells used in the experiment were cancer cell lines, and the implications of these observations remain to be validated in primary tissues or animal models.

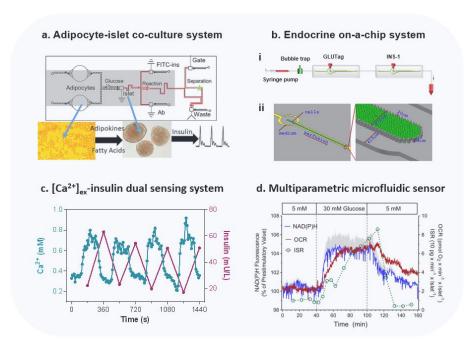


Figure 11. Multiplexed microfluidic sensing systems. (a) Top view of a microfluidic chip for investigation of the role of adipocytes in the control of islet function. Solid lines indicate the microfluidic channels. The large circles on the left represent the adipocyte chambers drilled through the glass (light image of adipocytes shown underneath). The shaded section of the chip indicates the parts that are heated during experiments. In this setup, the perfusate containing adipocyte-derived secretory products (dashed lines) is delivered into the islet chamber together with glucose from the side channel. Insulin secretion the islets is monitored by electrophoretic competitive immunoassays, fluorescence-labelled insulin (FITC-ins) and insulin antibodies are infused into the channel guided by electro-osmotic flow (red arrow). The laser-induced fluorescence (LIF) detection point, sited 1 cm beyond the injection cross (indicated by the star), monitors the dynamic concentration of insulin secretion. Reproduced with permission [193]. Copyright 2018, American Chemical Society. (b) Schematic of the endocrine system-on-chip: (i) The cells are loaded into their respective chambers via a syringe pump. Culture medium is supplied via the inlet. The perfusate from the outlet is collected for further analysis. The two chambers are joined by a connection tube; (ii) Dimensions of the three-dimensional microfluidic chip. Micropillars divide the microfluidic channel into a central cell culture compartment and two side channels for perfusion of the culture medium. Reproduced with permission [194]. Copyright 2017, IOP Publishing. (c) Simultaneous monitoring of dynamic Ca²⁺ and insulin in a biologically relevant environment. Oscillatory patterns of both Ca²⁺ and insulin well align with the set frequency. The temporal delay between the two measurements reflects the time required for the perfusion flow to travel from the optical window (for measuring Ca²⁺) to the channel outlet (for sample collection to measure insulin), which can be corrected based on the flow rate. Reproduced with permission [17]. Copyright 2020, American Chemical Society. (d) Multiparametric microfluidic sensor for simultaneous monitoring of various bioactive molecules during GSIS. The concentration of glucose is set to vary between 5 and 30 mM. Multiplexing is achieved by incorporation of respective indicators, i.e., NAD(P)H (blue trace) via autofluorescence, $\lambda_{ex}/\lambda_{em} = 366/450$ nm, oxygen consumption rate (OCR) via implanted miniaturised oxygen probe, and insulin secretion rate (ISR) via enzyme-linked immunosorbent assay (ELISA). Reproduced with permission [187]. Copyright 2017, Springer Nature.

The microfluidic sensing system is characterised by high spatial and temporal resolutions for tracing multiple physiological factors through the integration of different analytical modalities. For example, our recent work (a pseudo-islet study) has shown concurrent measurements of $[Ca^{2+}]_{ex}$ and insulin concentration via integrating optical modalities for on-chip monitoring of Ca^{2+} -induced fluorescence of Rhod-5N and off-chip insulin quantification via enzyme-linked immunosorbent assay (ELISA). The temporal resolutions for measuring $[Ca^{2+}]_{ex}$ and insulin are 10s and 1 minute, respectively (Figure 11c) [17]. In other work, a microfluidic chip was integrated with a fluorescence microscope for multiplexed imaging of Ca^{2+} (by Fura-2) and mitochondrial membrane potential (by Rh123) within the trapped islets. The concurrent monitoring of the excitation ratio of Fura-2 at 340/380 nm and the fluorescence of Rh123 at 535 nm revealed the dynamic changes of $[Ca^{2+}]_c$ and mitochondrial activity at the same time. These observations validated the feasibility of multi-parametric monitoring of signalling kinetics via an integrated system [200].

Schulze *et al* developed a multiparametric microfluidic sensor for simultaneous monitoring of oxygen consumption, [Ca²⁺]_c, insulin secretion and intracellular NAD(P)H, where insulin was measured off-chip by ELISA, and [Ca²⁺]_c and NAD(P)H were indicated by reading on-chip optical signals of Fura-2 and NAD(P)H (autofluorescence), respectively. The dynamic oxygen consumption was recorded by oxygen sensors (Pst3 sensor and Fibox4 meter) mounted on the inlet and outlet of the microfluidic chip. The pre-determined flow rate and perfusion distance would allow for temporal corrections for correlating the kinetics of molecules measured at different locations (Figure 11d) [187]. When necessary, other analytical techniques, such as patch-clamp [201], amperometry [202] and capillary electrophoresis immunoassay (CEI) [203, 204], can be incorporated into the microfluidic system [205].

2.6 Conclusions and Outlook

There is a wide recognition that Ca^{2+} acts as an indispensable messenger within and outside cells to signal cellular functions in a range of physiological and pathological processes [206], including but not limited to immune responses [207], brain function [208], cancer [209], cell death [210] and insulin secretion from pancreatic β -cells [211]. In general, Ca^{2+} oscillates in

different cellular domains as a result of dynamic Ca²⁺ exchange between intra- and extracellular compartments. The increases in [Ca²⁺]_{mito} and [Ca²⁺]_{ER} are usually related to the uptake of cytoplasmic Ca²⁺ into mitochondria and ER. Oscillations of Ca²⁺ within each of these cellular compartments are intertwined with critical steps of, for example, pulsatile insulin secretion in response to glucose stimulation. Specifically, [Ca²⁺]_c participates in the firing of action potentials to trigger exocytosis of insulin granules. [Ca²⁺]_{mito} oscillation induces oscillatory production of ATP, while [Ca²⁺]_{ER} buffers the sharp change in [Ca²⁺]_c to maintain cell vitality. Within the pancreatic β-cells, disruption of Ca²⁺ oscillations in the cytoplasm and mitochondria markedly attenuates pulsatile insulin secretion. Inhibition of Ca²⁺ transportation in ER, at least acutely in the first phase, augments [Ca²⁺]_c and insulin secretion. [Ca²⁺]_{ex} has also been found to be oscillatory in the vicinity of β -cells under glucose stimulation, due probably to Ca²⁺ influx via VGCC (that decreases [Ca²⁺]_{ex}) and Ca²⁺ extrusion pathways including exocytosis with insulin and export of cytoplasmic Ca²⁺ (that decrease [Ca²⁺]_{ex}). There is increasing evidence suggesting that extracellular Ca²⁺ may signal intercellular communication via CaSR, an unexpected pathway that may be responsible for the synchronisation of insulin secretion from a group of \beta-cells. Hitherto, it remains to be elucidated as to what are the intrinsic pacemakers that dictate the frequency and amplitudes of Ca²⁺ oscillations, and the extent to which cytoplasmic Ca²⁺ shapes the pulsatility of insulin secretion.

Understanding of Ca²⁺ signalling has been paired with the advent and advancement of contemporary Ca²⁺ sensors and sensing methodologies. Since the first observation of dynamic changes in intracellular Ca²⁺ by a bioluminescent protein (i.e. Aeq), three major types of Ca²⁺ sensors have been established and widely used, including chemically synthesised fluorescent Ca²⁺ indicators, GECIs and CSMs. Abundant synthetic fluorescent Ca²⁺ indicators have provided options for the spectral property and binding affinity, which are particularly suitable for sensing cytoplasmic Ca²⁺, albeit with limitations of poor localisation and the issue of leaching within cellular domains. GECIs can be precisely expressed in a specific subcellular compartment, but their organelle-targeting efficiency is often hampered by the expression level and maturation speed of the protein indicators [137]. Another aspect that may be overlooked is that fusion of GECIs with a tag sequence is likely to change their binding affinity (or K_d) towards Ca²⁺. *In situ* fluorescence titration is thus recommended to re-determine the modified binding kinetics after

the indicators are expressed in the cells. Such post-characterisation is necessary to validate their ability to sense Ca^{2+} in the specific target domain. CSMs are of limited use for measuring intracellular $[Ca^{2+}]$ due to their inevitable mechanical damage to the cell and are, therefore, mainly employed for monitoring $[Ca^{2+}]_{ex}$. However, CSMs are suitable for a point-of-care measurement, though not for mapping the kinetics or tracing the change of $[Ca^{2+}]_{ex}$ in multi-cellular or tissue level.

The demand for sensors competent for measurement of $[Ca^{2+}]_{ex}$ has stimulated the search for new-generation Ca^{2+} sensors or sensing methodologies. One straightforward strategy is to tune down the binding affinity of an indicator (e.g. BAPTA-based) to Ca^{2+} . This can be achieved by increasing the relative ratio of the fluorophore to the Ca^{2+} binding sites, either by conjugating more fluorophores or truncating carboxyl groups (the binding sites) of the Ca^{2+} chelator, or both. In addition, Ca^{2+} chelator-conjugated AIE-based indicators have been synthesised with low binding affinity to Ca^{2+} . Both modified BAPTA-based and AIE-based Ca^{2+} indicators have a sensing range between 0.5 and 3 mM, which is suitable for measurement of $[Ca^{2+}]_{ex}$, while maintaining excellent Ca^{2+} selectivity over other physiological metal ions. Other than CSMs, which measure electric potentials, optical indicators commonly face the issue of photobleaching, regardless of their applications for intra- or extracellular Ca^{2+} .

Recently, nano-structured Ca^{2+} sensors have been explored for sensing $[Ca^{2+}]_{ex}$. These sensors are typically based on the encapsulation/conjugation of Ca^{2+} -responsive materials into/onto materials at the nanoscale. The incorporation of diverse Ca^{2+} chelators and fluorophores into nano-materials has led to a library of Ca^{2+} sensors of varying sensing. Protected by biocompatible and viable matrix materials, nano-structured Ca^{2+} sensors exhibit minimal cytotoxicity and high photobleaching resistance. However, their applications in the long-term tracing of cellular Ca^{2+} are still currently restricted due to the aggregation of nanomaterials that is difficult to avoid.

Given the intimate involvement of Ca^{2+} in the complex signalling network, the development of multiplexed platforms capable of sensing Ca^{2+} and other biological targets is of major interest. At a single cell level, multiplexed sensing has been achieved by simultaneously utilising multiple indicators for different bioactive molecules including Ca^{2+} , ATP, pH and O_2 , in combination

with the autofluorescence of small molecules (e.g. NAD(P)H) and electrophysiological sensors (e.g. patch clamp). In the context of a group of cells or tissue, microfluidic chips appear to be an advantageous sensing platform for at least three reasons. First, microfluidic chips, as opposed to the conventional sensing experiment in a static setup, e.g., a petri dish, generate a dynamic culture environment, including continuous provision of refreshed culture media and chemical/physical stimulation for the biological subject of interest, which better mimics the physiological environment [199]. As such, cultured cells or tissues experience improved viability and sustained functionality, and cellular responses obtained in such a biomimetic system are more likely to reflect actual reactions that would occur in vivo. Second, microfluidic chips have high combability with a variety of sensing modules, the integration of which has uncovered the links of dynamic intra- and inter-cellular Ca²⁺ signalling and metabolic activity (e.g., glycolysis and ATP production) with insulin secretion. However, photocytotoxicity could be a concern for multiplexed sensing studies in the case that the optical module is incorporated (where external light excitation is applied). Third, the microfluidic platform permits the reconstruction of cell-cell or even organ-organ crosstalk, allowing delineation of complex intercellular or inter-organ communication.

Despite not the focus of this review, the advanced optical microscopy techniques have also made a great contribution to the understanding of intracellular activities. For example, the integration of laser-scanning microscopy and intravital microscopy with Ca²⁺ sensors (e.g., GECIs) has allowed for intracellular Ca²⁺ imaging in both transplanted islets [212, 213] and endogenous islets *in vivo* [214]. Similarly, monitoring of Zn²⁺ release from beta cells by intravital microscopy has been shown to be useful to trace insulin secretion [215].

 Ca^{2+} signalling continues to be a major target of interest in various fields of biomedical research. In the study of islets, decoding Ca^{2+} oscillations is expected to reveal how the pulsatile insulin secretion is coordinated and what factors modify the secretory response. To date, understanding of Ca^{2+} signalling in live cells/organisms has mainly relied on the improvement of Ca^{2+} sensors. Emerging innovative Ca^{2+} sensing materials and platforms, represented by the low-affinity Ca^{2+} indicator, nano-structured Ca^{2+} and microfluidic sensing platforms, are able to unveil new roles of $[Ca^{2+}]_{ex}$, particularly in intercellular communication and synchronised cellular behaviours. The convergence of intra- and intercellular Ca^{2+} signalling may shed light on fundamental

mechanisms relating to insulin pulsatility, which can potentially unlock useful therapeutic targets for T2D.

2.7 References

- 1. Berridge, M.J., M.D. Bootman, and H.L. Roderick, Calcium Signalling: dynamics, homeostasis and remodelling. *Nature Reviews Molecular Cell Biology*, 2003. **4**(7): p. 517.
- 2. Petersen, O.H., M. Michalak, and A. Verkhratsky, Calcium signalling: past, present and future. *Cell Calcium*, 2005. **38**(3-4): p. 161-169.
- 3. Semyanov, A., C. Henneberger, and A. Agarwal, Making sense of astrocytic calcium signals—from acquisition to interpretation. *Nature Reviews Neuroscience*, 2020. **21**(10): p. 551-564.
- 4. Kreutzberger, A.J., *et al.*, Reconstitution of calcium-mediated exocytosis of dense-core vesicles. *Science Advances*, 2017. **3**(7): p. e1603208.
- 5. Puri, B.K., Calcium signaling and gene expression. *Calcium Signaling*, 2020: p. 537-545.
- 6. Yamada, Y., K. Namba, and T. Fujii, Cardiac muscle thin filament structures reveal calcium regulatory mechanism. *Nature Communications*, 2020. **11**(1): p. 1-9.
- 7. Mannowetz, N., M.R. Miller, and P.V. Lishko, Regulation of the sperm calcium channel CatSper by endogenous steroids and plant triterpenoids. *Proceedings of the National Academy of Sciences*, 2017. **114**(22): p. 5743-5748.
- 8. Horigane, S.-i., *et al.*, Calcium signalling: a key regulator of neuronal migration. *The Journal of Biochemistry*, 2019. **165**(5): p. 401-409.
- 9. Stafford, N., et al., The plasma membrane calcium ATPases and their role as major new players in human disease. *Physiological Reviews*, 2017. **97**(3): p. 1089-1125.
- 10. Rodrigues, T., G.N.N. Estevez, and I.L. dos Santos Tersariol, Na⁺/Ca²⁺ exchangers: Unexploited opportunities for cancer therapy? *Biochemical Pharmacology*, 2019. **163**: p. 357-361.
- 11. Giorgi, C., *et al.*, Calcium dynamics as a machine for decoding signals. *Trends in Cell Biology*, 2018. **28**(4): p. 258-273.
- 12. Hofer, A.M. and E.M. Brown, Extracellular calcium sensing and signalling. *Nature Reviews Molecular Cell Biology*, 2003. **4**(7): p. 530-538.

- 13. Smith, I.F. and I. Parker, Imaging the quantal substructure of single IP₃R channel activity during Ca²⁺ puffs in intact mammalian cells. *Proceedings of the National Academy of Sciences*, 2009. **106**(15): p. 6404-6409.
- 14. Fill, M. and J.A. Copello, Ryanodine receptor calcium release channels. *Physiological Reviews*, 2002. **82**(4): p. 893-922.
- 15. Anderson, D.M., *et al.*, Widespread control of calcium signaling by a family of SERCA-inhibiting micropeptides. *Science Signaling*, 2016. **9**(457): p. ra119-ra119.
- 16. Oxenoid, K., *et al.*, Architecture of the mitochondrial calcium uniporter. *Nature*, 2016. **533**(7602): p. 269-273.
- 17. Huang, W., *et al.*, A Multiplexed Microfluidic Platform toward Interrogating Endocrine Function: Simultaneous Sensing of Extracellular Ca²⁺ and Hormone. *ACS Sensors*, 2020.
- 18. Uhlén, P. and N. Fritz, Biochemistry of calcium oscillations. *Biochemical and Biophysical Research Communications*, 2010. **396**(1): p. 28-32.
- 19. Ziv, N.E. and M.E. Spira, Axotomy induces a transient and localized elevation of the free intracellular calcium concentration to the millimolar range. *Journal of Neurophysiology*, 1995. **74**(6): p. 2625-2637.
- 20. Berlin, J., M. Cannell, and W.J. Lederer, Cellular origins of the transient inward current in cardiac myocytes. Role of fluctuations and waves of elevated intracellular calcium. *Circulation Research*, 1989, **65**(1): p. 115-126.
- 21. Danielczok, J.G., *et al.*, Red blood cell passage of small capillaries is associated with transient Ca²⁺-mediated adaptations. *Frontiers in Physiology*, 2017. **8**: p. 979.
- 22. Trump, B.F. and I.K. Berezesky, Calcium-mediated cell injury and cell death. *The FASEB Journal*, 1995. **9**(2): p. 219-228.
- 23. Frandsen, S.K., *et al.*, Direct therapeutic applications of calcium electroporation to effectively induce tumor necrosis. *Cancer Research*, 2012. **72**(6): p. 1336-1341.
- 24. Borghans, J.M., G. Dupont, and A. Goldbeter, Complex intracellular calcium oscillations A theoretical exploration of possible mechanisms. *Biophysical Chemistry*, 1997. **66**(1): p. 25-41.
- 25. Pasti, L., *et al.*, Intracellular calcium oscillations in astrocytes: a highly plastic, bidirectional form of communication between neurons and astrocytes *in situ*. *Journal of Neuroscience*, 1997. **17**(20): p. 7817-7830.

- 26. Hajnóczky, G., et al., Decoding of cytosolic calcium oscillations in the mitochondria. *Cell*, 1995. **82**(3): p. 415-424.
- 27. Samanta, K., G.R. Mirams, and A.B. Parekh, Sequential forward and reverse transport of the Na⁺ Ca²⁺ exchanger generates Ca²⁺ oscillations within mitochondria. *Nature Communications*, 2018. **9**(1): p. 1-10.
- 28. Ishii, K., K. Hirose, and M. Iino, Ca²⁺ shuttling between endoplasmic reticulum and mitochondria underlying Ca²⁺ oscillations. *EMBO Reports*, 2006. **7**(4): p. 390-396.
- 29. Wakai, T., *et al.*, Regulation of endoplasmic reticulum Ca²⁺ oscillations in mammalian eggs. *Journal of Cell Science*, 2013. **126**(24): p. 5714-5724.
- 30. Endo, M., M. Tanaka, and Y. Ogawa, Calcium induced release of calcium from the sarcoplasmic reticulum of skinned skeletal muscle fibres. *Nature*, 1970. **228**(5266): p. 34-36.
- 31. Campbell, K. and K. Swann, Ca²⁺ oscillations stimulate an ATP increase during fertilization of mouse eggs. *Developmental Biology*, 2006. **298**(1): p. 225-233.
- 32. Henquin, J.-C., Regulation of insulin secretion: a matter of phase control and amplitude modulation. *Diabetologia*, 2009. **52**(5): p. 739.
- 33. Hanley, P.J., *et al.*, Extracellular ATP induces oscillations of intracellular Ca²⁺ and membrane potential and promotes transcription of IL-6 in macrophages. *Proceedings of the National Academy of Sciences*, 2004. **101**(25): p. 9479-9484.
- 34. Simpson, A.W., Fluorescent measurement of [Ca²⁺]_C: basic practical considerations. *Calcium Signaling Protocols*, 2013: p. 3-36.
- 35. Suzuki, J., K. Kanemaru, and M. Iino, Genetically encoded fluorescent indicators for organellar calcium imaging. *Biophysical Journal*, 2016. **111**(6): p. 1119-1131.
- 36. Suzuki, J., K. Kanemaru, and M. Iino, Genetically encoded fluorescent indicators for organellar calcium imaging. *Biophysics Journal*, 2016. **111**(6): p. 1119-1131.
- 37. Takahashi, A., *et al.*, Measurement of intracellular calcium. *Physiological Reviews*, 1999. **79**(4): p. 1089-1125.
- 38. Carter, K.P., A.M. Young, and A.E. Palmer, Fluorescent sensors for measuring metal ions in living systems. *Chemical Reviews*, 2014. **114**(8): p. 4564-4601.
- 39. Dana, H., *et al.*, High-performance calcium sensors for imaging activity in neuronal populations and microcompartments. *Nature Methods*, 2019. **16**(7): p. 649-657.

- 40. Cerrone, M., *et al.*, Plakophilin-2 is required for transcription of genes that control calcium cycling and cardiac rhythm. *Nature Communications*, 2017. **8**(1): p. 1-16.
- 41. Huang, D., B. He, and P. Mi, Calcium phosphate nanocarriers for drug delivery to tumors: imaging, therapy and theranostics. *Biomaterials Science*, 2019. **7**(10): p. 3942-3960.
- 42. Cabrera, O., *et al.*, The unique cytoarchitecture of human pancreatic islets has implications for islet cell function. *Proceedings of the National Academy of Sciences*, 2006. **103**(7): p. 2334-2339.
- 43. Caicedo, A. Paracrine and autocrine interactions in the human islet: more than meets the eye. in *Seminars in Cell & Developmental Biology*. 2013. Elsevier.
- 44. Association, A.D., 2. Classification and diagnosis of diabetes: Standards of Medical Care in Diabetes—2021. *Diabetes Care*, 2021. **44**(Supplement 1): p. S15-S33.
- 45. Jensen, T., et al., Fasting of mice: a review. Laboratory Animals, 2013. 47(4): p. 225-240.
- 46. Sun, C., *et al.*, Effect of fasting time on measuring mouse blood glucose level. *International Journal of Clinical and Experimental Medicine*, 2016. **9**(2): p. 4186-4189.
- 47. Anderson, G.E., Y. Kologlu, and C. Papadopoulos, Fluctuations in postabsorptive blood glucose in relation to insulin release. *Metabolism*, 1967. **16**(7): p. 586-596.
- 48. Koerker, D.J., *et al.*, Synchronous, sustained oscillation of C-peptide and insulin in the plasma of fasting monkeys. *Endocrinology*, 1978. **102**(5): p. 1649-1652.
- 49. Stagner, J.I., E. Samols, and G.C. Weir, Sustained oscillations of insulin, glucagon, and somatostatin from the isolated canine pancreas during exposure to a constant glucose concentration. *The Journal of Clinical Investigation*, 1980. **65**(4): p. 939-942.
- 50. Lang, D., *et al.*, Cyclic oscillations of basal plasma glucose and insulin concentrations in human beings. *New England Journal of Medicine*, 1979. **301**(19): p. 1023-1027.
- 51. Porksen, N., *et al.*, Impact of sampling technique on appraisal of pulsatile insulin secretion by deconvolution and cluster analysis. *American Journal of Physiology-Endocrinology And Metabolism*, 1995. **269**(6): p. E1106-E1114.
- 52. Pørksen, N., The *in vivo* regulation of pulsatile insulin secretion. *Diabetologia*, 2002. **45**(1): p. 3-20.
- 53. Matthews, D., *et al.*, Pulsatile insulin has greater hypoglycemic effect than continuous delivery. *Diabetes*, 1983. **32**(7): p. 617-621.

- 54. Bratusch-Marrain, P., M. Komjati, and W. Waldhäusl, Efficacy of pulsatile versus continuous insulin administration on hepatic glucose production and glucose utilization in type I diabetic humans. *Diabetes*, 1986. **35**(8): p. 922-926.
- 55. O'Rahilly, S., R.C. Turner, and D.R. Matthews, Impaired pulsatile secretion of insulin in relatives of patients with non-insulin-dependent diabetes. *New England Journal of Medicine*, 1988. **318**(19): p. 1225-1230.
- 56. Lin, J.-M., *et al.*, Pulsatile insulin release from islets isolated from three subjects with type 2 diabetes. *Diabetes*, 2002. **51**(4): p. 988-993.
- 57. Gumbiner, B., *et al.*, Abnormalities of insulin pulsatility and glucose oscillations during meals in obese noninsulin-dependent diabetic patients: effects of weight reduction. *The Journal of Clinical Endocrinology & Metabolism*, 1996. **81**(6): p. 2061-2068.
- 58. Hunter, S.J., *et al.*, Association between insulin secretory pulse frequency and peripheral insulin action in NIDDM and normal subjects. *Diabetes*, 1996. **45**(5): p. 683-686.
- 59. Ashcroft, F.M., D.E. Harrison, and S.J. Ashcroft, Glucose induces closure of single potassium channels in isolated rat pancreatic β-cells. *Nature*, 1984. **312**(5993): p. 446-448.
- 60. Cook, D.L. and N. Hales, Intracellular ATP directly blocks K⁺ channels in pancreatic β-cells. *Nature*, 1984. **311**(5983): p. 271-273.
- 61. Yang, S.-N. and P.-O. Berggren, The role of voltage-gated calcium channels in pancreatic β-cell physiology and pathophysiology. *Endocrine Reviews*, 2006. **27**(6): p. 621-676.
- 62. Dean, P.M. and E. Matthews, Glucose-induced electrical activity in pancreatic islet cells. *The Journal of Physiology*, 1970. **210**(2): p. 255.
- 63. Jahn, R. and D. Fasshauer, Molecular machines governing exocytosis of synaptic vesicles. *Nature*, 2012. **490**(7419): p. 201-207.
- 64. Kindmark, H., *et al.*, Glucose-induced oscillations in cytoplasmic free Ca²⁺ concentration precede oscillations in mitochondrial membrane potential in the pancreatic β-cell. *Journal of Biological Chemistry*, 2001. **276**(37): p. 34530-34536.
- 65. Krippeit-Drews, P., M. Düfer, and G. Drews, Parallel oscillations of intracellular calcium activity and mitochondrial membrane potential in mouse pancreatic β-cells. *Biochemical and Biophysical Research Communications*, 2000. **267**(1): p. 179-183.

- 66. Balasubramanyam, M., L.P. Singh, and S. Rangasamy, Molecular intricacies and the role of ER stress in diabetes. 2012, Hindawi.
- 67. Gerbino, A., *et al.*, Glucose increases extracellular [Ca²⁺] in rat insulinoma (INS-1E) pseudoislets as measured with Ca²⁺-sensitive microelectrodes. *Cell Calcium*, 2012. **51**(5): p. 393-401.
- 68. Henquin, J.-C., *et al.*, Dynamics of glucose-induced insulin secretion in normal human islets. *American Journal of Physiology-Endocrinology and Metabolism*, 2015. **309**(7): p. E640-E650.
- 69. Grapengiesser, E., E. Gylfe, and B. Hellman, Glucose-induced oscillations of cytoplasmic Ca^{2+} in the pancreatic β -cell. *Biochemical and Biophysical Research Communications*, 1988. **151**(3): p. 1299-1304.
- 70. Valdeolmillos, M., *et al.*, Glucose-induced oscillations of intracellular Ca²⁺ concentration resembling bursting electrical activity in single mouse islets of Langerhans. *FEBS Letters*, 1989. **259**(1): p. 19-23.
- Quesada, I., *et al.*, Glucose induces opposite intracellular Ca^{2+} concentration oscillatory patterns in identified α-and β-cells within intact human islets of Langerhans. *Diabetes*, 2006. **55**(9): p. 2463-2469.
- 72. Bergsten, P., *et al.*, Synchronous oscillations of cytoplasmic Ca²⁺ and insulin release in glucose-stimulated pancreatic islets. *Journal of Biological Chemistry*, 1994. **269**(12): p. 8749-8753.
- 73. Jonas, J.-C., P. Gilon, and J.-C. Henquin, Temporal and quantitative correlations between insulin secretion and stably elevated or oscillatory cytoplasmic Ca²⁺ in mouse pancreatic β-cells. *Diabetes*, 1998. **47**(8): p. 1266-1273.
- 74. Tarasov, A.I., *et al.*, The mitochondrial Ca²⁺ uniporter MCU is essential for glucose-induced ATP increases in pancreatic β-cells. *PloS One*, 2012. **7**(7): p. e39722.
- 75. AINSCOW, E.K. and G.A. RUTTER, Mitochondrial priming modifies Ca²⁺ oscillations and insulin secretion in pancreatic islets. *Biochemical Journal*, 2001. **353**(2): p. 175-180.
- 76. Tarasov, A.I., *et al.*, Frequency-dependent mitochondrial Ca²⁺ accumulation regulates ATP synthesis in pancreatic β-cells. *Pflügers Archiv European Journal of Physiology*, 2013. **465**(4): p. 543-554.

- 77. Wiederkehr, A., *et al.*, Mitochondrial matrix calcium is an activating signal for hormone secretion. *Cell Metabolism*, 2011. **13**(5): p. 601-611.
- 78. Gilon, P., et al., Calcium signaling in pancreatic β-cells in health and in Type 2 diabetes. *Cell Calcium*, 2014. **56**(5): p. 340-361.
- 79. Gilon, P., *et al.*, Uptake and release of Ca²⁺ by the endoplasmic reticulum contribute to the oscillations of the cytosolic Ca²⁺ concentration triggered by Ca²⁺ influx in the electrically excitable pancreatic β-cell. *Journal of Biological Chemistry*, 1999. **274**(29): p. 20197-20205.
- 80. Arredouani, A., J.-C. Henquin, and P. Gilon, Contribution of the endoplasmic reticulum to the glucose-induced [Ca²⁺]_c response in mouse pancreatic islets. *American Journal of Physiology-Endocrinology and Metabolism*, 2002. **282**(5): p. E982-E991.
- 81. Arredouani, A., *et al.*, SERCA3 ablation does not impair insulin secretion but suggests distinct roles of different sarcoendoplasmic reticulum Ca²⁺ pumps for Ca²⁺ homeostasis in pancreatic β-cells. *Diabetes*, 2002. **51**(11): p. 3245-3253.
- 82. Ravier, M.A., *et al.*, Mechanisms of control of the free Ca²⁺ concentration in the endoplasmic reticulum of mouse pancreatic β-cells. *Diabetes*, 2011. **60**(10): p. 2533-2545.
- 83. Tornheim, K., Are metabolic oscillations responsible for normal oscillatory insulin secretion? *Diabetes*, 1997. **46**(9): p. 1375-1380.
- 84. Ristow, M., *et al.*, Deficiency of phosphofructo-1-kinase/muscle subtype in humans is associated with impairment of insulin secretory oscillations. *Diabetes*, 1999. **48**(8): p. 1557-1561.
- 85. Li, D., *et al.*, Imaging dynamic insulin release using a fluorescent zinc indicator for monitoring induced exocytotic release (ZIMIR). *Proceedings of the National Academy of Sciences*, 2011. **108**(52): p. 21063-21068.
- 86. Brown, E.M., *et al.*, Cloning and characterization of an extracellular Ca²⁺-sensing receptor from bovine parathyroid. *Nature*, 1993. **366**(6455): p. 575-580.
- 87. LeBoff, M.S., *et al.*, Regulation of parathyroid hormone release and cytosolic calcium by extracellular calcium in dispersed and cultured bovine and pathological human parathyroid cells. *The Journal of Clinical Investigation*, 1985. **75**(1): p. 49-57.

- 88. Komuves, L., *et al.*, Epidermal expression of the full-length extracellular calcium-sensing receptor is required for normal keratinocyte differentiation. *Journal of Cellular Physiology*, 2002. **192**(1): p. 45-54.
- 89. Lorget, F., *et al.*, High extracellular calcium concentrations directly stimulate osteoclast apoptosis. *Biochemical and Biophysical Research Communications*, 2000. **268**(3): p. 899-903.
- 90. Hofer, A.M., *et al.*, Intercellular communication mediated by the extracellular calcium-sensing receptor. *Nature Cell Biology*, 2000. **2**(7): p. 392.
- 91. Hills, C.E., *et al.*, Calcium-sensing receptor activation increases cell-cell adhesion and β-cell function. *Cellular Physiology and Biochemistry*, 2012. **30**(3): p. 575-586.
- 92. Gray, E., *et al.*, Activation of the extracellular calcium-sensing receptor initiates insulin secretion from human islets of Langerhans: involvement of protein kinases. *Journal of Endocrinology*, 2006. **190**(3): p. 703-710.
- 93. Kitsou-Mylona, I., *et al.*, A role for the extracellular calcium-sensing receptor in cell-cell communication in pancreatic islets of Langerhans. *Cellular Physiology and Biochemistry*, 2008. **22**(5-6): p. 557-566.
- 94. Calabrese, A., *et al.*, Connexin 36 controls synchronization of Ca²⁺ oscillations and insulin secretion in MIN6 cells. *Diabetes*, 2003. **52**(2): p. 417-424.
- 95. Grodsky, G.M. and L.L. Bennett, Cation requirements for insulin secretion in the isolated perfused pancreas. *Diabetes*, (1966): 910-910
- 96. Rorsman, P., *et al.*, Reduction of the cytosolic calcium activity in clonal insulin-releasing cells exposed to glucose. *Bioscience Reports*, 1983. **3**(10): p. 939-946.
- 97. Rutter, G.A., *et al.*, Stimulated Ca²⁺ influx raises mitochondrial free Ca²⁺ to supramicromolar levels in a pancreatic beta-cell line. Possible role in glucose and agonist-induced insulin secretion. *Journal of Biological Chemistry*, 1993. **268**(30): p. 22385-22390.
- 98. Varadi, A. and G.A. Rutter, Dynamic imaging of endoplasmic reticulum Ca²⁺ concentration in insulin-secreting MIN6 cells using recombinant targeted cameleons. *Diabetes*, 2002. **51**(suppl 1): p. S190-S201.

- 99. Yi, L., *et al.*, Dual Detection System for Simultaneous Measurement of Intracellular Fluorescent Markers and Cellular Secretion. *Analytical Chemistry*, 2016. **88**(21): p. 10368-10373.
- 100. Ridgway, E.B. and C.C. Ashley, Calcium transients in single muscle fibers. *Biochemical and Biophysical Research Communications*, 1967. **29**(2): p. 229-234.
- 101. Tsien, R.Y., New calcium indicators and buffers with high selectivity against magnesium and protons: design, synthesis, and properties of prototype structures. *Biochemistry*, 1980. **19**(11): p. 2396-2404.
- 102. Grynkiewicz, G., M. Poenie, and R.Y. Tsien, A new generation of Ca²⁺ indicators with greatly improved fluorescence properties. *Journal of Biological Chemistry*, 1985. **260**(6): p. 3440-3450.
- 103. Rizzuto, R., *et al.*, Rapid changes of mitochondrial Ca²⁺ revealed by specifically targeted recombinant aequorin. *Nature*, 1992. **358**(6384): p. 325-327.
- 104. Miyawaki, A., *et al.*, Fluorescent indicators for Ca²⁺ based on green fluorescent proteins and calmodulin. *Nature*, 1997. **388**(6645): p. 882-887.
- 105. Dyachok, O., *et al.*, Glucose-induced cyclic AMP oscillations regulate pulsatile insulin secretion. *Cell Metabolism*, 2008. **8**(1): p. 26-37.
- 106. Kindmark, H., *et al.*, Measurements of cytoplasmic free Ca²⁺ concentration in human pancreatic islets and insulinoma cells. *FEBS Letters*, 1991. **291**(2): p. 310-314.
- 107. Tsien, R.Y., A non-disruptive technique for loading calcium buffers and indicators into cells. *Nature*, 1981. **290**(5806): p. 527-528.
- 108. Moura, A., Membrane potential and intercellular calcium during glucose challenge in mouse islet of Langerhans. *Biochemical and Biophysical Research Communications*, 1995. **214**(3): p. 798-802.
- 109. Verkhratsky, A. and O.H. Petersen, *Calcium Measurement Methods*. 2010: Springer.
- 110. Tsien, R. and T. Pozzan, Measurement of cytosolic free Ca²⁺ with quin-2. *Methods in Enzymology*, 1989. **172**: p. 230-262.
- 111. Barreto-Chang, O.L. and R.E. Dolmetsch, Calcium imaging of cortical neurons using Fura-2 AM. *JoVE (Journal of Visualized Experiments)*, 2009(23): p. e1067.
- 112. Valeur, B. and M.N. Berberan-Santos, *Molecular fluorescence: principles and applications*. 2012: John Wiley & Sons.

- 113. Rorsman, P., *et al.*, Dual effects of glucose on the cytosolic Ca²⁺ activity of mouse pancreatic β-cells. *FEBS Letters*, 1984. **170**(1): p. 196-200.
- 114. Martin, F. and B. Soria, Glucoseminduced [Ca²⁺]_i oscillations in single human pancreatic islets. *Cell Calcium*, 1996. **20**(5): p. 409-414.
- 115. Kindmark, H., *et al.*, Oscillations in cytoplasmic free calcium concentration in human pancreatic islets from subjects with normal and impaired glucose tolerance. *Diabetologia*, 1994. **37**(11): p. 1121-1131.
- 116. Hellman, B., *et al.*, Glucose induces oscillatory Ca²⁺ signalling and insulin release in human pancreatic beta cells. *Diabetologia*, 1994. **37**(2): p. S11-S20.
- 117. Liu, Y.J., et al., Origin of slow and fast oscillations of Ca²⁺ in mouse pancreatic islets. *The Journal of Physiology*, 1998. **508**(2): p. 471-481.
- 118. Nunemaker, C.S., *et al.*, Glucose modulates [Ca²⁺]_i oscillations in pancreatic islets via ionic and glycolytic mechanisms. *Biophysical Journal*, 2006. **91**(6): p. 2082-2096.
- Thang, M., et al., The Ca²⁺ dynamics of isolated mouse β-cells and islets: implications for mathematical models. *Biophysical Journal*, 2003. **84**(5): p. 2852-2870.
- 120. Beauvois, M.C., *et al.*, Glucose-induced mixed [Ca²⁺]_c oscillations in mouse β-cells are controlled by the membrane potential and the SERCA3 Ca²⁺-ATPase of the endoplasmic reticulum. *American Journal of Physiology-Cell Physiology*, 2006. **290**(6): p. C1503-C1511.
- 121. Luciani, D.S., S. Misler, and K.S. Polonsky, Ca²⁺ controls slow NAD (P) H oscillations in glucose-stimulated mouse pancreatic islets. *The Journal of Physiology*, 2006. **572**(2): p. 379-392.
- 122. Li, J., *et al.*, Oscillations of sub-membrane ATP in glucose-stimulated beta cells depend on negative feedback from Ca²⁺. *Diabetologia*, 2013. **56**(7): p. 1577-1586.
- 123. Spence, M.T. and I.D. Johnson, *The molecular probes handbook: a guide to fluorescent probes and labeling technologies*. 2010: Live Technologies Corporation.
- 124. Miyazaki, J.-I., *et al.*, Establishment of a pancreatic β-cell line that retains glucose-inducible insulin secretion: special reference to expression of glucose transporter isoforms. *Endocrinology*, 1990. **127**(1): p. 126-132.
- 125. He, L., et al., Fluorescent chemosensors manipulated by dual/triple interplaying sensing mechanisms. *Chemical Society Reviews*, 2016. **45**(23): p. 6449-6461.

- 126. Wu, J., et al., New sensing mechanisms for design of fluorescent chemosensors emerging in recent years. *Chemical Society Reviews*, 2011. **40**(7): p. 3483-3495.
- 127. De Silva, A.P., *et al.*, Signaling recognition events with fluorescent sensors and switches. *Chemical Reviews*, 1997. **97**(5): p. 1515-1566.
- 128. Thomas, D., *et al.*, A comparison of fluorescent Ca²⁺ indicator properties and their use in measuring elementary and global Ca²⁺ signals. *Cell Calcium*, 2000. **28**(4): p. 213-223.
- 129. Bassnett, S., L. Reinisch, and D.C. Beebe, Intracellular pH measurement using single excitation-dual emission fluorescence ratios. *American Journal of Physiology-Cell Physiology*, 1990. **258**(1): p. C171-C178.
- 130. Perry, J.L., *et al.*, Use of genetically-encoded calcium indicators for live cell calcium imaging and localization in virus-infected cells. *Methods*, 2015. **90**: p. 28-38.
- 131. Rizzuto, R., *et al.*, Rapid changes of mitochondrial Ca²⁺ revealed by specifically targeted recombinant aequorin. *Nature*, 1992. **358**(6384): p. 325-327.
- 132. Nakazaki, M., *et al.*, Repetitive mitochondrial Ca²⁺ signals synchronize with cytosolic Ca²⁺ oscillations in the pancreatic beta-cell line, MIN6. *Diabetologia*, 1998. **41**(3): p. 279-286.
- 133. Xia, Z. and J. Rao, Biosensing and imaging based on bioluminescence resonance energy transfer. *Current Opinion in Biotechnology*, 2009. **20**(1): p. 37-44.
- 134. Palmer, A.E., *et al.*, Ca²⁺ indicators based on computationally redesigned calmodulin-peptide pairs. *Chemistry & Biology*, 2006. **13**(5): p. 521-530.
- 135. Nakai, J., M. Ohkura, and K. Imoto, A high signal-to-noise Ca²⁺ probe composed of a single green fluorescent protein. *Nature Biotechnology*, 2001. **19**(2): p. 137-141.
- 136. Mank, M. and O. Griesbeck, Genetically encoded calcium indicators. *Chemical Reviews*, 2008. **108**(5): p. 1550-1564.
- 137. Filippin, L., *et al.*, Improved strategies for the delivery of GFP-based Ca²⁺ sensors into the mitochondrial matrix. *Cell Calcium*, 2005. **37**(2): p. 129-136.
- 138. Idevall-Hagren, O., *et al.*, cAMP mediators of pulsatile insulin secretion from glucose-stimulated single β-cells. *Journal of Biological Chemistry*, 2010. **285**(30): p. 23007-23018.
- 139. Ammann, D., *Ion-selective microelectrodes: principles, design and application*. Vol. 50.2013: Springer Science & Business Media.

- 140. Kühtreiber, W.M. and L.F. Jaffe, Detection of extracellular calcium gradients with a calcium-specific vibrating electrode. *The Journal of Cell Biology*, 1990. **110**(5): p. 1565-1573.
- 141. Luxardi, G., *et al.*, Measurement of extracellular ion fluxes using the ion-selective self-referencing microelectrode technique. *Journal of Visualized Experiments: JoVE*, 2015(99).
- 142. Perez-Armendariz, E. and I. Atwater, Glucose-evoked changes in [K⁺] and [Ca²⁺] in the intercellular spaces of the mouse islet of Langerhans, in *Biophysics of the Pancreatic* β-Cell. 1986, Springer. p. 31-51.
- 143. Whitaker, M., Calcium in Living Cells. Vol. 99. 2010: Academic Press.
- 144. Han, M., *et al.*, Cytoplasmic delivery of quantum dots via microelectrophoresis technique. *Electrophoresis*, 2021. **42**(11): p. 1247-1254.
- 145. Misler, S., *et al.*, Electrical activity and exocytotic correlates of biphasic insulin secretion from β-cells of canine islets of Langerhans: Contribution of tuning two modes of Ca²⁺ entry-dependent exocytosis to two modes of glucose-induced electrical activity. *Channels*, 2009. **3**(3): p. 181-193.
- 146. Kendall, J.M., R.L. Dormer, and A.K. Campbell, Targeting aequorin to the endoplasmic reticulum of living cells. Biochemical and Biophysical Research Communications, 1992. **189**(2): p. 1008-1016.
- 147. Brini, M., *et al.*, Transfected aequorin in the measurement of cytosolic Ca²⁺ concentration ([Ca²⁺]_c): A critical evaluation. *Journal of Biological Chemistry*, 1995. **270**(17): p. 9896-9903.
- 148. Palmer, A.E. and R.Y. Tsien, Measuring calcium signaling using genetically targetable fluorescent indicators. *Nature Protocols*, 2006. **1**(3): p. 1057-1065.
- 149. Schefer, U., *et al.*, Neutral carrier based calcium(2+)-selective electrode with detection limit in the sub-nanomolar range. *Analytical Chemistry*, 1986. **58**(11): p. 2282-2285.
- 150. Suzuki, K., *et al.*, Design and synthesis of calcium and magnesium ionophores based on double-armed diazacrown ether compounds and their application to an ion sensing component for an ion-selective electrode. *Analytical Chemistry*, 1995. **67**(2): p. 324-334.
- 151. He, H., K. Jenkins, and C. Lin, A fluorescent chemosensor for calcium with excellent storage stability in water. *Analytica Chimica Acta*, 2008. **611**(2): p. 197-204.

- 152. Sui, B., *et al.*, A highly selective fluorescence turn-on sensor for extracellular calcium ion detection. *Chemistry-A European Journal*, 2016. **22**(30): p. 10351-10354.
- 153. Rusakov, D. and A. Fine, Extracellular Ca²⁺ depletion contributes to fast activity-dependent modulation of synaptic transmission in the brain. *Neuron*, 2003. **37**(2): p. 287-297.
- 154. Ishiwari, F., *et al.*, Bioinspired design of a polymer gel sensor for the realization of extracellular Ca²⁺ imaging. *Scientific Reports*, 2016. **6**.
- 155. Gao, M., *et al.*, Aggregation-induced emission probe for light-up and *in situ* detection of calcium ions at high concentration. *ACS Applied Materials & Interfaces*, 2018. **10**(17): p. 14410-14417.
- 156. Takesako, K., *et al.*, Low-affinity fluorescent indicator for intracellular calcium ions. *Analytical Communications*, 1997. **34**(12): p. 391-392.
- 157. Zhan, R., *et al.*, AIE polymers: synthesis, properties, and biological applications. *Macromolecular Bioscience*, 2016.
- 158. Moirangthem, M., *et al.*, An optical sensor based on a photonic polymer film to detect calcium in serum. *Advanced Functional Materials*, 2016. **26**(8): p. 1154-1160.
- 159. Ding, Y., *et al.*, A high-throughput fluorimetric microarray with enhanced fluorescence and suppressed "coffee-ring" effects for the detection of calcium ions in blood. *Scientific Reports*, 2016. **6**: p. 38602.
- 160. Li, E.S. and M.S. Saha, Optimizing calcium detection methods in animal systems: a sandbox for synthetic biology. *Biomolecules*, 2021. **11**(3): p. 343.
- 161. Kim, S., *et al.*, Bioinspired colorimetric detection of calcium (II) ions in serum using calsequestrin-functionalized gold nanoparticles. *Angewandte Chemie*, 2009. **121**(23): p. 4202-4205.
- 162. Si, D., *et al.*, Nanoparticle PEBBLE sensors for quantitative nanomolar imaging of intracellular free calcium ions. *Analytical Chemistry*, 2012. **84**(2): p. 978.
- 163. Yang, C., *et al.*, Continuous fluorescence imaging of intracellular calcium by use of ion-selective nanospheres with adjustable spectra. *ACS Applied Materials & Interfaces*, 2016. **8**(31): p. 19892-19898.

- 164. Bagheri, M. and M.Y. Masoomi, Sensitive ratiometric fluorescent Mmetal-organic framework sensor for calcium signaling in human blood ionic concentration media. *ACS Applied Materials & Interfaces*, 2020. **12**(4): p. 4625-4631.
- 165. Sun, Y. and Y. Xia, Shape-controlled synthesis of gold and silver nanoparticles. *Science*, 2002. **298**(5601): p. 2176-2179.
- 166. Reynolds, A.J., A.H. Haines, and D.A. Russell, Gold glyconanoparticles for mimics and measurement of metal ion-mediated carbohydrate—carbohydrate interactions. *Langmuir*, 2006. **22**(3): p. 1156-1163.
- 167. Clark, H.A., *et al.*, Subcellular optochemical nanobiosensors: probes encapsulated by biologically localised embedding (PEBBLEs). *Sensors and Actuators B: Chemical*, 1998. **51**(1): p. 12-16.
- 168. Buck, S.M., *et al.*, Nanoscale probes encapsulated by biologically localized embedding (PEBBLEs) for ion sensing and imaging in live cells. *Talanta*, 2004. **63**(1): p. 41-59.
- 169. Hun, X. and Z. Zhang, Preparation of a novel fluorescence nanosensor based on calcein-doped silica nanoparticles, and its application to the determination of calcium in blood serum. *Microchimica Acta*, 2007. **159**(3): p. 255-261.
- 170. Josefsen, L.B., *et al.*, Porphyrin-nanosensor conjugates. New tools for the measurement of intracellular response to reactive oxygen species. *Photochemical & Photobiological Sciences*, 2010. **9**(6): p. 801-811.
- 171. Webster, A., S.J. Compton, and J.W. Aylott, Optical calcium sensors: development of a generic method for their introduction to the cell using conjugated cell penetrating peptides. *Analyst*, 2005. **130**(2): p. 163-170.
- 172. Schulz, A., *et al.*, Dextran-coated silica nanoparticles for calcium-sensing. *Analyst*, 2011. **136**(8): p. 1722-1727.
- 173. Xie, X. and E. Bakker, Ion selective optodes: from the bulk to the nanoscale. *Analytical and Bioanalytical Chemistry*, 2015. **407**(14): p. 3899-3910.
- 174. Cui, Y., *et al.*, Luminescent functional metal–organic frameworks. *Chemical Reviews*, 2012. **112**(2): p. 1126-1162.
- 175. Li, B., *et al.*, Emerging multifunctional metal–organic framework materials. *Advanced Materials*, 2016. **28**(40): p. 8819-8860.

- 176. Kreno, L.E., *et al.*, Metal–organic framework materials as chemical sensors. *Chemical Reviews*, 2012. **112**(2): p. 1105-1125.
- 177. Tranchemontagne, D.J., *et al.*, Secondary building units, nets and bonding in the chemistry of metal–organic frameworks. *Chemical Society Reviews*, 2009. **38**(5): p. 1257-1283.
- 178. Lustig, W.P., *et al.*, Metal–organic frameworks: functional luminescent and photonic materials for sensing applications. *Chemical Society Reviews*, 2017. **46**(11): p. 3242-3285.
- 179. Lu, W.-G., *et al.*, Three-dimensional lanthanide anionic metal—organic frameworks with tunable luminescent properties induced by cation exchange. *Inorganic Chemistry*, 2009. **48**(15): p. 6997-6999.
- 180. Adewola, A.F., *et al.*, Microfluidic perifusion and imaging device for multi-parametric islet function assessment. *Biomedical Microdevices*, 2010. **12**(3): p. 409-417.
- 181. Silva, P.N., *et al.*, A microfluidic device designed to induce media flow throughout pancreatic islets while limiting shear-induced damage. *Lab on a Chip*, 2013. **13**(22): p. 4374-4384.
- 182. Tao, T., *et al.*, Engineering human islet organoids from iPSCs using an organ-on-chip platform. *Lab on a Chip*, 2019. **19**(6): p. 948-958.
- 183. Sokolowska, P., *et al.*, Islet-on-a-chip: Biomimetic micropillar-based microfluidic system for three-dimensional pancreatic islet cell culture. *Biosensors and Bioelectronics*, 2021. **183**: p. 113215.
- 184. Tan, W.-H. and S. Takeuchi, A trap-and-release integrated microfluidic system for dynamic microarray applications. *Proceedings of the National Academy of Sciences*, 2007. **104**(4): p. 1146-1151.
- 185. Sankar, K.S., *et al.*, Culturing pancreatic islets in microfluidic flow enhances morphology of the associated endothelial cells. *PloS One*, 2011. **6**(9): p. e24904.
- 186. Jun, Y., *et al.*, *In vivo*–mimicking microfluidic perfusion culture of pancreatic islet spheroids. *Science Advances*, 2019. **5**(11): p. eaax4520.
- 187. Schulze, T., *et al.*, A 3D microfluidic perfusion system made from glass for multiparametric analysis of stimulus-secretioncoupling in pancreatic islets. *Biomedical Microdevices*, 2017. **19**(3): p. 47.

- 188. Patel, S., *et al.*, Organoid microphysiological system preserves pancreatic islet function within 3D matrix. *Science Advances*, 2021. **7**(7): p. eaba5515.
- 189. Kin, T., *et al.*, Risk factors for islet loss during culture prior to transplantation. *Transplant International*, 2008. **21**(11): p. 1029-1035.
- 190. Ichii, H., et al., Shipment of Human Islets for Transplantation. American Journal of Transplantation, 2007. **7**(4): p. 1010-1020.
- 191. Misun, P.M., *et al.*, *In vitro* platform for studying human insulin release dynamics of single pancreatic islet microtissues at high resolution. *Advanced Biosystems*, 2020. **4**(3): p. 1900291.
- 192. Dhumpa, R., *et al.*, Measurement of the entrainment window of islets of Langerhans by microfluidic delivery of a chirped glucose waveform. *Integrative Biology*, 2015. **7**(9): p. 1061-1067.
- 193. Lu, S., C.E. Dugan, and R.T. Kennedy, Microfluidic chip with integrated electrophoretic immunoassay for investigating cell–cell interactions. *Analytical Chemistry*, 2018. 90(8): p. 5171-5178.
- 194. Nguyen, D.T.T., *et al.*, Endocrine system on chip for a diabetes treatment model. *Biofabrication*, 2017. **9**(1): p. 015021.
- 195. Thams, P. and K. Capito, Differential mechanisms of glucose and palmitate in augmentation of insulin secretion in mouse pancreatic islets. *Diabetologia*, 2001. **44**(6): p. 738-746.
- 196. Henquin, J.-C., Triggering and amplifying pathways of regulation of insulin secretion by glucose. *Diabetes*, 2000. **49**(11): p. 1751-1760.
- 197. Newsholme, P., *et al.*, Life and death decisions of the pancreatic β-cell: the role of fatty acids. *Clinical Science*, 2007. **112**(1): p. 27-42.
- 198. Xie, C., *et al.*, Enteroendocrine Hormone Secretion and Metabolic Control: Importance of the Region of the Gut Stimulation. *Pharmaceutics*, 2020. **12**(9): p. 790.
- 199. Huang, W.-K., *et al.*, Development of innovative tools for investigation of nutrient-gut interaction. *World Journal of Gastroenterology*, 2020. **26**(25): p. 3562.
- 200. Xing, Y., *et al.*, A pumpless microfluidic device driven by surface tension for pancreatic islet analysis. *Biomedical Microdevices*, 2016. **18**(5): p. 80.

- 201. Nam, Y.-J., *et al.*, Fabrication of glass micropipette device using reflow processes and its integration with microfluidic channels for patch clamp recording of cell. *IEEE Sensors Journal*, 2020. **20**(24): p. 14694-14702.
- 202. Agustini, D., M.F. Bergamini, and L.H. Marcolino-Junior, Tear glucose detection combining microfluidic thread based device, amperometric biosensor and microflow injection analysis. *Biosensors and Bioelectronics*, 2017. **98**: p. 161-167.
- 203. Wang, X., L. Yi, and M.G. Roper, Microfluidic device for the measurement of amino acid secretion dynamics from murine and human islets of Langerhans. *Analytical Chemistry*, 2016. **88**(6): p. 3369-3375.
- 204. Shackman, J.G., *et al.*, Dynamic monitoring of glucagon secretion from living cells on a microfluidic chip. *Analytical and Bioanalytical Chemistry*, 2012. **402**(9): p. 2797-2803.
- 205. Castiello, F.R., K. Heileman, and M. Tabrizian, Microfluidic perfusion systems for secretion fingerprint analysis of pancreatic islets: applications, challenges and opportunities. *Lab on a Chip*, 2016. **16**(3): p. 409-431.
- 206. Heilbrunn, L.V., Outline of general physiology. 1937.
- 207. Trebak, M. and J.-P. Kinet, Calcium signalling in T cells. *Nature Reviews Immunology*, 2019. **19**(3): p. 154-169.
- 208. Bading, H., Nuclear calcium signalling in the regulation of brain function. *Nature Reviews Neuroscience*, 2013. **14**(9): p. 593-608.
- 209. Monteith, G.R., N. Prevarskaya, and S.J. Roberts-Thomson, The calcium–cancer signalling nexus. *Nature Reviews Cancer*, 2017. **17**(6): p. 367.
- 210. Harr, M.W. and C.W. Distelhorst, Apoptosis and autophagy: decoding calcium signals that mediate life or death. *Cold Spring Harbor Perspectives in Biology*, 2010. **2**(10): p. a005579.
- 211. Seino, S., *et al.*, β-Cell signalling and insulin secretagogues: A path for improved diabetes therapy. *Diabetes, Obesity and Metabolism*, 2017. **19**: p. 22-29.
- 212. Speier, S., *et al.*, Noninvasive *in vivo* imaging of pancreatic islet cell biology. *Nature Medicine*, 2008. **14**(5): p. 574-578.
- 213. Salem, V., *et al.*, Leader β-cells coordinate Ca²⁺ dynamics across pancreatic islets *in vivo*. *Nature Metabolism*, 2019. **1**(6): p. 615-629.

- 214. Reissaus, C.A., *et al.*, A versatile, portable intravital microscopy platform for studying beta-cell biology *in vivo. Scientific Reports*, 2019. **9**(1): p. 8449.
- 215. Chen, S., *et al.*, *In vivo* ZIMIR imaging of mouse pancreatic islet cells shows oscillatory insulin secretion. *Frontiers in Endocrinology*, 2021. **12**: p. 613964.

CHAPTER 3: DISPARITIES IN THE GLYCAEMIC
AND INCRETIN RESPONSES TO
INTRADUODENAL GLUCOSE INFUSION
BETWEEN HEALTHY YOUNG MEN AND
WOMEN

Statement of Authorship

Title of the paper	Disparities in the glycaemic and incretin responses to intraduodenal glucose infusion between healthy young men and women
Publication status	Published
Publication details	Xie, C., Huang, W., Sun, Y., Xiang, C., Trahair, L., Jones, KL., Horowitz, M., Rayner, CK., Wu, T. (2023). "Disparities in the glycaemic and incretin responses to intraduodenal glucose infusion between healthy young men and women", <i>The Journal of Clinical Endocrinology & Metabolism</i> , dgad176

Principal Author

Candidate	Weikun Huang			
Contribution	Data collection and interpretation, methodology development, statistical analysis and drafting of the manuscript			
Overall percentage	35%			
Certification	This paper reports on original research I conducted during the period of my Higher Degree by Research candidature and is not subject to any obligations or contractual agreements with a third party that would constrain its inclusion in this thesis. I am the second primary author of this paper			
Signature		Date	September 2023	

Co-Author Contributions

By signing the Statement of Authorship, each author certifies that: i) the candidate's stated contribution to the publication is accurate (as detailed above); ii) permission is granted for the candidate to include the publication in the thesis; and iii) the sum of all co-author contributions is equal to 100% less the candidate's stated contribution.

Name of Co-Author	Cong Xie		
Contribution	Data collection and interpretation, statistical analysis and drafting of the manuscript.		
Signature		Date	September 2023

Name of Co-Author	Yixuan Sun			
Contribution	Data collection and review of the manuscript			
Signature		Date	September 2023	
Name of Co-Author	Chunjie Xiang			
Contribution	Data collection and review of the manuscript			
Signature		Date	September 2023	
Name of Co-Author	Laurence Trahair			
Contribution	Data interpretation and reviewing of the manuscript.			
Signature		Date	September 2023	
Name of Co-Author	Karen L. Jones			
Contribution	Data interpretation and reviewing of the manuscript.			
Signature		Date	September 2023	
Name of Co-Author	Michael Horowitz			
Contribution	Data interpretation and reviewing of the manuscript.			
Signature		Date	September 2023	
Name of Co-Author	Christopher K. Rayner			
Contribution	Conception and design of the study, data interpretation, reviewing of the manuscript, and guarantor of the paper.			
Signature		Date	September 2023	

Name of Co-Author	Tongzhi Wu					
Contribution	Conception and design of the study, data interpretation, reviewing of the manuscript, and guarantor of the paper.					
Signature		Date	September 2023			

3.1 Abstract

Pre-menopausal women are at a lower risk of type 2 diabetes (T2D) compared to men, but the underlying mechanism(s) remain elusive. The secretion of the incretin hormones, glucose-dependent insulinotropic polypeptide (GIP) and glucagon-like peptide-1 (GLP-1), from the small intestine is a major determinant of glucose homeostasis and may be influenced by sex. This study compared blood glucose and plasma insulin and incretin responses to intraduodenal glucose infusions in healthy young males and females. In Study 1, 9 women and 20 men received an intraduodenal glucose infusion at 2 kcal/min for 60 minutes. In Study 2, 10 women and 26 men received an intraduodenal glucose at 3 kcal/min for 60 minutes. Venous blood was sampled every 15 minutes for measurements of blood glucose, and plasma insulin, GLP-1 and GIP. In response to intraduodenal glucose at 2 kcal/min, the incremental area under the curve between t=0-60 minutes (iAUC_{0-60min}) for blood glucose and plasma GIP did not differ between the two groups. However, $iAUC_{0-60min}$ for plasma GLP-1 (P = 0.016) and insulin (P = 0.011) were ~2-fold higher in women than men. In response to intraduodenal glucose at 3 kcal/min, iAUC_{0-60min} for blood glucose, plasma GIP and insulin did not differ between women and men, but GLP-1 iAUC $_{0-60 \text{min}}$ was 2.5-fold higher in women (P = 0.012). Healthy young women exhibit comparable GIP but a markedly greater GLP-1 response to intraduodenal glucose than men. This disparity warrants further investigations to delineate the underlying mechanisms and may be of relevance to the reduced risk of diabetes in pre-menopausal women when compared to men.

Keywords: type 2 diabetes, blood glucose, incretin hormones, insulin, intraduodenal glucose, gender

3.2 Introduction

Compared with men, the risk of type 2 diabetes (T2D) is noticeably lower in women, particularly when the later are in the pre-menopausal phase [1-3]. Furthermore, in post-menopausal women, hormone replacement therapy (i.e. oestrogen and progestin) is associated with a reduced risk of T2D [4]. These observations are indicative of a sex-driven disparity in glucose metabolism.

There is recent evidence that oestrogen signalling is coupled to the secretion of the incretin hormone, glucagon-like peptide-1 (GLP-1), which, together with glucose-dependent

insulinotropic polypeptide (GIP), modulates the secretion of both insulin and glucagon from the pancreatic islets to drive glucose disposal in health and T2D [5]. For example, in ovariectomised mice, there are impairments in GLP-1 and insulin secretion, as well as glucose tolerance [6], while supplementation of oestradiol in ovariectomised mice augments GLP-1 secretion, associated with increased insulin, suppressed glucagon and improved glucose tolerance [6]. Moreover, 10-week treatment with oestradiol in a rodent model of menopause reduced energy intake and body weight, effects which were markedly attenuated by the GLP-1 receptor antagonist, exendin(9-39). These observations provide a strong support for an 'oestrogen-GLP-1' pathway in modulating metabolic health [7].

In humans, both GLP-1 and GIP are secreted mainly in response to meals, as a result of direct interaction between ingested nutrients and enteroendocrine L- and K-cells scattered along the gastrointestinal tract. There is a specific threshold, between 1-2 kcal/min, for glucose-induced GLP-1 secretion in the small intestine [8], while the secretion of GIP is more sensitive, which could be triggered by lesser glucose in the small intestine [8, 9]. In contrast to animal models, the impact of sex on nutrient-induced GLP-1 and GIP secretion has not been well studied and limited clinical studies have yielded inconsistent findings. It was reported that the postprandial GLP-1 response after a standardised breakfast is 50% higher in normal-weight young women than men [10]. In combined analyses of subjects with and without T2D, plasma GLP-1 levels following 75 g oral glucose, or a mixed meal were reported to be higher in women than men [11, 12]. In another study, while the GLP-1 response to 75 g oral glucose was ~20% higher in normoglycaemic women than men, there was no difference in GLP-1 secretion between men and women with prediabetes and T2D [13]. In pre-menopausal healthy women, the GLP-1 levels in response to 50 g oral glucose were shown to be substantially higher during the luteal than follicular phase [14]. However, it should also be appreciated that these studies did not take into account variation in the rate of gastric emptying, which exhibits a substantial inter-individual, but much lesser intra-individual, variation (~1-4 kcal/min) [15, 16], may be influenced by sex [17, 18] and, in women, the menstrual cycle [14, 19]. Consequently, any difference in gastric emptying, and by definition, exposure of nutrients to the small intestine, would affect the 'early' glycaemic response [16, 20, 21] and secretion of GLP-1 and GIP [8, 22-24]. For these reasons,

the lack of standardisation of gastric emptying may compromise the capacity to determine potential differences in GLP-1 and GIP secretion between men and women.

Accordingly, the current study compared plasma GLP-1 and GIP, as well as plasma insulin and blood glucose, in response to standardised intraduodenal glucose infusions, at two different rates within the physiological range of gastric emptying, between healthy young men and women.

3.3 Methods

3.3.1 Participants

We derived data from sixty-five healthy participants who were recruited from the community by advertisement for previous studies evaluating nutritional and/or pharmacological therapies for T2D [24-29]. Participants were excluded if they reported significant gastrointestinal symptoms, a history of gastrointestinal surgery, or a requirement for medication known to affect gastrointestinal function or appetite. Female participants who used oral contraceptives or were pregnant were also excluded. Participants were screened to exclude renal dysfunction (based on the estimated glomerular filtration rate) and/or liver disease (based on serum liver enzymes). The studies were approved by the Royal Adelaide Hospital Human Research Ethics Committee and conducted in accordance with the principles of the Declaration of Helsinki as revised in 2000, and all participants provided written informed consent.

3.3.2 Protocol

Healthy young female and male participants were evaluated in two independent experimental settings (i.e. Studies 1 & 2) (Table 1). In Study 1, 9 female and 20 male participants received an intraduodenal glucose infusion at a rate of 2 kcal/min. In Study 2, 10 female and 26 male participants received an intraduodenal glucose at 3 kcal/min. Female participants were studied exclusively during the follicular phase of the menstrual cycle to limit potential cyclical variations in gastrointestinal function [14]. All subjects were evaluated on a single study visit after refraining from strenuous physical activity for 24 hours and consuming a standardised evening meal (beef lasagne, McCain Foods, Victoria, Australia; 591 kcal) at 19: 00 pm the previous evening. Following the latter, subjects were instructed to abstain from food and nutrient

beverages, but were allowed to drink water until midnight, before attending our clinical research laboratory at The University of Adelaide the following day at ~0800 h.

Upon arrival, a multi-lumen silicone catheter (Dentsleeve International, Ontario, Canada) was inserted transnasally and allowed to pass into the duodenum by peristalsis, with its position monitored continuously by measurement of the antral and duodenal transmucosal potential difference, as discussed previously [30, 31]. An infusion port was positioned \sim 12 cm distal to the pylorus. An intravenous cannula was inserted into a forearm vein, which was kept warm for repeated sampling of 'arterialised' venous blood. Subsequently, a standardised glucose solution was infused via the infusion port at a rate of either 2 kcal/min (Study 1) or 3 kcal/min (Study 2) between t = 0 to 60 minutes. Blood samples were collected at t = 0, 15, 30, 45 and 60 minutes for measurements of blood glucose and plasma insulin, total GIP and GLP-1 concentrations. At the end of each study visit, participants were given a meal before they were discharged from the laboratory.

3.3.3 Measurement of blood glucose and plasma insulin, total GIP and GLP-1

Blood glucose concentrations were assessed using a glucometer (Optium Xceed, Abbott Laboratories, USA), and reported as the mean of duplicate measurements at each time point. Plasma insulin was measured by ELISA immunoassay (RRID: AB_287762, 10-1113, Mercodia, Uppsala, Sweden) with a sensitivity of 1.0 mU/L and intra- and inter-assay coefficients of variation (CVs) of 3.2% and 4.7%. Plasma total GIP was measured by radioimmunoassay (RRID: AB_518352) with some modifications of a previously published method [32]. The standard curve was prepared in buffer rather than extracted charcoal stripped serum and the radio-iodinated label was supplied by Perkin Elmer (Boston, MA, USA). The standard curve was prepared in buffer rather than extracted charcoal-stripped serum, and the radio-iodinated label was supplied by PerkinElmer. The sensitivity of the assay was 2 pmol/L, and the intra- and inter-assay CVs were 6.1% and 15.4%, respectively. Plasma total GLP-1 concentrations were measured by radioimmunoassay (RRID: AB_2757816, GLPIT-36HK; Millipore, Billerica, 1447475M

A, USA) with a sensitivity of 3 pmol/L and intra- and inter-assay CVs of 4.2% and 10.5%, respectively.

3.3.4 Statistical analysis

The incremental areas under the curve (iAUCs) (calculated as the total AUCs subtracting the baseline value) for blood glucose and plasma hormones were calculated using the trapezoidal rule. Demographic data for male and female subjects were compared using unpaired Student's t-tests after confirming the normality of distribution. Fasting blood glucose and plasma hormone concentrations and their iAUCs during intraduodenal glucose infusions in male and female participants were compared using unpaired Student's t-tests, or Mann-Whitney U tests if data were not normally distributed, before and after adjustment for body weight or BMI. The relationships of GLP-1 iAUC_{0-60min} with BMI and body weight in men were evaluated using univariate linear regression analysis. Blood glucose and plasma hormone responses to intraduodenal glucose infusions were also evaluated by two-way repeated measures analysis of variance (ANOVA) using group and time as factors. *Post hoc* comparisons, adjusted for multiple comparisons by Bonferroni's correction, were performed if ANOVAs revealed significant interactions. All analyses were performed using Prism 9.4 software (GraphPad, La Jolla, CA, USA). Data are presented as means ± SEM or medians (25% and 75% interquartile ranges); P < 0.05 was considered statistically significant.

3.4 Results

The demographic data of subjects in both studies are summarised in Table 1. There was no difference in age (female vs. male: 25.0 (21.5, 26.0) vs. 21.0 (19.0, 27.8) years, P = 0.19, in Study 1, and 25.0 (21.8, 27.0) vs. 23.5 (21.0, 28.0) years, P = 0.50, in Study 2) or BMI (female vs. male: 21.5 (20.1, 23.7) vs. 22.7 (21.8, 24.2) kg/m², P = 0.28, in Study 1, and 23.2 (20.2, 31.5) vs. 24.3 (22.7, 28.3) kg/m², P = 0.51, in Study 2) between female and male participants in either study (Table 1). However, in Study 1, female participants had a significantly lower body weight (55.0 (51.5, 62.3) vs. 67.8 (65.3, 79.5) kg, P = 0.001), and a trend for a lower body weight in Study 2 (71.4 \pm 7.1 vs. 82.7 \pm 4.8 kg, P = 0.09).

	Study 1 (intraduodenal glucose at 2 kcal/min)				Study 2 (intraduodenal glucose at 3 kcal/min)					
	Female (n = 9)	Male (n = 20)	P (no correction	P (corrected for body weight)	P (corrected for BMI)	Female (n = 10)	Male (n = 26)	P (no correction)	P (corrected for body weight)	P (corrected for BMI)
Age (years)	25.0 (21.5, 26.0)	21.0 (19.0, 27.8)	0.19	-	-	25.0 (21.8, 27.0)	23.5 (21.0, 28.0)	0.50	-	-
Weight (kg)	57.1 ± 2.9	72.9 ± 4.1	0.001	-	-	62.3 (54.3, 92.6)	73.8 (67.1, 90.1)	0.09	-	-
BMI (kg/m²)	21.5 (20.1, 23.7)	22.7 (21.8, 24.2)	0.28	-	-	23.2 (20.2, 31.5)	24.3 (22.7, 28.3)	0.51	-	-
Fasting blood glucose (mmol/L)	5.3 ± 0.2	5.2 ± 0.4	0.95	0.32	0.47	5.4 ± 0.2	5.4 ± 0.1	0.83	0.93	0.81
Glucose iAUC _{0-60min} (mmol/L*min)	135.7 ± 13.9	144.2 ± 10.4	0.75	0.35	0.44	99.8 ± 11.7	110.4 ± 8.0	0.47	0.59	0.51
Fasting plasma insulin (mU/L)	2.9 ± 0.4	2.4 ± 0.3	0.45	0.33	0.48	4.7 (2.4, 6.8)	4.7 (2.4, 6.8) 5.0 (2.2, 13.3)		0.18	0.51
Insulin iAUC _{0-60min} (mU/L*min)	1631.3 (1278.4, 2137.9)	834.3 (66.24, 1114.1)	0.005	0.011	0.025	1738.9 (1345.9, 4772.1)	1897.1 (1093.1, 4252.5)	0.99	0.86	0.85
Fasting plasma GIP (pmol/L)	10.9 ± 1.7	10.3 ± 1.4	0.81	0.61	0.62	11.2 (7.5, 16.5)	11.5 (6.6, 14.5)	0.79	0.96	0.95
GIP iAUC _{0-60min} (pmol/L*min)	1283.9 ± 121.7	1352.1 ± 105.3	0.96	0.82	0.78	1006.2 ± 131.6	1030.3 ± 68.6	0.86	0.74	0.83
Fasting plasma GLP-1 (pmol/L)	19.5 ± 2.0	23.0 ± 1.5	0.17	0.08	0.07	16.7 (14.6, 19.6)	15.7 (10.3, 20.7)	0.46	0.61	0.63
GLP-1 iAUC _{0-60min} (pmol/L*min)	524.8 ± 104.6	264.3 ± 57.2	0.025	0.016	0.039	640.5 (280.2, 1002.4)	205.5 (87.8, 274.3)	0.011	0.012	0.005

Table 1. Characteristics of study participants

Note: Normally distributed data are expressed as means \pm SEM, while data that are not normally distributed are expressed as median (25% and 75% interquartile range)

3.4.1 Blood glucose

Fasting blood glucose concentrations did not differ between the two groups in either study (Table 1). In both studies, during intraduodenal glucose infusion (t = 0-60 minutes), blood glucose increased progressively (time effect: P < 0.001 for each group), without a difference between the two groups (Study 1: P = 0.87 for group difference; Study 2: P = 0.35 for group difference, Figure 1A-B). Similarly, the blood glucose iAUC_{0-60min} did not differ between the two groups before, or after adjustment for body weight or BMI in either study (Table 1).

3.4.2 Plasma insulin

Fasting plasma insulin concentrations did not differ between the two groups in either study (Table 1). During intraduodenal glucose infusion (t = 0-60 minutes), plasma insulin increased progressively in both groups (time effect: P < 0.001 for each), with concentrations being higher in female than male subjects in Study 1 (group effect: P = 0.006, group by time interaction: P < 0.001), with a significant difference at t = 60 minutes, Figure 1C), but not in Study 2 (group effect: P = 0.97, group by time interaction: P = 0.74). Similarly, the insulin iAUC_{0-60min} was greater in female than male participants both before and after adjustment for body weight or BMI in Study 1, without any difference in Study 2 (Table 1).

3.4.3 Plasma total GIP

Fasting plasma total GIP did not differ between the two groups in either study (Table 1). During intraduodenal glucose infusion (t = 0-60 minutes), plasma GIP increased promptly and plateaued between t = 30-60 minutes (time effect: P < 0.001 each), without any difference between the two groups in either study (Study 1: P = 0.83 for group difference, P = 0.97 for group by time interaction; Study 2: P = 0.79 for group difference, P = 0.81 for group by time interaction, Figure 1 E-F). Similarly, the GIP iAUC_{0-60min} did not differ between the two groups, before or after adjustment for body weight or BMI, in either study (Table 1).

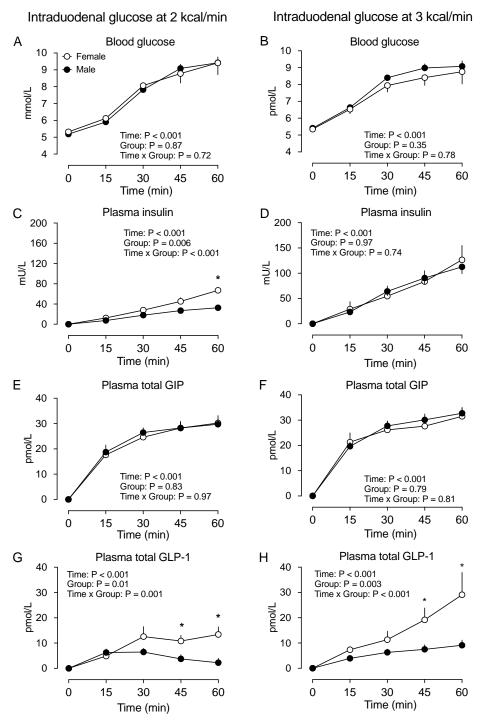


Figure 1. Blood glucose (A-B), plasma insulin (C-D), plasma total GIP (E-F), and plasma total GLP-1 (G-H) concentrations in response to intraduodenal glucose infusion at 2 kcal/min and 3 kcal/min in healthy male and female participants. Two-factor repeated-measures ANOVA, with group and time as factors, was used to compare the differences between males and females. *P < 0.05 for males vs. females. *Post hoc* comparisons, adjusted for multiple comparisons by Bonferroni's correction, were performed if ANOVAs revealed significant interactions. Data are means \pm SEM

3.4.4 Plasma total GLP-1

Fasting plasma total GLP-1 did not differ between the two groups in either study (Table 1). During intraduodenal glucose infusion at 2 kcal/min (t = 0-60 minutes), plasma total GLP-1 increased marginally in the first 30 minutes, but subsequently returned to the baseline level in male participants (time effect: P < 0.001). However, there were marked and sustained increases in plasma GLP-1 in female participants (time effect: P < 0.001). Accordingly, the GLP-1 response was greater in females (P = 0.01 for group difference; P = 0.001 for group by time interaction, with significant differences between t = 45-60 minutes). During intraduodenal glucose infusion at 3 kcal/min (t = 0-60 minutes), plasma total GLP-1 increased progressively in both male and female participants (time effect: P < 0.001 for each), with the magnitude of increase being substantially greater in females (P = 0.003 for group difference, P < 0.001 for group by time interaction, with significant differences between t = 45 to 60 minutes (Figure 1 G-H). The GLP-1 iAUC_{0-60min} was also greater in females, both before and after adjustment for body weight or BMI, in both studies (Table 1).

3.5 Discussion

The current study showed that the secretion of GLP-1 in response to small intestinal glucose infusion (at either 2 or 3 kcal/min) was substantially greater in healthy women than men. Although the latter was not accompanied by any difference in blood glucose, due probably to compensation for glucose disposal by other gluco-regulatory mechanisms in these healthy young participants, the sex-related disparity in GLP-1 secretion warrants further investigations to delineate the underlying mechanisms and clarify its relevance to the risk of T2D.

The use of intraduodenal infusions allowed standardisation of small intestinal exposure to glucose, by circumventing the influence of gastric emptying on postprandial incretin hormone secretion. The rates of intraduodenal glucose infusion, i.e. 2 and 3 kcal/min, were within the physiological range of gastric emptying, and were well tolerated. We observed that the plasma total GIP levels increased rapidly and plateaued after t = 30 minutes of intraduodenal glucose infusion, with a similar response to glucose infusion at 2 and 3 kcal/min. This secretory pattern of GIP is consistent with the distribution of GIP-releasing K-cells in the proximal small intestine

[5, 33]. By contrast, plasma GLP-1 was modestly elevated in response to glucose infusion at 2 kcal/min, and increased progressively following glucose infusion at 3 kcal/min, reflecting the need for glucose to exceed the absorptive capacity of the proximal small intestine and reach more distal regions of the intestine, where GLP-1-releasing L-cells predominate [5, 33].

Previous studies evaluating incretin responses to orally ingested meals or glucose have reported a modestly higher GLP-1 secretion (~20-50%) in women than men [10-13] or no difference between women and men [13, 34]. In the present study, we observed a profoundly higher GLP-1 response to intraduodenal glucose (at both 2 and 3 kcal/min) in healthy young women than men (>2 fold). The discrepancy between current and previous findings is likely to be attributable to the different study design. As discussed, gastric emptying varies substantially between individuals [16], and is often slower in women than age-matched men [17, 18], which would influence the nutrient exposure to the small intestine and confound comparisons of the secretory capacity of GLP-1 between women and men. In a previous study in healthy young women, the GLP-1 response to a 50 g oral glucose drink was found to be substantially greater during the luteal vs. follicular phase, in association with slower gastric emptying and attenuated postprandial blood glucose levels [14]. In the current study, female participants were evaluated in the follicular phase; it is, therefore, likely that the sex-related difference in GLP-1 response to intraduodenal glucose infusions could have been greater if female participants were studied in the luteal phase.

By contrast, we did not observe any sex-related disparity in GIP secretion in response to intraduodenal glucose. However, we noted that intraduodenal glucose infusions at 2 and 3 kcal/min appeared already to have achieved near-maximal GIP responses [24], which may have limited our ability to differentiate GIP secretion between the two groups.

Despite the differences in GLP-1 secretion in both experimental settings, insulin secretion was only modestly higher in women than men, following intraduodenal glucose infusion at 2 kcal/min, and there was no significant difference in blood glucose concentrations between the two groups in either setting. These observations may have reflected the fact that GIP is the major incretin hormone in health, and that other gluco-regulatory mechanisms beyond GLP-1 are involved in glucose disposal in healthy young participants. It is also plausible that the

observation window for blood glucose was too brief (only 60 minutes, within which blood glucose had not returned to baseline) to detect any potential differentiation in blood glucose.

Although the insulinotropic action of endogenous GIP is markedly diminished in T2D [31], the action of GLP-1 is largely preserved [5]. In a given individual, the greater GLP-1 response to small intestinal nutrient stimulation is also predictive of slower gastric emptying [35], which is highly desirable for limiting postprandial glycaemic excursions in the management of T2D [16, 21]. Dietary and/or pharmacological interventions that stimulate GLP-1 secretion are effective for slowing gastric emptying and reducing postprandial glycaemia in T2D [36-39]. Accordingly, the sex-related disparity in GLP-1 secretion may be relevant to glucose disposal in the context of dysglycaemia and T2D risk between women and men, and gaining an understanding of the underlying mechanism(s) may reveal novel therapeutic strategies for boosting endogenous GLP-1 secretion.

Preclinical evidence suggests a major role of oestrogen signalling in the incretin axis. In mice, ovariectomy is associated with a marked reduction in postprandial GLP-1 secretion, which can be restored by oestradiol replacement [6]. It would therefore be of interest to investigate whether the onset of menopause decreases GLP-1 secretion and, if so, whether oestrogen replacement therapy (or targeted activation of the intestinal oestrogen receptor) would correct this defect.

Several limitations should be noted in the current study. First, only young healthy male and female participants were enrolled. Generalisation of our findings to a wider population should be undertaken with caution. For example, there is evidence that both fasting and postprandial GLP-1 levels are reduced, at least modestly, with ageing [40]. Second, our sample size was relatively small, however, the findings were clear-cut. Third, although the cofounding factor of gastric emptying was circumvented, small intestinal transit which is likely to be a determinant of the nutrient-induced GLP-1 response was not evaluated in the current study. Fourthly, dietary patterns, which may also affect gastric motility [41] and incretin responses [42], were not evaluated. Fifth, the current study evaluated incretin responses to glucose only. Future studies involving other macronutrients or physiological meals are therefore warranted. Finally, we noted that, although BMI was well matched between the two groups in both study settings, female participants had lower body weight and hence less body fluid volume, which potentially

represents a confounder for the evaluation of plasma hormone concentrations. However, correction for body weight did not alter our conclusions. Moreover, we did not find any relationship between BMI/body weight and GLP-1 iAUC_{0-60min} in men (data not shown). Accordingly, we believe that the differences in body weight between the two groups are unlikely to be of major relevance to their disparate GLP-1 responses.

In summary, we have demonstrated that healthy young women exhibited comparable GIP and blood glucose, but a greater GLP-1 response, to intraduodenal glucose infusions at 2 and 3 kcal/min than men. These observations are indicative of a major disparity in GLP-1 secretion between women and men, which warrants further investigation of the underlying mechanisms and the relevance to the risk of impaired glucose tolerance and T2D.

3.6 References

- 1. International Diabetes Federation. *IDF Diabetes Atlas*, 10th edn. Brussels, Belgium: 2021.
- 2. Tramunt, B., *et al.* Sex differences in metabolic regulation and diabetes susceptibility. *Diabetologia* **63**, 453-461 (2020).
- 3. Heianza, Y., *et al.* Effect of postmenopausal status and age at menopause on type 2 diabetes and prediabetes in Japanese individuals: Toranomon Hospital Health Management Center Study 17 (TOPICS 17). *Diabetes Care* **36**, 4007-4014 (2013).
- 4. Margolis, K.L., *et al.* Effect of oestrogen plus progestin on the incidence of diabetes in postmenopausal women: results from the Women's Health Initiative Hormone Trial. *Diabetologia* **47**, 1175-1187 (2004).
- 5. Wu, T., Rayner, C.K. & Horowitz, M. Incretins. *Handbook of Experimental Pharmacology* **233**, 137-171 (2016).
- 6. Handgraaf, S., Dusaulcy, R., Visentin, F., Philippe, J. & Gosmain, Y. 17-beta Estradiol regulates proglucagon-derived peptide secretion in mouse and human alpha- and L cells. *JCI Insight* 3(2018).
- 7. Asarian, L., *et al.* Estradiol increases body weight loss and gut-peptide satiation after Roux-en-Y gastric bypass in ovariectomized rats. *Gastroenterology* **143**, 325-327 e322 (2012).

- 8. Schirra, J., *et al.* Gastric emptying and release of incretin hormones after glucose ingestion in humans. *Journal of Clinical Investigation* **97**, 92-103 (1996).
- 9. Horowitz, M., Edelbroek, M.A.L., Wishart, J.M. & Straathof, J.W. Relationship between oral glucose tolerance and gastric emptying in normal healthy subjects. *Diabetologia* **36**, 857-862 (1993).
- 10. Adam, T.C. & Westerterp-Plantenga, M.S. Nutrient-stimulated GLP-1 release in normal-weight men and women. *Hormone and Metabolic Research* **37**, 111-117 (2005).
- 11. Toft-Nielsen, M.B., *et al.* Determinants of the impaired secretion of glucagon-like peptide-1 in type 2 diabetic patients. *Journal of Clinical Endocrinology and Metabolism* **86**, 3717-3723 (2001).
- 12. Vollmer, K., *et al.* Predictors of incretin concentrations in subjects with normal, impaired, and diabetic glucose tolerance. *Diabetes* **57**, 678-687 (2008).
- 13. Faerch, K., *et al.* GLP-1 Response to Oral Glucose Is Reduced in Prediabetes, Screen-Detected Type 2 Diabetes, and Obesity and Influenced by Sex: The ADDITION-PRO Study. *Diabetes* **64**, 2513-2525 (2015).
- 14. Brennan, I.M., *et al.* Effects of the phases of the menstrual cycle on gastric emptying, glycemia, plasma GLP-1 and insulin, and energy intake in healthy lean women. *American Journal of Physiology-Gastrointestinal and Liver Physiology* **297**, G602-610 (2009).
- 15. Horowitz, M., *et al.* Relationships between oesophageal transit and solid and liquid gastric emptying in diabetes mellitus. *European Journal of Nuclear Medicine* **18**, 229-234 (1991).
- 16. Watson, L.E., *et al.* Gastric emptying in patients with well-controlled type 2 diabetes compared with young and older control subjects without diabetes. *Journal of Clinical Endocrinology and Metabolism* **104**, 3311-3319 (2019).
- 17. Datz, F.L., Christian, P.E. & Moore, J. Gender-related differences in gastric emptying. *Journal of Nuclear Medicine* **28**, 1204-1207 (1987).
- 18. Hutson, W.R., Roehrkasse, R.L. & Wald, A. Influence of gender and menopause on gastric emptying and motility. *Gastroenterology* **96**, 11-17 (1989).
- 19. Horowitz, M., *et al.* The normal menstrual cycle has no effect on gastric emptying. *British Journal for Obstetrics Gynaecology* **92**, 743-746 (1985).

- 20. Jones, K.L., *et al.* Relationships between gastric-emptying, intragastric meal distribution and blood-glucose concentrations in diabetes-mellitus. *Journal of Nuclear Medicine* **36**, 2220-2228 (1995).
- 21. Xie, C., *et al.* Gastric emptying in health and type 2 diabetes: An evaluation using a 75 g oral glucose drink. *Diabetes Research and Clinical Practice* **171**, 108610 (2021).
- 22. Pilichiewicz, A.N., *et al.* Load-dependent effects of duodenal glucose on glycemia, gastrointestinal hormones, antropyloroduodenal motility, and energy intake in healthy men. *American Journal Physiology-Endocrinology and Metabolism* **293**, E743-753 (2007).
- 23. Ma, J., *et al.* Effects of variations in duodenal glucose load on glycaemic, insulin, and incretin responses in type 2 diabetes. *Diabetic Medicine* **29**, 604-608 (2012).
- 24. Trahair, L.G., *et al.* Comparative effects of variations in duodenal glucose load on glycemic, insulinemic, and incretin responses in healthy young and older subjects. *Journal of Clinical Endocrinology and Metabolism* **97**, 844-851 (2012).
- 25. Thazhath, S.S., *et al.* Effects of intraduodenal hydroxycitrate on glucose absorption, incretin release, and glycemia in response to intraduodenal glucose infusion in health and type 2 diabetes: A randomised controlled trial. *Nutrition* **32**, 553-559 (2016).
- 26. Zhang, X., *et al.* Comparative effects of proximal and distal small intestinal glucose exposure on glycemia, incretin hormone Ssecretion, and the incretin effect in health and type 2 diabetes. *Diabetes Care* **42**, 520-528 (2019).
- 27. Marathe, C.S., *et al.* Small intestinal glucose exposure determines the magnitude of the incretin effect in health and type 2 diabetes. *Diabetes* **63**, 2668-2675 (2014).
- 28. Chaikomin, R., *et al.* Effects of intraluminal local anesthetic on upper gastrointestinal motor, sensory, and peptide hormone responses to intraduodenal glucose. *European Journal of Gastroenterology & Hepatology* **21**, 258-265 (2009).
- 29. Chang, J., *et al.* Effects of intraduodenal glutamine on incretin hormone and insulin release, the glycemic response to an intraduodenal glucose infusion, and antropyloroduodenal motility in health and type 2 diabetes. *Diabetes Care* **36**, 2262-2265 (2013).

- 30. Xie, C., *et al.* Role of endogenous glucagon-like peptide-1 enhanced by vildagliptin in the glycaemic and energy expenditure responses to intraduodenal fat infusion in type 2 diabetes. *Diabetes Obesity and Metabolism* **22**, 383-392 (2020).
- 31. Wu, T., *et al.* Effects of sitagliptin on glycemia, incretin hormones, and antropyloroduodenal motility in response to intraduodenal glucose infusion in healthy lean and obese humans and patients with type 2 diabetes treated with or without metformin. *Diabetes* **63**, 2776-2787 (2014).
- 32. Wishart, J., Morris, H.A. & Horowitz, M. Radioimmunoassay of gastric inhibitory polypeptide in plasma. *Clinical Chemistry* **38**, 2156-2157 (1992).
- 33. Xie, C., Jones, K.L., Rayner, C.K. & Wu, T. Enteroendocrine hormone secretion and metabolic control: importance of the region of the gut stimulation. *Pharmaceutics* **12**, 790 (2020).
- 34. Giezenaar, C., *et al.* Effects of randomized whey-protein loads on energy intake, appetite, gastric emptying, and plasma gut-hormone concentrations in older men and women. *American Journal of Clinical Nutrition* **106**, 865-877 (2017).
- 35. Xie, C., *et al.* Plasma GLP-1 response to oral and intraduodenal nutrients in health and type 2 diabetes-impact on gastric emptying. *Journal of Clinical Endocrinology and Metabolism* **107**, e1643-e1652 (2022).
- 36. Ma, J., *et al.* Effects of a protein preload on gastric emptying, glycemia, and gut hormones after a carbohydrate meal in diet-controlled type 2 diabetes. *Diabetes Care* **32**, 1600-1602 (2009).
- 37. Wu, T., *et al.* Effects of a D-xylose preload with or without sitagliptin on gastric emptying, glucagon-like peptide-1, and postprandial glycemia in type 2 diabetes. *Diabetes Care* **36**, 1913-1918 (2013).
- 38. Wu, T., *et al.* A protein preload enhances the glucose-lowering efficacy of vildagliptin in type 2 diabetes. *Diabetes Care* **39**, 511-517 (2016).
- 39. Watson, L., *et al.* A whey/guar "preload" improves postprandial glycaemia and glycated haemoglobin levels in type 2 diabetes: A 12-week, single-blind, randomized, placebo-controlled trial. *Diabetes Obesity and Metabolism* **21**, 930-938 (2019).

- 40. Pham, H., *et al.* Longitudinal changes in fasting and glucose-stimulated GLP-1 and GIP in healthy older subjects. *Journal of Clinical Endocrinology and Metabolism* **104**, 6201-6206 (2019).
- 41. Beckoff, K., *et al.* Effects of glucose supplementation on gastric emptying, blood glucose homeostasis, and appetite in the elderly. *American Journal of Physiology-Regulatory, Integrative and Comparative Physiology* **280**, R570-576 (2001).
- 42. O'Connor, K.L., *et al.* Altered appetite-mediating hormone concentrations precede compensatory overeating after severe, short-term energy deprivation in healthy adults. *Journal Nutrition* **146**, 209-217 (2016).

CHAPTER 4: SERUM ALANINE TRANSAMINASE
IS PREDICTIVE OF FASTING AND
POSTPRANDIAL INSULIN AND GLUCAGON
CONCENTRATIONS IN TYPE 2 DIABETES

Statement of Authorship

Title of the paper	Serum alanine transaminase is predictive of fasting and postprandial insulin and					
	glucagon concentrations in type 2 diabetes					
Publication status	Published					
	Huang, W., Xie, C., Wewer Albrechtsen, NJ., Sang M., Sun Z., Jones, KL., Horowitz,					
Publication details	M., Rayner, CK., Wu, T. (2023). "Serum alanine transaminase is predictive of fasting					
r ublication details	and postprandial insulin and glucagon concentrations in type 2 diabetes", Peptides,					
	171092.					

Principal Author

Candidate	Weikun Huang						
Contribution	Data collection and interpretation, statistical analysis, writing and revision of the manuscript						
Overall percentage	70%						
Certification	This paper reports on original research I conducted during the period of my Higher Degree by Research candidature and is not subject to any obligations or contractual agreements with a third party that would constrain its inclusion in this thesis. I am the primary author of this paper						
Signature		Date	September 2023				

Co-Author Contributions

By signing the Statement of Authorship, each author certifies that: i) the candidate's stated contribution to the publication is accurate (as detailed above); ii) permission is granted for the candidate to include the publication in the thesis; and iii) the sum of all co-author contributions is equal to 100% less the candidate's stated contribution.

Name of Co-Author	Cong Xie					
Contribution	Data interpretation and reviewing of the manuscript					
Signature		Date	September 2023			

Name of Co-Author	Nicolai J Wewer Albrechtsen								
Contribution	Data interpretation and reviewing of the manuscript								
Signature		Date September 2023							
Name of Co-Author	Miaomiao Sang	Miaomiao Sang							
Contribution	Data interpretation and reviewing o	f the manusc	ript						
Signature		Date September 2023							
Name of Co-Author	Zilin Sun								
Contribution	Data interpretation and reviewing of the manuscript								
Signature		Date September 2023							
Name of Co-Author	Karen L. Jones	I							
Contribution	Data interpretation and reviewing o	f the manusc	ript						
Signature		Date	September 2023						
Name of Co-Author	Michael Horowitz								
Contribution	Data interpretation and reviewing o	f the manusc	ript						
Signature		Date	September 2023						
Name of Co-Author	Christopher K. Rayner								
Contribution	Conception and design of the study, and guarantor of the paper.	data interpr	etation, reviewing of the manuscript,						
Signature		Date	September 2023						

Name of Co-Author	Tongzhi Wu		
Contribution	Conception and design of the study, and guarantor of the paper.	data interpr	etation, reviewing of the manuscript,
Signature		Date	September 2023

4.1 Abstract

The liver plays a key role in glucose homeostasis. Serum liver enzyme levels, including alanine transaminase (ALT), aspartate transaminase (AST) and gamma-glutamyl transferase (GGT), are reportedly predictive of the risk of T2D. However, the link between the liver enzyme profile and metabolic derangements in T2D, particularly the secretion of both insulin and glucagon, is not clear. This study evaluated its relationships with glycaemia, insulin and glucagon both during fasting and after an oral glucose load or a mixed meal in T2D. 15 healthy and 43 T2D subjects ingested a 75g glucose drink. 86 T2D subjects consumed a mixed meal. Venous blood was sampled for measurements of blood glucose and plasma insulin, C-peptide and glucagon. Blood glucose, plasma insulin, C-peptide and glucagon concentrations, both fasting and after oral glucose, correlated directly with ALT, while fewer and weaker correlations were observed with GGT or AST. Subgroup analysis in T2D subjects ascertained that plasma insulin, C-peptide and glucagon concentrations after oral glucose were higher with increasing ALT. Similar findings were observed in the T2D subjects who received a mixed meal. In conclusion, serum liver enzyme profile, particularly ALT, reflects dysregulated fasting and nutrient-stimulated plasma insulin and glucagon concentrations in T2D.

Keywords: alanine transaminase, insulin, glucagon, type 2 diabetes

4.2 Introduction

Hepatic glucose production and disposal are key metabolic processes in glucose homeostasis [1, 2]. During fasting, the liver releases glucose via both the breakdown of glycogen (glycogenolysis) and glucose synthesis from precursors including alanine and lactate (gluconeogenesis) [3]. During the postprandial phase, the liver is responsible for the disposal of about a third of ingested glucose [4]. Hepatic regulation of blood glucose is coordinated predominantly by insulin and glucagon released from the pancreatic islets; the secretion of insulin increases glucose uptake in the liver [5], while glucagon augments hepatic glucose production [6, 7]. Impairments in insulin secretion and hepatic insulin sensitivity, as well as an augmentation of both fasting and postprandial glucagon secretion, underpin the elevation of blood glucose in type 2 diabetes (T2D) [8, 9]. Accordingly, characterisation of the relationship between the secretion

of insulin and glucagon and liver function is potentially of major relevance to the understanding of the pathophysiology and rational management of T2D.

In clinical practice, a serum panel of liver enzymes, including gamma-glutamyl transferase (GGT), alanine transaminase (ALT), alkaline phosphatase (ALP) and aspartate transaminase (AST), are assessed usually under 'liver function tests' [10]. Liver enzyme levels are typically elevated in hepatic steatosis (particularly GGT and ALT), hepatocellular injury (ALT and AST), or cholestasis (ALP and GGT) [11]. ALT is released mainly by hepatocytes [12], but other 'liver' enzymes (particularly AST and ALP) are also produced by extra-hepatic tissues, so their elevations are not specific to the liver [13, 14]. There is increasing evidence that the liver enzyme profile is predictive of the risk of metabolic disorders, including T2D [14]. For example, a cross-sectional analysis revealed that plasma glucose at 2 hours after a 30g oral glucose load was associated directly with serum GGT in non-diabetic middle-aged men (n = 2419) [15]. In a subsequent cohort study of middle-aged men without diabetes (n = 7458), a relative or absolute increase in serum GGT was found to be an independent risk factor for the development of T2D [16]. Similarly, ALT and AST have been reported as potential markers of diabetes risk in individuals without hepatitis [17-22]. These observations necessitate a deeper understanding of the mechanistic links between metabolic derangement and liver enzymes.

In subjects with normal glucose tolerance, ALT, AST and GGT have been found to correlate positively with insulin levels during fasting and following a 75g oral glucose load [23]. Moreover, in healthy men and women, both GGT and ALT correlated positively with hepatic insulin resistance, assessed by the gold standard euglycaemic-hyperinsulinaemic clamp, with fasting glucagon related positively to ALT [24]. Accordingly, an increase in liver enzymes may represent an early marker of hepatic resistance to insulin and hyperglucagonaemia. Although T2D patients with increased liver fat and ALT also displayed greater hepatic insulin resistance than those with normal liver fat and ALT [25], the relationships of the secretion of both insulin and glucagon with serum liver enzyme levels in patients with T2D have not been well characterised. We have therefore examined the relationships of blood glucose, plasma insulin, C-peptide and glucagon during the fasting state and following a 75g oral glucose load and a mixed meal with liver enzymes in T2D.

4.3 Methods

4.3.1 Participants

T2D patients managed by diet and/or metformin monotherapy, and healthy controls matched for age, gender and body mass index (BMI), were recruited from the community by advertisement for studies to evaluate nutritional and/or pharmacological therapies for T2D in our centre (ACTRN12616001059459 and ACTRN1261600055415, ACTRN12612001005842 ACTRN12614001131640) [26-29]. After excluding subjects who participated in multiple protocols (n = 7) or had missing data (n = 3), a total of 15 healthy older subjects and 129 T2D patients were included in this retrospective analysis. In all subjects, during a screening visit, a fasting blood sample had been collected for serum biochemistry (including renal and liver function), and for HbA1c in the case of T2D, and analysed in a commercial laboratory (SA Pathology, Adelaide, Australia). None of the participants had gastrointestinal symptoms, eGFR of < 60 mL/min, or elevation of liver enzymes, including ALT, GGT, AST and ALP, more than two-fold the upper limit of the reference range. The studies were approved by the Royal Adelaide Hospital Human Research Ethics Committee and all participants provided written informed consent.

4.3.2 Protocol

Each subject was evaluated on a single occasion with either a 75g oral glucose challenge (Study 1), or a standardised mixed meal (Study 2). Prior to their study visit, subjects were instructed to refrain from intensive physical activity for 24 hours, and consumed a standardised evening meal (McCain beef lasagne, [592 kcal, McCain Foods, Melbourne, VIC, Australia], together with bread, a non-alcoholic beverage and one piece of fruit) at ~7 pm. Subjects then fasted from all food and nutrient beverages, but were allowed to drink water until midnight, before attending the clinical research laboratory at The University of Adelaide the following morning.

Study 1: oral glucose tolerance test (OGTT)

A total of 15 healthy subjects (9 males and 6 females, age 67.2 ± 2.3 years, BMI 30.3 ± 0.7 kg/m²) and 43 T2D patients (29 males and 14 females, age 65.7 ± 1.1 years, BMI 31.5 ± 0.7 kg/m², HbA1c $7.1 \pm 0.1\%$) (Table 1) were evaluated with a 75 g oral glucose challenge, during

which an intravenous (IV) cannula was inserted in one forearm vein for blood sampling and kept warm for collection of 'arterialised' venous blood. At t=0 minutes, a glucose drink (75 g glucose dissolved in water to a final volume of 300 mL) was consumed within 5 minutes, and subjects remained seated throughout the study. Blood samples were collected immediately before (t=0 minutes) and at t=15, 30, 60, 90, 120, 150 and 180 minutes after the glucose drink, and were centrifuged at 3200 rpm for 15 minutes at 4°C within 15 minutes of collection. Plasma was separated and stored at -80°C until subsequent assays were performed.

Study 2: mixed meal test

86 T2D subjects (54 males and 32 females, age 64.7 ± 0.7 years, BMI 29.9 ± 0.6 kg/m², HbA1c $6.6 \pm 0.1\%$) (Table 2) were evaluated in a similar procedure to Study 1, except that subjects consumed a semisolid meal comprising 65 g powdered potato (Deb Instant Mashed Potato; Continental, Epping, Australia) and 20 g glucose, reconstituted with 200 mL water and one egg yolk (368.5 kcal: 61.4 g carbohydrate, 7.4 g protein and 8.9 g fat) between t = 0-5 minutes. 'Arterialised' venous blood was sampled before (t = 0 minutes) and at t = 15, 30, 60, 90, 120, 180 and 240 minutes after the meal.

4.3.3 Measurements

Blood glucose concentrations were measured in duplicate at each time point using a glucometer (Optium Xceed; Abbott Laboratories, Lake Bluff, IL, USA), and the mean value was recorded. Plasma insulin concentrations were measured by ELISA (10-1113, Mercodia, Uppsala, Sweden), with a sensitivity of 1.0 mU/L, and intra- and inter-assay coefficients of variation (CVs) of 2.9% and 6.7% respectively. Plasma C-peptide concentrations were measured by ELISA (10-1136-01, Mercodia), with a sensitivity if 15 pmol/L and intra- and interassay CVs of 7.7% and 3.7% respectively. Plasma glucagon concentrations were determined by radioimmunoassay (RIA, GL-32k; Millipore, Billerica, MA, USA), with a sensitivity of 20 pg/mL, and intra- and inter-assay CVs of 10% and 3.1% respectively. We noted that there was a shift in the performance of the Millipore RIA kit after the introduction of a new batch of antibodies for glucagon in 2019 [30]. The glucagon data reported here were therefore derived from RIA kits produced before 2019, which we have validated against the highly specific sandwich ELISA kit that detects both the N- and C-terminus of glucagon (i.e. the Mercodia ELISA kit) [30]. Insulin

clearance was reflected by the molar ratio of C-peptide AUC_{0-180min} to insulin AUC_{0-180min} [31]. Whole-body insulin sensitivity and hepatic insulin resistance were assessed by the Matsuda index and homeostatic model assessment for insulin resistance (HOMA-IR), respectively. The Matsuda index was calculated by the following:

 $\sqrt{G_0 \times 18 \times I_0 \times mean \ glucose \ concentration} \times 18 \times mean \ insulin \ concentration}$ where G_0 was the fasting blood glucose (mmol/L), I_0 was the fasting plasma insulin (mU/L) [32]. HOMA-IR was calculated by the following [33]:

$$\frac{G_0 \times I_0}{22.5}$$

4.3.4 Statistical Analysis

Areas under the curves (AUC) for blood glucose, plasma insulin and plasma glucagon were calculated using the trapezoidal rule. Demographic data were either compared using one-way ANOVA (three subgroups) or unpaired Student's t-tests (designated subgroups) except for gender and medication use, which were compared by Chi-square tests.

In Study 1, the relationships between parameters (including the combined healthy and T2D subjects who received 75 g oral glucose) were examined by either Pearson correlation analyses (when the data were normally distributed) or Spearman correlation analyses (when the data were not normally distributed). Sensitivity analyses, which excluded healthy subjects, were also performed. Given the strong correlation between metabolic parameters and ALT, T2D subjects were also stratified into three subgroups, including T1 (ALT \leq 29 U/L, n = 15), T2 (ALT = 30-40 U/L, n = 15) and T3 (ALT > 40 U/L, n = 13) (Table 1). In Study 2, because the majority of the subjects had relatively low ALT values, they were divided into two subgroups, with Lower (\leq 29 U/L, n = 45) or Higher (\geq 30 U/L, n = 41) ALT levels (Table 2). Blood glucose, plasma insulin and plasma glucagon curves were compared between the subgroups by two-way repeated measures ANOVA using 'group' and 'time' as factors. If ANOVA revealed significant interactions, *post hoc* comparisons were performed with Bonferroni's correction. All analyses were performed with GraphPad Prism 9.0 (GraphPad Software, San Diego, CA, USA). Data are presented as means \pm SEM. P < 0.05 was considered statistically significant.

4.4 Results

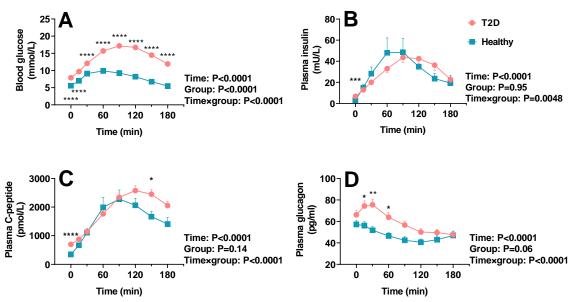


Figure 1. Blood glucose (A), plasma insulin (B), plasma C-peptide (C) and plasma glucagon (D) responses to a 75 g oral glucose load in healthy subjects (n = 15) and individuals with type 2 diabetes (T2D, n = 43) in Study 1. Repeated-measures two-way ANOVA was used to determine statistical differences. ANOVA results are reported as P values for differences between groups, over time, and due to group by time interactions. *Post hoc* comparisons were adjusted by Bonferroni's correction. Data are means \pm SEM. *P < 0.05, **P < 0.01, ***P < 0.005, ****P < 0.001 for healthy vs. T2D.

Both protocols were well tolerated. Demographic and biochemical data of subjects included in Studies 1 and 2 are summarised in Table 1 and Table 2, respectively. In Study 1, healthy and T2D subjects were well matched for age, BMI and gender, but ALT was higher, and AST non-significantly higher, in the T2D group (Table 1). As expected, blood glucose concentrations, both fasting (P < 0.0001) and after oral glucose (group effect: P < 0.0001, group by time interaction: P < 0.0001), were substantially higher in T2D than healthy subjects (Figure 1A). Fasting insulin was higher (P < 0.0001), and the insulin response to oral glucose occurred later (peak at ~120 minutes vs. 60 minutes) in T2D subjects (P = 0.0048 for group by time interaction, Figure 1B). Similarly, fasting C-peptide was higher (P < 0.0001), and the C-peptide response to oral glucose occurred later (~120 minutes vs 90 minutes) in T2D subjects (group by time interaction: P < 0.0001, Figure 1C). Fasting glucagon was numerically (P = 0.4) higher in T2D subjects. However, while plasma glucagon was suppressed after oral glucose in healthy subjects, it increased to a peak at t = 30 minutes in the T2D group before returning to baseline. Accordingly, the glucagon response to oral glucose was greater in T2D than healthy subjects

(group by time interaction: P < 0.0001) (Figure 1D). In T2D subjects in Study 2, blood glucose, plasma insulin, and plasma glucagon all increased following the mixed meal, with glucose and insulin peaking at around 90 minutes and glucagon peaking at around 30 minutes after the meal, as reported previously [28, 29, 34].

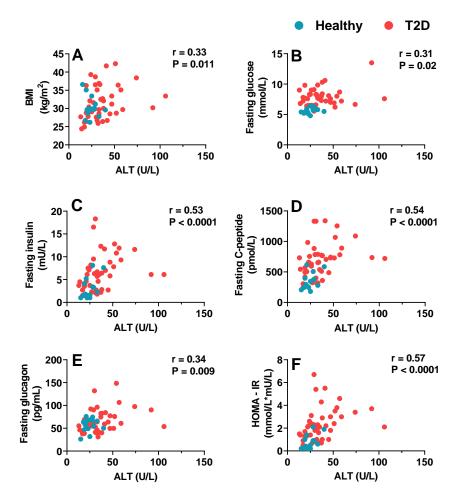


Figure 2. Relationships of BMI (A), fasting blood glucose (B), plasma insulin (C), plasma C-peptide (D), plasma glucagon (E) and HOMA-IR (F) with alanine transaminase (ALT) in the combined subjects without (n = 15) and with type 2 diabetes (T2D, n = 43) in Study 1. Spearman correlation analysis was employed to examine these relationships.

Table 1. Characteristics of healthy and type 2 diabetes (T2D) participants in Study 1

Parameters	Healthy (n = 15)	T2D (n = 43)						
rarameters	Healthy (II = 15)	Overall	T1 (n = 15)	T2 (n = 15)	T3 (n = 13)	P		
Gender (M/F)	9/6	29/14	13/2	9/6	7/6	0.2		
Age (year)	67.2 ± 2.3	65.7 ± 1.1	66.4 ± 2.1	64.9 ± 1.3	65.9 ± 1.4	0.9		
BMI (kg/m^2)	30.3 ± 0.7	31.5 ± 0.7	29.6 ± 1.0	31.7 ± 1.1	33.5 ± 1.2	0.08		
HbA1c (%)		7.1 ± 0.1	6.9 ± 0.2	7.2 ± 0.2	7.2 ± 0.2	0.3		
Medication (Diet/Metformin)		4/39	3/12	1/14	0/13	0.17		
Total Bili (µmol/L)	10.9 ± 1.4	11.7 ± 0.8	12.9 ± 1.3	10.3 ± 1.0	12.0 ± 1.3	0.4		
GGT (U/L)	23.8 ± 3.2	43.3 ± 6.8	23.0 ± 4.2	37.5 ± 10.6	73.2 ± 13.1	0.008		
ALP (U/L)	74.7 ± 4.1	76.8 ± 3.5	66.1 ± 2.8	80.5 ± 7.6	84.8 ± 4.7	0.07		
ALT (U/L)	24.4 ± 1.7	$36.7 \pm 2.9****$	20.8 ± 1.1	33.3 ± 0.8	59.0 ± 4.6	< 0.0001		
AST (U/L)	23.0 ± 1.2	28.6 ± 2.0	20.5 ± 1.1	25.3 ± 1.0	41.6 ± 3.9	< 0.0001		
Fasting glucose (mmol/L)	5.6 ± 0.1	$7.9 \pm 0.2****$	7.7 ± 0.3	7.9 ± 0.3	8.1 ± 0.5	0.7		
Fasting insulin (mU/L)	3.0 ± 0.6	$6.7 \pm 0.6****$	4.7 ± 0.5	6.9 ± 1.3	8.6 ± 0.8	0.03		
Fasting C-peptide (pmol/L)	346.1 ± 34.3	$698.7 \pm 42.9****$	557.5 ± 49.4	694.1 ± 82.3	866.8 ± 68.4	0.003		
Insulin clearance	11.8 ± 1.5	12.6 ± 0.7	15.3 ± 1.3	11.2 ± 1.1	11.1 ± 1.2	0.027		
Fasting glucagon (pg/mL)	57.2 ± 3.7	66.2 ± 3.8	57.1 ± 3.6	64.8 ± 7.2	78.2 ± 7.8	0.08		
HOMA-IR (dL/mg*L/mU)	0.8 ± 0.2	$2.3 \pm 0.2****$	1.6 ± 0.2	2.4 ± 0.5	3.1 ± 0.3	0.02		

Data are means \pm SEM. The Mann-Whitney test (or unpaired student t-test for normally distributed data) was used to evaluate differences between the healthy and T2D groups, except that the distribution of gender and medication were compared using a Chi-square analysis. * $^{*}P < 0.05$, ** $^{*}P < 0.01$, *** $^{*}P < 0.005$, **** $^{*}P < 0.001$ for healthy vs. T2D (overall). T2D subjects were stratified into three subgroups, including T1 (ALT \leq 29 U/L, n = 15) T2 (ALT = 30-40 U/L, n = 15) and T3 (ALT > 40, n = 13). One-way ANOVA was used to determine statistical differences between the three subgroups, except that the distribution of gender and medication were compared using Chi-square analysis.

4.4.1 Relationships between metabolic parameters and liver enzymes in fasting and after an oral glucose load and before and after a mixed meal

In the pooled analysis of both healthy and T2D subjects who received oral glucose (Study 1), BMI (r = 0.33, P = 0.011), fasting blood glucose (r = 0.31, P = 0.02), plasma insulin (r = 0.53, P < 0.0001), plasma C-peptide (r = 0.54, P < 0.0001) and plasma glucagon (r = 0.34, P = 0.009), as well as HOMA-IR (r = 0.57, P < 0.0001), correlated directly with ALT (Figure 2). The relationship between HbA1c and ALT (r = 0.28, P = 0.07) did not reach significance (Table 3). BMI (r = 0.29, P = 0.03), HbA1c (r = 0.38, P = 0.01), fasting plasma insulin (r = 0.41, P = 0.001), C-peptide (r = 0.36, P = 0.005) and HOMA-IR (r = 0.43, P = 0.0007) correlated directly with GGT, but no significant correlations between fasting blood glucose or plasma glucagon and GGT were observed (Table 3). Likewise, fasting plasma insulin (r = 0.42, P = 0.001), C-peptide (r = 0.47, P = 0.002), glucagon (r = 0.30, P = 0.024) and HOMA-IR (r = 0.45, P = 0.0005) correlated directly with AST. The relationship between fasting blood glucose and AST (r = 0.23, r = 0.078) did not reach significance, and there were no significant correlations observed of either BMI or HbA1c with AST (Table 3).

Table 2. Characteristics of Study 2 participants in the total group and classified according to serum ALT

Parameters	Overall	Lower $(n = 45)$	Higher (n = 41)	P
Gender (M/F)	54/32	26/19	28/13	0.3
Age (year)	64.7 ± 0.7	65.6 ± 0.9	63.7 ± 1.1	0.18
BMI (kg/m^2)	29.9 ± 0.6	29.0 ± 0.8	30.9 ± 0.7	0.04
HbA1c (%)	6.6 ± 0.1	6.5 ± 0.1	6.8 ± 0.1	0.14
Medication (Diet/Metformin)	37/49	19/26	18/23	0.9
Total Bili (µmol/L)	10.1 ± 0.7	9.3 ± 0.6	10.9 ± 1.2	0.63
GGT (U/L)	38 ± 4.9	25.0 ± 2.0	43.4 ± 4.1	< 0.0001
ALP(U/L)	74.1 ± 2.0	74.6 ± 2.8	73.6 ± 2.8	0.8
ALT(U/L)	31.4 ± 1.8	20.6 ± 0.8	43.3 ± 2.6	< 0.0001
AST(U/L)	26.8 ± 1.0	22.3 ± 0.7	31.5 ± 1.6	< 0.0001
Fasting glucose (mmol/L)	8.1 ± 0.2	8.1 ± 0.2	8.2 ± 0.2	0.9
Fasting insulin (mU/L)	6.6 ± 0.6	5.1 ± 0.5	8.3 ± 1.1	0.007
Fasting glucagon (pg/mL)	74.1 ± 2.1	71.2 ± 2.5	77.2 ± 3.3	0.1
Matsuda index (dL/mg*L/mU)	7.3 ± 0.6	8.8 ± 0.9	5.7 ± 0.7	0.0007
HOMA-IR (mmol/L*mU/L)	2.5 ± 0.2	1.8 ± 0.2	3.0 ± 0.4	0.006

Data are means \pm SEM. Participants were divided into two subgroups, with lower (\leq 29 U/L, n = 45) or higher (\geq 30 U/L, n = 41) ALT levels. Mann-Whitney test (or unpaired student t-test for normally distributed data) was used to determine the statistical difference between the Lower and Higher subgroups, except that the distribution of gender and medication were compared using Chi-square analysis.

After the 75g oral glucose load, the $AUC_{0-180min}$ for blood glucose (r = 0.27, P = 0.04), plasma insulin (r = 0.35, P = 0.007), C-peptide (r = 0.33, P = 0.01) and glucagon (r = 0.44, P = 0.0006)

correlated directly (Figure 3A-D), whereas insulin clearance (r = -0.35, P = 0.008) and the Matsuda index correlated inversely (r = -0.57, P < 0.0001), with ALT in the pooled analysis (Figure 3E-F). The Matsuda index also correlated inversely with GGT (r = -0.37, P = 0.004), but there was no significant correlation between the AUC_{0-180min} for glucose, insulin, C-peptide or glucagon and GGT (Table 3). There was a direct relationship between the glucagon AUC_{0-180min} and AST (r = 0.38, P = 0.004), and an inverse relationship between the Matsuda index and AST (r = -0.46, P = 0.0004). However, no significant correlations were observed between the AUC_{0-180min} for glucose, insulin or C-peptide and AST, nor between any of the aforementioned parameters and ALP, in the pooled analysis (Table 3).

Table 3. Relationships between liver enzyme levels and baseline characteristics in healthy and T2D subjects (n = 58 in total) in Study 1

	GGT		ALP		ALT		AST	
Parameters	r	P	r	P	r	P	r	P
BMI (kg/m²)	0.29	0.03	0.03	0.8	0.33	0.011	0.15	0.28
HbA1c (%)	0.38	0.01	0.02	0.9	0.28	0.07	0.25	0.11
Fasting glucose (mmol/L)	0.18	0.17	0.04	0.7	0.31	0.02	0.24	0.08
Glucose AUC _{0-180min} (mmol/L*min)	0.13	0.34	0.05	0.7	0.27	0.04	0.2	0.13
Fasting insulin (mU/L)	0.41	0.001	0.10	0.4	0.53	< 0.0001	0.42	0.001
Insulin AUC _{0-180min} (mU/L*min)	0.19	0.15	0.13	0.3	0.35	0.007	0.23	0.07
Fasting C-peptide (pmol/L)	0.36	0.005	0.15	0.27	0.54	< 0.0001	0.4	0.002
C-peptide AUC _{0-180min} (pmol/L*min)	0.21	0.1	0.24	0.07	0.33	0.01	0.2	0.1
Insulin clearance	-0.14	0.3	-0.02	0.9	-0.35	0.008	-0.2	0.1
Fasting glucagon (pg/mL)	0.01	0.94	-0.02	0.9	0.34	0.009	0.30	0.024
Glucagon AUC _{0-180min} (pg/mL*min)	0.1	0.47	0.1	0.4	0.44	0.0006	0.38	0.004
Matsuda index (dL/mg*L/mU)	-0.37	0.004	-0.16	0.2	-0.57	< 0.0001	-0.46	0.0004
HOMA-IR (mmol/L*mU/L)	0.43	0.0007	0.12	0.4	0.57	< 0.0001	0.44	0.0005

Spearman test (or Pearson test for normally distributed data) was used to determine the relationship.

Sensitivity analysis was also conducted between metabolic parameters and ALT in Study 1 by excluding significant outliers (Figure S1 and S2), which did not affect the aforementioned relationships, except that the correlation between the $AUC_{0-180min}$ for blood glucose and ALT became less apparent (r = 0.25, P = 0.058). After the exclusion of healthy subjects, the relationships between the metabolic parameters and liver enzymes were generally unchanged, except that the correlations of liver enzymes with blood glucose were no longer apparent (Table S1).

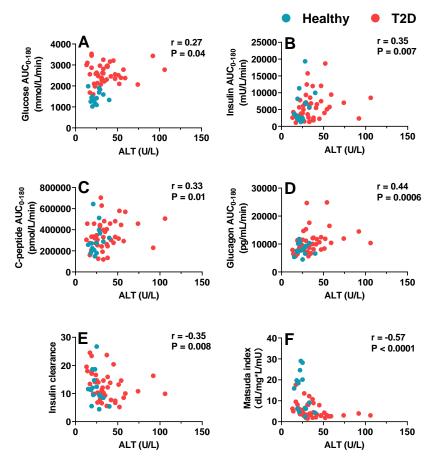


Figure 3. Relationships of the area under the curve (AUC) for blood glucose (A), plasma insulin (B), plasma C-peptide (C), plasma glucagon (D) between t=0-180 minutes, insulin clearance (E) and Matsuda index (F) with alanine transaminase (ALT) in the combined subjects without (n=15) and with type 2 diabetes (T2D, n=43) in Study 1. Spearman correlation analysis was employed to examine these relationships.

There were also direct relationships between the plasma insulin concentration after a mixed meal and liver enzymes (GGT and ALT) in Study 2, although no relationships between plasma glucagon concentrations and liver enzymes were evident, most likely due to the small inter-individual variations in liver enzymes (data not shown).

4.4.2 Blood glucose and plasma insulin, C-peptide and glucagon in T2D subjects classified according to ALT

The demographic data of subjects in each subgroup are summarised in Table 1. GGT (P = 0.008) and AST (P < 0.0001) were higher in subgroups with higher ALT, and BMI and ALP also tended to be higher. However, neither the distribution of gender, age, or HbA1c differed between the three subgroups. While blood glucose concentrations did not differ over 180 minutes following

the 75 g oral glucose challenge between the three subgroups of T2D subjects (Table 1 and Figure 4A), plasma insulin concentrations were higher in subgroups with higher ALT both during fasting (P = 0.03, Table 1) and after the oral glucose load (group by time interaction: P = 0.01, Figure 4B). Similarly, plasma C-peptide concentrations were higher in subgroups with higher ALT at fasting (P = 0.003, Table 1) and after oral glucose load (group effect: P = 0.056, Figure 4C). Plasma glucagon concentrations were numerically higher during fasting (P = 0.08, Table 1), but significantly higher after oral glucose (group by time interaction: P < 0.0019, Figure 4D), in subgroups with higher ALT. In addition, both insulin clearance (P = 0.027, Figure 4E) and the Matsuda index decreased (P = 0.016, Figure 4F), while HOMA-IR increased (P = 0.02, Table 1), with increasing ALT.

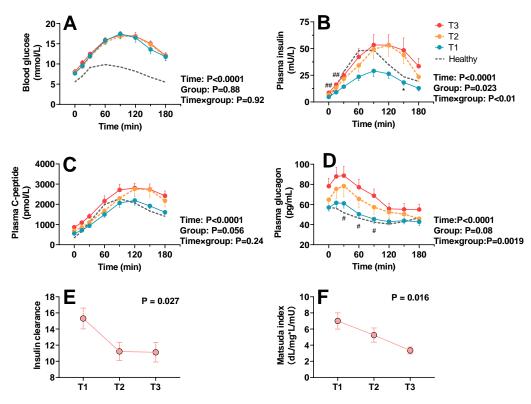


Figure 4. Blood glucose (A), plasma insulin (B), plasma C-peptide (C) and plasma glucagon (D) in response to a 75 g oral glucose load in subgroups of individuals with type 2 diabetes (T2D), stratified by ALT, i.e. T1 (low ALT, n = 15), T2 (intermediate ALT, n = 15) and T3 (high ALT, n = 13) in Study 1. Relevant curves for healthy participants were added to the figures for reference purposes but were not included in the statistical analysis. Repeated-measures two-way ANOVA was used to determine statistical differences. ANOVA results are reported as P values for differences by groups, the difference over time and differences due to group by time interaction. *Post hoc* comparisons were adjusted by Bonferroni's correction. Data are means \pm SEM. *P < 0.05 for T1 vs. T2; *P < 0.05, **P < 0.01 for T1 vs. T3 (E) and (F) show the insulin clearance and Matsuda index of the three ALT subgroups, respectively. One-way ANOVA was used to determine the statistical differences.

The demographic data in T2D subjects in Study 2 stratified into lower and higher ALT subgroups are summarised in Table 2. There were no differences in gender distribution, age, HbA1c, ALP or the use of metformin between the two subgroups. As in Study 1, GGT and AST were elevated in the subgroup with higher ALT in Study 2 (Table 2). Blood glucose concentrations did not differ between the two subgroups at baseline or after the meal (Figure 5A). Both fasting (P = 0.007) and meal-induced insulin concentrations were higher in the subgroup with higher ALT (group by time interaction: P = 0.019, Figure 5B). While fasting glucagon concentrations were numerically higher, postprandial glucagon concentrations were significantly higher in the subgroup with higher ALT (group by time interaction: P = 0.016, Figure 5C). In addition, a lower Matsuda index (P = 0.0007) and a higher HOMA-IR (P = 0.006) were observed in the subgroup with higher ALT (Table 2).

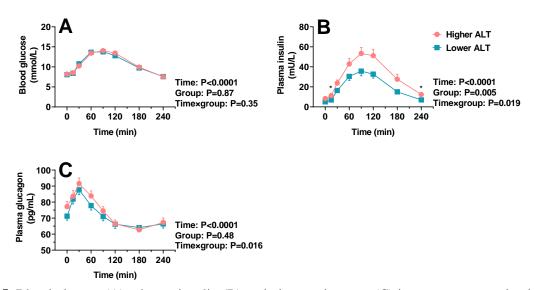


Figure 5. Blood glucose (A), plasma insulin (B) and plasma glucagon (C) in response to a mixed meal in the two subgroups of individuals with type 2 diabetes in Study 2, i.e. lower ALT group (n = 45) and higher ALT group (n = 41). Repeated-measures two-way ANOVA was used to determine statistical differences. ANOVA results are reported as P values for differences by groups, the difference over time and differences due to group by time interaction. *Post hoc* comparisons were adjusted by Bonferroni's correction. Data are means \pm SEM. *P < 0.05, **P < 0.01, for the subgroup of high vs. low ALT.

4.5 Discussion

While associations of serum liver enzymes with insulin resistance and future risk of T2D in normoglycaemic individuals have been increasingly appreciated, links to specific metabolic

derangements in T2D remain poorly characterised. The present study showed that T2D patients with relatively good glycaemic control and managed by diet and/or metformin displayed higher serum liver enzyme levels compared to age- and BMI-matched healthy controls, and most importantly that circulating glucose, insulin, C-peptide and glucagon concentrations, both fasting and after oral glucose, correlated closely with serum liver enzymes, particularly ALT. In T2D subjects, subgroup analysis indicated that higher ALT was predictive of greater insulin resistance, higher insulin and glucagon responses to both an oral glucose load and a mixed meal, even in the absence of differences in glycaemia. Together, these findings suggest that serum liver enzymes, particularly ALT, represent biomarkers for diabetogenic changes in insulin and glucagon secretion (and action) in T2D.

The observed relationships between metabolic parameters and liver enzymes in T2D subjects represent a substantial development from prior knowledge in non-diabetic subjects. As reported in the latter [20, 23, 35], we observed that both insulin resistance (HOMA-IR) and the insulin response to 75 g oral glucose correlated directly with ALT, AST and GGT in the T2D group. A direct relationship between fasting glucagon and some liver enzymes (ALT and GGT) has been observed in healthy individuals [35]. To our knowledge, there is no report on the relationship between circulating glucagon concentrations (either during fasting or in response to nutrient loads) and liver enzymes in patients with T2D. Therefore, the current study has added an important new insight into the link of liver enzymes to metabolic derangements in T2D. Together, these findings are indicative of the development of hepatic resistance to both insulin and glucagon signalling in the course of T2D, i.e. insulin and glucagon secretion may be exaggerated to compensate for reduced hepatocyte sensitivity to these hormones [36], which may predispose to the deterioration of glycaemic control [37-40]. The mechanism underlying the relationship between liver enzymes and glucagon secretion in T2D is not clear. There is recent evidence that hyperglucagonaemia in metabolic diseases, such as non-alcoholic fatty liver disease, may be driven by elevated circulating amino acid levels due to impaired amino acid catabolism in the face of hepatic glucagon resistance [41]. It may also reflect, in part, reduced metabolism of pancreatic hormones due to compromised liver function. In keeping with this concept, hepatic insulin clearance, as assessed by the C-peptide to insulin ratio, was reduced in T2D subjects with elevated ALT. The diminished insulin sensitivity associated with T2D may

also be of relevance to hyperglucagonaemia, since there is a counter-regulatory relationship between insulin and glucagon [42].

We recognise that serum liver enzymes are often inter-related – for example, individuals with T2D who have higher ALT levels frequently also exhibit raised AST and GGT concentrations. Relative to other liver enzymes, ALT appeared to have a closer relationship to metabolic parameters, probably due to the higher specificity of ALT for reflecting liver dysfunction [10, 14]. Subgroup analysis in T2D patients revealed that an increase in ALT was predictive of augmented insulin and glucagon secretion after an oral glucose load. Similar observations were evident in an independent group of T2D patients after a standardised mixed meal. However, the reasons accounting for elevated ALT in T2D were not further examined in the current study. In people with non-alcoholic fatty liver disease, adipose tissue insulin resistance and liver triglyceride content have been shown to be major determinants of plasma ALT levels [43]. It is therefore plausible that the accumulation of liver fat in the context of insulin resistance in T2D may be relevant to inter-individual variations in ALT. However, we note that liver enzyme levels were, at most, only modestly elevated in the T2D subjects in our study, so the degree of hepatic steatosis may not have been great. Imaging of liver fat content, e.g. by ultrasound, would add insights into this aspect.

Despite substantial differences in the insulin and glucagon responses to oral glucose and a mixed meal between subgroups of T2D subjects with different ALT levels, blood glucose concentrations did not differ between the subgroups. Similarly, the direct relationship between ALT and glycaemia after the oral glucose challenge was no longer evident after excluding the healthy subjects. This is likely to reflect the fact that the development of insulin and glucagon resistance occurs in advance of deterioration in blood glucose control, and that the T2D subjects included in the current study were at a relatively 'early' stage of T2D and were able to compensate for hepatic insulin and glucagon resistance. Further studies are, therefore, warranted to evaluate the potential for liver enzymes to both characterise the pathological defects of T2D and inform interventional strategies (e.g. focussing on normalising liver enzymes) to prevent or delay the progression of the disease.

Several limitations should also be acknowledged when interpreting our findings. First, the current observational study involves only a small number of participants, lacks a healthy control in Study 2, and does not provide information about the impact of liver enzymes on future metabolic outcomes, so that a large longitudinal study involving well-matched healthy subjects as a reference in both settings is warranted. Second, the T2D subjects included in the current study were relatively homogenous, with well-controlled glycaemia and without large variations in liver enzymes, which limited the capacity to demonstrate relationships with metabolic parameters. Accordingly, evaluations involving a full spectrum of T2D patients with both normal and abnormally elevated liver enzyme levels are needed. Third, the current study has focussed only on the links of insulin and glucagon secretion with liver enzymes. Concurrent measurements of other metabolic targets, such as the incretin hormone glucagon-like pepetide-1 (GLP-1) and insulin-degrading enzyme (IDE), may yield complimentary insights. Finally, given recent evidence that circulating amino acids and fatty acids are key mediators in communication between the liver and the pancreatic islets, measurements of these may shed light on the observed dysregulated insulin and glucagon concentrations in relation to liver enzymes.

In summary, our study has revealed close relationships between metabolic derangements, including insulin resistance and hyperglucagonaemia, and serum liver enzymes in individuals with relatively well-controlled T2D. That ALT was predictive of exaggerated insulin and glucagon responses to an oral glucose load or a mixed meal, in the absence of differences in glycaemia, suggests that ALT may represent an 'early' biomarker of metabolic dysfunction during the progression of T2D.

4.6 References

- 1. Han, H.-S., Kang, G., Kim, J.S., Choi, B.H. & Koo, S.-H. Regulation of glucose metabolism from a liver-centric perspective. *Experimental & Molecular Medicine* **48**, e218-e218 (2016).
- Adeva-Andany, M.M., Pérez-Felpete, N., Fernández-Fernández, C., Donapetry-García, C.
 & Pazos-García, C. Liver glucose metabolism in humans. *Bioscience Reports* 36(2016).
- 3. Sherwin, R.S. Role of liver in glucose homeostasis. *Diabetes Care* **3**, 261-265 (1980).

- 4. Ferrannini, E., *et al.* The disposal of an oral glucose load in healthy subjects: a quantitative study. *Diabetes* **34**, 580-588 (1985).
- 5. Iozzo, P., *et al.* Insulin stimulates liver glucose uptake in humans: an 18F-FDG PET Study. *Journal of Nuclear Medicine* **44**, 682-689 (2003).
- 6. Liljenquist, J., *et al.* Evidence for an important role of glucagon in the regulation of hepatic glucose production in normal man. *The Journal of Clinical Investigation* **59**, 369-374 (1977).
- 7. Ramnanan, C., Edgerton, D., Kraft, G. & Cherrington, A. Physiologic action of glucagon on liver glucose metabolism. *Diabetes, Obesity and Metabolism* **13**, 118-125 (2011).
- 8. D'alessio, D. The role of dysregulated glucagon secretion in type 2 diabetes. *Diabetes, Obesity and Metabolism* **13**, 126-132 (2011).
- 9. Campbell, J.E. & Newgard, C.B. Mechanisms controlling pancreatic islet cell function in insulin secretion. *Nature Reviews Molecular Cell Biology* **22**, 142-158 (2021).
- 10. Hall, P. & Cash, J. What is the real function of the liver 'function' tests? *The Ulster Medical Journal* **81**, 30 (2012).
- 11. Hoekstra, L.T., *et al.* Physiological and biochemical basis of clinical liver function tests: a review. *Annals of Surgery* **257**, 27-36 (2013).
- 12. Pratt, D.S. & Kaplan, M.M. Evaluation of abnormal liver-enzyme results in asymptomatic patients. *New England Journal of Medicine* **342**, 1266-1271 (2000).
- 13. Giannini, E.G., Testa, R. & Savarino, V. Liver enzyme alteration: a guide for clinicians. *Cmaj* **172**, 367-379 (2005).
- 14. Limdi, J. & Hyde, G. Evaluation of abnormal liver function tests. *Postgraduate Medical Journal* **79**, 307-312 (2003).
- 15. Trell, E., *et al.* Two-hour glucose and insulin responses after a standardized oral glucose load in relation to serum gamma-glutamyl transferase and alcohol consumption. *Acta Diabetologia Latina* **18**, 311-317 (1981).
- 16. Perry, I.J., Wannamethee, S.G. & Shaper, A.G. Prospective study of serum γ-glutamyltransferase and risk of NIDDM. *Diabetes Care* **21**, 732-737 (1998).
- 17. Miyamori, D., *et al.* Prediction of new onset of diabetes mellitus during a 10-year period by using a combination of levels of alanine aminotransferase and γ-glutamyl transferase. *Endocrine Journal*, EJ20-0823 (2021).

- 18. Fraser, A., *et al.* Alanine aminotransferase, γ-glutamyltransferase, and incident diabetes: the British Women's Heart and Health Study and meta-analysis. *Diabetes Care* **32**, 741-750 (2009).
- 19. Song, S., *et al.* ALT/AST as an Independent Risk Factor of Gestational Diabetes Mellitus Compared with TG/HDL-C. *International Journal of General Medicine* **15**, 115 (2022).
- 20. Vozarova, B., *et al.* High alanine aminotransferase is associated with decreased hepatic insulin sensitivity and predicts the development of type 2 diabetes. *Diabetes* **51**, 1889-1895 (2002).
- 21. Chen, S.C.-C., *et al.* Liver fat, hepatic enzymes, alkaline phosphatase and the risk of incident type 2 diabetes: a prospective study of 132,377 adults. *Scientific Reports* **7**, 1-9 (2017).
- 22. Wannamethee, S.G., Shaper, A.G., Lennon, L. & Whincup, P.H. Hepatic enzymes, the metabolic syndrome, and the risk of type 2 diabetes in older men. *Diabetes Care* **28**, 2913-2918 (2005).
- 23. Succurro, E., *et al.* One-hour post-load plasma glucose levels are associated with elevated liver enzymes. *Nutrition, Metabolism and Cardiovascular Diseases* **21**, 713-718 (2011).
- 24. Bonnet, F., *et al.* Liver enzymes are associated with hepatic insulin resistance, insulin secretion, and glucagon concentration in healthy men and women. *Diabetes* **60**, 1660-1667 (2011).
- 25. Gastaldelli, A., *et al.* Relationship between hepatic/visceral fat and hepatic insulin resistance in nondiabetic and type 2 diabetic subjects. *Gastroenterology* **133**, 496-506 (2007).
- 26. Rayner, C.K., *et al.* Effects of sustained treatment with lixisenatide on gastric emptying and postprandial glucose metabolism in type 2 diabetes: a randomized controlled trial. *Diabetes Care* **43**, 1813-1821 (2020).
- 27. Jones, K.L., *et al.* Effects of lixisenatide on postprandial blood pressure, gastric emptying and glycaemia in healthy people and people with type 2 diabetes. *Diabetes, Obesity and Metabolism* **21**, 1158-1167 (2019).
- 28. Watson, L.E., *et al.* A whey/guar "preload" improves postprandial glycaemia and glycated haemoglobin levels in type 2 diabetes: a 12-week, single-blind, randomized, placebo-controlled trial. *Diabetes, Obesity and Metabolism* **21**, 930-938 (2019).

- 29. Wu, T., *et al.* A protein preload enhances the glucose-lowering efficacy of vildagliptin in type 2 diabetes. *Diabetes Care* **39**, 511-517 (2016).
- 30. Wu, T., *et al.* Measurement of plasma glucagon in humans: A shift in the performance of a current commercially available radioimmunoassay kit. *Diabetes, Obesity & Metabolism* **24**, 1182-1184 (2022).
- 31. Meier, J.J., Holst, J.J., Schmidt, W.E. & Nauck, M.A. Reduction of hepatic insulin clearance after oral glucose ingestion is not mediated by glucagon-like peptide 1 or gastric inhibitory polypeptide in humans. *American Journal of Physiology-Endocrinology and Metabolism* **293**, E849-E856 (2007).
- 32. Matsuda, M. & DeFronzo, R.A. Insulin sensitivity indices obtained from oral glucose tolerance testing: comparison with the euglycemic insulin clamp. *Diabetes Care* **22**, 1462-1470 (1999).
- 33. Matthews, D.R., *et al.* Homeostasis model assessment: insulin resistance and β-cell function from fasting plasma glucose and insulin concentrations in man. *Diabetologia* **28**, 412-419 (1985).
- 34. Huang, W., *et al.* The 'early' postprandial glucagon response is related to the rate of gastric emptying in patients with type 2 diabetes. *Peptides*, 170941 (2023).
- 35. Bonnet, F., *et al.* Liver enzymes are associated with hepatic insulin resistance, insulin secretion, and glucagon concentration in healthy men and women. *Diabetes* **60**, 1660-1667 (2011).
- 36. Wewer Albrechtsen, N.J., *et al.* Hyperglucagonemia correlates with plasma levels of non-branched-chain amino acids in patients with liver disease independent of type 2 diabetes. *American Journal of Physiology-Gastrointestinal and Liver Physiology* **314**, G91-G96 (2018).
- 37. Sinha, R., *et al.* Prevalence of impaired glucose tolerance among children and adolescents with marked obesity. *New England Journal of Medicine* **346**, 802-810 (2002).
- 38. Dowse, G.K., *et al.* Abdominal obesity and physical inactivity as risk factors for NIDDM and impaired glucose tolerance in Indian, Creole, and Chinese Mauritians. *Diabetes Care* **14**, 271-282 (1991).

- 39. Sung, K.-C., Jeong, W.-S., Wild, S.H. & Byrne, C.D. Combined influence of insulin resistance, overweight/obesity, and fatty liver as risk factors for type 2 diabetes. *Diabetes Care* **35**, 717-722 (2012).
- 40. Hazlehurst, J.M., Woods, C., Marjot, T., Cobbold, J.F. & Tomlinson, J.W. Non-alcoholic fatty liver disease and diabetes. *Metabolism* **65**, 1096-1108 (2016).
- 41. Richter, M.M., et al. The liver– α -cell axis in health and in disease. Diabetes **71**, 1852-1861 (2022).
- 42. Wewer Albrechtsen, N.J., *et al.* Evidence of a liver–alpha cell axis in humans: hepatic insulin resistance attenuates relationship between fasting plasma glucagon and glucagonotropic amino acids. *Diabetologia* **61**, 671-680 (2018).
- 43. Maximos, M., *et al.* The role of liver fat and insulin resistance as determinants of plasma aminotransferase elevation in nonalcoholic fatty liver disease. *Hepatology* **61**, 153-160 (2015).

4.7 Supplementary Information

Table S1. Relationships between liver enzyme levels and baseline characteristics of T2D subjects in Study 1

	GGT		ALT		AST	
Parameters	r	P	r	P	r	P
BMI (kg/m ²)	0.37	0.02	0.38	0.01	0.24	0.11
HbA1c (%)	0.38	0.01	0.28	0.07	0.25	0.11
Fasting glucose (mmol/L)	0.07	0.7	0.05	0.8	0.08	0.6
Glucose AUC _{0-180min} (mmol/L/min)	-0.02	0.9	0.005	0.97	0.08	0.62
Fasting insulin (mU/L)	0.41	0.007	0.4	0.006	0.34	0.001
Insulin AUC _{0-180min} (mU/L*min)	0.2	0.2	0.34	0.03	0.24	0.12
Fasting C-peptide (pmol/L)	0.36	0.017	0.42	0.005	0.33	0.03
C-peptide AUC _{0-180min} (pmol/L*min)	0.15	0.35	0.25	0.1	0.18	0.3
Insulin clearance	-0.16	0.3	-0.36	0.017	-0.23	0.14
Fasting glucagon (pg/mL)	0.005	0.97	0.34	0.02	0.34	0.025
Glucagon AUC _{0-180min} (pg/mL*min)	0.1	0.46	0.44	0.003	0.4	0.009
HOMA-IR (dL/mg*L/mU)	0.43	0.002	0.46	0.0017	0.39	0.01
Matsuda index (mmol/L*mU/L)	-0.35	0.02	-0.50	0.0006	-0.43	0.005

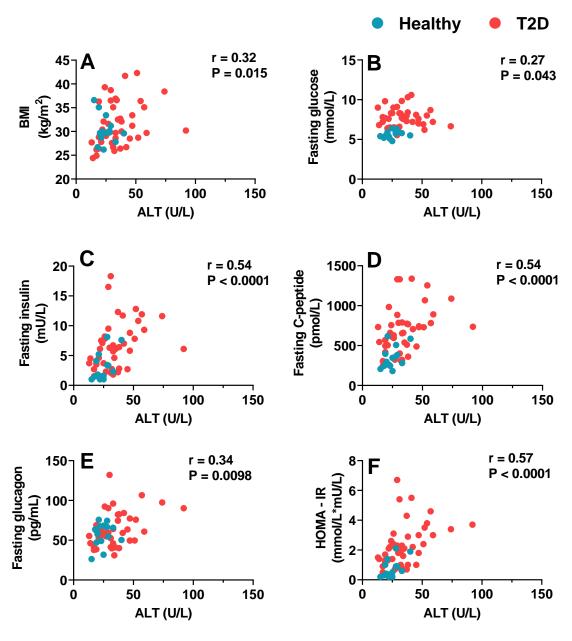


Figure S1. The relationships of BMI (A), fasting blood glucose (B), plasma insulin (C), C-peptide (D) glucagon (E) and HOMA-IR (F) with alanine transaminase (ALT) in the combined subjects without and with type 2 diabetes (T2D) after excluding significant outliers (1 in ALT level, 1 in fasting glucagon and 1 in HOMR-IR from T2D group). Spearman correlation analysis was employed to examine these relationships.

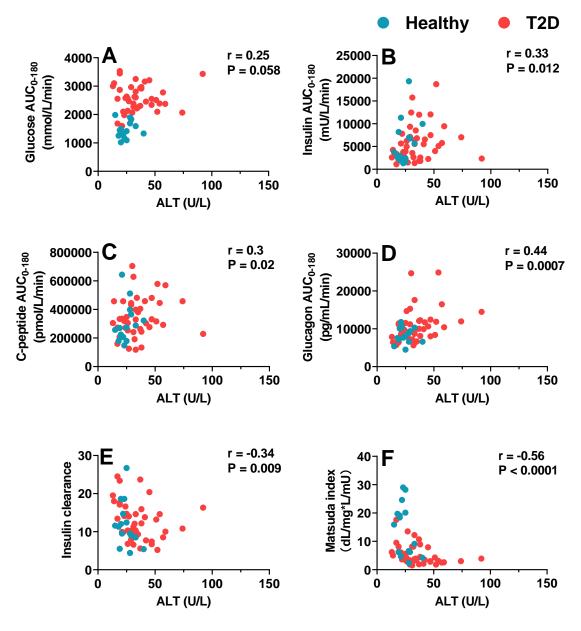


Figure S2. Relationships of the area under the curve (AUC) for blood glucose (A), plasma insulin (B), C-peptide (C), glucagon (D) between t=0-180 minutes, insulin clearance (E) and Matsuda index (F) with alanine transaminase (ALT) in the combined subjects without and with type 2 diabetes (T2D) after excluding significant outliers (1 in ALT level and 1 in glucagon AUC $_{0\text{-}180\text{min}}$ from T2D group) in Study 1. Spearman correlation analysis was employed to examine these relationships.

CHAPTER 5: THE 'EARLY' POSTPRANDIAL
GLUCAGON RESPONSE IS RELATED TO THE
RATE OF GASTRIC EMPTYING IN PATIENTS
WITH TYPE 2 DIABETES

Statement of Authorship

Title of the paper	The 'early' postprandial glucagon response is related to the rate of gastric emptying in patients with type 2 diabetes
Publication status	Published
Publication details	Huang, W., Xie, C., Wewer Albrechtsen, NJ., Jones, KL., Horowitz, M., Rayner, CK., Wu, T. (2023). "The 'early' postprandial glucagon response is related to the rate of gastric emptying in patients with type 2 diabetes", <i>Peptides</i> , 170941.

Principal Author

Candidate	Weikun Huang		
Contribution	Data collection and interpretation, statistical analysis, writing and revision of the manuscript		
Overall percentage	70%		
Certification	This paper reports on original research I conducted during the period of my Higher Degree by Research candidature and is not subject to any obligations or contractual agreements with a third party that would constrain its inclusion in this thesis. I am the primary author of this paper		
Signature		Date	September 2023

Co-Author Contributions

By signing the Statement of Authorship, each author certifies that: i) the candidate's stated contribution to the publication is accurate (as detailed above); ii) permission is granted for the candidate to include the publication in the thesis; and iii) the sum of all co-author contributions is equal to 100% less the candidate's stated contribution.

Name of Co-Author	Cong Xie		
Contribution	Data interpretation and reviewing of the manuscript		
Signature	Date September 2023		

Name of Co-Author	Nicolai J Wewer Albrechtsen			
Contribution	Data interpretation and reviewing of the manuscript			
Signature		Date	September 2023	
Name of Co-Author	Karen L. Jones			
Contribution	Data interpretation and reviewing of the manuscript			
Signature		Date	September 2023	
Name of Co-Author	Michael Horowitz			
Contribution	Data interpretation and reviewing of the manuscript			
Signature		Date	September 2023	
Name of Co-Author	Christopher K. Rayner			
Contribution	Conception and design of the study, data interpretation, reviewing of the manuscript, and guarantor of the paper.			
Signature		Date	September 2023	
Name of Co-Author	Tongzhi Wu			
Contribution	Conception and design of the study, data interpretation, reviewing of the manuscript, and guarantor of the paper.			
Signature		Date	September 2023	

5.1 Abstract

Gastric emptying (GE) is a major determinant of the postprandial glycaemic and insulinaemic responses in health and type 2 diabetes (T2D). However, the effect of GE on the postprandial glucagon response, which is characteristically augmented in T2D, is unknown. This study examined the relationship between plasma glucagon and GE of a standardised mixed meal in individuals with well-controlled T2D. 89 T2D patients (HbA1c $6.6 \pm 0.1\%$) consumed a mashed potato meal labelled with 100 µL ¹³C-octanoic acid between 0-5 minutes. Venous blood was sampled frequently over 4h for measurements of blood glucose and plasma glucagon. The gastric half-emptying time (T50) was calculated by quantification of ¹³C in the breath. Blood glucose peaked at t = 90 minutes after the meal. Plasma glucagon increased to its peak at t = 30 minutes and then decreased to a nadir at t = 180min. The T50 was 68.3 ± 1.6 min. The incremental area under the plasma glucagon curve between t = 0-30 minutes (glucagon iAUC_{0-30min}) was related inversely to the T50 (r = -0.23, P = 0.029), while the increase in blood glucose at t=30 minutes was related directly to the glucagon iAUC_{0-30min} (r = 0.25, P = 0.018). Accordingly, subjects with relatively faster GE exhibited higher postprandial glucagon and glucose levels (ANOVA: P < 0.01 for each). In well-controlled T2D, the early postprandial glucagon response to a mixed meal is partly related to the rate of GE, and predictive of the initial glycaemic response. These observations indicate that a reduction in plasma glucagon may contribute to the effect of dietary and pharmacological strategies which reduce postprandial glycaemia in T2D by slowing GE.

Keywords: gastric emptying, postprandial glycaemia, glucagon secretion, carbohydrate meal, type 2 diabetes

5.2 Introduction

Glucagon, released by the pancreatic α -cells, is an important counter-regulatory hormone of insulin for maintaining glucose homeostasis [1, 2]. While insulin resistance, and consequently a relative deficiency in insulin secretion, are characteristic pathophysiological features of type 2 diabetes (T2D), there is persuasive evidence that excessive glucagon secretion is important in the development of both fasting and postprandial dysglycaemia. Fasting plasma glucagon levels are markedly elevated in subjects with T2D compared to healthy individuals [3, 4]. Moreover, the

suppression of plasma glucagon levels following an oral glucose load or a mixed meal is markedly attenuated in T2D [5-7].

The mechanisms responsible for the regulation of glucagon secretion are complex and heterogeneous [8, 9]. In health, the secretion of glucagon is upregulated when there is a reduction in blood glucose to prevent or counteract hypoglycaemia, whereas hyperglycaemia induced by oral or intravenous administration of glucose is associated with a suppression of plasma glucagon levels [10, 11]. Unlike glucose, both amino acids and long-chain fatty acids are potent stimuli for glucagon secretion [12-15]. Accordingly, both the nutrient composition of the meal and the rate of its absorption from the gut are of relevance to the postprandial glucagon response.

The delivery of ingested nutrients from the stomach into the small intestine is tightly controlled; gastric emptying (GE) occurs at a relatively constant caloric rate in the range of 1 to 4 kcal/min in health [16]. GE is, accordingly, a key determinant of postprandial digestion and the appearance of digestive products in the circulation [17]. While it has been appreciated for a long time that GE in individuals with longstanding and complicated diabetes is frequently delayed (i.e. gastroparesis) [18], it has been recognised only more recently that T2D, associated with few complications, irrespective of overall glycaemic control, is often associated with accelerated GE [19, 20], which, in the context of relative or absolute reduction in insulin secretion, exacerbates glycaemic excursions following ingestion of carbohydrate [21]. With a mixed meal, GE also influences the digestion and absorption of protein and fat, which may modulate postprandial insulin and glucagon secretion and hence, indirectly influence the blood glucose excursion.

We hypothesised that the secretion of glucagon following a mixed meal in T2D would be influenced by the rate of GE and predictive of the postprandial glycaemic response. Accordingly, we have now examined the relationships between the postprandial glucagon response to a mixed meal and GE, and the rise in blood glucose with change in glucagon, in a cohort of patients with well-controlled T2D.

5.3 Research Design and Methods

5.3.1 Subjects

The current data were derived from two studies reported previously (clinical trial registrations ACTRN12612001005842 and ACTRN12614001131640) [22, 23]. After excluding individuals who participated in both studies (n = 5), a total of 89 subjects with T2D (56 male and 33 female, age 64.6 ± 0.7 years, BMI 29.9 ± 0.5 kg/m², HbA1c $6.6 \pm 0.1\%$) diagnosed by the American Diabetes Association criteria were included in this analysis. All participants were managed by diet (n = 37) and/or metformin monotherapy (n = 52) (the latter at a stable dose of 500 to 3000 mg per day for at least 3 months). None had gastrointestinal symptoms, a history of kidney or liver disease, gastrointestinal surgery, or was using other medications known to affect gastrointestinal function or appetite. The studies were approved by the Royal Adelaide Hospital Human Research Ethics Committee, and all participants provided written informed consent.

5.3.2 Study protocol

Each subject was evaluated on a single study day. On the evening before the study day, subjects consumed a standardised beef lasagne meal (592 kcal, McCain Foods, Melbourne VIC, Australia), together with bread, a non-alcoholic beverage and one piece of fruit, at ~7 pm. Subjects who routinely took an evening dose of metformin were instructed to withhold that dose until the end of the study. Subjects then fasted from all food and nutrient beverages, but were allowed to drink water until midnight, prior to attending the laboratory the following morning. Upon arrival, an intravenous cannula was inserted into a forearm vein for repeated blood sampling; subjects remained seated throughout the study. Between t = 0 and 5 minutes, subjects ate a semisolid meal comprising 65 g powdered potato (Deb Instant Mashed Potato; Continental, Epping, Australia) and 20 g glucose, reconstituted with 200 mL water and one egg yolk containing $100 \mu L$ ^{13}C -octanoic acid (368.5 kcal: 61.4 g carbohydrate, 7.4 g protein and 8.9 g fat). Breath samples were collected immediately before, and every 5 minutes after meal ingestion in the first hour and then every 15 minutes for a further 3 hours for the assessment of GE. "Arterialised" venous blood was sampled before the meal (t = 0 minutes) and at t = 15, 30, 60, 90, 120, 180 and 240 minutes for measurement of blood glucose and plasma glucagon. Blood

samples were placed in ice-cold EDTA tubes and were centrifuged at 3200 rpm for 15 minutes at 4 °C. Plasma was separated and stored at -80 °C before the glucagon assay.

5.3.3 Measurement of blood glucose, plasma glucagon and GE

Blood glucose concentrations were measured in duplicate at each time point by a glucometer (Optium Xceed; Abbott Laboratories, Lake Bluff, IL, USA), and computed as the mean values. Plasma glucagon concentrations were determined by radioimmunoassay (RIA, GL-32k; Millipore, Billerica, MA, USA), with a sensitivity of 20 pg/mL, intra- and inter-assay CVs of 10% and 3.1%, respectively. We noted that several commercial glucagon RIA kits exhibit considerable cross-reactivity with L-cell products such as glicentin [24] and that there was a shift in the performance of the Millipore RIA kit after the introduction of a new batch of antibody for glucagon in 2019 [25]. For this reason, the glucagon data reported were derived from the RIA kits produced before 2019, which we have further validated against the highly specific sandwich ELISA kit that detects both the N- and C-terminus of glucagon (i.e. the Mercodia ELISA kit) [25].

The ¹³CO₂ concentration in breath samples was measured by an isotope ratio mass spectrometer for computation of the gastric half-emptying time (T50) using the Wagner-Nelson formula as described previously [26]. The accuracy of the method has been validated against the gold standard technique of scintigraphy in patients with T2D [27].

5.3.4 Statistical analysis

Incremental areas under the curve (iAUC) for blood glucose and plasma glucagon were calculated using the trapezoidal rule. The relationships between pre-defined parameters were examined by either Pearson correlation analyses (if the data passed the normality test) or Spearman correlation analyses (when the data were not normally distributed), as reported in figure legends. Subjects were also stratified into three subgroups based on their GE T50 values, i.e. the fast GE group, the intermediate GE group and the slow GE group (Table 1). Homeostatic model assessment for insulin resistance (HOMA-IR) was calculated by fasting blood glucose × fasting plasma insulin / 22.5. Demographic data in these subgroups were compared using

one-way ANOVA except for gender, which was compared by Chi-square test. Blood glucose and plasma glucagon concentrations in the T50 subgroups were compared by two-way repeated measures ANOVA using 'group' and 'time' as factors. *Post hoc* comparisons were performed with Bonferroni's correction if ANOVA revealed significant interactions. All analyses were performed with GraphPad Prism 9.0 (GraphPad Software, San Diego, CA, USA). Data are presented as means \pm SEM. P < 0.05 was considered statistically significant.

Table 1. Characteristics of subjects with fast gastric emptying (GE), intermediate GE and slow GE

	Fast GE (n = 29)	Intermediate GE (n = 31)	Slow GE (n = 29)	P
T50 (minute)	52.8 ± 1.0	66.6 ± 0.8	85.5 ± 1.5	< 0.0001
Gender (male/female)	22/7	20/11	14/15	0.09
Age (year)	64.8 ± 1.3	64.2 ± 1.2	65.0 ± 1.2	0.89
BMI (kg/m^2)	30.0 ± 0.9	29.1 ± 0.9	30.6 ± 0.9	0.52
HbA1c (%)	6.8 ± 0.1	6.7 ± 0.1	6.5 ± 0.1	0.14
Diet/Metformin	6/23	15/16	16/13	0.018
HOMA-IR	3.1 ± 0.6	2.1 ± 0.3	2.0 ± 0.2	0.12

Data are means \pm SEM. One-way ANOVA was used to determine statistical differences between the subgroups, except that the distribution of gender and the use of metformin was compared using Chi-squared analysis.

5.4 Results

5.3.1 Blood glucose, plasma glucagon and GE

All participants tolerated the study well. After the meal, blood glucose concentrations increased from 8.1 ± 0.1 mmol/L to a peak of 14 ± 0.3 mmol/L at 90 minutes, followed by a gradual decline towards baseline (Figure 1A). Plasma glucagon concentrations increased promptly from 75.2 ± 2.3 pg/mL to a peak of 91.5 ± 2.7 pg/ml at t = 30 minutes, followed by a gradual decline to a nadir of 64.9 ± 2.0 pg/mL at t = 180 minutes before returning to baseline (Figure 1B). The GE T50 ranged from 39 to 116 minutes, with a mean of 68.3 ± 1.6 minutes (Figure 1C).

5.4.2 Relationships between blood glucose and GE

The rises in blood glucose from baseline at t = 30 minutes (r = -0.39, P < 0.001), t = 60 minutes (r = -0.53, P < 0.0001) and t = 90 minutes (r = -0.31, P = 0.0028) were related inversely to the T50 (Figure 2 A-C). The iAUCs for blood glucose between t = 0.60 minutes (r = -0.43, P < 0.0001), between t = 0.120 minutes (r = -0.38, P < 0.001) and between t = 0.180 minutes (r = -0.180 minutes (r = -0.180

= -0.21, P = 0.049) were also related inversely to the T50 (Figure 2 D-F). In contrast, the changes in blood glucose from baseline between t = 120-240 minutes were not related significantly to the T50 (data not shown). There was also no significant correlation between the blood glucose $iAUC_{0-240min}$ and the T50 (data not shown).

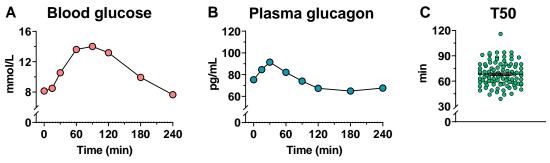


Figure 1. Concentrations of (A) blood glucose and (B) plasma glucagon and (C) the gastric half-emptying time (T50) in response to a standardised meal in patients with type 2 diabetes (n = 89).

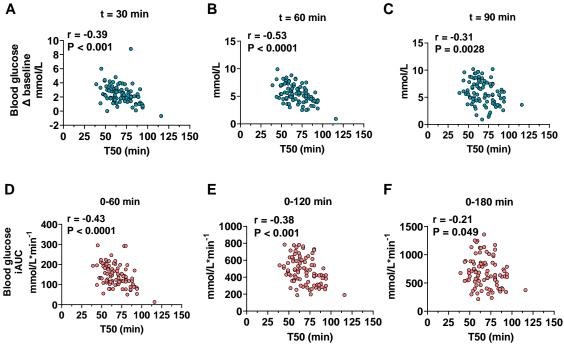


Figure 2. (A-C) Relationships of the changes in blood glucose from the baseline at t = 30, 60 and 90 minutes and (D-F) the blood glucose incremental areas under the curves (iAUCs) between t = 0-60, t = 0-120 and t = 0-180 minutes, with the gastric half-emptying time (T50) after a mixed meal in patients with type 2 diabetes (n = 89). Pearson correlation analysis was employed to examine these relationships.

5.4.3 Relationships between plasma glucagon and GE

There was no significant correlation between fasting plasma glucagon and the T50. After the meal, plasma glucagon correlated inversely with the T50 at t=15 minutes (r=-0.33, P=0.0016) and directly at t=120 minutes (r=0.21, P=0.048) (Figure 3 A-B). Moreover, the glucagon iAUC_{0-30min} (r=-0.23, P=0.029) was related inversely to T50 (Figure 3C). There was also a tendency for a weak inverse relationship between the glucagon iAUC_{0-60min} and T50 (r=-0.18, P=0.096) (Figure 3D).

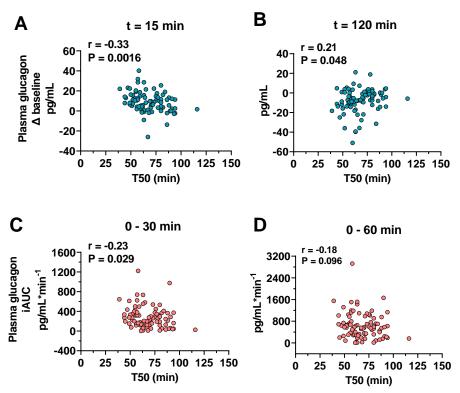


Figure 3. (A-B) Relationships of plasma glucagon at t = 15 and 120 minutes after a mixed meal and (C-D) the glucagon incremental areas under the curves (iAUCs) between t = 0-30 minutes and t = 0-60 minutes with the gastric half-emptying time (T50) in patients with type 2 diabetes (n = 89). The Spearman correlation analysis was employed to examine these relationships.

5.4.4 Relationships between blood glucose and plasma glucagon

There was no significant correlation between fasting blood glucose and fasting plasma glucagon. At t=30 minutes, both the change in blood glucose from baseline (r=0.25, P=0.018) and the glucose $iAUC_{0-30min}$ (r=0.23, P=0.032) were related directly to the $iAUC_{0-30min}$ for plasma glucagon (Figure 4 A-B).

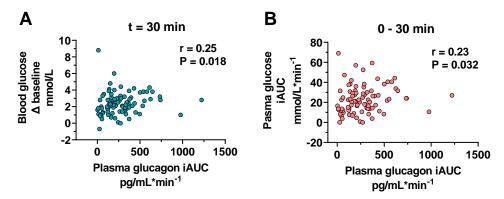


Figure 4. Relationship of (A) the change in blood glucose from baseline at t = 30 minutes and (B) the blood glucose incremental area under the curve (iAUC) between t = 0-30 minutes with the plasma glucagon iAUC_{0-30min}. Spearman correlation analysis was employed to examine these relationships.

5.4.5 Blood glucose and plasma glucagon levels in subgroups with fast, medium and slow GE

The demographic data of the three subgroups are shown in Table 1. Neither age, sex distribution, BMI, HOMA-IR or HbA1c differed between the three subgroups. Although the proportion of subjects treated with metformin was higher in the fast than slow GE group (Table 1), basal blood glucose and plasma glucagon did not differ between the three subgroups (Figure 5).

After the meal, blood glucose concentrations differed between the subgroups (group effect: P = 0.048, group by time interaction: P < 0.0001), with concentrations being higher between t = 30-90 minutes in the fast GE than slow GE subgroup (P < 0.01 each), and between t = 60-120 minutes in intermediate GE than Slow GE subgroups (P < 0.05 each) (Figure 5A). There was a significant group by time interaction for plasma glucagon (P = 0.0072), with concentrations being significantly higher at t = 15 and 30 minutes in the fast GE than the slow GE subgroup (P < 0.05 each) (Figure 5B).

5.5 Discussion

The present study indicates that, in well-controlled T2D, the early postprandial increase in plasma glucagon is related to the rate of GE. We also found that the glucagon response is predictive of early postprandial glycaemia. Together, these findings support the concept that GE,

which is frequently dysregulated in T2D, may influence the postprandial glucagon response and, hence, postprandial glycaemia.

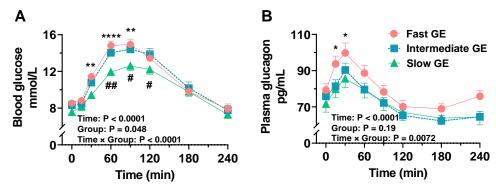


Figure 5. Concentrations of blood glucose (A) and plasma glucagon (B) in response to a standardised mixed meal (consumed between t=0.5 minutes) in type 2 diabetes patients with fast gastric emptying (GE) (n = 29), intermediate GE (n = 31) and slow gastric emptying (n = 29). Repeated-measures two-way ANOVA was used to determine statistical difference. ANOVA results are reported as P values for differences by groups, difference over time and difference due to group by time interaction. *Post hoc* comparisons were adjusted by Bonferroni's correction. Data are means \pm SEM. *P < 0.05, **P < 0.01, ***P < 0.005, ****P < 0.001 for Fast GE vs. Slow GE. *P < 0.05, **P < 0.01 for Intermediate GE vs. Slow GE.

Both the increments in blood glucose during t = 30-90 minutes and the glucose iAUC up to 3 hours after the meal correlated inversely with the T50 in T2D patients. These observations support the concept that GE is an important determinant of the postprandial blood glucose response to oral glucose or carbohydrate-containing meals in both health and T2D [28-31]. Importantly, they also extend insights derived from the 75 g oral glucose tolerance test, which revealed a fundamental shift in the relationship between the blood glucose response to oral glucose and GE in T2D when compared with health. In healthy subjects, the blood glucose response to oral glucose correlates directly with the rate of GE at 30 minutes, but inversely at 120 minutes [32], whereas in T2D this relationship remains direct over 120 minutes [28]. Together, these findings suggest that GE determines the majority of the postprandial glycaemic response in T2D.

We have shown that GE influences the appearance of exogenous glucose to modulate postprandial glycaemia in T2D [33]. In the current study, we demonstrated that the 'early' postprandial glucagon response to a mixed meal in T2D is related inversely to the T50 (i.e. directly to the rate of GE). It is noteworthy that, although delayed GE is prevalent in patients

with longstanding and complicated diabetes, GE in those with uncomplicated T2D is often accelerated [34]. Accordingly, the exaggerated glucagon secretion often seen at ~30 minutes after mixed meals in patients with T2D [5, 35-37] may be accounted for, at least in part, by the presence of rapid GE in this group. The exact mechanisms underlying this phenomenon remain elusive, but may reflect the impact of GE on the digestion and absorption of dietary protein and fat, since both amino acids and fatty acids are potent stimuli of the pancreatic α -cells [12-15]. It is also noted that suppression of glucagon is most evident following intravenous, but not oral, glucose administration (75 g) in both health and T2D [38], suggesting that gastrointestinal exposure to nutrients potentiates glucagon secretion. Indeed, the incretin hormone glucosedependent insulinotropic polypeptide (GIP), which is mainly released from the proximal small intestine and dependent on the rate of GE [39], is known to increase glucagon secretion, particularly during hypoglycaemia. Moreover, GE controls the delivery of nutrients into the small intestine. The subsequent small intestinal distension and/or the release of neurotransmitters arising from the nutrient-gut interaction may activate intestinal vagal nerves, leading to increased glucagon secretion from the pancreas [40-43]. However, the extent to which this potential mechanism may have contributed to postprandial glucagon secretion is unclear. Interestingly, the relationship between the change in plasma glucagon from baseline and the T50 became direct at t = 120 minutes. This shift is likely to be driven by the greater rise in blood glucose in subjects with more rapid GE. In keeping with this concept, our subgroup analysis showed that subjects with faster GE exhibited substantially higher blood glucose concentrations between t = 30-120minutes. We noted that the proportion of patients treated with metformin was higher in the fast than slow GE subgroup. However, the impact of this confounding factor was minimised by our instruction to patients to withhold their evening dose prior to the study. Attesting to the negligible impact of the use of metformin on the study outcomes, there was no significant difference in basal blood glucose or plasma glucagon between the subgroups.

Of note, the initial glucagon response was predictive of the postprandial blood glucose excursion within the first 30 minutes. This is consistent with previous observations made after an oral glucose load [44] or a mixed meal tolerance test [45] in individuals with prediabetes and T2D. It is also noteworthy that insulin sensitivity, as assessed by HOMA-IR, did not differ between the three subgroups, suggesting that the relationship between postprandial blood glucose and plasma

glucagon was independent of variations in insulin sensitivity. Taken together, these findings support a role for GE in regulating glucagon secretion to influence the glycaemic response to meals, at least during the early postprandial phase. Accordingly, in addition to their glucagonostatic action, slowing of GE by the glucagon-like peptide-1 (GLP-1) receptor agonists may contribute to the suppression of postprandial glucagon and glycaemia in T2D [33, 46-48].

Several limitations should be noted in interpreting our findings. First, the current study is observational in its nature and involved only patients with relatively well-controlled T2D; future intervention studies involving the modulation of GE in people with and without T2D are required to validate our interpretation. Second, the blood glucose concentrations were measured by a glucometer. To minimise the potential incidental errors, blood glucose was measured in duplicate at each timepoint. Third, the systemic appearance of digestive products (i.e. amino acids and fatty acids) that directly stimulate glucagon secretion was not measured in the current study. Further studies are warranted to clarify the relative contributions of different nutrients to the postprandial glucose and glucagon response in relation to GE. Fourth, GLP-1 and insulin concentrations were not reported in this study. Although the secretion of GLP-1 and insulin would be expected to suppress glucagon secretion [49], we have recently shown that the GLP-1 and insulin responses to an oral nutrient load are not related to GE T2D [28, 50], probably reflecting the inter-individual variations in the L-cell responsiveness to intestinal nutrient stimulation and the delayed insulin secretion in T2D. Fifth, the test meal was high in carbohydrates, so may not represent a meal typically recommended in T2D. It would be of interest to evaluate the impact of GE on the glucagon response to meals of different macronutrient compositions (e.g. rich in dietary protein). Finally, given that only patients with relatively well-controlled T2D and few complications were studied, caution should be exercised when generalising our findings to a wider T2D community.

In summary, our study indicates that the 'early' postprandial glucagon response to a mixed meal in well-controlled T2D patients is related to the rate of GE, and is predictive of the initial postprandial glucose excursion. These observations shed light on the mechanism underlying postprandial glucagon hypersecretion, and support the use of interventions that retard GE for the management of postprandial hyperglycaemia in T2D.

5.6 References

- 1. Müller, T., Finan, B., Clemmensen, C., DiMarchi, R. & Tschöp, M. The new biology and pharmacology of glucagon. *Physiological Reviews* **97**, 721-766 (2017).
- 2. Pereira, M.J., *et al.* Direct effects of glucagon on glucose uptake and lipolysis in human adipocytes. *Molecular and Cellular Endocrinology* **503**, 110696 (2020).
- 3. Reaven, G., Chen, Y.-D., Golay, A., Swislocki, A. & Jaspan, J. Documentation of hyperglucagonemia throughout the day in nonobese and obese patients with noninsulin-dependent diabetes mellitus. *The Journal of Clinical Endocrinology & Metabolism* **64**, 106-110 (1987).
- 4. Gastaldelli, A., *et al.* Influence of obesity and type 2 diabetes on gluconeogenesis and glucose output in humans: a quantitative study. *Diabetes* **49**, 1367-1373 (2000).
- 5. Müller, W.A., Faloona, G.R., Aguilar-Parada, E. & Unger, R.H. Abnormal alpha-cell function in diabetes: response to carbohydrate and protein ingestion. *New England Journal of Medicine* **283**, 109-115 (1970).
- 6. Dimitriadis, G.D., Pehling, G.B. & Gerich, J.E. Abnormal glucose modulation of islet A-and B-cell responses to arginine in non-insulin-dependent diabetes mellitus. *Diabetes* **34**, 541-547 (1985).
- 7. Knop, F.K., Vilsbøll, T., Madsbad, S., Holst, J.J. & Krarup, T. Inappropriate suppression of glucagon during OGTT but not during isoglycaemic iv glucose infusion contributes to the reduced incretin effect in type 2 diabetes mellitus. *Diabetologia* **50**, 797-805 (2007).
- 8. Hughes, J.W., Ustione, A., Lavagnino, Z. & Piston, D.W. Regulation of islet glucagon secretion: Beyond calcium. *Diabetes, Obesity and Metabolism* **20**, 127-136 (2018).
- Adeva-Andany, M.M., Funcasta-Calderón, R., Fernández-Fernández, C., Castro-Quintela,
 E. & Carneiro-Freire, N. Metabolic effects of glucagon in humans. *Journal of Clinical & Translational Endocrinology* 15, 45-53 (2019).
- 10. OHNEDA, A., *et al.* Abnormal response of pancreatic glucagon to glycemic changes in diabetes mellitus. *The Journal of Clinical Endocrinology & Metabolism* **46**, 504-510 (1978).
- 11. Gerich, J., *et al.* Comparison of the suppressive effects of elevated plasma glucose and free fatty acid levels on glucagon secretion in normal and insulin-dependent diabetic

- subjects. Evidence for selective alpha-cell insensitivity to glucose in diabetes mellitus. *The Journal of Clinical Investigation* **58**, 320-325 (1976).
- 12. Unger, R.H., Aguilar-Parada, E., Müller, W.A. & Eisentraut, A.M. Studies of pancreatic alpha cell function in normal and diabetic subjects. *The Journal of Clinical Investigation* **49**, 837-848 (1970).
- 13. Wise, J.K., Hendler, R. & Felig, P. Evaluation of alpha-cell function by infusion of alanine in normal, diabetic and obese subjects. *New England Journal of Medicine* **288**, 487-490 (1973).
- 14. Hong, J., *et al.* The short-term effect of fatty acids on glucagon secretion is influenced by their chain length, spatial configuration, and degree of unsaturation: studies *in vitro*. *Metabolism* **54**, 1329-1336 (2005).
- 15. Collins, S., Salehi, A., Eliasson, L., Olofsson, C. & Rorsman, P. Long-term exposure of mouse pancreatic islets to oleate or palmitate results in reduced glucose-induced somatostatin and oversecretion of glucagon. *Diabetologia* **51**, 1689-1693 (2008).
- 16. Phillips, L.K., Deane, A.M., Jones, K.L., Rayner, C.K. & Horowitz, M. Gastric emptying and glycaemia in health and diabetes mellitus. *Nature Reviews Endocrinology* **11**, 112-128 (2015).
- 17. Goyal, R.K., Guo, Y. & Mashimo, H. Advances in the physiology of gastric emptying. *Neurogastroenterology & Motility* **31**, e13546 (2019).
- 18. Bharucha, A.E., *et al.* Relationship between glycemic control and gastric emptying in poorly controlled type 2 diabetes. *Clinical Gastroenterology and Hepatology* **13**, 466-476. e461 (2015).
- 19. Watson, L.E., *et al.* Gastric emptying in patients with well-controlled type 2 diabetes compared with young and older control subjects without diabetes. *The Journal of Clinical Endocrinology & Metabolism* **104**, 3311-3319 (2019).
- 20. Xie, C., *et al.* Gastric emptying in health and type 2 diabetes: An evaluation using a 75 g oral glucose drink. *Diabetes Research and Clinical Practice* **171**, 108610 (2021).
- 21. Gonlachanvit, S., *et al.* Effect of altering gastric emptying on postprandial plasma glucose concentrations following a physiologic meal in type-II diabetic patients. *Digestive Diseases and Sciences* **48**, 488-497 (2003).

- 22. Wu, T., *et al.* A protein preload enhances the glucose-lowering efficacy of vildagliptin in type 2 diabetes. *Diabetes Care* **39**, 511-517 (2016).
- 23. Watson, L.E., *et al.* A whey/guar "preload" improves postprandial glycaemia and glycated haemoglobin levels in type 2 diabetes: a 12-week, single-blind, randomized, placebo-controlled trial. *Diabetes, Obesity and Metabolism* **21**, 930-938 (2019).
- 24. Wewer Albrechtsen, N.J., *et al.* Hyperglucagonaemia analysed by glucagon sandwich ELISA: nonspecific interference or truly elevated levels? *Diabetologia* **57**, 1919-1926 (2014).
- 25. Wu, T., et al. Measurement of plasma glucagon in humans: A shift in the performance of a current commercially available radioimmunoassay kit. *Diabetes, Obesity and Metabolism* **24**, 1182-1184 (2022).
- 26. Sanaka, M., Nakada, K., Nosaka, C. & Kuyama, Y. The Wagner–Nelson method makes the [13C]-breath test comparable to radioscintigraphy in measuring gastric emptying of a solid/liquid mixed meal in humans. *Clinical and Experimental Pharmacology and Physiology* **34**, 641-644 (2007).
- 27. Trahair, L.G., *et al.* Measurement of gastric emptying using a 13C-octanoic acid breath test with Wagner-Nelson analysis and scintigraphy in type 2 diabetes. *Experimental and Clinical Endocrinology Diabetes* (2022).
- 28. Jalleh, R.J., et al. Relationships of glucose, GLP-1 and insulin secretion with gastric emptying after a 75g glucose load in type 2 diabetes. The Journal of Clinical Endocrinology & Metabolism (2022).
- 29. Horowitz, M., Edelbroek, M., Wishart, J. & Straathof, J. Relationship between oral glucose tolerance and gastric emptying in normal healthy subjects. *Diabetologia* **36**, 857-862 (1993).
- 30. Jones, K., *et al.* Gastric emptying in early noninsulin-dependent diabetes mellitus. *Journal of Nuclear Medicine* **37**, 1643-1648 (1996).
- 31. Wang, X., *et al.* Disparities in gastric emptying and postprandial glycaemia between Han Chinese and Caucasians with type 2 diabetes. *Diabetes Research and Clinical Practice* **159**, 107951 (2020).

- 32. Marathe, C.S., *et al.* Relationships of early and late glycemic responses with gastric emptying during an oral glucose tolerance test. *The Journal of Clinical Endocrinology & Metabolism* **100**, 3565-3571 (2015).
- 33. Rayner, C.K., *et al.* Effects of sustained treatment with lixisenatide on gastric emptying and postprandial glucose metabolism in type 2 diabetes: a randomized controlled trial. *Diabetes Care* **43**, 1813-1821 (2020).
- 34. Jalleh, R.J., *et al.* Normal and disordered gastric emptying in diabetes: recent insights into (patho)physiology, management and impact on glycaemic control. *Diabetologia* (2022).
- 35. Thorburn, A., Litchfield, A., Fabris, S. & Proietto, J. Abnormal transient rise in hepatic glucose production after oral glucose in non-insulin-dependent diabetic subjects.

 Diabetes Research and Clinical Practice 28, 127-135 (1995).
- 36. Dunning, B.E. & Gerich, J.E. The role of α-cell dysregulation in fasting and postprandial hyperglycemia in type 2 diabetes and therapeutic implications. *Endocrine Reviews* **28**, 253-283 (2007).
- 37. Chen, X., Maldonado, E., DeFronzo, R.A. & Tripathy, D. Impaired suppression of glucagon in obese subjects parallels decline in insulin sensitivity and beta-cell function. *The Journal of Clinical Endocrinology & Metabolism* **106**, 1398-1409 (2021).
- 38. Bagger, J.I., Knop, F.K., Lund, A., Holst, J.J. & Vilsbøll, T. Glucagon responses to increasing oral loads of glucose and corresponding isoglycaemic intravenous glucose infusions in patients with type 2 diabetes and healthy individuals. *Diabetologia* 57, 1720-1725 (2014).
- 39. Wu, T., Rayner, C.K., Young, R.L. & Horowitz, M. Gut motility and enteroendocrine secretion. *Current Opinion in Pharmacology* **13**, 928-934 (2013).
- 40. Andrews, P.L. & Sanger, G.J. Abdominal vagal afferent neurones: an important target for the treatment of gastrointestinal dysfunction. *Current Opinion in Pharmacology* **2**, 650-656 (2002).
- 41. Berthoud, H.-R., Fox, E.A. & Powley, T.L. Localization of vagal preganglionics that stimulate insulin and glucagon secretion. *American Journal of Physiology-Regulatory, Integrative and Comparative Physiology* **258**, R160-R168 (1990).
- 42. Dockray, G.J. Gastrointestinal hormones and the dialogue between gut and brain. *The Journal of Physiology* **592**, 2927-2941 (2014).

- 43. Egerod, K.L., *et al.* Profiling of G protein-coupled receptors in vagal afferents reveals novel gut-to-brain sensing mechanisms. *Molecular Metabolism* **12**, 62-75 (2018).
- 44. Ichikawa, R., *et al.* Basal glucagon hypersecretion and response to oral glucose load in prediabetes and mild type 2 diabetes. *Endocrine Journal* **66**, 663-675 (2019).
- 45. Henkel, E., Menschikowski, M., Koehler, C., Leonhardt, W. & Hanefeld, M. Impact of glucagon response on postprandial hyperglycemia in men with impaired glucose tolerance and type 2 diabetes mellitus. *Metabolism* **54**, 1168-1173 (2005).
- 46. Jones, K.L., *et al.* Exenatide once weekly slows gastric emptying of solids and liquids in healthy, overweight people at steady-state concentrations. *Diabetes, Obesity and Metabolism* **22**, 788-797 (2020).
- 47. Halawi, H., *et al.* Effects of liraglutide on weight, satiation, and gastric functions in obesity: a randomised, placebo-controlled pilot trial. *The Lancet Gastroenterology & Hepatology* **2**, 890-899 (2017).
- 48. Jones, K.L., *et al.* Effects of lixisenatide on postprandial blood pressure, gastric emptying and glycaemia in healthy people and people with type 2 diabetes. *Diabetes, Obesity and Metabolism* **21**, 1158-1167 (2019).
- 49. Wu, T., Rayner, C.K. & Horowitz, M. Incretins. in *Metabolic Control* (ed. Herzig, S.) 137-171 (Springer International Publishing, Cham, 2016).
- 50. Xie, C., *et al.* Plasma GLP-1 response to oral and intraduodenal nutrients in health and type 2 diabetes—impact on gastric emptying. *The Journal of Clinical Endocrinology and Metabolism* **107**, e1643-e1652 (2022).

CHAPTER 6: EFFECTS OF A BITTER
SUBSTANCE, DENATONIUM BENZOATE, ON
PANCREATIC HORMONE SECRETION: AN EX
VIVO EVALUATION USING BOTH A RODET
β-CELL LINE AND ISOLATED MOUSE ISLETS

Statement of Authorship

Title of the paper	Effects of a bitter substance, denatonium benzoate, on pancreatic hormone secretion: an $ex\ vivo$ evaluation using both a rodent β -cell line and isolated mouse islets
Publication status	To be published
Publication details	Huang, W., O'Hara, SE., Xie, C., Liu, N., Rayner, CK., Nicholas, LM., Wu, T. (2023). "Effects of bitter substance, denatonium benzoate, on pancreatic hormone secretion: an <i>ex vivo</i> evaluation using both a rodent β-cell line and isolated mouse islets"

Principal Author

Candidate	Weikun Huang		
Contribution	Data collection and interpretation, statistical analysis, writing and revision of the manuscript		
Overall percentage	70%		
Certification	This paper reports on original research I conducted during the period of my Higher Degree by Research candidature and is not subject to any obligations or contractual agreements with a third party that would constrain its inclusion in this thesis. I am the primary author of this paper		
Signature		Date	September 2023

Co-Author Contributions

By signing the Statement of Authorship, each author certifies that: i) the candidate's stated contribution to the publication is accurate (as detailed above); ii) permission is granted for the candidate to include the publication in the thesis; and iii) the sum of all co-author contributions is equal to 100% less the candidate's stated contribution.

Name of Co-Author	Stephanie E. O'Hara		
Contribution	Data collection and interpretation, drafting and reviewing of the manuscript		
Signature		Date	September 2023

Name of Co-Author	Cong Xie			
Contribution	Data collection and interpretation, and reviewing of the manuscript			
Signature		Date	September 2023	
Name of Co-Author	Ning Liu			
Contribution	Data collection and interpretation, and reviewing of the manuscript			
Signature		Date	September 2023	
Name of Co-Author	Christopher K. Rayner			
Contribution	Data interpretation and reviewing of the manuscript			
Signature		Date	September 2023	
Name of Co-Author	Lisa M. Nicholas			
Contribution	Conception and design of the study, data interpretation, reviewing of the manuscript, and guarantor of the paper.			
Signature		Date	September 2023	
Name of Co-Author	Tongzhi Wu			
Contribution	Conception and design of the study, data interpretation, reviewing of the manuscript, and guarantor of the paper.			
Signature		Date	September 2023	

6.1 Abstract

There is increasing evidence linking bitter taste receptor (BTR) signalling to glucose homeostasis. In both rodents and humans, exposure of the gastrointestinal tract to bitter tasting substances, e.g. quinine and denatonium benzoate (DB), triggers glucagon-like peptide 1 (GLP-1) release to augment insulin secretion and reduce postprandial glycaemia. However, the effects of bitter substances beyond the gut have been poorly characterised. This study examined the effect of DB on insulin secretion from a rodent β-cell line, INS-1 832/13, and isolated mouse islets and explored the potential underlying mechanisms. At both 2.8 mM ('2.8G') and 16.7 mM ('16.7G') glucose concentrations, a relatively low concentration of DB was sufficient to induce insulin secretion dose-dependently. In contrast, at higher DB concentrations, insulin release was diminished due to cellular apoptosis. Diazoxide (a K_{ATP} channel opener) reduced DB-stimulated insulin secretion both in INS-1 832/13 cells and islets. However, probenecid (a BTR inhibitor) only reduced insulin secretion in the β-cell line, but not islets. That DB markedly increased GLP-1 secretion from islets and that blocking GLP-1 receptors by exending-39 substantially reduced DB-stimulated insulin secretion, suggests a paracrine regulation of insulin secretion within islets. In support of this, DB also stimulated glucagon and somatostatin secretion at both 2.8G and 16.7G. In conclusion, the bitter substance, DB, stimulates insulin secretion from pancreatic β-cells. This effect is mediated in part by the closure of K_{ATP} channels and stimulation of BTRs within β -cells, but is also indirectly influenced by a complex paracrine network within islets, involving GLP-1.

6.2 Introduction

Mammals can distinguish different tastes (i.e. sour, sweet, bitter, salty and umami) via distinct taste-specific sensing pathways [1]. A family of type 2 G-protein-coupled receptors (T2Rs) detect bitter taste and hence are known as bitter taste receptors (BTRs), while type 1 taste receptors heterodimerise to detect sweet (T1R2/T1R3) and umami (T1R1/T1R3) tastes [2]. In contrast to the signalling of sweet and umami tastes, which usually signal energy-rich foods and enhance the desire to eat [3, 4], bitter taste is considered aversive and serves to prevent the ingestion of potentially poisonous substances [5]. However, recent evidence has suggested that bitter taste signalling is associated with a range of health benefits, such as activation of immune

responses to infectious pathogens and maintenance of metabolic homeostasis [6]. Indeed, insensitivity to bitter substances (e.g. phenylthiocarbamide and 6-n-propylthiouracil) due to polymorphism of T2Rs is associated with a preference for fatty foods and hence increased energy intake in healthy female subjects [7]. Furthermore, a T2R haplotype which results in a functionally compromised T2R9 is associated with an increased risk of type 2 diabetes (T2D) in Amish individuals [8]. Accordingly, there is substantial interest in utilising bitter substances to stimulate the BTR signalling pathways for the management of metabolic diseases, such as obesity and T2D [9-11].

Because of the abundant expression of BTRs along the gastrointestinal tract and their co-localisation with enteroendocrine cells, investigations in relation to the metabolic effects of bitter substances have been largely centred around the gut [12]. Various bitter substances, including denatorium benzoate (DB), quinine, the fluoroquinolone antibiotic ofloxacin, berberine and bitter herbal extracts [8, 13, 14], have been shown to stimulate the release of the incretin hormone glucagon-like peptide-1 (GLP-1) from enteroendocrine L-cells. In db/db mice, oral administration of DB (1 mg/kg body weight) increased plasma GLP-1 concentrations and reduced the blood glucose response to an oral glucose load [15]. Similarly, in diet-induced obese mice, acute stimulation of intestinal T2R108 by the bitter substance, KDT501 (isohumulone 150 mg/kg, a derivative of hops), augmented plasma GLP-1 concentration by 3 folds and lowered postprandial glycaemia. Moreover, oral administration of KDT501 over 28 days (150 mg/kg) resulted in substantial reductions in body weight and body fat, as well as an improvement in insulin sensitivity [16]. Metabolic benefits of bitter substances have also been reported in humans. For example, oral administration of bitter Gentiana lutea root extract increased the GLP-1 response to a mixed meal by ~50% and reduced 24-hour energy intake by 22% in healthy subjects [17]. In healthy men, intraduodenal infusion of quinine (600 mg) increased plasma insulin and GLP-1 and lowered plasma glucose after a mixed-nutrient drink [18].

However, the potential for bitter substances to modulate the function of tissues outside of the gastrointestinal tract has received little attention. The observations that intraperitoneal injection of quinine enhanced postprandial insulin secretion in rats [19], and that intravenous infusion of quinine increased plasma insulin and reduced plasma glucose concentrations in human subjects, in the absence of gastrointestinal exposure [20, 21], suggest a direct effect of bitter substances on

pancreatic islet function. Indeed, DB (0.1 and 0.3 mM) stimulated insulin secretion dose-dependently in rodent pancreatic islets. Interestingly, this was reportedly mediated by decreasing the activity of ATP-sensitive potassium (K_{ATP}) channels rather than by T2R receptors [22].

In addition to the direct effect on β -cells, paracrine pathways may also be a potential target of DB to modulate insulin secretion. Three major endocrine cells, including α -, β - and δ -cells are densely packed in both rodent and human islet cells, and their secretory activities are interactive via cell contact and local blood flow [23]. For example, insulin secretion can be potentiated by glucagon released from α -cells and inhibited by somatostatin secretion from δ -cells [24]. There is recent recognition that α -cells are an additional source of GLP-1 secretion [25, 26], particularly in the face of systemic inflammation and islet stress [27, 28]. Given the known effect of bitter substances to stimulate intestinal GLP-1 secretion, it is likely that they also drive intra-islet GLP-1 secretion to modulate insulin secretion indirectly [29].

Therefore, this study examined the effects of the bitter substance, DB, on insulin secretion from a rodent β -cell line, INS-1 832/13, and isolated mouse pancreatic islets, and explored potential signalling pathways. The effects of DB on other pancreatic islet hormones, including GLP-1, glucagon and somatostatin, were also characterised.

6.3 Methods

6.3.1 Culture of INS-1 832/13 cells

The rat insulinoma cell line INS-1 832/13 was purchased (Merck, Australia) and cultured in RPMI 1640 supplemented with 10% fetal bovine serum (FBS, Gibco, USA), 10 mM HEPES, 2 mM L-glutamine, 1 mM sodium pyruvate, and 50 μ M β -mercaptoethanol in a 37°C incubator containing 5% CO₂. Cells were passaged approximately every 3-4 days (about 80-100% confluence). All INS-1 832/13 cell lines were routinely tested and were negative for mycoplasma.

6.3.2 Isolation of mouse pancreatic islets

Pancreatic islets from 8-week-old healthy male C57BL6 mice were isolated via density medium separation as reported previously [30, 31]. First, the bile duct was ligated and 3 mL ice-cold

Collagenase P (1 mg/mL, Roche, Australia) in Hanks' Balanced Saline Buffer (HBSS, Sigma-Aldrich, Australia) was injected via the ampulla of Vater to inflate the pancreas, which was then harvested and digested at 37°C for 16 minutes. Subsequently, 30 mL ice-cold HBSS was added to stop digestion, followed by manual shaking to achieve complete dissociation. The dissociated pancreas was then filtered through a 0.5 mm cell strainer (PluriSelect, Germany) and centrifuged at 200 g, 4 °C for 1 minute. The pellet was re-suspended in 12 mL Histopaque 1077 (Sigma, Australia) and 8 mL HBSS was slowly added on top. The separation medium was then centrifuged at 1070 g, 4 °C, for 24 minutes. The supernatant was washed twice with HBSS, after which islets were manually picked under a stereomicroscope into RPMI 1640 medium supplemented with 10% FBS and 100 U/mL Penicillin-Streptomycin (Gibco, USA). Islets were recovered in the medium overnight in a humidified atmosphere containing 5% CO₂ before functional experiments.

6.3.3 Hormone secretion study

For investigation of insulin secretion from INS-1 832/13 cells, cells were plated at a density of 2x10⁵ cells per well onto a 24-well plate coated with 100 μg/mL Poly-D-lysine. On day 5, after 2 hours starvation in secretion assay buffer (SAB), containing 114 mM NaCl, 4.7 mM KCl, 1.2 mM KH₂PO₄, 1.16 mM MgSO₄, 25.5 mM NaHCO₃, 2.6 mM CaCl₂, 20 mM HEPES, and 0.2% BSA supplemented with 2.8 mM glucose, cells were stimulated in fresh SAB for 1 hour. Following this, supernatant was collected and stored at –20 °C until analysis. Cells were harvested for measurement of protein content using PierceTM BCA protein assay kit (ThermoFisher Scientific, Australia).

For investigation of islet hormone secretion, isolated islets were incubated in pre-warmed modified Krebs-Ringer bicarbonate buffer (KRBB, 114 mM NaCl, 4.7 mM KCl, 1.2 mM KH₂PO₄, 1.16 mM MgSO₄•7H₂O, 25.5 mM NaHCO₃, 10 mM HEPES) supplemented with 2.8 mM glucose at 37 °C for 1 hour. Islets (n = 20 islets for assessment of insulin, glucagon and somatostatin secretion; n = 120 islets for assessment of GLP-1 secretion) were then stimulated in fresh KRBB for 1 hour. Following this, supernatant was collected and stored at –20 °C until analysis.

To study the effect of DB on pancreatic hormone secretion, both INS-1 832/13 cells and isolated islets were exposed to 0, 0.1, 0.5, 1, 3 and 5 mM DB under low glucose (2.8 mM, '2.8G') and high glucose concentrations (16.7 mM, '16.7G'). To investigate the signalling pathways involved in the potentiation of insulin secretion by DB, insulin secretion was also measured in the presence and absence of 250 μM diazoxide (a K_{ATP} channel opener) [32], 0.5 μM exendin₉₋₃₉ (Ex₉₋₃₉, a GLP-1 receptor antagonist, Bachem, Germany) [33] and 1 mM probenecid (a BTR antagonist, Santa Cruz, USA) [34] at both 2.8G and 16.7G. All chemicals were purchased from Sigma-Aldrich unless specified otherwise.

6.3.4 Hormone measurements

All hormones were measured by ELISA with details provided in Supplemental Table S1. Insulin secretion from INS-1 832/13 cells was normalised to cell protein content as measured by BCA assay, while hormones secreted from the islets were normalised to the number of islets.

6.3.5 Analysis of RNA-sequencing datasets

While the expression of T2Rs has been reported in human islets [35], their expression profile in specific islet cells has not been characterised. Therefore, we determined the expression of T2Rs in α -, β - and δ -cells in both mice and humans using publicly deposited sequencing datasets (GSE80673 and GSE81547) [36, 37]. Data from both control mice and healthy human subjects were extracted for analysis using R (4.3.1) and Tidyverse (2.0.0). The count table was normalised to reads per kilobase per million mapped reads (RPKM) and the normalised counts were used to determine the expression level of T2R genes in specific islet cells. The R package ggplot2 was used to visualise the expression of T2R genes.

6.3.6 Assessment of cell apoptosis and viability

Cell vitality, including the level of early cell apoptosis marker, Caspase 3/7, and live/dead cell ratio was assessed using CellEvent (ThermoFisher, USA), and calcein/propidium iodide (PI) staining, respectively. For the CellEvent assay, islets were stimulated in a 96-well plate and INS-1 832/13 cells in a 24-well plate under the same conditions as in the hormone secretion study. CellEvent dye was then added to the stimulation buffer (1:400 dilution) and incubated for 10 minutes before fluorescence measurement ($\lambda_{ex}/\lambda_{em} = 495/540$ nm) using a plate reader

(Synergy H1, BioTek, USA). For calcein/PI staining, islets were transferred to a staining buffer containing 10 μ M calcein and 5μ g/mL PI in phosphate-buffered saline (PBS, 137 mM NaCl, 3 mM KCl, 10 mM NaHPO₄, 1.8 mM K₂HPO₄) after 1-hour stimulation in 16.7G and incubated at 37 °C for 30 minutes [38]. Fluorescence images were acquired using a confocal microscope (FV3000, Olympus, Australia) with filters at $\lambda_{ex}/\lambda_{em} = 360/449$ nm and 535/617 nm for calcein and PI respectively.

6.3.7 Statistical analysis

All statistical analyses were performed in GraphPad Prism 9.0 (GraphPad Software, USA). Data are presented as means \pm SEM. Glucose-stimulated (2.8G versus 16.7G) hormone secretion (without DB) was analysed by a paired Student's t-test. The effect of DB on hormone secretion, apoptosis and cell viability at either 2.8G or 16.7G was determined by a one-way ANOVA. All other data were analysed by a two-way ANOVA with DB and another concurrent treatment (i.e. diazoxide, probenecid, or Ex_{9-39}) as factors. For both the one- and two-way ANOVA, Tukey's correction was applied for *post hoc* comparison where appropriate. P < 0.05 was considered statistically significant.

6.4 Results

6.4.1 DB potentiates insulin secretion at both low and high glucose concentrations in INS-1 832/13 cells and mouse pancreatic islets

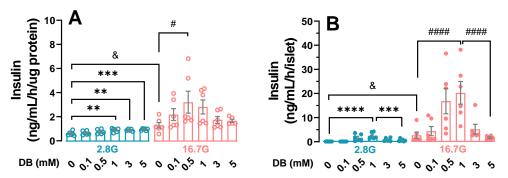


Figure 1. Effects of DB (0-5 mM) on insulin secretion from (A) INS-1 832/13 cells, and (B) mouse pancreatic islets at 2.8 mM (2.8G) and 16.7 mM (16.7G) glucose (n = 5-9 each). Paired student's t-test was used to determine the statistical difference between hormone secretion at 2.8G and 16.7G; $^{\&}P < 0.05$ for 2.8G vs. 16.7G. One-way ANOVA was used to evaluate the difference in hormone response to different concentrations of DB at either 2.8G or 16.7G. *Post hoc* comparisons were adjusted by Tukey's correction. $^{*}P < 0.05$, $^{**}P < 0.01$, $^{***}P < 0.005$, $^{***}P < 0.001$ for 2.8G; $^{*}P < 0.05$, $^{**}P < 0.005$, $^{***}P < 0.005$, $^{***}P < 0.001$ for 16.7G.

As expected, insulin secretion was higher at 16.7G vs. 2.8G in INS-1 832/13 cells. At 2.8G, insulin secretion from INS-1 832/13 cells was gradually augmented with increasing doses of DB from 0.1 to 5 mM (P < 0.0001). At 16.7G, insulin secretion increased substantially and peaked at 0.5 mM DB, followed by a progressive decline at higher concentrations (P = 0.0077, Figure 1A). In isolated islets, insulin secretion was also higher at 16.8G vs. 2.8G. There was an effect of DB on insulin secretion at both 2.8G and 16.7G (P < 0.0001 each). Under both glucose conditions, insulin secretion was highest at 0.5-1 mM DB and declined towards the control level at 5 mM DB (Figure 1B).

6.4.2 A high concentration of DB induces cell apoptosis.

High concentrations of DB (> 3 mM) have been reported to induce cell apoptosis and reduce cell viability in airway epithelial cells [39]. Thus the impact of DB on cell vitality, including the level of early cell apoptosis marker and live/dead cell ratio was assessed. Treatment of islets with 5 mM, but not 0.5 mM DB, resulted in a significant increase in the level of activated Caspase-3/7 (P < 0.05; Figures 2A and B). These findings were also replicated in INS-1 832/13 cells (P < 0.05; Figure S1A). Furthermore, it was observed in these cells that treatment with 5 mM, but not 0.5 mM DB, led to changes in cell morphology with the cells appearing more rounded in shape. However, there was no effect of DB on cell viability in islets (Figure 5C).

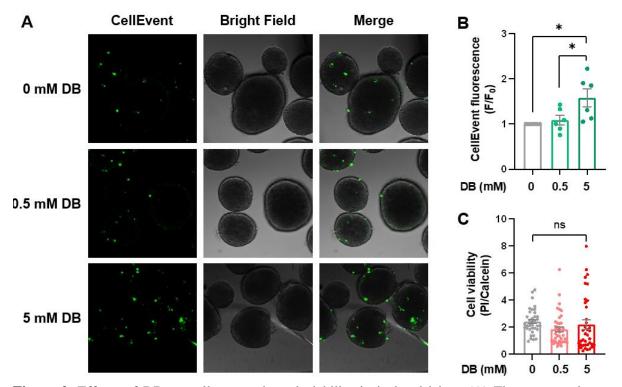


Figure 2. Effects of DB on cell apoptosis and viability in isolated islets. (A) Fluorescence images of mouse pancreatic islets stained with CellEvent in the presence of 0, 0.5 or 5 mM DB. (B) Fluorescence intensity ratio of islets stained with CellEvent in the presence of 0.5 and 5 mM DB relative to control (n = 6). (C) Cell viability calculated by the relative fluorescence intensity of propidium iodide (PI) to the fluorescence of calcein (n = 37-40). One-way ANOVA was used to determine the statistical difference between the groups with Tukey's correction applied in the *post hoc* comparisons. *P < 0.05 for 0 mM DB vs. 5 mM DB.

6.4.3 Potentiation of insulin secretion by DB is dependent on the closure of the K_{ATP} channel and BTR signalling in β -cells

In view of the potent effect of DB on stimulating insulin secretion at 0.5 mM, this concentration was selected to identify signalling pathways that may be involved in DB-stimulated insulin release. Insulin secretion from either INS-1 832/13 cells or islets was unaffected by diazoxide (K_{ATP} channel opener) at 2.8G. While diazoxide suppressed DB-stimulated insulin secretion from INS-1 832/13 cells by 38% at 16.7G (P = 0.0016 for the overall treatment effect of diazoxide), there was no interaction between diazoxide and DB (Figure 3A). By contrast, diazoxide suppressed DB-stimulated insulin secretion from islets by 78% with significant interaction with glucose (P = 0.0018; Figure 3B).

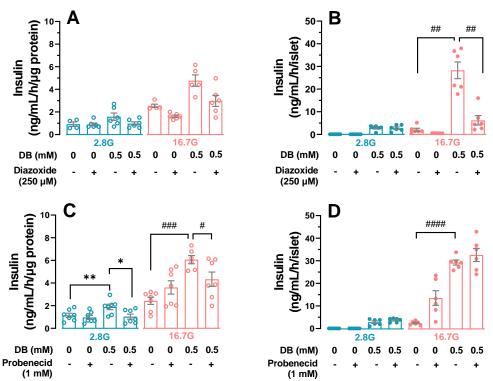


Figure 3. Effects of diazoxide (A-B) and probenecid (C-D) on insulin secretion from INS-1 832/13 cells and mouse pancreatic islets in the presence and absence of 0.5 mM DB at both 2.8 mM glucose (2.8G, blue) and 16.7 mM glucose (16.7G, red) (n = 6-8). Two-way ANOVA was used to determine the treatment effect of each compound and their interaction at either 2.8G or 16.7G. *Post hoc* comparisons were performed with Tukey's correction, if ANOVA revealed a significant interaction or treatment effect; $^*P < 0.05$, $^{**P} < 0.01$, $^{***P} < 0.005$, $^{***P} < 0.001$ at 2.8G; $^{**P} < 0.05$, $^{***P} < 0.005$, $^{****P} < 0.001$ at 16.7G.

To understand the relevance of T2R-signalling in mediating the effects of DB on potentiating insulin secretion, we first examined the expression of T2R genes in mouse and human α -, β - and δ -cells. Several T2R subtypes (T2R108, T2R135, T2R137 and T2R138) were found to be expressed in mouse islet cells, particularly α -cells. In human islets, there was more diverse expression of T2Rs across the different islet cells (Figure S3). Next, we examined the effect of the BTR inhibitor, probenecid, on DB-stimulated insulin secretion from both INS-1 832/13 cells and isolated islets. There was a significant interaction between probenecid and DB on insulin secretion in INS-1 832/13 cells at both 2.8G and 16.7G (both P < 0.01), such that DB-induced insulin secretion was reduced by probenecid by 45% at 2.8G and 34% at 16.7G, respectively (P < 0.05 each). However, probenecid had no impact on insulin secretion in isolated islets (Figures 3C and D). One explanation for this could be that DB-stimulated insulin secretion from islets

may involve a substantial contribution from the paracrine factors which maintain the elevation in insulin secretion despite the inhibition of bitter taste signalling.

6.4.4 Intra-islet GLP-1 may play a role in mediating the effects of DB on insulin secretion from isolated islets.

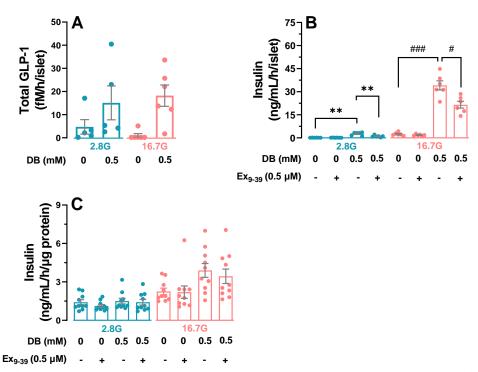


Figure 4. Intra-islet GLP-1 secretion in response to 0.5 mM DB at 2.8 mM glucose (2.8G, blue) and 16.7 mM glucose (16.7G, red) (A), and DB-stimulated insulin secretion in the absence and presence of the GLP-1 receptor antagonist, exendin₉₋₃₉ (Ex₉₋₃₉), from pancreatic islets (B) and INS-1 832/13 cells (C) (n = 5-10). Two-way ANOVA was used to determine treatment effects and interaction at either 2.8G or 16.7G. *Post hoc* comparisons were performed with Tukey's correction, if ANOVA revealed a significant interaction or treatment effect; $^*P < 0.05$, $^{**P} < 0.01$, $^{***P} < 0.005$, $^{****P} < 0.001$ for 2.8G; $^{**P} < 0.05$, $^{***P} < 0.01$, $^{****P} < 0.005$, $^{****P} < 0.001$ for 16.7G.

The lack of effect of probenecid on insulin secretion in isolated islets indicated the presence of insulin-stimulating factor(s) arising from the effect of DB on other islet cell types. Indeed, there was increased GLP-1 secretion from islets exposed to 0.5 mM DB at both 2.8G and 16.7G (overall effect of DB treatment: P < 0.01). However, there was no significant treatment effect of glucose or an interaction between glucose and DB on GLP-1 release from islets (Figure 4A). Moreover, treatment with both DB and the GLP-1 receptor antagonist, Ex₉₋₃₉, reduced insulin secretion by 62% at 2.8G and by 37% at 16.7G (P < 0.001 each). Ex₉₋₃₉ in the absence of DB did

not affect insulin secretion (Figure 4B). In contrast to the response in islets, Ex_{9-39} with or without DB did not affect insulin secretion from INS-1 832/13 cells (Figure 4C).

6.4.5 Effect of DB on somatostatin and glucagon secretion from mouse pancreatic islets

Similar to insulin, somatostatin secretion from isolated islets was higher at 16.7G vs. 2.8G (P < 0.05; Figure 5A). At both 2.8G and 16.7G, treatment of DB (0.1-0.5 mM) was associated with an increase in somatostatin secretion (P<0.01 each)). However, higher concentrations of DB (1 – 5 mM) did not further affect somatostatin secretion at 2.8G but led to a reduction in somatostatin secretion at 16.7G. As expected, glucagon secretion was lower at 16.7G compared to 2.8G (P < 0.05; Figure 5B). At both 2.8G and 16.7G, DB treatment resulted in a dose-dependent increase in glucagon secretion, which peaked at 5 mM DB (P < 0.05 each).

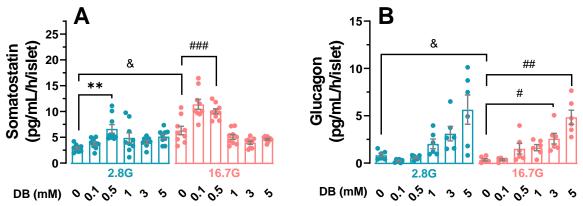


Figure 5. Effects of DB (0-5 mM) on somatostatin (A) and glucagon (B) secretion from mouse pancreatic islets at 2.8 mM (2.8G) and 16.7 mM (16.7G) glucose (n = 5-9 each). Paired student's t-test was used to examine the difference between hormone secretion at 2.8G and 16.7G without the addition of DB; $^{\&}$ P < 0.05 for 2.8G vs. 16.7G. One-way ANOVA was used to evaluate the difference in hormone response to different concentrations of DB at either 2.8G or 16.7G. *Post hoc* comparisons were adjusted by Tukey's correction. * P < 0.05, ** P < 0.01 for 2.8G; * P < 0.05, ** P < 0.005, for 16.7G.

6.5 Discussion

This study has shown that the bitter substance, DB, is a potent insulin secretagogue, capable of driving insulin secretion by closure of K_{ATP} channels and stimulation of BTR within β -cells, but also indirectly by a paracrine action of GLP-1 signalling within the islet. However, exposure to DB at high concentrations may induce islet cell apoptosis, leading to an impairment in insulin secretion. Furthermore, we observed abundant gene expression of a variety of BTRs in α - and δ -cells of both mouse and human islets, and that, beyond insulin, DB was potent at stimulating

both glucagon and somatostatin secretion from isolated islets. These observations highlight the possibility of a complex interaction of bitter substances with extra-gastrointestinal tissues, an aspect necessitating careful consideration in the development of bitter-tasting compounds for the management of metabolic disorders.

A limited number of studies have reported the of bitter substances, including DB and quinine, on insulin secretion from pancreatic β -cells and isolated rodent islets at high glucose concentrations, and the involvement of K_{ATP} channels in driving β -cell depolarisation and insulin secretion [22, 40]. The present study, however, is the first to demonstrate the stimulatory effect of DB on insulin secretion from a β-cell line and isolated mouse islets at both low and high glucose concentrations. Given that diazoxide, at a concentration sufficient to achieve the complete opening of K_{ATP} channels [41], did not affect DB-stimulated insulin secretion at 2.8G and only partially attenuated DB-stimulated insulin release at 16.7G suggests that additional signalling pathways are mediating the effects of DB. Using publicly available sequencing datasets [36, 37], we showed that T2Rs are expressed across the different islet cells in both mice and humans. Importantly, blockade of T2Rs with probenecid (which is known to inhibit at least T2R118 and 138 [42]) attenuated DB-stimulated insulin secretion from INS-1 832/13 cells, supporting a functional role of BTR-signalling within β -cells to drive insulin release. Interestingly, probenecid did not affect DB-induced insulin secretion from isolated islets at either 2.8G or 16.7G. These discrepant observations on the effect of probenecid between INS-1 832/13 cells and isolated islets are indicative of the involvement of paracrine effects of other islet cells, which are concurrently exposed to DB, in governing insulin secretion. It is also worth mentioning that probenecid (2 mM) has been shown to potentiate forskolin-induced insulin secretion from INS-1 cells by inhibiting cAMP efflux [43], although it alone (1 mM) did not affect insulin release from islets [44]. Therefore, a potential off-target effect of probenecid beyond inhibiting BTR signalling cannot be ruled out. Alternatively, it is possible that paracrine effects mediated by BTR signalling may not be sufficiently blocked by probenecid at the level of islets [34, 42].

In the present study, we showed for the first time that DB is able to stimulate intra-islet GLP-1 secretion and that blocking GLP-1 signalling using the GLP-1 receptor antagonist, Ex₉₋₃₉, markedly attenuated DB-stimulated insulin secretion from isolated islets. Of note, the latter effect was evident at both 2.8G and 16.7G, i.e. independent of glucose concentrations, which is

in contrast to the glucose-dependent insulinotropic action of circulating GLP-1 [45]. The apparent disparity in the action of intra-islet vs. extra-islet GLP-1 signalling may have reflected the involvement of other organs in coordinating circulating GLP-1-mediated insulin secretion. In addition, DB-stimulated GLP-1 secretion from intestinal L-cells and mouse duodenal tissue also occurs in the absence of hyperglycaemia [15]. This was also the case in the islets. Given the major role of intra-islet GLP-1 in mediating DB-induced insulin release, future studies are warranted to understand the relative contribution of intra-islet versus intestinal GLP-1 to the metabolic benefits of DB and other bitter substances.

Exposure of isolated islets to DB was also associated with increased glucagon and somatostatin secretion, reflecting the complexity of the interaction between DB and the islets. That somatostatin secretion was reduced, while glucagon remained augmented, in response to DB at high concentrations could be due to the higher resistance of α-cells to metabolic stress in comparison to β - and δ -cells [46, 47]. The mechanisms responsible for the stimulation of glucagon and somatostatin were not investigated in the current study, but are likely to involve both direct signalling pathways on respective endocrine cells, potentially through the K_{ATP} on these cells, and also complex paracrine effects arising from neighbouring cells. Therefore, established α - and δ -cell lines (e.g. α TC1-6 cells [48] and Rin14B cells [49], respectively) can also be used to identify the cell-autonomous effects of DB on hormone secretion. The relative contributions of glucagon and somatostatin signalling to DB-stimulated insulin secretion may also be studied by administering glucagon or somatostatin receptor inhibitors, but these were not available at the time of thesis submission. Of note, glucagon secretion did not significantly change at the stimulatory concentration of DB (0.5 mM) for GLP-1. Therefore, it would be of interest to understand how intra-islet GLP-1 is preferentially released by a low dose of DB and whether it plays a major role in glucose metabolism.

Limitations of the current study should be acknowledged. First, only islets from male mice were used. Previous studies have shown that glucose-stimulated insulin secretion from isolated islets was higher in females than males for both humans and rodents [50, 51]. Accordingly, further studies to investigate the effects of DB on pancreatic hormone secretion from the islets of female mice are warranted. Moreover, *in vivo* evaluation was not performed in the present study, so the

metabolic impact of DB-stimulated pancreatic hormone secretion observed *ex vivo* remains to be defined.

In summary, the present study shows that DB can directly drive insulin secretion from pancreatic islets. This effect is mediated by both the closure of K_{ATP} channels and stimulation of BTR pathways within β -cells, and is also indirectly governed by a complex paracrine network within islets including intra-islet GLP-1 signalling. These observations highlight the pleiotropic actions of bitter substances on endocrine tissues outside of the gut, which warrants careful consideration in the development of bitter-tasting compounds for the management of metabolic disorders. For example, the current findings also call for attention to potential 'off-target' effects arising from the administration of bitter-tasting medicines.

6.6 References

- 1. Chandrashekar, J., et al. T2Rs function as bitter taste receptors. Cell 100, 703-711 (2000).
- 2. Lossow, K., *et al.* Comprehensive analysis of mouse bitter taste receptors reveals different molecular receptive ranges for orthologous receptors in mice and humans. *Journal of Biological Chemistry* **291**, 15358-15377 (2016).
- 3. Loper, H.B., La Sala, M., Dotson, C. & Steinle, N. Taste perception, associated hormonal modulation, and nutrient intake. *Nutrition Reviews* **73**, 83-91 (2015).
- 4. Lazutkaite, G., Soldà, A., Lossow, K., Meyerhof, W. & Dale, N. Amino acid sensing in hypothalamic tanycytes via umami taste receptors. *Molecular Metabolism* **6**, 1480-1492 (2017).
- 5. Wang, Q., Liszt, K.I. & Depoortere, I. Extra-oral bitter taste receptors: New targets against obesity? *Peptides* **127**, 170284 (2020).
- 6. Lee, S.-J., Depoortere, I. & Hatt, H. Therapeutic potential of ectopic olfactory and taste receptors. *Nature Reviews Drug Discovery* **18**, 116-138 (2019).
- 7. Shafaie, Y., Koelliker, Y., Hoffman, D.J. & Tepper, B.J. Energy intake and diet selection during buffet consumption in women classified by the 6-n-propylthiouracil bitter taste phenotype. *The American Journal of Clinical Nutrition* **98**, 1583-1591 (2013).
- 8. Dotson, C.D., *et al.* Bitter taste receptors influence glucose homeostasis. *PloS One* **3**, e3974 (2008).

- 9. Suh, H.-W., *et al.* A bitter herbal medicine Gentiana scabra root extract stimulates glucagon-like peptide-1 secretion and regulates blood glucose in db/db mouse. *Journal of Ethnopharmacology* **172**, 219-226 (2015).
- 10. Rezaie, P., Bitarafan, V., Horowitz, M. & Feinle-Bisset, C. Effects of bitter substances on GI function, energy intake and glycaemia-Do preclinical findings translate to outcomes in humans? *Nutrients* **13**, 1317 (2021).
- 11. Saeed, F., *et al.* Bitter melon (Momordica charantia): a natural healthy vegetable. *International Journal of Food Properties* **21**, 1270-1290 (2018).
- 12. Xie, C., *et al.* Role of intestinal bitter sensing in enteroendocrine hormone secretion and metabolic control. *Frontiers in Endocrinology* **9**, 576 (2018).
- 13. Yu, Y., *et al.* Berberine induces GLP-1 secretion through activation of bitter taste receptor pathways. *Biochemical Pharmacology* **97**, 173-177 (2015).
- 14. Shin, M.-H., *et al.* Gentiana scabra extracts stimulate glucagon-like peptide-1 secretion via G protein-coupled receptor pathway. *BioChip Journal* **6**, 114-119 (2012).
- 15. Kim, K.-S., Egan, J.M. & Jang, H.-J. Denatonium induces secretion of glucagon-like peptide-1 through activation of bitter taste receptor pathways. *Diabetologia* **57**, 2117-2125 (2014).
- 16. Kok, B.P., *et al.* Intestinal bitter taste receptor activation alters hormone secretion and imparts metabolic benefits. *Molecular Metabolism* **16**, 76-87 (2018).
- 17. Mennella, I., *et al.* Microencapsulated bitter compounds (from Gentiana lutea) reduce daily energy intakes in humans. *British Journal of Nutrition* **116**, 1841-1850 (2016).
- 18. Rose, B.D., *et al.* Comparative effects of intragastric and intraduodenal administration of quinine on the plasma glucose response to a mixed-nutrient drink in healthy men: relations with glucoregulatory hormones and gastric emptying. *The Journal of Nutrition* **151**, 1453-1461 (2021).
- 19. Okitolonda, W., Pottier, A.-M. & Henquin, J.-C. Glucose homeostasis in rats treated acutely and chronically with quinine. *European Journal of Pharmacology* **132**, 179-185 (1986).
- Okitolonda, W., Delacollette, C., Malengreau, M. & Henquin, J.-C. High incidence of hypoglycaemia in African patients treated with intravenous quinine for severe malaria.
 British Medical Journal (Clinical Research Ed) 295, 716-718 (1987).

- 21. Taylor, T.E., Molyneux, M.E., Wirima, J.J., Fletcher, K.A. & Morris, K. Blood glucose levels in Malawian children before and during the administration of intravenous quinine for severe falciparum malaria. *New England Journal of Medicine* **319**, 1040-1047 (1988).
- 22. Straub, S.G., Mulvaney-Musa, J., Yajima, H., Weiland, G.A. & Sharp, G.W. Stimulation of insulin secretion by denatonium, one of the most bitter-tasting substances known. *Diabetes* **52**, 356-364 (2003).
- 23. Hartig, S.M. & Cox, A.R. Paracrine signaling in islet function and survival. *Journal of Molecular Medicine* **98**, 451-467 (2020).
- 24. Caicedo, A. Paracrine and autocrine interactions in the human islet: more than meets the eye. in *Seminars in Cell & Developmental Biology*, Vol. 24 11-21 (Elsevier, 2013).
- 25. Rouillé, Y., Martin, S. & Steiner, D.F. Differential processing of proglucagon by the subtilisin-like prohormone convertases PC2 and PC3 to generate either glucagon or glucagon-like peptide (*). *Journal of Biological Chemistry* **270**, 26488-26496 (1995).
- 26. Furuta, M., *et al.* Severe defect in proglucagon processing in islet α-cells of prohormone convertase 2 null mice. *Journal of Biological Chemistry* **276**, 27197-27202 (2001).
- 27. Nie, Y., et al. Regulation of pancreatic PC1 and PC2 associated with increased glucagon-like peptide 1 in diabetic rats. *The Journal of Clinical Investigation* **105**, 955-965 (2000).
- 28. Ellingsgaard, H., *et al.* Interleukin-6 enhances insulin secretion by increasing glucagon-like peptide-1 secretion from L cells and alpha cells. *Nature Medicine* **17**, 1481-1489 (2011).
- 29. Huang, W., *et al.* Sensing intra-and extra-cellular Ca²⁺ in the islet of Langerhans. *Advanced Functional Materials* **32**, 2106020 (2022).
- 30. Nicholas, L.M., *et al.* Mitochondrial transcription factor B2 is essential for mitochondrial and cellular function in pancreatic β-cells. *Molecular Metabolism* **6**, 651-663 (2017).
- 31. Nicholas, L.M., *et al.* Exposure to maternal obesity programs sex differences in pancreatic islets of the offspring in mice. *Diabetologia* **63**, 324-337 (2020).
- 32. Mariot, P., Gilon, P., Nenquin, M. & Henquin, J.-C. Tolbutamide and diazoxide influence insulin secretion by changing the concentration but not the action of cytoplasmic Ca²⁺ in beta-cells. *Diabetes* **47**, 365-373 (1998).

- 33. Raufman, J.-P., Singh, L. & Eng, J. Exendin-3, a novel peptide from Heloderma horridum venom, interacts with vasoactive intestinal peptide receptors and a newly described receptor on dispersed acini from guinea pig pancreas. Description of exendin-3 (9-39) amide, a specific exendin receptor antagonist. *Journal of Biological Chemistry* **266**, 2897-2902 (1991).
- 34. Greene, T.A., *et al.* Probenecid inhibits the human bitter taste receptor TAS2R16 and suppresses bitter perception of salicin. *PloS One* **6**, e20123 (2011).
- 35. Amisten, S., Salehi, A., Rorsman, P., Jones, P.M. & Persaud, S.J. An atlas and functional analysis of G-protein coupled receptors in human islets of Langerhans. *Pharmacology & Therapeutics* **139**, 359-391 (2013).
- 36. DiGruccio, M.R., *et al.* Comprehensive alpha, beta and delta cell transcriptomes reveal that ghrelin selectively activates delta cells and promotes somatostatin release from pancreatic islets. *Molecular Metabolism* **5**, 449-458 (2016).
- 37. Enge, M., *et al.* Single-cell analysis of human pancreas reveals transcriptional signatures of aging and somatic mutation patterns. *Cell* **171**, 321-330. e314 (2017).
- 38. Palasis, K.A., *et al.* Optical fibre-enabled photoswitching for localised activation of an anti-cancer therapeutic drug. *International Journal of Molecular Sciences* **22**, 10844 (2021).
- 39. Wen, X., *et al.* Denatonium inhibits growth and induces apoptosis of airway epithelial cells through mitochondrial signaling pathways. *Respiratory Research* **16**, 1-9 (2015).
- 40. Henquin, J., Horemans, B., Nenquin, M., Verniers, J. & Lambert, A. Quinine-induced modifications of insulin release and glucose metabolism by isolated pancreatic islets. *FEBS Letters* **57**, 280-284 (1975).
- 41. Gembal, M., Gilon, P. & Henquin, J.-C. Evidence that glucose can control insulin release independently from its action on ATP-sensitive K⁺ channels in mouse B cells. *The Journal of Clinical Investigation* **89**, 1288-1295 (1992).
- 42. Masamoto, M., Mitoh, Y., Kobashi, M., Shigemura, N. & Yoshida, R. Effects of bitter receptor antagonists on behavioral lick responses of mice. *Neuroscience Letters* **730**, 135041 (2020).

- 43. Peschke, E., *et al.* Receptor (MT1) mediated influence of melatonin on cAMP concentration and insulin secretion of rat insulinoma cells INS-1. *Journal of Pineal Research* **33**, 63-71 (2002).
- 44. Campbell, I.L. & Taylor, K.W. The effect of metabolites, papaverine, and probenecid on cyclic AMP efflux from isolated rat Islets of Langerhans. *Biochimica et Biophysica Acta* (*BBA*)-General Subjects **676**, 357-364 (1981).
- 45. Wu, T., Rayner, C.K. & Horowitz, M. Incretins. *Metabolic Control*, 137-171 (2016).
- 46. Marroqui, L., *et al.* Pancreatic α-cells are resistant to metabolic stress-induced apoptosis in type 2 diabetes. *EBioMedicine* **2**, 378-385 (2015).
- 47. Jones, B., Tan, T. & Bloom, S. Minireview: glucagon in stress and energy homeostasis. *Endocrinology* **153**, 1049-1054 (2012).
- 48. Watada, H., *et al.* PDX-1 induces insulin and glucokinase gene expressions in αTC1 clone 6 cells in the presence of betacellulin. *Diabetes* **45**, 1826-1831 (1996).
- 49. AMIRANOFF, B., LORINET, A.M. & LABURTHE, M. A clonal rat pancreatic δ cell line (Rin 4B) expresses a high number of galanin receptors negatively coupled to a pertussis-toxin-sensitive cAMP-production pathway. *European Journal of Biochemistry* **195**, 459-463 (1991).
- 50. Li, T., Jiao, W., Li, W. & Li, H. Sex effect on insulin secretion and mitochondrial function in pancreatic beta cells of elderly Wistar rats. *Endocrine Research* **41**, 167-179 (2016).
- 51. Hall, E., *et al.* Sex differences in the genome-wide DNA methylation pattern and impact on gene expression, microRNA levels and insulin secretion in human pancreatic islets. *Genome Biology* **15**, 1-22 (2014).

6.7 Supplementary Information

Table S1. Details of ELISA kits for hormone measurements

Hormone	Brand	Catalogue Number	Sensitivity
Insulin	Millipore	EZRMI-13K	0.2 ng/mL
GLP-1	Millipore	MPEZGLP1T36K	1.5 pM
Somatostatin	Phoenix Pharmaceuticals	EK-060-03	0.13 ng/mL
Glucagon	Mercodia	10-1281-01	1.5 pM

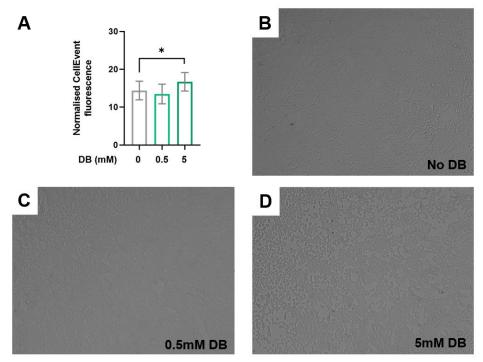


Figure S1. Apoptosis and morphology of INS-1 832/13 cells after acute DB stimulation in high glucose condition (16.7 mmol/L). (A) The normalised CellEvent fluorescence (per mg protein weight) in INS-1 832/13 cells after 1-hour stimulation with different concentrations of DB. Statistical difference between the designated groups was compared by paired Student's t-test (n = 6); *P < 0.05. (B-D) The morphology of INS-1 832/13 cell after 1-hour treatment in the absence and presence of DB (0.5 mM and 5 mM).

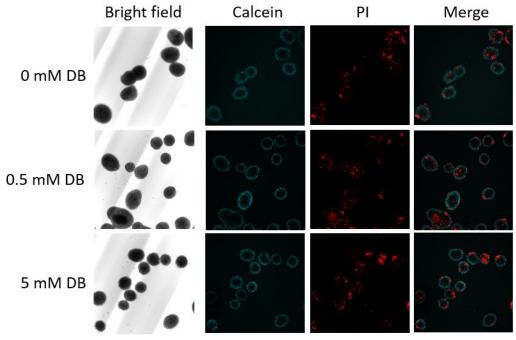


Figure S2. Propidium iodide and calcein staining of mouse pancreatic islets showing the dead (red) and live cells (blue), respectively.

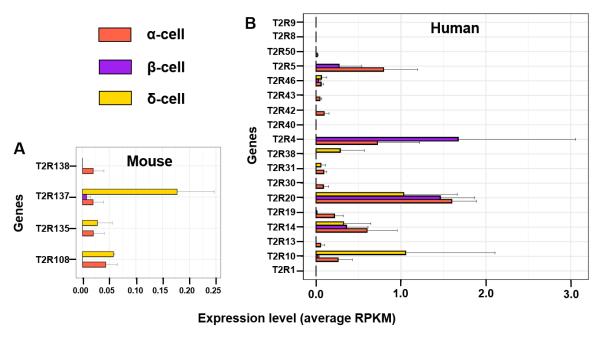


Figure S3. Expression of bitter taste receptors (T2Rs) in (A) mouse islet cells and (B) human islet cells. Data were extracted and analysed using publically deposited sequencing data GSE80673 (mouse) and GSE81547 (human).

CHAPTER 7: DEVELOPMENT OF A

GUT-ON-A-CHIP PLATFORM TO MONITOR

GLP-1 SECRETION FROM PRIMARY

INTESTINAL TISSUE

Statement of Authorship

Title of the paper	Development of a gut-on-a-chip platform to monitor GLP-1 secretion from primary intestinal tissue
Publication status	To be published
	Huang, W., Zhao, J., Xie, C., Ebendorff-Heidepriem, H., Priest, C., Young, RL.,
Publication details	Rayner, CK., Wu, T. (2023). "Development of a gut-on-a-chip platform to monitor
	GLP-1 secretion from primary intestinal tissue"

Principal Author

Candidate	Weikun Huang		
Contribution	Study design, data collection and interpretation, statistical analysis, writing and revision of the manuscript		
Overall percentage	80%		
Certification	This paper reports on original research I conducted during the period of my Higher Degree by Research candidature and is not subject to any obligations or contractual agreements with a third party that would constrain its inclusion in this thesis. I am the primary author of this paper		
Signature		Date	September 2023

Co-Author Contributions

By signing the Statement of Authorship, each author certifies that: i) the candidate's stated contribution to the publication is accurate (as detailed above); ii) permission is granted for the candidate to include the publication in the thesis; and iii) the sum of all co-author contributions is equal to 100% less the candidate's stated contribution.

Name of Co-Author	Jiangbo Zhao		
Contribution	Study design, data interpretation and reviewing of the manuscript		
Signature		Date	September 2023

Name of Co-Author	Cong Xie		
Contribution	Data collection and reviewing of the manuscript		
Signature		Date	September 2023
Name of Co-Author	Heike Ebendorff-Heidepriem		
Contribution	Study design, data interpretation and reviewing of the manuscript		
Signature		Date	September 2023
Name of Co-Author	Craig Priest		
Contribution	Data interpretation and reviewing of the manuscript		
Signature		Date	September 2023
Name of Co-Author	Richard L. Young		
Contribution	Data collection and interpretation, and reviewing of the manuscript		
Signature		Date September 2023	
Name of Co-Author	Christopher K. Rayner		
Contribution	Conception and design of the study, data interpretation and reviewing of the manuscript.		
Signature		Date	September 2023
Name of Co-Author	Tongzhi Wu		
Contribution	Conception and design of the study, data interpretation, reviewing of the manuscript, and guarantor of the paper.		
Signature		Date	September 2023

7.1 Abstract

Glucagon-like peptide-1 (GLP-1), secreted from enteroendocrine L-cells along the intestinal epithelium, is a key regulator of glucose metabolism and energy homeostasis in both health and type 2 diabetes (T2D). Understanding the mechanisms and triggers of GLP-1 secretion is of major importance to the management of metabolic disorders, but has been reliant largely on ex vivo experimental platforms involving static incubation of immortalised cell lines, which lack resemblance to the native L-cells, or of primary intestinal tissues, which are incapable of monitoring dynamic GLP-1 secretion under biomimetic conditions over a sustained period. This work, therefore, aimed to develop a microfluidic 'gut-on-a-chip' (GOC) platform to enable the monitoring of dynamic GLP-1 secretion from primary mouse intestinal tissue in a biomimetic environment. To this end, the GLP-1 secretion capacity of different regions of mouse small intestine, as well as the potential factors that may influence GLP-1 release or measurement, were investigated to guide the design of a GOC platform. A polymethyl methacrylate (PMMA) microchip was fabricated via micromachining with the capacity to immobilise a segment of intestinal tissue and facilitate two parallel perfusion flows via peristaltic micro-fluidic pumps. Finally, a well-established GLP-1 secretagogue, taurocholic acid, was perfused onto the luminal surface of mouse small intestine in an off-and-on mode as a proof-of-concept demonstration. The dynamic changes in GLP-1 concentrations evident in the serosal-side channel over 2 hours and preservation of tissue integrity compared to static incubated tissues indicate superior performance of the GOC platform to interrogate dynamic GLP-1 secretion from primary intestinal tissue. This novel GOC platform has high potential to advance understanding of the mechanisms underlying GLP-1 release, and to screen for novel GLP-1 secretagogues for therapeutic development.

Keywords: gastrointestinal function, incretin, glucagon-like peptide-1, gut-on-a-chip, microfluidics, type 2 diabetes

7.2 Introduction

The epithelium of the gastrointestinal (GI) tract comprises a range of distinct enteroendocrine cells (EECs), capable of detecting luminal contents via different chemo-sensors to release GI hormones and regulate subsequent GI motility, energy intake and glucose metabolism [1-4].

Despite representing only ~1% of all GI epithelial cells, these EECs constitute the largest endocrine organ in the human body [5, 6] and are increasingly targeted for the management of metabolic disorders, including type 2 diabetes (T2D) [7, 8]. Of particular importance to the latter are L-cells and K-cells, which release the so-called 'incretin' hormones, glucagon-like peptide-1 (GLP-1) and glucose-dependent insulinotropic polypeptide (GIP), both of which potently augment insulin secretion and glucose disposal in a glucose-dependent manner in health [9]. In T2D, the insulinotropic action of GIP is markedly diminished, while the effect of GLP-1 remains relatively intact [10, 11]. GLP-1 also slows gastric emptying, inhibits glucagon secretion and suppresses energy intake [12]. Accordingly, there is a critical need to understand the mechanisms responsible for GLP-1 release and identify novel approaches to boost GLP-1 secretion for the management of T2D.

Evaluation of intestinal GLP-1 secretion by monitoring circulating GLP-1 levels has been challenging due to its low concentrations in the peripheral circulation. Moreover, this approach has limited value for both mechanistic studies and screening for interventional compounds. *Ex vivo* setups using immortalised GLP-1-secreting cells have been utilised extensively, but the relevance of findings derived from immortalised cell lines is often limited due to their intrinsic variations from native L-cells, including the generally wider secretory repertoire and lower cell differentiation [13]. An *ex vivo* preparation using primary intestinal tissue from animals and humans has the advantage of maintaining native cell-cell connections and polarity, with correspondingly improved translatability. However, the conventionally employed tissue-based bio-release system (in a petri dish or well) suffers from a short experimental window due to the progressive loss of tissue viability, a high demand to access primary tissue, and the inability to demonstrate dynamic EEC secretory activity.

In this context, 'gut-on-a-chip' (GOC) devices are emerging as precision biomimetic platforms to study gut function [14]. These devices are micro-scale 3D intestinal culture systems, which can be functionalised with dynamic perfusion modalities to control the micro-environment precisely, recapitulating defined physiological activities and properties of the gut, including peristaltic activity [15]. The constant refreshing of culture media during the perfusion also provides the intestinal tissue with continuous nutrient support, extending the integrity and functionality of the cultured intestinal tissue from several hours to several days [16, 17]. These

unique features of GOC devices have stimulated the development of several sophisticated experimental platforms to investigate EEC activity [18]. For example, an automated microfluidic platform was developed for high-throughput imaging of intracellular Ca²⁺ in NCI-H716 cells in response to various sweet and bitter stimuli, although hormone secretion was not measured [19]. In another study, GLUTag cells (a murine GLP-1 secreting cell line) were co-cultured with INS-1 cells (an insulin-secreting cell line) in two joint perfusion chambers to study the effects of anti-diabetic compounds on GLP-1 and insulin secretion [20]. However, these models involved immortalised intestinal cell lines and thus may not recapitulate the native intestinal tissue response to intraluminal contents. The potential for a GOC system to host primary intestinal tissues for long-term monitoring of dynamic secretory activity, particularly GLP-1 release, has not been reported.

In this work, we demonstrate the development of a GOC system that integrates primary mouse small intestinal tissues and a microfluidic perfusion system to monitor dynamic GLP-1 release in response to luminal stimuli. In order to understand the GLP-1 secretory capacity of intestinal tissues, we first investigated GLP-1 secretion from different segments of mouse small intestine in response to a well-established physiological GLP-1 secretagogue, taurocholic acid (TCA) [21]. Subsequently, a microfluidic device was designed and fabricated via Computer Numerical Control (CNC) machining, and customised to (1) host a segment of mouse small intestine, (2) enable targeted stimulation on either the luminal or serosal side of the tissue via two independent perfusion flows, and (3) continuously sample the perfusates to evaluate GLP-1 outputs. To demonstrate proof-of-concept, a segment of mouse small intestine was loaded onto the chip, with 4 cycles of 'on' and 'off' perfusion with TCA to the luminal surface, to examine both GLP-1 secretion, and the morphology of the tissue sample.

7.3 Methods

7.3.1 Preparation of mouse small intestinal tissues

Mouse small intestinal tissue was prepared via direct surgical dissection as previously reported [22]. Healthy 6-hour fasted or unfasted 8-week male C57BL/6 mice were humanely killed by cervical dislocation according to ethical approval from the animal welfare committee of The University of Adelaide (Approval Number: M2021-071). The entire small intestine was removed

and pinned on a Sylgard-coated (Dow Corning, USA) petri dish containing ice-cold Krebs solution containing 118 mM NaCl, 4.7 mM KCl, 25 mM NaHCO₃, 1 mM citric acid, 1.2 mM MgSO₄, 1.5 mM CaCl₂, 1.3 mM NaH₂PO₄, and 5 mM D-glucose [23]. For GLP-1 release study, Krebs solution was supplemented with 0.1 mM DPPIV inhibitor (linagliptin) and protease inhibitor (1 tablet per 10 mL buffer) to prevent GLP-1 degradation. Excessive connective tissue was removed from the basolateral side of the intestine, which was then opened by a midline incision along the mesenteric border.

To understand the overall secretory capability of primary intestinal tissues, an off-chip GLP-1 secretion study was performed first. Briefly, segments of the small intestine, including the duodenum (< 7 cm distal to the pylorus), jejunum, and ileum (< 4 cm proximal to ileocecal valve) [24], were dissected into ~5 mm-long pieces, and then weighed before being loaded onto a 96-well plate containing the stimuli in 200 µL Krebs. Tissues were stimulated at 37°C for 1 hour in a cell incubator, after which supernatants were collected and stored at -20 °C until analysis. TCA (2.8 mM) and glucose (300 mM) were used as test stimuli, both of which have been shown to induce GLP-1 secretion potently from primary intestinal tissues, or *in vivo* [25, 26]. All chemicals were purchased from Sigma unless specified otherwise.

7.3.2 Design, fluidic simulation and fabrication of the microfluidic device

The structure of the GOC device was designed and visualised in AutoCAD while the fluid dynamics were simulated in COMSOL 5.6 (COMSOL Multiphysics, Sweden). The parameters of the simulation followed the principle of the previous report [27], except that the flow rate at the two inlets was set as $100 \,\mu\text{L/min}$ to achieve an experiment sampling frequency shorter than 2 minutes for GLP-1 assays.

The GOC device was fabricated using a milling machine (RoboDrill 3-axis, Fanuc, Japan) at the Australian National Fabrication Facility South Australian Node. The surface diameters of the device were verified using a laser confocal microscope (OLS5000, Olympus, Japan).

7.3.3 Optical examination of the dimensions of the microfluidic channels

An optical microscope (BX51, Olympus, Japan) was used to examine the overall appearance and dimensions of the fabricated microfluidic channels and chip, while an optical profiler Contour

GT-I (Bruker, Germany) was used to measure precise chip dimensions via vertical scanning interferometry (VSI). To expand the view, $5\times$ and 0.55 were applied to the objective and multiplier, respectively. Three repeated measurements were conducted, and mean values were calculated.

7.3.4 Experimental characterisation of on-chip fluidic dynamics

A perfusion system was configured to facilitate two independent and continuous flows through the microchip (Figure S2). The two inlets of the microchip were connected to two precision peristaltic pumps (L100-1S-2, Longer, China) via silicone tubing (1 mm OD \times 1 mm wall thickness, Longer, China). Each outlet was also connected to a silicone tubing to collect effluents into 1.5 mL Eppendorf tubes. Prior to all perfusion experiments, the tubing and microchip were treated with sequential perfusion of 70% ethanol, deionised (DI) water and Krebs supplemented with 1% BSA (15 minutes each) at 500 μ L/min for cleaning and blocking the surface. Both diluted food colouring solution, 10% in deionised (DI) water, and reconstituted human GLP-1 (Bachem, Germany) in Krebs solution were perfused through the luminal channel of the microchip to visualise flows and characterise the experimental fluidic dynamics.

7.3.5 On-chip study of GLP-1 secretion from small intestinal tissue

The duodenum from C57BL/6 mice was dissected into a 2.5 cm long opened tissue, and loaded into the tissue chamber of the microfluidic chip. Krebs buffers supplemented with 0.1 mM linagliptin, protease inhibitor and 1% BSA for perfusion were placed in a water bath maintained at 40 °C so that the temperature of the buffer was 37 °C on entry to the chip. Upon loading, the intestinal tissue was equilibrated by perfusing for 20 minutes with control Krebs buffer before commencing secretion experiments.

7.3.6 Measurement of GLP-1 concentrations

The concentrations of active GLP-1 in the off-chip incubation samples and on-chip perfusion samples were measured by ELISA (EGLP35K, Millipore, USA), with a detection limit of 6.6 pg/mL.

7.3.7 Hematoxylin and eosin (H&E) staining of intestinal tissues

Post-infusion intestinal tissues were fixed in 10% formalin solution overnight at room temperature. On the second day, fixed tissues were cleaned with DI water before storage in 70% ethanol. The tissues were then embedded into paraffin and sliced at 5 μ M thickness using a microtome (Leica RM2235), after which the slides were stained using the H&E coverstainer (Agilent CS10030).

7.3.8 Statistical analysis

Changes in GLP-1 concentration in response to each stimulus were calculated by dividing the GLP-1 concentration at each time point by the baseline concentration at the serosal channel. Data are presented as means \pm SEM unless specified. Differences in GLP-1 concentration were standardised to tissue weight where relevant, and compared using paired Student's t-test. P < 0.05 was considered statistically significant.

7.4 Results and Discussion

7.4.1 Off-chip characterisation of GLP-1 release from mouse small intestine

To facilitate the design of the GOC platform, it is critical to understand how GLP-1 is secreted from intestinal tissues *ex vivo*, particularly the magnitude of secretion in response to physiologically relevant stimuli and the experimental conditions that influence its secretion and measurement. These include the impact of stimulation time, implementation of a fasting protocol prior to the collection of intestinal tissue, and the addition of BSA in the perfusate.

As expected, tissue weight decreased progressively from the duodenum towards the ileum (Figure S1A), due to decreasing wall thickness [28]. We first examined the GLP-1 response of different sections of the mouse small intestine to a physiological GLP-1 secretagogue, TCA, at low physiological concentration (2.8 mM). As shown in Figure 1A, treatment with TCA (2.8 mM) over 1 hour increased GLP-1 secretion from all regions of the small intestine from unfasted mice (each P < 0.05), with the magnitude numerically, but not significantly, greater in the duodenum (5.5 ± 0.9 pg/mL per mg tissue) than jejunum (1.0 ± 0.06 pg/mL per mg tissue) or ileum (3.1 ± 0.5 pg/mL per mg tissue). This is consistent with previous reports in which TCA

treatment potently stimulated GLP-1 secretion from mouse intestinal tissue *ex vivo* (100 µmol/L in culture medium) [29] and human subjects *in vivo* (75mg/mL in rectal infusion buffer) [30]. The density of L-cells is higher in the distal than proximal small intestine in rodents [31, 32], so the observed higher basal and TCA-evoked GLP-1 secretion from the duodenum may reflect a higher secretory activity and/or sensitivity to TCA in proximally located L-cells, compared to their distal counterparts.

We did not observe a significant difference in TCA-evoked GLP-1 response between 0.5-hour and 1-hour of incubation (Figure 1B), however 2-hour incubation led to significantly decreased GLP-1 concentrations (P < 0.05 each). This suggests that GLP-1 was promptly released and that maximum levels occurred within a relatively short period of TCA exposure. The inability of prolonged TCA exposure to increase GLP-1 concentrations is aligned with the concept of negative feedback regulation of GLP-1-signalling on its subsequent secretion [33, 34]. The decrease in GLP-1 concentrations from 1-hour to 2-hour TCA exposure may also parallel an increase in GLP-1 degradation, despite the presence of DPPIV and protease inhibition in the buffer.

Fasting acts to return metabolism to baseline and reduce variability in physiological parameters in metabolic studies [35]. Indeed, a fasting period of at least 6 hours has been widely adopted in glucose tolerance tests in mice to characterise postprandial glucose-evoked responses of glucoregulatory hormones, including GLP-1. Therefore, it is relevant to understand whether fasting influences GLP-1 secretion from primary intestinal tissues. We therefore compared the GLP-1 response to TCA and glucose in primary intestinal tissues of fasted and unfasted mice. As shown in Figure 1C, the relative increase in glucose-induced GLP-1 secretion was ~4-fold higher in the duodenal tissue of fasted compared to unfasted mice (P < 0.05). Similarly, the TCA-induced increase in GLP-1 was more than 2-fold higher in the duodenum in fasted animals (P<0.05). However, glucose and TCA-evoked GLP-1 release from the jejunum or ileum did not differ between fasted and unfasted mice. This regional difference in the impact of fasting on GLP-1 response likely reflects the fact that a 6-hour fast, while sufficient to clear the stomach and duodenum, may not be long enough for the distal jejunum and ileum. In metabolic studies of mice and humans, an overnight fast longer than 10 hours may be more appropriate [36, 37].

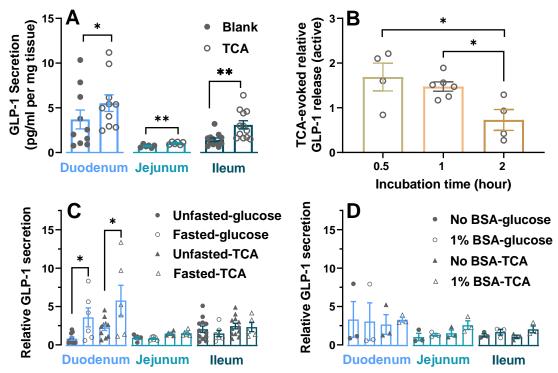


Figure 1. GLP-1 secretion from mouse small intestine. (A) GLP-1 secretion from small intestine regions in the absence (blank) and presence of 2.8 mM taurocholic acid (TCA, n = 6-12). (B) TCA-evoked relative GLP-1 secretion from jejunum after 0.5, 1 and 2 hours stimulation (n = 4-6). (C) Relative GLP-1 secretion (normalised to respective control levels) from small intestinal segments of unfasted and 6-hour fasted mice in response to either 5% glucose (dots) or 2.8 mM TCA (triangles) (n = 6-12). (D) GLP-1 secretion (normalised to respective control levels) from small intestine regions in response to glucose (dots) or TCA (triangles) in the absence or presence of 1% BSA (n = 3). Data are means \pm SEM. Paired Student's t-test was used to determine group differences. *P < 0.05, ***P < 0.01, ***P < 0.005, ****P < 0.001.

BSA is often provided as a nutrient source for endocrine cells and acts as a decoy substrate for proteases in *ex vivo* hormone secretion studies; it also prevents non-specific binding of secreted hormones to plastic surfaces [38, 39]. However, BSA may directly and markedly enhance the secretory activity of the endocrine cells [40], a fact that may explain the inconsistent use of BSA in GLP-1 secretion studies [3, 41]. We examined the impact of BSA on the measurement of GLP-1 in the presence or absence of intestinal tissue. As shown in Figure S1B, less than 10% of added GLP-1, in the range of 100 to 1000 pM, was detected by active GLP-1 ELISA kits in the absence of BSA in tissue-free incubation, while supplementation of 1% BSA increased the detected GLP-1 to the expected values. This difference is likely to have reflected non-specific binding of GLP-1 to plastic surfaces in the absence of BSA. By contrast, the presence of 1% BSA did not significantly improve evoked GLP-1 responses to glucose or TCA in the presence of intestinal tissue (Figure 1D). Accordingly, the impact of BSA on GLP-1 secretion and/or

detection appeared to be negligible when intestinal tissue was present, probably because the protein products released from the tissue are sufficient to substitute for the functions of BSA.

These *ex vivo* experiments have established the capability of primary small intestinal tissue in fasted or unfasted mice to respond to physiological stimuli (glucose and TCA) and release GLP-1 at levels reliably detected by a commercial ELISA kit. Although GLP-1 responses to TCA varied between different small intestinal regions, we opted to use duodenum for proof-of-concept demonstration in subsequent experiments as this section is generally thicker and is easier to be positioned on the chip. While implementation of a fasting protocol may increase GLP-1 responses, we opted to collect duodenal tissues from unfasted mice to ensure that the GOC platform is capable of detecting suboptimal GLP-1 signals. Finally, although the effect of BSA on GLP-1 secretion was not apparent in static tissue incubations, it was added to the perfusion buffer during on-chip perfusion of duodenal tissue to limit the non-specific binding of GLP-1 to the larger surface areas of the plastic perfusion tubes and the microfluidic chip.

7.4.2 Design, fabrication and characterisation of the GOC device

The conventional static tissue bio-release system has several intrinsic drawbacks when studying the endocrine function of intestinal tissues, including potential inhibition of secretion arising from negative feedback regulation, degradation of accumulated GLP-1, stimulation of both luminal and serosal sides of the tissue, and an inability to dynamically profile secretion. To circumvent these issues, the design of the GOC platform should: (1) immobilise an intestinal tissue of a size that releases GLP-1 at detectable levels under the target sampling frequency and flow rate (detailed below); (2) provide two independent perfusion channels for flexible delivery of stimuli to the mucosa or serosa, as well as removal and collection of perfusates for subsequent profiling of dynamic GLP-1 secretion.

As shown in Figure 2A, the GOC device consists of two perfusion channels, top and bottom, separated by a tissue chamber and a polycarbonate (PC) membrane. The use of dual independent perfusion channels allows for constant refreshing of media and permits delivery of stimuli to the luminal or serosal surface of the intestinal tissue, an advantage compared to conventional static incubation. The dual channels also permit the customisation of independent flows on both sides of the intestinal tissue for specific purposes. The shape of the tissue chamber was designed to fit

the intestinal sample so that no additional tissue processing is needed, and the assembly of the device can be simplified. A porous PC membrane with a pore size of 3 μ m was built in the tissue chamber to physically support the tissue during perfusion while also allowing for permeation of bioactive molecules between the media in the top and bottom channels, i.e. serosal and luminal channels, respectively.

The dimensions of the perfusion channel and tissue chamber are detailed in Figure S2. The height of the top channel, tissue chamber, and bottom channel is 1 mm (Figure S4 and Table S1) to host a 2.5×0.5 cm intestinal tissue sample, and to permit detectable GLP-1 secretion at flow rates under 100 µL/min under a target sampling frequency of 2 minutes based on *ex vivo* GLP-1 secretion studies in static culture systems. Each layer of the device is fabricated from transparent poly(methyl methacrylate) (PMMA), so the immobilised intestinal tissue can be visualised throughout the perfusion (displayed in Figure 2B-D). Two O-rings are embedded in the two layers with perfusion channels to prevent the leaking of perfusate from the interstitial space between the top channel layer and tissue chamber. The simulated fluidic dynamics of the integrated channels, with an object occupying the tissue chamber as a surrogate for intestinal tissue, show that the flow speed is identical across the horizontal plane of both perfusion channels. This indicates that the mucosa and serosa of the tissue will be exposed to homogenised flow, ensuring all cells receive uniform chemical and physical stimulation. When assembling the device, a section of small intestinal tissue was loaded onto the tissue chamber with the mucosa facing the membrane and the bottom channel flow.

The loaded tissue with an actual length of 2.7-3.0 cm is clamped by extruding the proximal end of the tissue into the interstitial space between the top layer and tissue chamber layer (Figure 2F). Previous reports have utilised a circular clamp to immobilise all edges of the intestinal tissue [17] which achieved complete immobilisation of the tissue and separation of the two perfusion channels, but often caused significant damage around the entire tissue. In another work, intestinal tissue was adhered to the underlying membrane using cyanoacrylate glue [16]. This is likely to impact the secretory activity of the tissue as the adhesive fully covers the surface of the tissue, which, on one hand, may directly stimulate the tissue and, on the other hand, hinder the interaction between the perfusate and cells. By contrast, the current clamping mechanism

minimises tissue damage, while achieving immobilisation of the tissue and separation between luminal and serosal sides during perfusion.

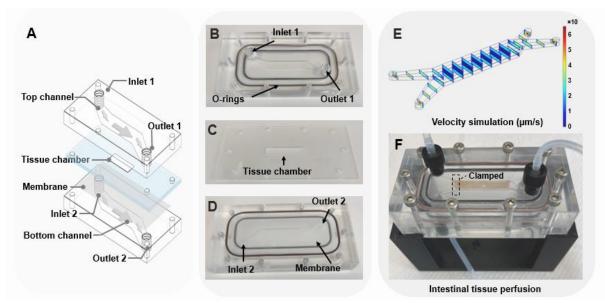


Figure 2. Design, fabrication and perfusion dynamics of the gut-on-a-chip (GOC) device. (A) Schematic of the structure of the GOC device, which is composed of (from top to bottom) a top channel, tissue chamber, membrane and a bottom channel. (B) The top channel, (C) tissue chamber, and (D) bottom channel covered with a polycarbonate membrane (blue colour) fabricated from polymethyl methacrylate (PMMA). Two O-rings are embedded around the top and bottom channels to prevent the leaking of buffer. (E) Fluidic dynamics in the GOC device simulated by COMSOL. (F) The assembled GOC device with a section of mouse intestinal tissue mounted in the tissue chamber.

7.4.3 Characterisation of fluidic dynamics and on-chip GLP-1 secretion from primary intestinal tissue

To characterise the permeation of molecules between the luminal and serosal chambers of the GOC device, the fluorescent dye, calcein, was perfused into the bottom channel as a surrogate for luminal stimulation. As shown in Figure 3A, calcein fluorescence was detected in the top channel, suggesting permeation from the bottom to top. As the flow rate decreased from 500 μ L/min to 100 μ L/min, the concentration of calcein increased substantially, as reflected by fluorescence intensity (Figure 3A). Therefore, a perfusion rate of 100 μ L/min should allow effective permeation of stimulatory molecules into the tissue, and enable the collection of a 200 μ L sample every 2 minutes (100 μ L is required for the GLP-1 assay). When an intestinal tissue sample was loaded on the membrane, the fluorescence detected in the top channel was

substantially blunted, indicating excellent separation of the two champers in our setup, without leakage (Figure 3B).

The fluidic dynamics were then characterised by perfusing GLP-1 in artificially oscillating concentrations. The travel time within the device suggests that buffer flows from the pump to the sampling tubes at a flow rate of 100 µL/min in 12.1 minutes. As shown in the uncalibrated results for GLP-1, there was an actual delay of 12 minutes from the switch of GLP-1-containing buffer at the reservoir to the detection of GLP-1 concentration rise (Figure S5). After this adjustment, the four detected peaks in GLP-1 were well matched to GLP-1 perfusion (8-minute blank + 12-minute GLP-1) during the entire perfusion study (Figure 3C). It is worth noting that the decrease in GLP-1 concentrations during the artificial oscillation did not return to baseline, suggesting that the 8-minute wash-out with blank buffer may be insufficient to remove GLP-1 in the tissue chamber, or that the duration of the nadir was too brief to be recorded under the current measurement frequency. Therefore, the blank-TCA cycle was set to provide 12 minutes blank buffer and 8 minutes TCA in the subsequent proof-of-concept experiment (detailed below), to better separate the GLP-1 response to the programmed stimulation.

TCA-induced GLP-1 secretion occurred predominantly in the top channel of the GOC platform, which faced the serosal side of the intestinal tissue specimen, consistent with GLP-1 secretion into the basolateral side of L-cells [42]. After calibration for fluid travel time, GLP-1 concentrations increased ~0-4 minutes after the end of each TCA stimulation rather than immediately on TCA application, i.e. 8-12 minutes after each switch-on of the TCA cycle. This is consistent with a previous report of a delay of ~10 minutes between the stimulation of primary intestinal tissue and GLP-1 release [43]. There is evidence suggesting that the effect of bile acids on GLP-1 secretion requires access to basolaterally located G protein-coupled bile acid receptors which may, in part, account for this delay in GLP-1 release [29].

It is worth noting that the magnitude of the TCA-induced GLP-1 response detected in the GOC device (around 15% of baseline) was smaller in dynamic than static incubations, where the TCA-induced GLP-1 release was 2.3-fold of baseline. Two factors may be responsible for this variation in GLP-1 response. First, the media volume per mg tissue ratio was approximately 12 times higher in the dynamic perfusion system and markedly diluted GLP-1 concentration.

Second, not all secreted GLP-1 egressed the serosal surface and entered the serosal channel, as a portion of GLP-1 was detected in the luminal channel (around 40-50% of the baseline level in the serosal channel, Figure 3D). Third, while the serum concentration of total BAs is around 3 µM [44, 45], postprandial BA concentrations can increase to over 10 mM in mice and humans [46, 47]. In contrast to well-based intestinal tissue with TCA in the static system, the luminal surface of intestinal tissue loaded on the chip was exposed to a very low concentration of TCA, without immediate TCA stimulation at the serosal side. Therefore, administration of TCA at higher concentrations is likely to improve the magnitude of serosal GLP-1 responses on-chip.

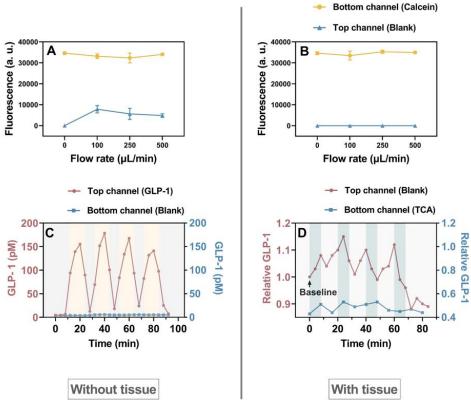


Figure 3. On-chip characterisation of fluidic dynamics of the gut-on-a-chip (GOC) device in the absence and presence of intestinal tissue. Fluorescence intensity of calcein was detected in the efflux from both sides of the channels when calcein was perfused into the bottom channel under different flow rates (A) in the absence and (B) in the presence of mouse intestinal tissue ($\lambda_{ex}/\lambda_{em} = 470/525$ nm) (n = 6 each). (C) Monitoring of dynamic GLP-1 concentration measured in the efflux from the top (red curve) and bottom (blue curve) channel in the absence of tissue. GLP-1 concentrations were switched between 0 and 100 pM in the top channel to mimic GLP-1 secretion from the serosal side of intestinal tissue for 4 cycles. In each cycle, perfusion with blank buffer and GLP-1-supplemented buffer lasted 8 and 12 minutes, respectively. (D) Monitoring of dynamic GLP-1 concentrations in the top channel (serosa side, red curve) and bottom channel (mucosa side, blue curve) in the GOC device during off-and-on stimulation with 2.8 mM taurocholic acid (TCA) over 4 cycles. In each cycle, perfusion with blank buffer and TCA buffer lasted 12 minutes and 8 minutes in the bottom channel (mucosa side), respectively.

7.4.4 Assessment of tissue morphology after static incubation and dynamic perfusion

The viability of the intestinal tissue in a dynamic perfusion system can be maintained for up to 72 hours [16]. Therefore, we assessed morphological changes in small intestinal tissues after on-chip perfusion using H&E staining in comparison with tissues after static incubation. The morphology of freshly isolated intestine in Figure 4A and S6 shows normal mucosa architecture with clearly defined villi and crypts, and muscularis propria consisting of an inner circular muscle layer and an outer longitudinal muscle layer. As in previous studies, intestinal tissue structures were maintained after both static incubation and dynamic perfusion [17, 48], although villi appeared blunted and distorted. This is likely due to the fragility of the mucosa after 2 hours in warm buffer, and thus the preparation procedures for histological staining would inevitably cause substantial damage to the villi, particularly when straightening the tissues on the histology pads.

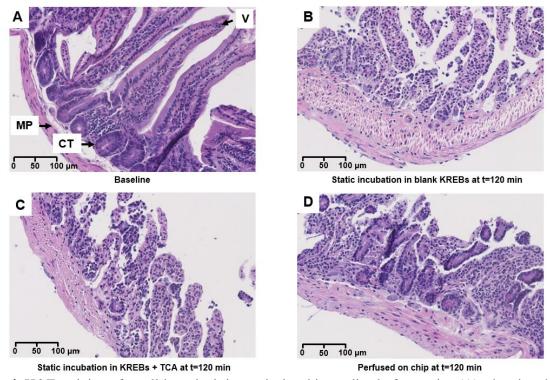


Figure 4. H&E staining of small intestinal tissues isolated immediately from mice (A), showing the villi (V), crypt (CT) and muscularis propria (MP). (B) and (C) show the morphology of small intestinal tissues after 2-hour static incubation in blank Krebs and Krebs supplemented with 2.8 mM TCA in a 96-well plate respectively. (D) shows small intestinal tissue after dynamic perfusion with 4 cycles of on-and-off stimulation with 2.8 TCA over 2 hours in a gut-on-a-chip device. Scale bars are 0-100 μm.

7.5 Conclusions

Understanding the mechanisms and triggers of intestinal GLP-1 secretion represents a key area in the development of gut-based therapies for metabolic diseases, particularly T2D. The present work reports a unique GOC platform, based on a microfluidic chip, to investigate dynamic GLP-1 secretion from primary intestinal tissue. The design of the microfluidic chip permits the immobilisation of intestinal tissue with minimal physical stress and provides homogenised flows for continuous nutrient support and controlled stimulation through two independent perfusion channels at the luminal and serosal surfaces. Upon integration with a temperature-controlled buffer reservoir and peristaltic pumps, the GOC platform can precisely control the micro-environment of the mucosa and serosa of intestinal tissue. The dynamic GLP-1 secretion profile of primary intestinal tissue in response to a physiological GLP-1 secretagogue (TCA) was successfully recorded on the GOC platform. Importantly, this platform shows advantages over conventional static incubation in preserving the integrity of the tissue for at least 2 hours. This novel device holds the potential for numerous biomedical applications, including mechanistic studies to gain deeper insights into GLP-1 secretion and high throughput screening of GLP-1 secretagogues for therapeutic development.

7.6 References

- 1. Gribble, F.M. & Reimann, F. Enteroendocrine cells: chemosensors in the intestinal epithelium. *Annual Review of Physiology* **78**, 277-299 (2016).
- 2. Murphy, K.G. & Bloom, S.R. Gut hormones and the regulation of energy homeostasis. *Nature* **444**, 854-859 (2006).
- 3. Xiong, Y., *et al.* Activation of FFA1 mediates GLP-1 secretion in mice. Evidence for allosterism at FFA1. *Molecular and Cellular Endocrinology* **369**, 119-129 (2013).
- 4. Xie, C., *et al.* Role of bile acids in the regulation of food intake, and their dysregulation in metabolic disease. *Nutrients* **13**, 1104 (2021).
- 5. Ahlman, H. & Nilsson, O. The gut as the largest endocrine organ in the body. *Annals of Oncology* **12**, S63-S68 (2001).

- 6. Martin, A.M., Sun, E.W. & Keating, D.J. Mechanisms controlling hormone secretion in human gut and its relevance to metabolism. *Journal of Endocrinology* **244**, R1-R15 (2020).
- 7. Khursheed, R., *et al.* Treatment strategies against diabetes: Success so far and challenges ahead. *European Journal of Pharmacology* **862**, 172625 (2019).
- 8. Brandt, S.J., Götz, A., Tschöp, M.H. & Müller, T.D. Gut hormone polyagonists for the treatment of type 2 diabetes. *Peptides* **100**, 190-201 (2018).
- 9. Wu, T., Rayner, C.K. & Horowitz, M. Incretins. *Metabolic Control*, 137-171 (2016).
- 10. Wu, T., *et al.* Effects of sitagliptin on glycemia, incretin hormones, and antropyloroduodenal motility in response to intraduodenal glucose infusion in healthy lean and obese humans and patients with type 2 diabetes treated with or without metformin. *Diabetes* **63**, 2776-2787 (2014).
- 11. Nauck, M.A., *et al.* Preserved incretin activity of glucagon-like peptide 1 [7-36 amide] but not of synthetic human gastric inhibitory polypeptide in patients with type-2 diabetes mellitus. *The Journal of Clinical Investigation* **91**, 301-307 (1993).
- 12. Cheang, J.Y. & Moyle, P.M. Glucagon-like peptide-1 (GLP-1)-based therapeutics: current status and future opportunities beyond type 2 diabetes. *ChemMedChem* 13, 662-671 (2018).
- 13. Kuhre, R.E., *et al.* Peptide production and secretion in GLUTag, NCI-H716 and STC-1 cells: a comparison to native L-cells. *Journal of Molecular Endocrinology* **56**, 201 (2016).
- 14. Ashammakhi, N., *et al.* Gut-on-a-chip: Current progress and future opportunities. *Biomaterials* **255**, 120196 (2020).
- 15. Kim, H.J., Huh, D., Hamilton, G. & Ingber, D.E. Human gut-on-a-chip inhabited by microbial flora that experiences intestinal peristalsis-like motions and flow. *Lab on a Chip* **12**, 2165-2174 (2012).
- 16. Richardson, A., *et al.* A microfluidic organotypic device for culture of mammalian intestines *ex vivo*. *Analytical Methods* **12**, 297-303 (2020).
- 17. Amirabadi, H.E., *et al.* Intestinal Explant Barrier Chip: Long-term intestinal absorption screening in a novel microphysiological system using tissue explants. *Lab on a Chip* **22**, 326-342 (2022).

- 18. Marrero, D., *et al.* Gut-on-a-chip: Mimicking and monitoring the human intestine. *Biosensors and Bioelectronics* **181**, 113156 (2021).
- 19. Hsiao, Y.-H., Hsu, C.-H. & Chen, C. A high-throughput automated microfluidic platform for calcium imaging of taste sensing. *Molecules* **21**, 896 (2016).
- 20. Nguyen, D.T.T., Van Noort, D., Jeong, I.-K. & Park, S. Endocrine system on chip for a diabetes treatment model. *Biofabrication* **9**, 015021 (2017).
- 21. Wu, T., *et al.* Effects of taurocholic acid on glycemic, glucagon-like peptide-1, and insulin responses to small intestinal glucose infusion in healthy humans. *The Journal of Clinical Endocrinology & Metabolism* **98**, E718-E722 (2013).
- 22. Keating, D.J. & Spencer, N.J. Release of 5-hydroxytryptamine from the mucosa is not required for the generation or propagation of colonic migrating motor complexes. *Gastroenterology* **138**, 659-670. e652 (2010).
- 23. Symonds, E.L., *et al.* Mechanisms of activation of mouse and human enteroendocrine cells by nutrients. *Gut* **64**, 618-626 (2015).
- 24. Casteleyn, C., Rekecki, A., Van der Aa, A., Simoens, P. & Van Den Broeck, W. Surface area assessment of the murine intestinal tract as a prerequisite for oral dose translation from mouse to man. *Laboratory Animals* **44**, 176-183 (2010).
- 25. Sun, E.W., *et al.* Mechanisms controlling glucose-induced GLP-1 secretion in human small intestine. *Diabetes* **66**, 2144-2149 (2017).
- 26. Potthoff, M.J., *et al.* Colesevelam suppresses hepatic glycogenolysis by TGR5-mediated induction of GLP-1 action in DIO mice. *American Journal of Physiology-Gastrointestinal and Liver Physiology* **304**, G371-G380 (2013).
- 27. Huang, W., *et al.* A multiplexed microfluidic platform toward interrogating endocrine function: Simultaneous sensing of extracellular Ca²⁺ and hormone. *ACS Sensors* 5, 490-499 (2020).
- 28. Nylund, K., Hausken, T., Ødegaard, S., Eide, G. & Gilja, O. Gastrointestinal wall thickness measured with transabdominal ultrasonography and its relationship to demographic factors in healthy subjects. *Ultraschall in der Medizin-European Journal of Ultrasound*, E225-E232 (2012).

- 29. Brighton, C.A., *et al.* Bile acids trigger GLP-1 release predominantly by accessing basolaterally located G protein–coupled bile acid receptors. *Endocrinology* **156**, 3961-3970 (2015).
- 30. Wu, T., *et al.* Effects of rectal administration of taurocholic acid on glucagon-like peptide-1 and peptide YY secretion in healthy humans. *Diabetes, Obesity and Metabolism* **15**, 474-477 (2013).
- 31. Evans, G.S. & Potten, C.S. The distribution of endocrine cells along the mouse intestine: a quantitative immunocytochemical study. *Virchows Archiv B* **56**, 191-199 (1988).
- 32. Hansen, C.F., Vrang, N., Sangild, P.T. & Jelsing, J. Novel insight into the distribution of L-cells in the rat intestinal tract. *American Journal of Translational Research* 5, 347 (2013).
- 33. Toft-Nielsen, M.-B., Madsbad, S. & Holst, J.J. Continuous subcutaneous infusion of glucagon-like peptide 1 lowers plasma glucose and reduces appetite in type 2 diabetic patients. *Diabetes Care* **22**, 1137-1143 (1999).
- 34. Näslund, E., *et al.* GLP-1 slows solid gastric emptying and inhibits insulin, glucagon, and PYY release in humans. *American Journal of Physiology-Regulatory, Integrative and Comparative Physiology* **277**, R910-R916 (1999).
- 35. Jensen, T.L., Kiersgaard, M., Sørensen, D.B. & Mikkelsen, L. Fasting of mice: a review. *Laboratory Animals* **47**, 225-240 (2013).
- 36. Ayala, J.E., *et al.* Standard operating procedures for describing and performing metabolic tests of glucose homeostasis in mice. *Disease Models & Mechanisms* 3, 525-534 (2010).
- 37. Tschritter, O., *et al.* Assessing the shape of the glucose curve during an oral glucose tolerance test. *Diabetes Care* **26**, 1026-1033 (2003).
- 38. Francis, G.L. Albumin and mammalian cell culture: implications for biotechnology applications. *Cytotechnology* **62**, 1-16 (2010).
- 39. Jeyachandran, Y.L., Mielczarski, J.A., Mielczarski, E. & Rai, B. Efficiency of blocking of non-specific interaction of different proteins by BSA adsorbed on hydrophobic and hydrophilic surfaces. *Journal of Colloid and Interface Science* **341**, 136-142 (2010).
- 40. Straub, S.G. & Sharp, G.W. Massive augmentation of stimulated insulin secretion induced by fatty acid–free BSA in rat pancreatic islets. *Diabetes* **53**, 3152-3158 (2004).

- 41. O'Halloran, F., *et al.* A casein hydrolysate increases GLP-1 secretion and reduces food intake. *Food Chemistry* **252**, 303-310 (2018).
- 42. Holst, J.J., Jepsen, S.L. & Modvig, I. GLP-1–Incretin and pleiotropic hormone with pharmacotherapy potential. Increasing secretion of endogenous GLP-1 for diabetes and obesity therapy. *Current Opinion in Pharmacology* **63**, 102189 (2022).
- 43. Kuhre, R.E., *et al.* Bile acids are important direct and indirect regulators of the secretion of appetite-and metabolism-regulating hormones from the gut and pancreas. *Molecular Metabolism* **11**, 84-95 (2018).
- 44. Myant, N.B. *The Biology of Cholesterol and Related Steroids*, (Butterworth-Heinemann, 2014).
- 45. Song, P., Zhang, Y. & Klaassen, C.D. Dose-response of five bile acids on serum and liver bile Acid concentrations and hepatotoxicty in mice. *Toxicological Sciences* **123**, 359-367 (2011).
- 46. Baghdasaryan, A., *et al.* Inhibition of intestinal bile acid absorption improves cholestatic liver and bile duct injury in a mouse model of sclerosing cholangitis. *Journal of Hepatology* **64**, 674-681 (2016).
- 47. Van Deest, B., Fordtran, J., Morawski, S. & Wilson, J. Bile salt and micellar fat concentration in proximal small bowel contents of ileectomy patients. *The Journal of Clinical Investigation* **47**, 1314-1324 (1968).
- 48. Sjögren, E., Eriksson, J., Vedin, C., Breitholtz, K. & Hilgendorf, C. Excised segments of rat small intestine in Ussing chamber studies: A comparison of native and stripped tissue viability and permeability to drugs. *International Journal of Pharmaceutics* **505**, 361-368 (2016).

7.7 Supplementary Information

Table S1. Height of different sections of fabricated top and bottom (unit: μ m)

Area	Inlet	Middle channel	Outlet
Top layer	999.1 ± 0.2	986.1 ± 1	991.4 ± 1.0
Bottom layer	999.4 ± 0.2	1002.9 ± 1.3	1001.1 ± 0.2

Data are means \pm SD. n = 23 at each section

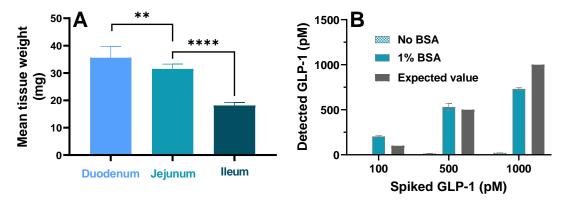


Figure S1. (A) Averaged tissue weight of \sim 0.5 cm (length) * 0.5 cm (width) from mouse small intestine regions used in the biorelease study (n = 10). (B) The detection of 100-500 pM GLP-1 by active GLP-1 kits in the absence and presence of 1% BSA (n = 3). Data are means \pm SEM. Paired student t-test was used to determine statistical difference. *P < 0.05, **P < 0.01, ***P < 0.005, ****P < 0.001.

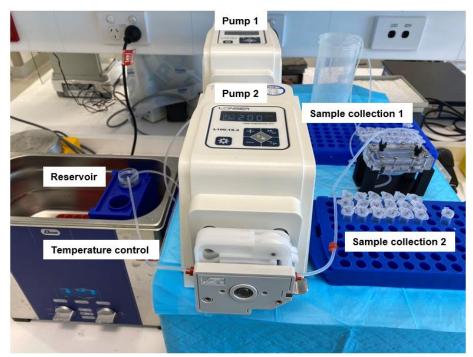


Figure S2. The gut-on-a-chip platform. Perfusion media were maintained in a water bath and delivered to the microfluidic chip via peristaltic pumps. Perfusion efflux was collected into two sets of tubes with a sampling frequency of 2 minutes per sample at each channel.

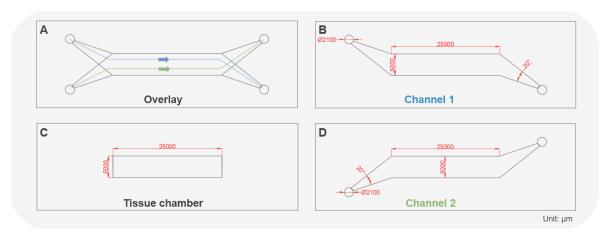


Figure S3. The layout and dimensions of different layers of the gut-on-a-chip device (unit: μ m). (A) Schematic of the overlay structure of the device with the demonstration of the two parallel flows, including a flow in the luminal channel (blue) and a flow in the serosal channel (green). Detailed dimensions of luminal channel (B), tissue chamber (C) and serosal channel (D).

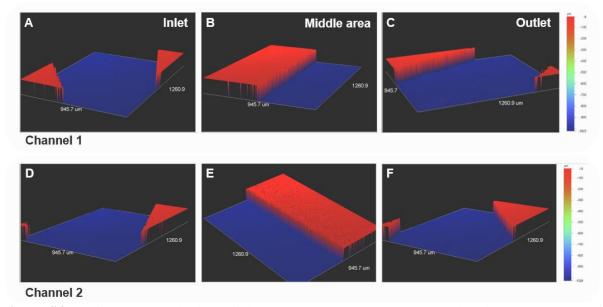


Figure S4. Surface characterisation of channel 1 (top channel) and channel 2 (bottom channel) of the gut-on-a-chip device fabricated by micro-machining. (A-C) show the detailed measurements of channel 1 at the inlet, middle area, and outlet, respectively. (D-F) show the detailed measurements of channel 2 at the inlet, middle area, and outlet, respectively.

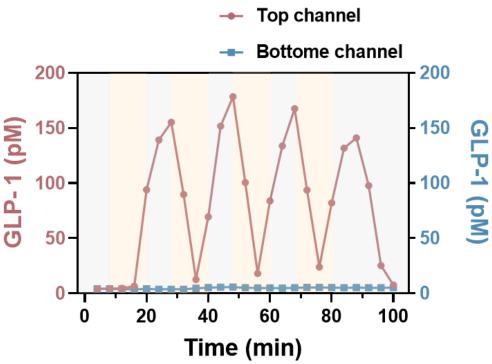


Figure S5. Dynamic GLP-1 concentration measured in the efflux of the top (red curve) and bottom (blue curve) channels in the absence of tissue. GLP-1 concentrations were switched between 0 and 100 pM in the top channel to mimic the GLP-1 secretion for 4 cycles. In each cycle, blank buffer and GLP-1 buffer perfusions last 8 and 12 minutes, respectively.

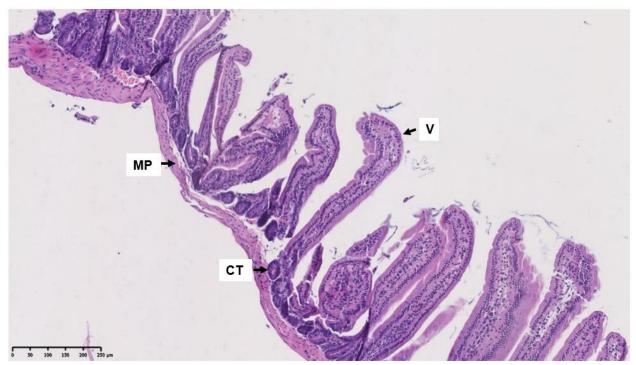


Figure S6. H&E staining of small intestinal tissues immediately after isolation from mice showing the villi (V), crypt (CT) and muscularis propria (MP). Scale bar shows 0-250 μm.

CHAPTER 8: A MULTIPLEXED MICROFLUIDIC
PLATFORM TOWARDS INTERROGATING
ENDOCRINE FUNCTION: SIMULTANEOUS
SENSING OF EXTRACELLULAR CA²⁺ AND
HORMONE

Statement of Authorship

Title of the paper	A multiplexed microfluidic platform toward interrogating endocrine function: simultaneous sensing of extracellular Ca ²⁺ and hormone
Publication status	Published
Publication details	Huang, W., Wu, T., Shallan, A., Kostecki, R., Rayner, CK., Priest, C., Ebendorff-Heidepriem, H., Zhao, J., (2020). "A multiplexed microfluidic platform towards interrogating endocrine function: simultaneous sensing of extracellular Ca ²⁺ and hormone", <i>ACS Sensors</i> , 5(2):490-499

Principal Author

Candidate	Weikun Huang			
Contribution	Data collection and interpretation, statistical analysis, writing and revision of the manuscript			
Overall percentage	80%			
Certification	This paper reports on original research I conducted during the period of my Higher Degree by Research candidature and is not subject to any obligations or contractual agreements with a third party that would constrain its inclusion in this thesis. I am the primary author of this paper.			
Signature		Date	September 2023	

Co-Author Contributions

By signing the Statement of Authorship, each author certifies that: i) the candidate's stated contribution to the publication is accurate (as detailed above); ii) permission is granted for the candidate to include the publication in the thesis; and iii) the sum of all co-author contributions is equal to 100% less the candidate's stated contribution.

Name of Co-Author	Tongzhi Wu		
Contribution	Conception and design of the study, data interpretation, reviewing of the manuscript, and guarantor of the paper.		
Signature		Date	September 2023

Name of Co-Author	Aliaa Shallan			
Contribution	Data collection and interpretation, and reviewing of the manuscript			
Signature		Date	September 2023	
Name of Co-Author	Roman Kostecki			
Contribution	Data collection and interpretation, and reviewing of the manuscript			
Signature		Date	September 2023	
Name of Co-Author	Christopher K. Rayner			
Contribution	Data interpretation and reviewing of the manuscript			
Signature		Date	September 2023	
Name of Co-Author	Craig Priest			
Contribution	Data interpretation and reviewing of the manuscript			
Signature	_	Date	September 2023	
Name of Co-Author	Heike Ebendorff-Heidepriem			
Contribution	Data interpretation and reviewing of the manuscript			
Signature		Date	September 2023	
Name of Co-Author	Jiangbo Zhao			
Contribution	Conception and design of the study, data interpretation, reviewing of the manuscript, and guarantor of the paper.			
Signature	-	Date	September 2023	

8.1 Abstract

Extracellular Ca²⁺ ([Ca²⁺]_{ex}) is an important regulator of various physiological and pathological functions, including intercellular communication for synchronised cellular activities (e.g., coordinated hormone secretion from endocrine tissues). Yet rarely is it possible to concurrently quantify the dynamic changes of [Ca²⁺]_{ex} and related bioactive molecules with high accuracy and temporal resolution. This work aims to develop a multiplexed microfluidic platform to enable monitoring oscillatory [Ca²⁺]_{ex} and hormone(s) in a biomimetic environment. To this end, a low-affinity fluorescent indicator, Rhod-5N, is identified as a suitable sensor for a range of [Ca²⁺]_{ex} based on its demonstrated high sensitivity and selectivity to Ca²⁺ in biomedical samples, including human serum and cell culture medium. A microfluidic chip is devised to allow for immobilisation of microscale subjects (analogous to biological tissues), precise control of the perfusion gradient at sites of interest, and integration of modalities for fluorescence measurement and enzyme-linked immunosorbent assay. As this analytical system is demonstrated to be viable to quantify the dynamic changes of Ca²⁺ (0.2-2 mM) and insulin (15-150 mU L⁻¹) concurrently, with high temporal resolution, it has the potential to provide key insights into the essential roles of [Ca²⁺]_{ex} in the secretory function of endocrine tissues and to identify novel therapeutic targets for human diseases.

8.2 Introduction

The advent of various Ca^{2+} -responsive sensors and advanced instruments has revealed the indispensable role of Ca^{2+} signalling in numerous physiological and pathological processes [1-6]. Three types of non-destructive Ca^{2+} sensors have been used to unravel the physiological roles of Ca^{2+} , i.e., chemically engineered fluorescent indicator molecules, genetically encoded Ca^{2+} indicators (GECI) and Ca^{2+} -selective microelectrodes (CSM) (Figure 1A) [7]. In comparison to CSM, synthetic indicators and GECI have inherently higher spatial and temporal resolution and are extensively utilised to characterise concentrations of Ca^{2+} ([Ca^{2+}]) in different cellular domains, such as cytoplasm (50-1000 nM), mitochondria (0.1-100 μ M), and endoplasmic reticulum (50-500 μ M) (Figure 1B) [8].

Of note, the majority of the fluorescence-based indicators are used to interrogate the functions of intracellular Ca^{2+} ($[Ca^{2+}]_i$), due to their effective sensing range spanning from nM to μ M [9]. The limited usage of those indicators in the extracellular matrix (ECM), where $[Ca^{2+}]$ fluctuates in the high concentration range (0.5-3 mM) [10,11], has retarded understanding of how $[Ca^{2+}]_{ex}$ mediates various biological processes to maintain the physiological homeostasis [12-15], e.g., facilitating intercellular communication, [16] and synchronising tissue-level activity [17]. A system for sensing $[Ca^{2+}]_{ex}$ should have the ability to: (1) quantify dynamic changes of $[Ca^{2+}]_{ex}$ (in the order of mM scale) with high accuracy; (2) respond to Ca^{2+} in an instantaneous manner; and (3) allow for multiplexed sensing of $[Ca^{2+}]_{ex}$ and other biological molecule(s) of interest to reveal their underlying correlations. Concurrent measurement of $[Ca^{2+}]_{ex}$ and hormone(s) is critical, for instance, to advance knowledge of the relationship between variations in $[Ca^{2+}]_{ex}$ and dynamic secretion of insulin in the pancreatic islets. Yet hitherto, few, if any, sensing systems have met all the requirements specified above.

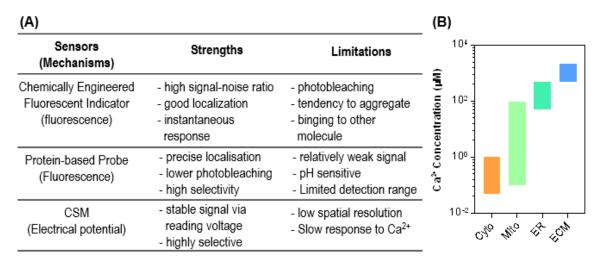


Figure 1. (A) Summary of strengths and limitations of the state-of-the-art non-destructive Ca^{2+} sensors. (B) Snapshot of typical intracellular or extracellular $[Ca^{2+}]$ present in different cellular domains, including $[Ca^{2+}]$ in cytoplasm (Cyto, 50-1000 nM), mitochondria (Mito, 0.1-100 μ M), endoplasmic reticulum (ER, 50-500 μ M), and extracellular matrix (ECM, 0.5-3 mM).

In this work, we demonstrate the integration of a microfluidic sensing system with a light-induced fluorescence (LIF) detection set-up and enzyme-linked immunosorbent assay (ELISA) to quantify $[Ca^{2+}]_{ex}$ and the concentration of a hormone (insulin) simultaneously, with high temporal resolution. Firstly, we identified that a derivative indicator of 1, 2-bis(o-aminophenoxy)ethane-N, N, N', N'-tetraacetic acid (BAPTA), Rhod-5N, provides an

effective sensing range of 0.33-33 mM Ca²⁺ in a biomimetic environment, which is sufficient to evaluate [Ca²⁺]_{ex} in tissues of interest. Emerging indicators for sensing high [Ca²⁺], including gold nanoparticles (GNP) [18,19], photonic polymer [20,21] and aggregation-induced emission (AIE) fluorogen [22,23], were excluded in the present study, due to their limitations in instantaneously quantifying [Ca²⁺] under a fluidic flow at microscale. Based on a series of fluidic dynamic simulations, we devised, fabricated, characterised and validated a microfluidic chip to immobilise the microscale subjects – a surrogate for biological tissue – and mimic physiological conditions for the trapped subjects. We then demonstrated the simultaneous and real-time sensing of [Ca²⁺]_{ex} (via LIF) and an exemplar hormone, insulin (via ELISA) by our analytical set-up, in which the concentrations of Ca²⁺ and insulin were oscillated to mimic their pulsatile patterns in vivo. We established a satisfactory quantification of [Ca²⁺]_{ex} (0.2-2 mM) and insulin (15-150 mU/L) in the extracellular medium, with temporal resolutions up to 10 s. Our work on this multiplexed microfluidic chip will enable the development of a high-throughput platform to analyse the interrelation of [Ca²⁺]_{ex} and the secretory functions of endocrine tissues, which is key to understanding the complex (patho)physiology relating to metabolic health, and to identifying novel therapeutic targets for human diseases.

8.3 Experimental Sections

8.3.1 Determination of dissociation constant (K_d)

The K_d that describes the dynamic interaction between Ca^{2+} , Rhod-5N (noted as N), and their complex molecule (noted as CaN) can be calculated as follow:

$$K_{d} = \frac{[Ca^{2+}] \times [N]}{[CaN]} \tag{1}$$

$$[Ca^{2+}] = K_d \left(\frac{F - F_{\min}}{F_{\max} - F} \right) \tag{2}$$

$$F' = F_{\text{max}'} \left(\frac{[Ca^{2+}]}{K_d + [Ca^{2+}]} \right)$$
 (3)

$$y = V_{\text{max}} \times \frac{x^{n_{\text{h}}}}{k^{n_{\text{h}}} + x^{n_{\text{h}}}} \tag{4}$$

In Equation (1), $[Ca^{2+}]$, [N] and [CaN] are the equilibrium concentrations of Ca^{2+} , Rhod-5N and their complex, respectively. The concentration of Ca^{2+} can be calculated by Equation (2), where F is the fluorescence Ca^{2+} -bound Rhod-5N, F_{max} is the fluorescence when all Rhod-5N molecules are bound and F_{min} is the background fluorescence in the absence of Ca^{2+} . Equation (2) can be rearranged into Equation (3) by subtracting F_{min} from F and F_{max} to acquire F' and F_{max} '. Subsequently, K_d can be computed by fitting the experimentally detected data into Hill's function as formulated in Equation (4), where y, V_{max} , x and k correspond to F', F_{max} ', $[Ca^{2+}]$ and K_d , respectively. If n_h approximates 1, it indicates a monomer binding reaction [27].

8.3.2 Fluidic dynamics simulation

COMSOL Multiphysics 5.3 (COMSOL Inc., Sweden) was employed to simulate the fluid dynamics in the microfluidic channels. The geometry for the simulation study was imported from the mask design in AutoCAD. The 2D simulation under a general environment pressure level of 1 atm and a temperature of 293.15 K was performed using the 'laminar flow' model and the 'incompressible flow' model. The former is valid for the microfluidic chip with a typically small Reynold number (<< 2100), and the latter is based on Navier-Stokes equations. The material used in the simulation was defined as water, with a density of 1000 kg m⁻³ and a dynamic viscosity of 0.001 Pa s. Boundary conditions of inlet 1 and 2 were defined with a fluid velocity of 10 μ m/s and 20 μ m/s for indicator inlet (arbitrary unit). No-slip (zero velocity) boundary condition was imposed on the channel walls. No mass transport was set through the walls of the device. At the outlet, the pressure was set as 1 atm with suppressed backflow. The physics-controlled mesh was used for the mesh sequence type and selected as extra-fine.

8.3.3 Microfluidic chip fabrication

The single-layer PDMS microfluidic chip was fabricated via soft lithography. Briefly, the proposed chip structure was written on Borofloat 33 glass via direct laser writing with a beam diameter of 10 µm. SU8 50 photoresist (MicroChem, Australia) was spun on a clean silicon wafer washed by acetone to prepare a 250 µm thick photoresist layer. The photoresist was exposed to UV radiation using a mask aligner. Areas exposed through the mask were cross-linked while unexposed photoresist was dissolved after developing with SU8 developer (MicroChem, Australia). The template was then treated with hexamethyldisilazane (Sigma,

Australia) to form an anti-adhesion layer so that the cured PDMS could be removed without damaging the template. PDMS (SYLGARD 184 Silicone Elastomer, MicroChem, Australia) was prepared by mixing monomer and curing agent at a ratio of 10:1, degassed and cast on the template. PDMS was then cured in an oven at 65 °C for 3 h. The cured PDMS device was gently peeled off from the template and bonded to a microscopic glass slide after air plasma cleaning. Inlets and outlets were drilled using Haris UniCore biopsy punches (Ted Pella).

8.3.4 Dual-sensing of oscillating Ca²⁺ and insulin

Ca²⁺-free Dulbecco's Modified Eagle Medium (DMEM) (without insulin, Thermo Fisher, Australia) and insulin-supplied DMEM, containing 2 mM Ca²⁺ and 150 mU/L insulin were delivered into the microfluidic chip via inlet 1 and 2, respectively, with a total flow rate of 5 μL/min. The Calibrator 5 in the insulin ELISA kit (Mercodia, Sweden), containing 200 mU/L insulin, was used to supplement the DMEM to prepare the insulin-supplied DMEM. Indicator solution, 100 µM Rhod-5N (Life Technologies, USA) in pH7.4 PBS (prepared as described in Supporting Information), was loaded into the channel via inlet 3 at 5 µL/min, so that the 1:1 mixing with the upstream flow of DMEM resulted in reaching the optimal concentration of Rhod-5N (50 µM) at the optical window. To generate oscillating concentrations of insulin and Ca²⁺, the ratios of the flow rates were finely tuned between two values in each group and each ratio lasted 180 seconds. After insulin carried by fluid flowed through the chip device and discharged from the outlet (Figure S1A), the effluent was collected to quantify insulin content via the same ELISA kit. Note that a minimum sample volume of 25 μL is required by the insulin ELISA. Considering the flow rate was 10 μL/min at the outlet, the sampling time was set as 3 minutes to provide sufficient sample volume for insulin quantification following the protocol provided by the manufacturer (Supporting Information).

8.4 Results and Discussion

8.4.1 Fluorometric characterisations of Rhod-5N

The fluorometric property of Rhod-5N in response to a series of high [Ca²⁺] (up to 2 mM) was studied in PBS buffer (pH 7.4), commonly used in biomedical research. DI water with almost zero ionic strength was applied as a control experiment. As shown in Figure 2A, Rhod-5N is

switched on with the addition of 0.5-2 mM [Ca²⁺], amplifying fluorescence intensity up to 80 times that of Rhod-5N only. Both the Ca²⁺-induced fluorescence of Rhod-5N in PBS (pH 7.4, Figure 2A) and DI water (Figure S2A) show a dominant broad emission band peaking at around 580 nm, accompanied by a spectral shoulder from 610 nm to 675 nm. For the same range of [Ca²⁺], the fluorescence intensity of Rhod-5N in PBS buffer was slightly lower than that in DI water (Figure S2B). This is attributable to the shielding effect on Ca²⁺ imposed by other cations in PBS, which retards Ca²⁺ binding with Rhod-5N, i.e., a lower amount of Rhod-5N-Ca²⁺ complex was formed in a buffering environment with high ionic strength, which, therefore, would result in a higher K_d of Rhod-5N to Ca²⁺. The combined advantages of the increased K_d of Rhod-5N in buffer and high bio-compatibility of the PBS (isotonic and non-toxic to most cells) are favourable features for monitoring the dynamic $[Ca^{2+}]_{ex}$.

For the same range of $[Ca^{2+}]$, the fluorescence intensity of 25 μ M Rhod-5N (in DI water) was higher than that of 2.5 μ M Rhod-5N (Figure S2C). The fluorescence intensity plateau appeared for 2.5 μ M Rhod-5N at around 0.25 mM Ca^{2+} , lower than that for 25 μ M Rhod-5N (1.25 mM Ca^{2+}). That the performance of Rhod-5N is concentration-dependent prompted the need to examine a wide range of Rhod-5N concentrations, from 2.5 μ M to 250 μ M (in PBS, pH 7.4) in this study, with different $[Ca^{2+}]$. As shown in Figure 2B, the largest fluorescence enhancement was observed for Rhod-5N at 50-100 μ M across 0-2 mM Ca^{2+} , exhibiting two orders of magnitude amplification against the background fluorescence. A concentration-quenching behaviour of Rhod-5N in the presence of Ca^{2+} (i.e., a decrease of the fluorescence intensity of Ca^{2+} -bounded Rhod-5N) was observed when the concentration of Rhod-5N increased over 100 μ M, which however can be avoided by employing Rhod-5N at the concentration of 50 μ M (Figure 2B). Thus, 50 μ M Rhod-5N was used in the following experiment of quantifying $[Ca^{2+}]_{ex}$ under physiologically relevant conditions.

Given that [Ca²⁺] will be ultimately analysed in the context of a physiological environment, the preservation of the sensing selectivity of Rhod-5N to Ca²⁺ was examined. For this purpose, the fluorescence intensities of Rhod-5N with and without Ca²⁺ were measured in the presence of other common extracellular cations at physiological concentrations, including Mg²⁺ (1 mM), Na⁺ (150 mM), K⁺ (5 mM), Fe²⁺ (50 μ M), Cu²⁺ (50 μ M), Zn²⁺ (50 μ M), Al³⁺ (50 μ M). In the absence of Ca²⁺, Rhod-5N was non- or weakly- fluorescent in the presence of other metal ions, except for

 Zn^{2+} , which induced a minor increase of Rhod-5N fluorescence (Fig. 2C). By contrast, the fluorescence intensity of Rhod-5N was markedly increased in the presence of 1 mM Ca^{2+} and other ions, apart from the groups with Cu^{2+} or Zn^{2+} . The latter is in good agreement with previous studies, where Cu^{2+} and Zn^{2+} were shown to display higher binding affinities with the BAPTA-based indicator than that of Ca^{2+} [24,25]. As such, Cu^{2+} and Zn^{2+} are expected to compete with Ca^{2+} to form Cu^{2+} -/ Zn^{2+} - bound Rhod-5N complexes, thereby diminishing the fluorescence originating from the Ca^{2+} -bound Rhod-5N complex.

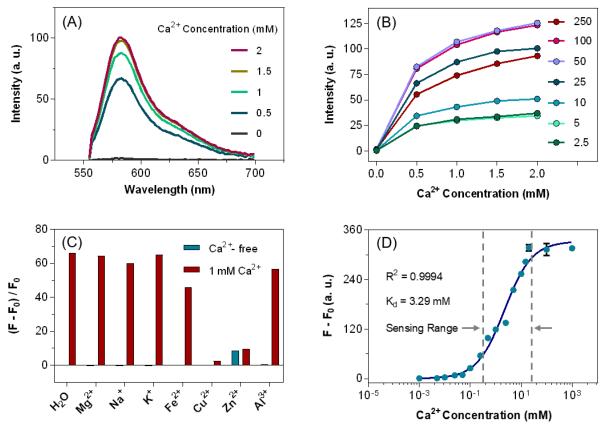


Figure 2. Fluorometric characterisations of Rhod-5N with various [Ca²⁺] ($\lambda_{ex} = 530$ nm, $\lambda_{em} = 580$ nm). (A) Variations of emission of 25 μM Rhod-5N (in PBS, pH 7.4) in response to different [Ca²⁺]. (B) Fluorescence intensities of 2.5-250 μM Rhod-5N as a function of different [Ca²⁺] up to 2 mM. (C) In the presence of various common extracellular cations, relative fluorescence changes (F-F₀)/F₀ of 50 μM Rhod-5N with (red bars) and without (blue bars) Ca²⁺ addition. The concentrations of the presented cations are consistent with those in the extracellular environment, i.e., Mg²⁺ (1 mM), Na⁺ (150 mM), K⁺ (5 mM), Fe²⁺ (50 μM), Cu²⁺ (50 μM), Zn²⁺ (50 μM) and Al³⁺ (50 μM). (D) The fluorometric titration curve of 50 μM Rhod-5N, obtained by fitting the fluorescence enhancement at 580 nm via Hill's equation, where Hill's coefficient (n_h) was determined as 0.94 ± 0.06 and K_d was computed as 3.29 ± 0.41 mM, with an R² of 0.9994. The fluorescence enhancement is given by the filled circles with error bars from 1 μM to 1 M Ca²⁺ in cell culture medium at 37 °C. Apart from further notation, all Rhod-5N was prepared in PBS buffer (pH 7.4), Ca²⁺ and other cations were dissolved in DI water. C-D: F and F₀ represent the fluorescence of Rhod-5N in the presence and absence of the respective metal ions.

The observed interference by Zn²⁺ and Cu²⁺ prompted the investigation into how much the sensing capability and sensitivity of Rhod-5N towards Ca²⁺ would be perturbed by physiologically relevant ions; therefore, a solution containing all the above-mentioned extracellular metal ions was prepared (termed "ions-supplied solution"). As shown in Figure S2D-E, Rhod-5N maintained a high sensitivity and responsivity to Ca²⁺ (0.5-2 mM) in the ions-supplied solution, evidenced by the continuous increase of fluorescence intensity at 580 nm. The Ca²⁺-induced relative fluorescence change of Rhod-5N increased even in a more linear fashion in the ions-supplied solution compared to DI water (Figure S2F). These observations confirm that the excellent selectivity of Rhod-5N towards Ca²⁺ over other metal ions can be retained in physiological solutions.

The effective sensing range of an indicator is typically defined as $0.1\text{-}10\times K_d$, so an indicator suited to monitoring dynamic $[Ca^{2+}]_{ex}$ must bear with a high value of K_d in the extracellular environment. Though K_d of Rhod-5N is specified as 0.32 mM by the manufacturer (Ca^{2+}) in a solution with an ionic strength of 100 mM at room temperature) [7], it is important that we re-determine the K_d under the conditions the indicator would be employed [26]. As such, the fluorescence of Rhod-5N as a function of $[Ca^{2+}]$ was measured in DMEM at 37 °C, which is a common environment for cell culture *in vitro* and has an ionic strength of 167.22 mM. By fitting the fluorescence data with Hill's equation as derived in Equations (1-4), K_d of Rhod-5N towards Ca^{2+} at ionic strength of DMEM was computed to be 3.29 ± 0.41 mM ($R^2 = 0.9994$), with Hill's coefficient (n_h) at 0.94 ± 0.06 , suggesting 1:1 binding ratio of Rhod-5N to Ca^{2+} [27]. The fitting results and the fluorometric titration data clearly define the sensing window to Ca^{2+} from 0.33-33 mM ($0.1-10 \times K_d$, visualised by two dashed lines in Figure 2D), within which Rhod-5N displays relatively linear fluorescence changes in response to Ca^{2+} . Thus, the sensing capacity of Rhod-5N to extracellular Ca^{2+} is validated in conditions with physiological concentrations of ions.

The K_d obtained via Hill's fitting as mentioned above, also known as apparent K_d , was one order of magnitude larger than the value provided by the manufacturer (0.32 mM). In line with our theoretical prediction (details in Supporting Information), there could be three reasons for this discrepancy. First, other cations, glucose, or amino acids in the cell culture medium may bind

with the carboxyl groups (binding units) of Rhod-5N, competing with the binding of Rhod-5N to Ca^{2+} . Second, the ionic environment and increasing amount of $CaCl_2$ during the titration analysis may impose a shielding effect on Ca^{2+} as discussed in Equations (S1-4), which in turn results in a lower effective $[Ca^{2+}]$ to bind with the indicator (Figure S3A) [28], and a smaller effective dissociation constant (K_{ed}) of 1.31 ± 0.20 mM (Figure S3B). In the interests of convenient comparison, the apparent K_d is used throughout the manuscript. Third, K_d could be reduced to almost half when the titrations were conducted at 37 °C compared to 20 °C, as reported by Grynkiewicz *et al* [29].

In addition, with the continuous exposure of Rhod-5N (50 μ M) to ambient light up to 7 days, little variations in Ca²⁺-induced fluorescence were observed (Figure S3C), which attests to the high photostability of this indicator under the environment light. Taken together, Rhod-5N (50 μ M) has been demonstrated to give rise to high sensitivity, high selectivity, enhanced K_d, and robust fluorescent signal in a biomimetic environment, favouring the viability of this indicator for detecting dynamic variations of [Ca²⁺]_{ex}.

8.4.2 Design principle and fluidic dynamics

To realise the multiplexed sensing of [Ca²⁺]_{ex} and hormone(s), a PDMS microfluidic chip was designed and fabricated via soft lithography in accordance with the following criteria: (1) allowing immobilisation of biological subjects and manipulation of the microenvironment, and (2) enabling compatibility with the set-ups for simultaneous quantification of fluorescence signals and hormone(s) of interest. As shown in Figure 3A, the microfluidic chip features: (1) double Y-shape inlets to introduce cell culture media and Rhod-5N, respectively, (2) two serpentine channels, following the double Y-shape inlets, to enhance the mixing efficiency of reagents, (3) U-shape cups to trap and immobilise the subjects of interest, (4) an optical window for fluorescence detection, and (5) an outlet to collect hormone for analysis. The modular functions of the microfluidic chip are discussed as follows, with structural dimensions illustrated and/or characterised in Figure S4-5.

8.4.3 Flow velocity profile

Two Y-shape channels are implemented in different locations of the microfluidic chip, which allows tuning of the microenvironment by the delivery of customised perfusion fluid (via Port 1&2, with regulated ratios between media) and introducing the fluorescent indicator for sensing (via Port 3), respectively.

To understand the stream dynamics in the microfluidic chip, three input flows in the canals via ports 1, 2, and 3 (P_1 , P_2 , and P_3) are conceived, with constant flow rates of Q_1 , Q_2 and Q_4 , respectively (Figure 3B (i)). In accordance with the mass conservation law, the flow rate in each branch canal can be interrelated as: $Q_5 = Q_4 + Q_3 = Q_4 + Q_1 + Q_2$, where Port 4 is the outlet with flow rate Q_5 . As revealed by the 2D computational fluidic dynamic (CFD) of COMSOL (Figure 3B (ii)), the velocity profile of each channel exhibits the features of laminar flow, showing the highest value in the centre of the channels, but approaching zero at the wall. The specific velocity (denoted as V) in the profile is also indicated as $V_5 = V_4 + V_3 = V_4 + V_1 + V_2$, consistent with the flow rate, Q_5 , in each branch.

Under laminar flow, the mixing of molecules in the channels relies on a relatively slow diffusion process which is dependent on the specific diffusion coefficient of the molecule [30]. To ensure the complete mixing of the perfused media prior to their arrival at the site of interest (e.g., U-shape cups or optical window), two serpentine channels, around 40 cm and 20 cm long, are built into the microfluidic chip following the respective Y-shaped inlets. The trapping site is embedded in the middle of the former serpentine channel, the second half of which is designed to collect and mix the effluent from each cup. The latter serpentine channel is used to enhance the mixing of the fluorescent indicator with the fluid from the U-shape cups.

The serpentine channels not only extend the distance that the molecules travel, but also facilitate the mixing of the co-flowing solutions when they pass the curved section (due to the centrifugal forces) [31]. To visualise the mixing process, food colouring and DI water were delivered into the microfluidic channel via inlet 1&2, respectively. As shown in Figure 3C, the food colouring molecules diffused gradually with DI water as the co-fluid flowed through the serpentine channel, the mixing efficiency of which was quantitatively characterised via fluorescence imaging in section 2.3.

8.4.4 U-shape cups for trapping

The capacity for immobilising biological subjects (e.g., tissues) and collecting the effluent from the trapping site is of significance for interrogating the secretory function of the subjects concerned. To this end, U-shape cups are devised and implemented in between two columns in the former serpentine channel (Figure 3A&D).

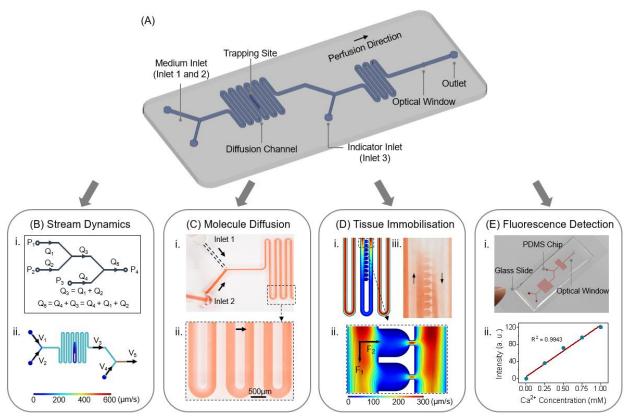


Figure 3. Design, simulation and characterisations of the microfluidic chip. (A) Overall layout of the microfluidic chip. (B) (i) Stick diagram of the microfluidic channels, where arrows indicate the fluidic flow in each branch. The formulae underneath suggest the relationship between the flows according to the mass conservation law; (ii) Velocity mapping of the microfluidic channels via 2D CFD simulation. (C) (i) Perfusion and mixing of water and food colouring in the channels. Food colouring and water were delivered 1:1 into the microfluidic chip via the medium inlet at a total flow rate of 5 μL/min (inlet 1 channel is illustrated with the parallel dashed lines for visualisation); (ii) Close-up view showing the mixing process of the water and food colouring from two separate flows to a homogenised mixture (left to right indicated by an arrow). (D) (i) Velocity mapping of the fluidic dynamics at the trapping site and the serpentine channels in the vicinity; (ii) Close-up view of the flow velocity at the cup, where perfusion flow is divided into a main stream (F_1) along the main channel, and a partial stream (F_2) directing into the cup; (iii) Progressive variations of perfusion speed across the cups due to the division of the streams by F_1 and F₂ (indicated by food colouring). (E) (i) Outlook of the microfluidic chip assembled on a glass slide. The optical window, visible to the naked eyes, is used for detecting the fluorescence of Rhod-5N; (ii) Fluorescence intensity of Rhod-5N as a function of [Ca²⁺], measured in triplicates. Error bars indicate the standard deviation of three repeat measurements ($\lambda_{ex} = 530$ nm, $\lambda_{em} = 580$ nm). Arrows indicate the perfusion directions.

As shown in Figure 3D (i), the fluidic dynamics relevant to the U-shape cups were evaluated by 2D CFD simulations. The decrease of velocity downstream of the trapping site suggests that a substantial portion of the flow would be directed through the cups, as visualised by the gradual diffusion of food colouring in the sequential cups in Figure 3D (iii). The close-up view at the trapping site indicates that the perfusion in the channel is governed by two flows: the main flow F₁ guiding downward along the serpentine channel, and the side flow F₂ directing a partial fluidic stream into the cup (Figure 3D (ii)). Based on the Darcy-Weisbach equation, the flow ratio of F₂ versus F₁ in this configuration is larger than 1 (i.e., a higher volumetric flow rate directing into the cup compared with the main channel, due to the lower resistance in the U-shape cup) [32,33]. The subjects of interest would primarily be guided by F₂ to accomplish trapping in the cup. Figure 3D also shows that each narrow cross-section channel (neck of a cup in connection with the adjacent main channel) has an increased flow velocity, which helps maintain the trapping of the subjects during continuous perfusion. Once the U-shape cup is occupied, the flow resistance in the corresponding cup increases substantially, leading to a reduction of flow in the side stream, and facilitating the loading of subjects to the next pocket (Figure S6A). The use of these pockets is also advantageous to reduce shear stress, thus preserving the viability of trapped subjects [34].

To mimic the loading of biological subjects for hormone secretion analysis, specifically pancreatic islets (usually $200 \pm 20~\mu m$ in diameter), and advance the understanding of the flow in the chip, three groups of polyethylene (PE) microspheres ($\emptyset = 90\text{-}100~\mu m$, $180\text{-}210~\mu m$ and $210\text{-}250~\mu m$, $\rho = 1.08~g~cm\text{-}3$) were loaded into the chip. As shown in Figure S6B-E, only the microspheres of $180\text{-}210~\mu m$ in diameter can be individually captured by each cup in a sequential manner, without dislodgement under continuous flow. In contrast, the smaller microspheres ($90\text{-}100~\mu m$) were stacked in the cups (Figure S7) while the larger ones ($210\text{-}250~\mu m$) were not observed due to the complete clogging of the channels (data not shown). These results, therefore, validate that the fabricated chip with the given dimension and trapping site is suitable to selectively immobilise the designated subjects for the secretory activity study.

8.4.5 Optical window for fluorescence readout

An optical window (500 μ m in diameter) is incorporated downstream of the second serpentine channel (Figure 3E (i)), which is visually distinctive from the main channel without inducing a delay in refreshing sample. The on-chip fluorescence of Rhod-5N was measured at the optical window via an in-house built LIF set-up with a bifurcated optical fibre (Figure S1B-D). In accordance with the on-chip fluorescence of Rhod-5N as a function of [Ca²⁺], we confirmed that the variations of multiple measurements (n = 3) were negligible, suggesting complete mixing and high stability of the binding between Rhod-5N and Ca²⁺ (Figure 3E (ii)).

8.4.6 Generation of a dynamic microenvironment

In order to characterise the concentration of perfusate at the trapping site (unoccupied) in our microfluidic configuration, calcein and DI water were perfused into the channel via inlet 1 and inlet 2, respectively. Serial concentrations of calcein (1-9 μ M) were generated by adjusting the flow rate ratios between calcein and DI water in the range of 1:9–9:1, while maintaining a constant total flow rate of 2 μ L/min. As shown in Figure 4A, when tuning up the ratio of calcein flow rate, the width of the green band (fluorescence of calcein) gradually increased from top to bottom.

To examine whether the targeted concentrations of calcein were achieved homogeneously in the trapping site, the fluorescence intensity of the region of interest (ROI) in the ten U-shape cups was measured and averaged to plot against the theoretical concentrations of calcein (Figure 4B). As shown in the on-chip measurement, a linear fluorescence intensity as a function of calcein concentration was observed when the concentration of calcein increased from 1 μ M to 9 μ M (R² = 0.9989, red fitting curve). This is highly consistent with the linear fluorescence of calcein (0-10 μ M) measured by the plate reader (R² = 0.9995, blue fitting curve), where the fluorescence was measured in a 96-well plate with the same concentrations. These results validate the capacity of our microfluidic chip to homogenise a series of perfusing chemical gradients at the trapping site with tunable concentrations. It is desirable that multiple captured biological subjects can be exposed to identical stimuli for a uniform response. This means the applicable range of flow rate must ensure homogenising of the gradient across the cups. As shown in Figure 4C (left panel), when calcein and DI water were delivered at a flow rate ratio of 1:1, homogenous fluorescence

was observed across ten cups at a flow rate of 3 μ L/min. As the flow rate increased to 6 μ L/min, a shadow appeared in the first cup due to its lower fluorescence intensity (indicated by the circle in the middle panel of Figure 4C), suggesting the incomplete mixing of calcein and DI water. Increasing the flow rate to 20 μ L/min resulted in an extension of this shaded area, corresponding to a further decrease in mixing efficiency under the higher flow rate (Figure 4C, right panel).

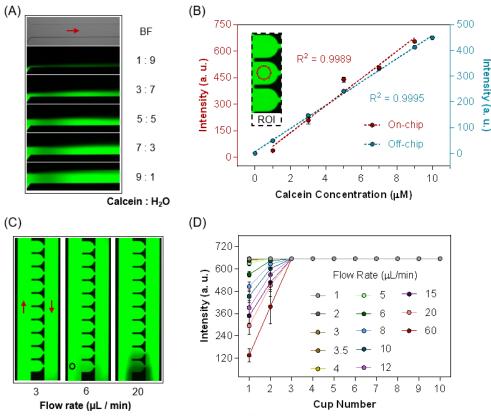


Figure 4. Characterisations of on-chip mixing efficiency under varying perfusion conditions. (A) Fluorescent image of the medium inlet with varying flow rate ratios of calcein versus DI water ranging from 1:9 to 9:1 at a constant total flow rate of 2 µL/min. The top panel shows the bright field image of the channel with a red arrow indicating the direction of perfusion. (B) Fluorescence of a series of calcein (0-10 μM) measured on the microfluidic chip (on-chip) and in a microplate (off-chip). The fluorescence was obtained by averaging the fluorescence intensities of ten cups (one signal of one ROI in each cup) and of three repeat measurements in a microplate, respectively. The dashed curves show the linear fitting of the experimental results (filled circles). Error bars indicate standard deviations of the measured fluorescence intensities of ten cups (on-chip) or the triplicate measurements (off-chip). (C) Fluorescence at the trapping site under different total flow rates of 3-20 µL/min with 1:1 co-perfusion of calcein and DI water. The shadow appearing in the first two cups (at the bottom) increases when the total flow rate exceeds 3 µL/min. The black circle (middle panel) tags the first cup with exposure to the perfusion fluid. (D) Variations of fluorescence at the trapping site under various flow rates (1-60 μ L/min). The cup numbered 1 notes that it was the first exposed to the flow, and the following cups are numbered 2-10. Error bars indicate standard deviations of the fluorescence intensity of an ROI in a cup. All measurements were carried out at $\lambda_{ex} = 475$ nm and $\lambda_{em} = 515$ nm, with cups unoccupied.

The applicable flow rates were further refined by studying the change in fluorescence of calcein in each cup under a series of flow rates. As shown in Figure 4D, in the range of 1-3 μ L/min, the identical fluorescence intensity across ten cups suggests a homogeneous distribution of calcein at the trapping site. When the flow rate increased over 3.5 μ L/min, the fluorescence intensity in the first cup started to decrease. Further increase of the flow rate over 6 μ L/min resulted in a fluorescence drop in the first two cups. These results demonstrate that the maximum flow rate for the complete mixing of calcein (Q_c) ($D_c = 3.3 \times 10^{-6}$ cm² s) [35] is 3 μ L/min with the current chip configuration.

 Q_c can be used as a benchmark value to define the upper bound flow rate for other molecules (Q_a) with different diffusion coefficients. For instance, glucose is widely used as a nutrient stimulus during the study of secretory activity (e.g. insulin secretion from the pancreatic islets). According to Equations (S5-10), the maximum flow rate of glucose is calculated to be 6.09 μ L/min at room temperature (around 23 °C) and 6.38 μ L/min at 37 °C. Since the flow rate typically applied during biomimetic studies is around 5 μ L/min [36,37] the calculated maximum flow rate for glucose suggests the suitability of the configuration of the current microfluidic chip for this purpose.

8.4.7 Biomedical applications

The demonstrated characteristics of both Rhod-5N and the (integrated) microfluidic system imply their potential for broad biomedical applications. To this end, we examined the fluorescence of Rhod-5N in response to human serum Ca²⁺ at concentrations ranging from hypocalcaemia to hypercalcaemia (Figure 5A). In addition, we compared the Ca²⁺-induced fluorescence of Rhod-5N in cell culture medium with and without fetal bovine serum (FBS), respectively (Figure 5B). Lastly, we investigated the feasibility of using the microfluidic chip for multiplexed sensing by simultaneously recording and quantifying the dynamic [Ca²⁺]_{ex} and insulin concentrations, both of which were oscillating to mimic their pulsatile patterns *in vivo* (Figure 5C and D).

As shown in Figure 5A, the fluorescence enhancement of Rhod-5N exhibited a behaviour of concentration-dependence on [Ca²⁺] in both unfiltered and filtered serum samples, where [Ca²⁺] spans from 0.24 mM to 3.21 mM. Under such experimental setups, Ca²⁺-induced fluorescence of

Rhod-5 at hypocalcaemia and hypercalcaemia can be readily distinguishable from that at normocalcaemia (the measured fluorescence data provided in Figure S8A). These observations suggest that Rhod-5N may potentially be developed as a fluorescence-based diagnostic tool for hypocalcaemia and hypercalcemia which are in close relation to a number of diseases such as nutritional deficiency and cancers, respectively [38,39].

Similar to other fluorescence-based sensors used for measuring [Ca²⁺] in serum [20,21], Rhod-5N exhibits distinctive fluorescent signals over a broad range of [Ca²⁺] in raw serum samples (unfiltered). In addition, Rhod-5N is commercially available and can be readily accessed without conducting a sophisticated synthesis. However, the fluorescence change of Rhod-5N in response to variations of Ca²⁺ is not visually distinctive. This would limit the use of Rhod-5N as a convenient diagnostic tool for abnormal serum Ca² that can be read by naked eyes [18].

Intriguingly, the slopes of the fluorescence enhancement differed slightly in the filtered and unfiltered sera, with a slower increase observed in the unfiltered serum (Figure 5A and Figure S8A). This is likely due to the presence of various Ca^{2+} -bound proteins and ionised Ca^{2+} in the unfiltered serum samples (i.e., the altered equilibrium between Ca^{2+} -protein complex and ionised Ca^{2+}), both of which may have given rise to different fluorescence strengths upon binding with the indicator. The clarification of the respective weighing of the fluorescence arising from ionised Ca^{2+} and bound Ca^{2+} in the unfiltered serum is beyond the scope of this study. Nevertheless, our data suggest that a higher protein content would result in a higher K_d of Rhod-5N (i.e., the presence of protein suppressed the formation of (ionised) Ca^{2+} -bound Rhod-5N complex) [40,41].

Given that hormone secretion would be studied with the provision of an *in vitro* culture medium, e.g., DMEM with 10% FBS and thus with the interference by proteins, the fluorescent responses of Rhod-5N to varying [Ca²⁺] in DMEM with and without FBS were compared (static measurements conducted in a microplate). Similar to Figure 5A, the fluorescence enhancement of Rhod-5N exhibited a linear dependence as a function of logarithmic [Ca²⁺] in the cell medium samples (Figure 5B). In addition, a divergence was observed between the fluorescence enhancements of DMEM only and DMEM + FBS (Figure 5B). Apart from the suppressing effect of protein on Ca²⁺-Rhod-5N interaction, the divergence is also related to the higher background

fluorescence (F₀) measured in DMEM + FBS relative to DMEM only (Figure S8B). The raised background can be accounted for by the presence of a small amount of Ca^{2+} in FBS, which resulted in an increase of Ca^{2+} -induced fluorescence in DMEM+FBS for $[Ca^{2+}] \le 0.1$ mM (inset image in Figure S8B, but this perturbation appeared to be negligible when the introduced $[Ca^{2+}]$ increased over 0.5 mM). These results suggest that, (1) Rhod-5N is a competent indicator for measuring $[Ca^{2+}]_{ex}$ in a cell culture medium, e.g., DMEM or DMEM+FBS; and (2) different calibration curves are required for a precise quantification of $[Ca^{2+}]$ in the presence of proteins.

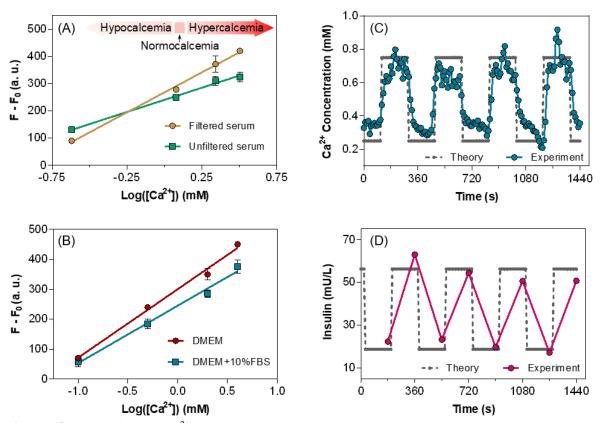


Figure 5. Quantifying $[Ca^{2+}]_{ex}$ (ionised) in various biomedical scenarios. (A) The linearity of fluorescence enhancement of Rhod-5N observed for a widespread range of $[Ca^{2+}]$ in unfiltered and filtered human serum samples. (B) The linearity of fluorescence enhancement of Rhod-5N observed for a widespread range of $[Ca^{2+}]$ in DMEM with and without FBS (10%), respectively. Of note, $[Ca^{2+}]$ in (A) and (B) are expressed in logarithmic concentration, and their concentrations range from hypocalcaemia and normocalcaemia to hypercalcaemia. The measurements in (A) and (B) were performed in a 96-well microplate, with $\lambda_{ex} = 530$ nm and $\lambda_{em} = 580$ nm. (C-D) Simultaneous sensing of oscillatory $[Ca^{2+}]$ and insulin concentrations via the multiplexed microfluidic sensing platform. $[Ca^{2+}]$ and insulin concentrations were artificially oscillated between 0.25-0.75 mM and 18.75-56.25 mU/L, respectively.

In the multiplexed sensing experiment, insulin and Ca²⁺ within the designated concentrations were co-perfused into the microfluidic chip in a pulsatile manner, for which DMEM was used as

the fluidic medium. Since the presence of insulin attenuated the relative change of Ca^{2+} -induced fluorescence of Rhod-5N (Figure S9A), the calibration curve was needed for the quantification of $[Ca^{2+}]$ in the presence of insulin. As shown in Figure S9B, we found this calibration curve fits well with the Hill function ($R^2 = 0.9983$), with the respective k and n_h at 0.42 ± 0.11 mM and 1.52 ± 0.91 . As the fitting parameters were obtained from a narrow concentration range of Ca^{2+} , the numerical values of k and n_h obtained here are only used to quantify Ca^{2+} and they do not have physicochemical implications. To eliminate any photobleaching interference on the indicator, an interval of 10 seconds between each cycle of signal acquisition was applied throughout all the measurements, where the excitation duration was set at 200 ms.

With regard to the quantification of insulin, one potential concern is the nonspecific binding of insulin to the chip. Although the chip channels were pre-treated with a blocking agent, BSA, the loss of insulin due to its contact with perfusion surfaces cannot be avoided. To enable retrieving the exact concentration of perfused insulin, the loss of insulin as aforementioned must be considered, i.e., the measured insulin should undergo a calibration. To obtain the calibration factor, the (theoretical) concentration of insulin in the stock solution as prepared was compared with the concentration of insulin from the chip outlet. As indicated in Figure S9D, a relatively constant loss of 49% was observed from a series of samples containing different concentrations of insulin, suggesting that a factor of 49% should be used as a correction factor. It is worth noting that all the above experimentally measured insulin concentrations were determined on the basis of the standard curve given by the calibrators of the ELISA kit (Figure S9C).

In Figure 5C-D, a continuous dual-sensing of oscillatory [Ca²⁺] and insulin is demonstrated, with the temporal frequency and concentration dynamics approximating their pulsatile patterns *in vivo*.^[41] The measured duration and intensity of oscillating [Ca²⁺] are in line with the theoretical prediction of [Ca²⁺] at the optical window (Figure 5C, Figure S10A & C). These observations validate the ability of the microfluidic system to track the dynamic [Ca²⁺]_{ex} in the range of 0.2-2 mM at the trapping site. They further indicate the oscillation period of [Ca²⁺] around 360 s, which is in good agreement with the switching frequency of the perfusion set-up. Compared to the theoretical timing (vertical grey-dash line), about 50 seconds of the rising edge was observed when switching the low concentration of Ca²⁺ to the high level. This transition time reflects the duration between the flow arriving at the first cup and the flow exiting the trapping site (details

in Supporting Information). With regard to determining the insulin concentration, the oscillation within 7.5-75 mU/L at the outlet, corresponding to 15-150 mU/L at the trapping site, was obtained by using the aforementioned calibration factor (Figure 5D and Figure S10B&D). Relative to the theoretical insulin concentration, our measurement represented an accurate retrieval with less than a 5% deviation. In terms of the temporal response, insulin signals displayed a time delay of around 80 s, which is approximately the perfusion time (75 s) from the optical window to the outlet (Figure S11). Overall, this sensing platform is competent to record the physiological oscillations and durations of [Ca²⁺] and insulin and allows for retrieving and evaluating the oscillations of target molecules at any position on the chip. However, its extension to other specific experiments requires careful evaluation and possible optimisation to suit the specific purpose.

8.5 Conclusions

Our work has established a fluorescent sensing method enabling the quantification of [Ca²⁺]_{ex} (0.2-2 mM), based upon a cost-effective and easily accessible indicator, Rhod-5N, that exhibits highly predictable fluorescence changes in different concentrations of Ca²⁺ in biomedical media, including human serum and cell culture medium with and without FBS. We have designed and fabricated a microfluidic chip that can refine, tune and homogenise the concentrations of chemical gradients in the perfusion fluid under physiologically analogous flow rates for the generation of a dynamic micro-environment. By integrating the chip with the modalities of LIF detection set-up and ELISA, we showed that this microfluidic sensing system can simultaneously measure the dynamic changes of both [Ca²⁺]_{ex} and a hormone (insulin) with a high temporal resolution. Compared with the recently developed sensors for [Ca²⁺]_{ex} [19,22,23,44], our microfluidic platform provides a unique opportunity for continuous and multiplexed sensing of Ca²⁺ and hormone in a biomimetic environment, which is critical to evaluate the link between [Ca²⁺]_{ex} and the secretory function of endocrine tissues. However, in addition to the lack of automation capacity for sample collection, the present system is shown to detect dynamic insulin with a temporal resolution of 3 minutes (because of the minimal volume of the sample required for the ELISA). By contrast, capillary electrophoresis immunoassay has attained a 10-second temporal resolution at the cost of complicating the experimental setups.^[45] The future biological applications of this platform may provide valuable insights into the roles of [Ca²⁺]_{ex} in biological

events, and potentially lead to the identification of novel targets for the development of new therapies.

8.6 References

- 1. Berridge, M. J., Lipp, P., Bootman, M. D. The versatility and universality of calcium signalling. *Nature Review Molecular Cell Biology* **2000**, *1*, 11-21.
- 2. Berridge, M. J., Bootman, M. D., Roderick, H. L. Calcium signalling: dynamics, homeostasis and remodelling. *Nature Review Molecular Cell Biology* **2003**, *4*, 517-529.
- 3. Delling, M., DeCaen, P. G., Doerner, J. F., Febvay, S., Clapham, D. E. Primary cilia are specialized calcium signallin organelles. *Nature* **2013**, *504*, 311-314.
- 4. Courjaret, R., Machaca, K. Mid-range Ca²⁺ signalling mediated by functional coupling between store-operated Ca²⁺ entry and IP 3-dependent Ca²⁺ release. *Nature Communications* **2014**, *5*, 3916
- 5. Zhou, Q., Yen, A., Rymarczyk, G., Asai, H., Trengrove, C., Aziz, N., Kirber, M. T., Mostoslavsky, G., Ikezu, T., Wolozin, B., Bolotina, V. M. Impairment of PARK14-dependent Ca²⁺ signalling is a novel determinant of Parkinson's disease. *Nature Communications* **2016**, *7*, 10332
- 6. Grienberger, C., Konnerth, A. Imaging calcium in neurons. *Neuron* **2012**, *73*, 862-885.
- 7. Life Technologies Inc., *The Molecular Probes Handbook*, (Eds: I. Johnson, M. Spence), USA **2010**.
- 8. Bagur, R., Hajnóczky, G. Intracellular Ca²⁺ sensing: its role in calcium homeostasis and signaling. *Molecular Cell*, **2017**, *66*, 780-788.
- 9. Simpson, A. W. Fluorescent measurement of [Ca²⁺]_C: basic practical considerations. *Methods in Molecular Biology* **2013**, *937*, 3-36.
- 10. Schaafsma, G. in *Calcium in Human Biology*, (Eds: B. C. E. Nordin), Springer, London, UK 1988, 241-259.
- 11. Carroll, M. F., Schade, D. S. A practical approach to hypercalcemia. *American Family Physician* **2003**, *67*, 1959-1966.
- 12. Hofer, A. M., Brown, E. M. Extracellular calcium sensing and signalling. *Nature Review Molecular Cell Biology* **2003**, *4*, 530-538.

- 13. Zhang, C., Miller, C. L., Brown, E. M., Yang, J. J. The calcium sensing receptor: from calcium sensing to signaling. *Science China: Life Science* **2015**, *58*, 14-27.
- 14. Hills, C. E., Younis, M. Y. G., Bennett, J.; Siamantouras, E.; Liu, K.; Squires, P. E. Calcium-sensing receptor activation increases cell-cell adhesion and β-cell function. *Cellular Physiology and Biochemistry* **2012**, *30*, 575-586.
- 15. Brown, E. M. Role of the calcium-sensing receptor in extracellular calcium homeostasis.

 *Best Practice & Research Clinical Endocrinology & Metabolism 2013, 27, 333-343.
- 16. Torres, A., Wang, F., Xu, Q., Fujita, T., Dobrowolski, R., Willecke, K., Takano, T., Nedergaard, M. Extracellular Ca²⁺ acts as a mediator of communication from neurons to glia. *Science Signalling* **2012**, *5* (208), ra8
- 17. Squires, P. E., Jones, P. M., Younis, M. Y., Hills, C. E. in Hills, *Vitamines and Hormones* **2014**, *95*, 249-267.
- 18. Kim, S., Park, J. W., Kim, D., Kim, D., Lee, I.-H., Jon, S. Bioinspired colorimetric detection of calcium (II) ions in serum using calsequestrin-functionalized gold nanoparticles. *Angewandte Chemie* **2009**, *121*, 4202-4205.
- 19. Kim, S., Kim, J., Lee, N. H., Jang, H. H., Han, M. S. A colorimetric selective sensing probe for calcium ions with tunable dynamic ranges using cytidine triphosphate stabilized gold nanoparticles. *Chemical Communications* **2011**, *47*, 10299-10301.
- Moirangthem, M., Arts, R., Merkx, M., Schenning, A. P. An optical sensor based on a photonic polymer film to detect calcium in serum. *Advanced Functional Materials* 2016, 26, 1154-1160.
- 21. Ding, Y., Ling, J., Qiao, Y., Li, Z., Sun, Z., Cai, J., Guo, Y., Wang, H. A high-throughput fluorimetric microarray with enhanced fluorescence and suppressed "coffee-ring" effects for the detection of calcium ions in blood. *Scientific Reports* **2016**, *6*, 38602
- 22. Ishiwari, F., Hasebe, H., Matsumura, S., Hajjaj, F., Horii-Hayashi, N., Nishi, M., Someya, T., Fukushima, T. Bioinspired design of a polymer gel sensor for the realization of extracellular Ca²⁺ imaging. *Scientific Reports* **2016**, *6*, 24275
- 23. Gao, M., Li, Y., Chen, X., Li, S., Ren, L., Tang, B. Z. Aggregation-induced emission probe for light-up and *in situ* detection of calcium ions at high concentration. *ACS Applied Materials & Interfaces* **2018**, *10* (*17*), 14410-14417.

- Minta, A., Kao, J., Tsien, R. Y. Fluorescent indicators for cytosolic calcium based on rhodamine and fluorescein chromophores. *Journal of Biological Chemistry* 1989, 264, 8171-8178.
- 25. Collot, M., Loukou, C., Yakovlev, A. V., Wilms, C. D., Li, D., Evrard, A., Zamaleeva, A., Bourdieu, L., Léger, J.-F., Ropert, N., Eilers, J., Oheim, M., Feltz, A., Mallet, J. Calcium Rubies: A family of red-emitting functionalizable indicators suitable for two-photon Ca²⁺ imaging. *Journal of the American Chemical Society* 2012, 134, 14923-14931.
- 26. Ribou, A.-C., Salmon, J.-M., Vigo, J., Goyet, C. Measurements of calcium with a fluorescent probe Rhod-5N: Influence of high ionic strength and pH. *Talanta* **2007**, *71*, 437-442.
- 27. Gesztelyi, R., Zsuga, J., Kemeny-Beke, A., Varga, B., Juhasz, B., Tosaki, A. The Hill equation and the origin of quantitative pharmacology. *Archive for History Exact Sciences* **2012**, *66*, 427-438.
- 28. McGuigan, J. A., Lüthi, D., Buri, A. Calcium buffer solutions and how to make them: a do it yourself guide. *The Canadian Journal of Physiology and Pharmacology* **1991**, *69*, 1733-1749.
- 29. Grynkiewicz, G., Poenie, M., Tsien, R. Y. A new generation of Ca²⁺ indicators with greatly improved fluorescence properties. *Journal of Biological Chemistry* **1985**, *260*, 3440-3450.
- 30. Taylor & Francis Group, *CRC Handbook of Chemistry and Physics 95th Edition*, (Eds: W. M. Haynes, D. R. Lide, T. J. Bruno), CRC Press, Boca Raton, FL, USA **2014**.
- 31. Clark, J., Kaufman, M., Fodor, P. S. Mixing Enhancement in Serpentine Micromixers with a Non-Rectangular Cross-Section. *Micromachines* **2018**, *9*, 107
- 32. Marusic-Paloka, E. Incompressible newtonian flow through thin pipes. *Applied Mathematics and Scientific Computing*, (Eds: Z. Drmač, V. Hari, L. Sopta, Z. Tutek, K. Veselić), Springer, Boston, MA, USA **2003**, 123-142.
- 33. Tan, W.-H., Takeuchi, S., A trap-and-release integrated microfluidic system for dynamic microarray applications. *Proceedings of the National Academy of Sciences* **2007**, *104* (4), 1146-1151.

- 34. Xing, Y., Nourmohammadzadeh, M., Mendoza-Elias, J. E.; Chan, M.; Chen, Z.; McGarrigle, J. J.; Oberholzer, J.; Wang, Y. A pumpless microfluidic device driven by surface tension for pancreatic islet analysis. *Biomedical Microdevices* **2016**, *18*, 80,
- 35. Yoshida, N., Tamura, M., Kinjo, M. Fluorescence correlation spectroscopy: a new tool for probing the microenvironment of the internal space of organelles. *Single Molecules* **2000**, *1*, 279-283.
- 36. Choe, A., Ha, S. K., Choi, I., Choi, N., Sung, J. H. Microfluidic Gut-liver chip for reproducing the first pass metabolism. *Microdevices* **2017**, *19*, 4,
- 37. Kimura, H., Ikeda, T., Nakayama, H., Sakai, Y., Fujii, T. An on-chip small intestine–liver model for pharmacokinetic studies. *Journal of Laboratory Automation* **2015**, *20*, 265-273.
- 38. Schafer, A. L., Shoback, D. M., Hypocalcemia: Definition, etiology, pathogenesis, diagnosis, and management. *Primer on the Metabolic Bone Diseases and Disorders of Mineral Metabolism* **2018**, 646-653.
- .39. Minisola, S., Pepe, J., Piemonte, S., Cipriani, C., The diagnosis and management of hypercalcaemia. *British Medical Journal* **2015**, *350*, h2723
- 40. Chiancone, E., Thulin, E., Boffi, A., Forsen, S.; Brunori, M. Evidence for the interaction between the calcium indicator 1, 2-bis (o-aminophenoxy) ethane-N, N, N', N'-tetraacetic acid and calcium-binding proteins. *Journal of Biological Chemistry* **1986**, *261*, 16306-16308.
- 41. Harkins, A., Kurebayashi, N., Baylor, S. Resting myoplasmic free calcium in frog skeletal muscle fibers estimated with fluo-3. *Biophysics Journal* **1993**, *65*, 865-881.
- 42. Baker, A. J., Brandes, R., Schreur, J., Camacho, S. A., Weiner, M. W. Protein and acidosis alter calcium-binding and fluorescence spectra of the calcium indicator indo-1. *Biophysics Journal* **1994**, *67*, 1646-1654.
- 43. Pørksen, N. The *in vivo* regulation of pulsatile insulin secretion. *Diabetologia* **2002**, *45*, 3-20
- 44. Tastanova, A., Folcher, M., Müller, M., Camenisch, G.; Ponti, A.; Horn, T.; Tikhomirova, M. S.; Fussenegger, M., Synthetic biology-based cellular biomedical tattoo for detection of hypercalcemia associated with cancer. *Science Translational Medicine* 2018, 10 (437), eaap8562

45. Yi, L., Bandak, B., Wang, X., Bertram, R., Roper, M. G., Dual detection system for simultaneous measurement of intracellular fluorescent markers and cellular secretion. *Analytical Chemistry* **2016**, *88* (21), 10368-10373.

8.7 Supplementary Information

8.7.1 Chemicals and reagents

Ca²⁺, Mg²⁺, K⁺, and Na⁺ ions were provided in the form of chlorate salts (Chem-Supply, Adelaide, Australia). Other cations, including Fe²⁺, Cu²⁺, Zn²⁺, and Al³⁺ were provided in the form of perchlorate salts (Sigma-Aldrich, St. Louis, USA). Na₂HPO₄ and KH₂PO₄ for preparing phosphate-buffered saline (PBS) were purchased from Chem-Supply, Australia. All the salts were in analytical grade and used without further purification. Calcein (> 93%) was purchased from Sigma, Australia. Calcein indicator supplied in powder form was dissolved in a freshly prepared solvent for studies as described below.

PBS buffer was prepared by dissolving 4 g NaCl, 0.1 g KCl, 0.71 g Na₂HPO₄ and 0.12 g KH₂PO₄ in 500 mL DI water. The pH of PBS was then adjusted to 7.4 under monitoring by a pH meter (827 pH Lab Metrohm, Australia). The pH meter was calibrated by standard solutions with pH 4, 7 and 9 (Metrohm, Australia) prior to the measurement. A stock solution of 200 mM Ca²⁺ was prepared by dissolving 588.08 mg CaCl₂•2H₂O (MW = 147.02) into 20 mL DI water. For Rhod-5N in DI water, a stock solution of 0.1 mM Rhod-5N (MW = 900.034), prepared by dissolving 500 µg Rhod-5N into 5.56 mL DI water, was diluted into 5 µM and 50 µM with DI water, respectively. For Rhod-5N in PBS solution, 1mM stock solution was prepared by dissolving the same amount of Rhod-5N in 555.6 µL PBS buffer. This stock solution was diluted with PBS buffer for target concentrations when in use. 0.5 mM calcein stock solution was prepared by dissolving 62.25 mg calcein (MW = 622.53) in 200 mL PBS buffer, which would be diluted into 10 µM with PBS buffer for use. Ca²⁺, Rhod-5N and calcein solutions were used without further adjustment on pH. Blue polyethylene (PE) microspheres (φ = 180-212 μm, 90-100 µm and 210-250µm) for simulating the tissue loading were obtained from Cospheric, USA. Fetal bovine serum (FBS) was obtained from Thermo Fisher Scientific, Australia. All glassware used during the experiment was thoroughly cleaned in accordance with standard cleaning procedures.

8.7.2 Fluorescence detection by plate reader (off-chip measurement)

50 μ L Ca²⁺ and 50 μ L Rhod-5N solutions were mixed in a 96-well assay plate (black plate, clear bottom, Corning, USA), where the Ca²⁺ samples were diluted into the detection concentration as shown in the results. The fluorescence was measured by Synergy H4 Hybrid Multi-Mode Microplate Reader (BioTek, USA). With the exposure to 535 nm excitation light, the emission spectra from 555 nm to 700 nm of Rhod-5N were obtained. To characterise the concentration-dependent fluorescence of calcein, the volume ratio of calcein solution (10 μ M) versus DI water was set from 1:9 to 9:1 with a total volume of 100 μ L. The excitation was 470 nm and the emission spectra were recorded from 490 nm to 700 nm.

All measurements were carried out at room temperature except for the Ca²⁺ titration experiment which was conducted at 37 °C. The scanning speed was set at 2 nm with the bandpass at 9 nm. The gain rate was set as 60% with a read height of 8 mm. Each spectrum here was measured in duplicates and triplicates for Rhod-5N and calcein, respectively.

To investigate the photostability of Rhod-5N, the indicator was placed in an ambient environment and exposed to light in the lab from 0 (no exposure, aluminium foil blocked) to 7 days. The fluorescence of Rhod-5N in response to various [Ca²⁺] was measured in triplicate by a plate reader upon the completion of the proposed exposure duration.

8.7.3 Calibration of effective Ca²⁺ concentration ([Ca²⁺]_e)

 Ca^{2+} is subject to the shielding effect imposed by other ionised species in the ionic solution. The effective concentration of Ca^{2+} ($[Ca^{2+}]_e$) available for binding with the indicator is thus smaller than the ionised concentration of Ca^{2+} ($[Ca^{2+}]_{ic}$). While the apparent K_d is computed with $[Ca^{2+}]_{ic}$, the effective dissociation constant (K_{ed}) can be extracted if the calibrated $[Ca^{2+}]_e$ is used. The relationship between $[Ca^{2+}]_e$ and $[Ca^{2+}]_{ic}$ can be given by:

$$[C\alpha^{2+}]_e = \gamma_i \times [C\alpha^{2+}]_{ic} \tag{S1}$$

where γ_i describes the relationship between the effective concentration and the ionised concentration of an ion species under a specific condition.

For an ionic solution, γ_i of the specific ion is determined by the ionic strength of the solution and the temperature of the environment. γ_i can be calculated via the Davis formula when I < 0.5 mol/L [1]:

$$\log(\gamma_i) = -a \times z_i^2 \left(\frac{\sqrt{I}}{1 + \sqrt{I}} - 0.3 \times I \right)$$
 (S2)

where a is the coefficient constant, z_i is the valence of the ion, and I (mol/L) is the ionic strength of a solution. The coefficient constant can be determined as:

$$a = 1.82 \times 10^6 \times (\varepsilon T)^{-3/2}$$
 (S3)

where T is the absolute temperature, and the dielectric constant ε of water at 37 °C is 74.12 [2]. a is calculated to be 0.52.

The ionic strength of a solution is expressed as [3]:

$$I = \frac{1}{2} \sum c_i z_i^2 \tag{S4}$$

where c_i is the ionised concentration of an ion. Based on the ionic species in the cell culture medium (for Ca^{2+}) and in PBS (for Rhod-5N) as listed in Table S2, the background ionic strength was determined at 167.22 mM.

According to Equation (S1-4), the addition of Ca^{2+} during the titration experiment could vary the $[Ca^{2+}]_e$, as shown in Figure S3A. By plotting the fluorescence intensity of Rhod-5N against $[Ca^{2+}]_e$ (Figure S3B), the effective dissociation constant (K_{ed}) was computed as 1.31 ± 0.20 mM, with n_h at 0.88 ± 0.041 (R² = 0.9996).

8.7.4 Surface characterisations of the microfluidic chip

An optical microscope (Olympus BX51, Olympus, Japan) was used to examine the microfluidic channels (Figure S5A-F). An optical profiler Contour GT-I (Bruker, Germany) was used to examine the dimensions of the chip (Figure S5G-H), where the VSI mode was selected, 5× and 0.55 were applied on the objective and multiplier, respectively. Three PDMS chip replicas were

measured, and the averaged values of the measurements were used to compare with the chip design to determine the accuracy of the fabrication procedure.

As shown in Table S3, the dimensions of the PDMS chip, in general, undergo shrinkage in comparison to the values set in the design. There are two factors contributing to the shrinkage. Firstly, the PDMS was poured into the mould to form the structure, thus the dimension of the resultant PDMS chip was smaller than the mould. Secondly, since the curing process was performed in the mould with incubation at 70 °C, the PDMS would shrink when cooling down to room temperature (thermal expansion coefficient of PDMS: 300×10⁻⁶ /°C) [4]. Table S3 shows that the PDMS chips bear with different errors for different dimensions, typically <10% for the width and height of the main channel, and the opening and base of the tissue array, whereas ~25% for finer structures, such as the walls and cross-channel sections of the tissue cups.

Perfusion set-up and pre-preparations. A microfluidic perfusion system was set up to investigate the fluid dynamics in the microfluidic chip as depicted in Figure S1. The perfusion system was controlled by a microfluidic pump syringe driver (NanoJet Stereotaxic Syringe Pump, Chemyx, USA). The designated solutions were perfused from 500 µl glass syringes (SGE, Trajan, USA) to the connected fluorinated ethylene propylene (FEP) tubing (1/16" OD× .010", IDEX, USA) and the inlets of the chip in downstream. The FEP tubing was connected to the syringe via a 10-32 female and male lure adapter (IDEX, USA). The effluent from the chip was collected for insulin measurement via ELISA kit.

Prior to perfusions, the microfluidic chip and glass syringes were filled with 70% ethanol to prevent the entrapment of bubbles, followed by 3 times rinses with DI water. For insulin detection experiment, an additional treatment with 3% bovine serum albumin (BSA) for 15 minutes was performed prior to the experiments to reduce the non-specific adsorption of protein onto PDMS. DI water, ethanol and 3% BSA were processed by syringe filter (pore size $0.45 \, \mu m$, Minisart, Germany) before the perfusion.

8.7.5 On-chip imaging and fluorescence detection

The perfusion of food colouring was observed by Nikon SMZ25 Stereo microscope. To obtain a broad view of the channels, magnification, zoom factor and objective were $0.5\times$, $1.0\times$ and $0.5\times$,

respectively, with an exposure time of 250 ms. For a close-up view of the trapping site, the parameters were adjusted to $1.5\times$, $3.0\times$ and $0.5\times$ with an exposure time of 400 ms.

The on-chip fluorescence was measured by an in-house built portable fluorescence detection system as shown in Figure S1B-D. The 532 nm excitation light from Match Box laser generator (Integrated Optics, Lithuania) was delivered into a bifurcated fibre (FG200UEA, THORLABS, USA). The output laser beam from the fibre, after coupling with an optical objective, was focused onto the optical window of the chip (Figure S1C). The fluorescence was collected and delivered by the adjacent branch of the fibre to QEPro spectrometer (Ocean Optics, UK). Note that each sample was recorded with 5 repeated spectral measurements. A 532 nm long-pass filter (THORLABS, USA) was placed in front of the spectrometer to remove the interference from the scattered excitation light. To prevent the errors from the stage vibration, the microfluidic chip attached on a glass slide was tightly mounted on an aluminium slide holder (Figure S1D). The position of the chip was precisely controlled by a micro-stepper (LST-15FC60-40R-XYZ, Lambda Scientific) in a stepwise manner.

The imaging of calcein was completed by Nikon Ti-E inverted fluorescence microscope. The exposure time was set as 400 ms with the gain rate at level 1. The acquired fluorescence images were analysed by image processing software, Fiji. With the software, the fluorescence was measured by drawing a 23×23 Region of Interest (ROI) within the trapping site and reading the fluorescence intensity of the ROI.

8.7.6 Analysis of diffusion and flow rate in the channel

The diffusion of molecules in a microfluidic channel, i.e. the travelling distance (d) of molecules over a certain period of time (t), can be described as:

$$d^2 = 2 \cdot D \cdot t \tag{S5}$$

where D is the diffusion coefficient of the molecules and t is the travelling time. According to the Stokes-Einstein equation, D can be calculated by:

$$D = \frac{k_b T}{6\pi r \mu} \tag{S6}$$

where k_b is the Boltzmann constant, T is the absolute temperature and r is the hydrodynamic radius. The mixing time (τ) required for achieving a homogeneous distribution of the molecules can be expressed as [5]:

$$\tau \sim \frac{w^2}{D} \tag{S7}$$

Assuming two laminar flows are carried with velocity (v):

$$v = \frac{Q}{wh} \tag{S8}$$

where Q is the volumetric flow rate. As such, the product of Equation (S7-8) leads to the minimum length (L) that is required for complete mixing of two solutions, which can be written as:

$$L = \frac{Qw}{hD} \tag{S9}$$

For a given channel length for fluid travelling, the maximum volumetric flow rate to ensure the thorough mixing of flows in a channel is calculated as:

$$Q = \frac{LhD}{w} \tag{S10}$$

8.7.7 Preparation and loading of Polyethylene (PE) microspheres suspension

Blue PE microspheres (\emptyset = 180-212 μ m and 90-100 μ m) were used as an analogous object of the loading of tissue into the microfluidic channels. The preparation of microsphere suspension followed the protocol by the manufacturer. Briefly, 30 mg PE microspheres were dispersed in 1 mL 0.1% Tween 80 (Sigma, USA) to prepare a 30 mg/mL stock suspension. Prior to the loading, the stock suspension was diluted into 0.1 mg/mL with 0.1% Tween 80 and inlet 2 and inlet 3 were blocked by inserting a long tube around 10 cm. The microfluidic chip was preconditioned by perfusing ethanol, followed by DI water. After that, a 1 mL pipette tip was inserted into inlet 1 and a 5 cm tubing was inserted into the outlet, followed by loading the microsphere suspension via inlet 1. By plugging off the tubing from the outlet, the microsphere suspension commenced to perfusion into the channel and underwent subsequent trapping at the U-shape cups.

8.7.8 Calibration curve of Ca²⁺-induced fluorescence of Rhod-5N (on-chip)

Since Ca^{2+} -induced fluorescence of Rhod-5N in the microfluidic chip is likely to deviate from that measured in a microplate, we conducted an on-chip-based standard calibration curve of the fluorescence intensity of the indicator as a function of $[Ca^{2+}]$ to improve the sensing accuracy.

As shown in Table S4, with a total flow rate of 4 μ L/min, Ca²⁺-free DMEM and DMEM containing 4 mM Ca²⁺ were delivered into the microfluidic chip via inlet 1 and inlet 2 at varying flow rate ratios to generate serial concentrations of Ca²⁺. Meanwhile, Rhod-5N (100 μ M in PBS, pH 7.4) was loaded into the channels (inlet 3) at a constant flow rate of 4 μ L/min; the optimal concentration of 50 μ M Rhod-5N was obtained after mixing with the perfused flow from inlets 1&2. In response to varying Ca²⁺ concentrations, the variations of fluorescence intensity at 580 nm (emission peak of Rhod-5N) were recorded.

Each measurement was repeated three times with an interval of 30 seconds. When adjusting the flow rate for a different [Ca²⁺], the fluorescence was recorded only after stable signals were observed.

8.7.9 Temporal characterisation of the on-chip perfusion

For any selected flow rate, the fluid travelling from the inlet, via optical window to the outlet undergoes a time difference. To obtain a corrected temporal readout, the volume of each section of the channel and the corresponding time duration were listed in Table S5 and Figure S9. In short, when tuning the ratio of the flow rate at the inlets to obtain oscillating [Ca^{2+}], a time delay of ~130 seconds ($t_1 + t_2 + t_3$) takes place for such a change at the optical window. When the perfusion flow arrives at the trapping site, a substantial portion flows through the U-shape cups and it would travel a shorter distance before reaching the optical window compared with the flow passing the main channel. Consequently, the early arrival of this portion of flow at the optical window initiates the change in Ca^{2+} -induced fluorescence around 10 seconds earlier than the calculation, i.e. 10-second reduction in t_2 . In addition, the transition periods between the two concentrations reflect the time from the flow arrives at the 1st U-shape cup to completely refresh the trapping site. For the dual-sensing of Ca^{2+} -induced fluorescence and insulin concentration, a

time delay of ~75 seconds (t₄) can be predicted due to the distance between the optical window and sample tube.

8.7.10 Measurement of Ca^{2+} -induced fluorescence of Rhod-5N in serum or cell culture medium with FBS

To investigate the fluorescent response of Rhod-5N to serum Ca^{2+} , a human serum sample was used (obtained from our current Biobank with approval from the Central Adelaide Local Health Network Human Research Committee). The concentrations of ionised Ca^{2+} (1.21 mM) and total Ca^{2+} (2.64 mM) were examined by the test for Blood Biochemistry at SA Pathology, Australia. To clarify the impact of serum protein on the sensing performance, 600 μ L serum was filtered by a centrifugal filter with a pore size of 3kDa (around 380 μ L filtered serum was collected). Both the filtered and unfiltered serum samples were either 5 times diluted with pH 7.4 PBS buffer or supplemented with 200 mM Ca^{2+} stock solution to adjust $[Ca^{2+}]$ from hypocalcemia to hypercalcemia (up to 3.2 mM Ca^{2+} in our test).

To prepare different concentrations of Ca²⁺ in the cell culture media, the stock solution of Ca²⁺ was added into DMEM with or without FBS, where the mixture of DMEM with 10% FBS was obtained by adding 1 mL FBS to 9 mL Ca²⁺-free DMEM.

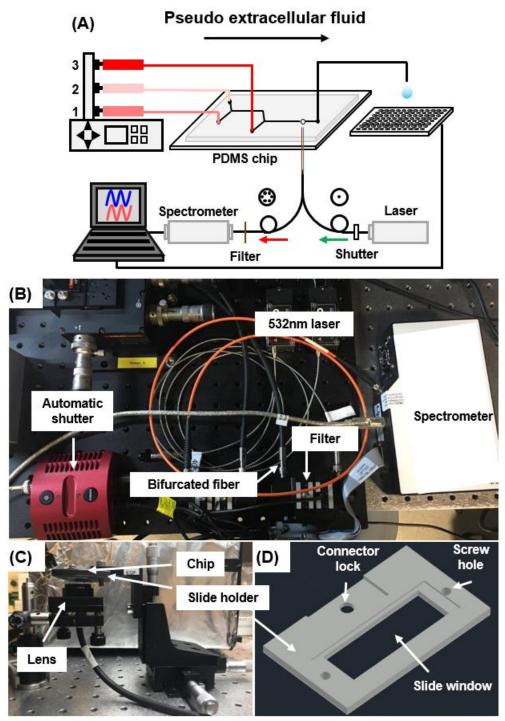


Figure S1. Schematic and experimental set-up of the multiplexing microfluidic platform for Ca²⁺ and insulin sensing. (A) Schematic of the microfluidic perfusion system incorporated with a fluorescence detection system and ELISA kit. (B) Major optical components include a matchbox laser, 532 nm long-pass filter, an automatic shutter and a spectrometer. (C) The glass slide fixed in an aluminium slide holder was placed onto the position adjuster. (D) Schematic of the slide holder for mounting the glass slide.

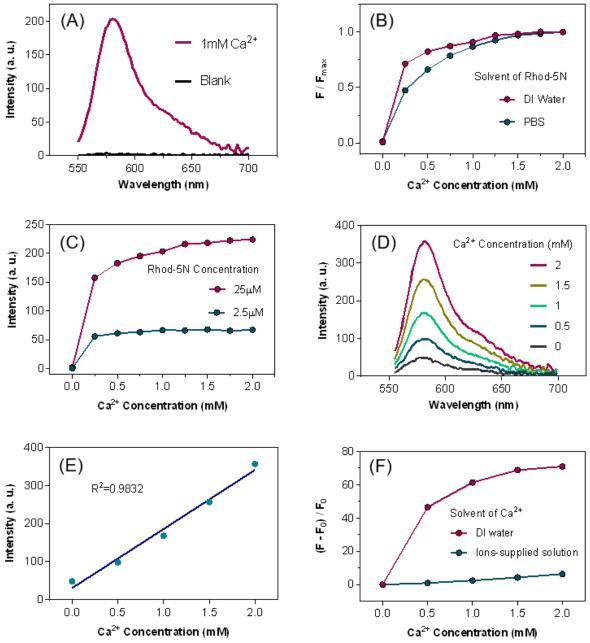


Figure S2. Fluorometric characterisations of Rhod-5N for different [Ca²⁺] under various conditions. (A) Emission spectra of 25 μM Rhod-5N (DI water) in response to 1 mM Ca²⁺ (DI water) and in the absence of Ca²⁺. (B) Fluorescence intensities of 25 μM Rhod-5N in DI water and PBS as a function of 0-2 mM Ca²⁺, respectively. (C) Ca²⁺-induced fluorescence of 2.5 μM and 25 μM Rhod-5N in DI water. (D) Emission spectra of 50 μM Rhod-5N (PBS, pH7.4) in response to increasing concentration of Ca²⁺ (ions-supplied solution). (E) Fluorescence intensity of 50 μM Rhod-5N (PBS, pH7.4) in response to increasing concentration of Ca²⁺ (ions-supplied solution). (F) Relative fluorescence intensity of 50 μM Rhod-5N (PBS, pH7.4) to Ca²⁺ in DI water (red) and in ions-supplied solution (blue). F_0 and F were the fluorescence of the indicator in the absence and presence of Ca²⁺, respectively. ($\lambda_{ex} = 535$ nm, $\lambda_{em} = 580$ nm)

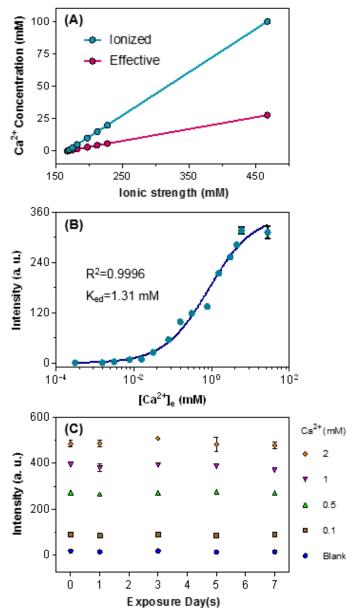


Figure S3. Calibrations of K_{ed} and investigation of photostability of Rhod-5N. (A) Comparison of ionised Ca^{2+} concentration ($[Ca^{2+}]_{ic}$) and effective Ca^{2+} concentration ($[Ca^{2+}]_e$) in different ionic strengths. (B) Fitting of $[Ca^{2+}]_e$ (solid dots) via Hill's function. The effective dissociation constant (K_{ed}) was determined as 1.31 ± 0.20 mM with n_h of 0.88 ± 0.041 ($R^2 = 0.9996$). (C) Ca^{2+} -induced fluorescence of Rhod-5N with the exposure to ambient light from 0-7 days.

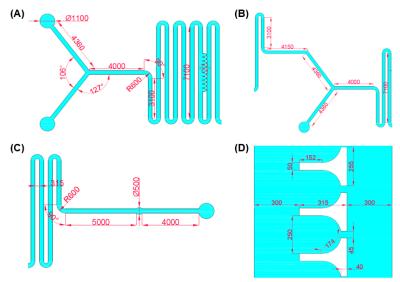


Figure S4. The layout and dimension of the microfluidic chip design (unit: μ m). (A) Overall layout of the microfluidic chip, which consisted of three inlets, two sections of serpentine channels, a tissue trapping site consisting of ten U-shape cups embedded in the first serpentine channel, an optical window and an outlet. (B-D) Detailed dimensions of the chip structure.

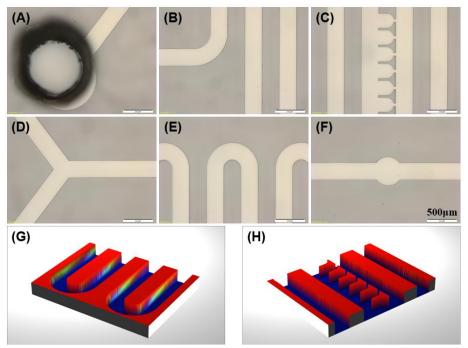


Figure S5. The microfluidic chip imaged by an optical microscope and optical profiler, respectively. (A-F) Zoom-in view of the respective microscale parts of the chip under an optical microscope. The well-defined structures are highly consistent with the chip design. (G-H) Illustrative 3D images of the chip by optical profiler, suggesting the good surface properties of the fabricated PDMS device.

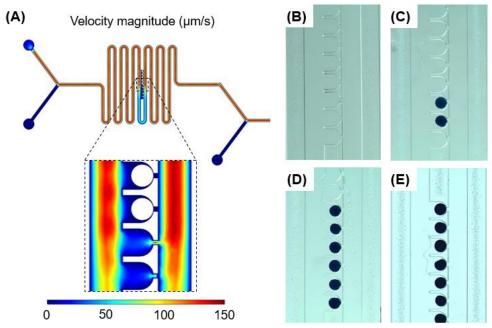


Figure S6. PE microspheres trapping in the microfluidic chip ($\emptyset = 180-210 \, \mu m$). (A) Velocity mapping in the microfluidic channels with particles occupying the first five cups. The inset shows a detailed view of the occupied cups and the following empty cups. (B-D) Continuous loading of microspheres under hydrodynamic force. (E) Completion of the particle trapping, where all the cups were occupied by a single particle.

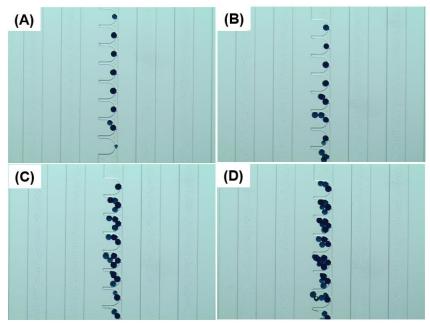


Figure S7. PE microspheres loading in the microfluidic chip ($\emptyset = 90\text{-}100 \,\mu\text{m}$). (A) The first few particles distributed in the cups in a relatively even manner. (B-D) Microspheres were stacked within each cup during the continuous loading.

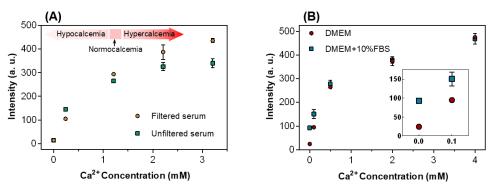


Figure S8. Measuring Ca^{2+} -induced fluorescence of Rhod-5N in different media. (A) Fluorescence intensity of Rhod-5N as a function of $[Ca^{2+}]$ in filtered and unfiltered serum samples; (B) Fluorescence intensity of Rhod-5N as a function of $[Ca^{2+}]$ in a cell culture medium DMEM with and without 10% FBS.

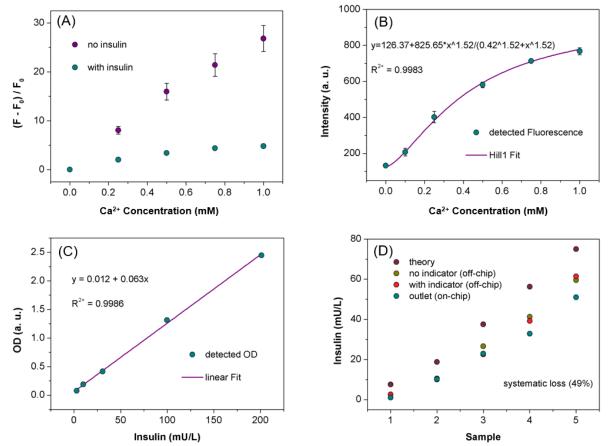


Figure S9. Calibration curves for Ca^{2+} -insulin dual-sensing. (A) Comparison of relative enhancement of Ca^{2+} -induced fluorescence of Rhod-5N in the absence and presence of insulin, where F is the fluorescence of Rhod-5N with the addition of the specific concentration of Ca^{2+} and F_0 is the fluorescence of Rhod-5N without any Ca^{2+} (on-chip measurement). Error bars indicate the standard deviation of triplicate measurements. (B) Calibration curve of Ca^{2+} -induced fluorescence as a function of $[Ca^{2+}]$ (on-chip measurement). Error bars indicate the standard deviation of triplicate measurements. (C) Standard curve for insulin quantification, obtained by measuring the OD of the calibrators of the ELISA kit (a 96-well microplate measurement). (D) Determination of insulin concentrations of the samples as named in the legend. The systematic loss was calculated by: (theoretical concentration – experimental concentration)/theoretical concentration. (A-B: $\lambda_{ex} = 535$ nm, $\lambda_{em} = 580$ nm; C-D: $\lambda_{ex} = 450$ nm)

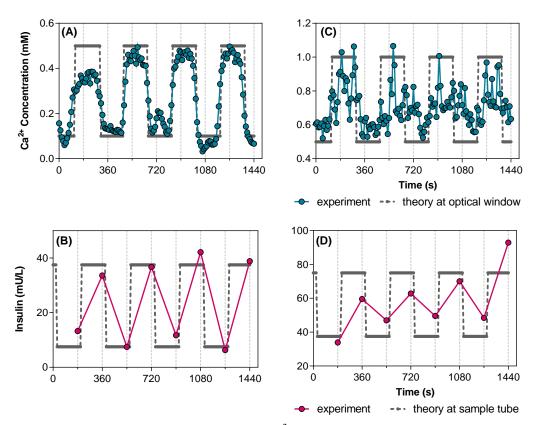


Figure S10. Simultaneous sensing of oscillatory Ca^{2+} and insulin with different concentrations. (A-B) Ca^{2+} and insulin oscillate between 0.1-0.5 mM and 7.5-37.5 mU/L, respectively; (C-D) Ca^{2+} and insulin oscillate between 0.5-1.0 mM and 37.5-75mU/L, respectively.

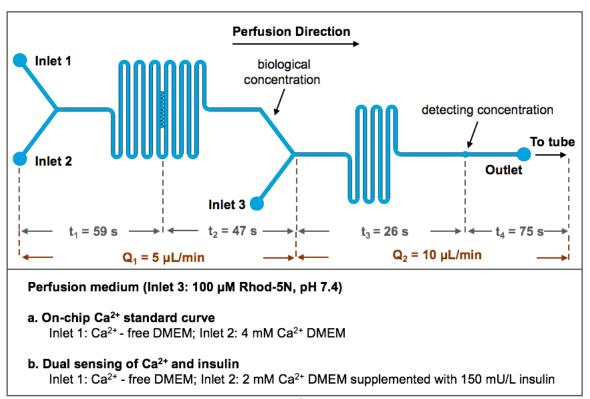


Figure S11. The perfusion setting for the on-chip Ca²⁺ detections. Briefly, two DMEM media containing varying concentrations of Ca²⁺ were pumped into the channel via inlet 1 and inlet 2. While the total flow rate of inlet 1 and inlet 2 were constant, the ratio of the flow rate at inlet 1 to inlet 2 was altered to obtain serial concentrations of Ca²⁺ in the channel. The Rhod-5N solution was pumped into the channel at inlet 3 at the same flow rate as the total flow rate of inlet 1 and inlet 2. The time intervals of fluid travelling are indicated for different sections of the channel.

Detection a | To establish the on-chip Ca^{2+} -induced fluorescence curve (without protein), Ca^{2+} -free DMEM and DMEM containing 4 mM Ca^{2+} were delivered into the channel via inlet 1 and inlet 2, respectively;

Detection b | To examine the dual-sensing capability of the microfluidic system, Ca^{2+} -free DMEM and DMEM containing 2 mM Ca^{2+} and 150 mU/L insulin were delivered into the channel via inlet 1 and inlet 2, respectively.

Table S1. Flow rate settings and corresponding concentrations of Ca²⁺ and insulin at the optical window

[Ca ²⁺] _B	[Ca ²⁺] _D	Insulin	Flow Rate (μL/min)				RI
(mM)	(mM)	(mU/L)	Inlet 1	Inlet 2	Inlet 3	Outlet	
0.2	0.1	7.5	4.5	0.5	5	10	9:1
0.5	0.25	18.75	3.75	1.25	5	10	3:1
1	0.5	37.5	2.5	2.5	5	10	1:1
1.5	0.75	56.25	1.25	3.75	5	10	1:3
2.0	1.0	75	0	5	5	10	0:5

Table S2. The concentrations of the ionic components in the sensing environment

Components	Concentration (mM)
${ m MgSO_4}$	0.407
KCl	4.017
NaH_2PO_4	0.4528
Na_2HPO_4	5.0
NaCl	123.2
NaHCO ₃	22.02
KH ₂ PO ₄	0.9

Table S3. Comparison of the dimensions of the design and fabricated device

	Main ch	annel (µm)		U-shape cups (μm)			
Structure	Width	Height	Opening	Wall	Cross channel	Base	Body
Design	300	250	250	50	45	255	315
Chip	289 ± 2	236 ± 7.9	235.8 ± 3.6	37.5 ± 2	55.6 ± 2.1	226.2 ± 2.1	285.4 ± 2.1
Error (%)	3.7	5.6	5.68	25	23.56	9.3	9.4

Table S4. Flow rate setting and the corresponding concentration of Ca²⁺

$[Ca^{2+}]_T$	$[Ca^{2+}]_D$	Flow Rate (µL/min)				$\mathbf{R}_{\mathbf{I}}$
(mM)	(mM)	Inlet 1	Inlet 2	Inlet 3	Outlet	
0	0	4	0	4	8	4:0
0.5	0.25	3.5	0.5	4	8	7:1
1.0	0.5	3	1	4	8	3:1
1.5	0.75	2.5	1.5	4	8	5:3
2.0	1	2	2	4	8	1:1

Table S5. The channel volume of different sections of the chip and the corresponding travelling time of the perfusion medium

Channel Section	V (µL)	Q (μL/min)	t (s)
1. inlet – trapping site	4.9	5	59
2. trapping site − 2 nd joint	3.93	5	47
3. 2 nd joint – optical window	4.3	10	26
4. optical window – tube	12.3	10	75

^{*} Section 4 includes the travel distance via a 25cm long tubing with an internal radius of 125 μm.

8.7.11 Supporting references

- 1. Davies, C. W.; Shedlovsky, T. Ion association. *Journal of the Electrochemical Society* **1964**, *111*, 85C-86C.
- 2. Malmberg, C.; Maryott, A. Dielectric constant of water from 0° to 1000 °C. *Journal of Research of the National Bureau of Standards* **1956**, *56*, 1-8.
- 3. McGuigan, J. A. S.; Kay, J. W.; Elder, H. Y. Ionised concentrations in calcium and magnesium buffers: Standards and precise measurement are mandatory. *Progress in Biophysics & Molecular Biology* **2017**, *126*, 48-64.
- 4. Park, C.-S.; Joo, K.-I.; Kang, S.-W.; Kim, H.-R. A PDMS-coated optical fiber Bragg grating sensor for enhancing temperature sensitivity. *Journal of the Optical Society of Korea* **2011**, *15*, 329-334.
- 5. Tabeling, P. *Introduction to Microfluidics*, Oxford University Press, New York, USA **2005**.

CHAPTER 9: CONCLUSIONS AND

PERSPECTIVES

The studies included in this thesis have yielded novel insights into the regulation of intestinal and pancreatic hormone secretion, including the role of sex, gastric emptying (GE), liver function and bitter taste signalling, and led the establishment of two microfluidic 'organ-on-a-chip' platforms for investigation of the secretory function of primary intestinal tissues and pancreatic islets.

The secretion and action of both intestinal and pancreatic hormones are key to the maintenance of glucose homeostasis, particularly after meals. Men are known to be at greater risk of developing type 2 diabetes (T2D) than women. There is recent preclinical evidence suggesting that sex is a major determinant of intestinal hormone secretion, which may account for the sex-driven disparity in T2D risk. In the study reported in **Chapter 3**, we found that the GLP-1 response to intraduodenal glucose infusion at rates within the physiological range (2 and 3 kcal/min) was substantially greater in healthy women than in age- and BMI-matched men, although no difference in GIP secretion or blood glucose was observed between the two groups. The lack of difference in glycaemia in this study is probably due to the inclusion of healthy young volunteers in the study with intact compensatory extra-gastrointestinal mechanisms of glucose disposal. Further studies are warranted to investigate the mechanisms responsible for the disparity in the GLP-1 response to small intestinal glucose between healthy men and women and the sex-related pathogenesis of dysglycaemia.

Counter-regulation of pancreatic hormones (insulin and glucagon) governs both hepatic glucose production and disposal. Altered liver function, as reflected by increased circulating liver enzyme levels, has been appreciated as a key determinant of hepatic insulin sensitivity and future risk of T2D. However, the relationships of metabolic derangements, including insulin resistance and hyperglucagonaemia, with the liver enzyme profile in individuals with T2D had not been well characterised. The study reported in **Chapter 4** showed that circulating insulin, C-peptide and glucagon concentrations, both fasting and after oral glucose, correlated closely with serum liver enzymes, particularly ALT, in individuals with T2D relatively well-controlled by diet and/or metformin. That ALT is predictive of exaggerated insulin and glucagon concentrations during fasting and after an oral glucose load or a mixed meal, in the absence of differences in blood glucose, corroborates its potential as an 'early' biomarker for diabetogenic changes in insulin and glucagon secretion (and action) in T2D.

As discussed above, patients with T2D often display an exaggerated glucagon response to meals, in addition to insulin resistance. It is noteworthy that postprandial glucagon secretion can be directly stimulated by amino acids and long-chain fatty acids following their absorption. Our group has recently shown that T2D patients with few complications, regardless of glycaemic control, frequently exhibit abnormally rapid GE, which may contribute to post-absorptive stimulation of glucagon secretion. The study reported in **Chapter 5** showed, in a cohort of T2D patients with relatively good glycaemic control, that the 'early' postprandial phase of the glucagon response (0-30 minutes) to a standardised mixed meal was related inversely to the gastric half-emptying time (T50) (i.e., related directly to the rate of GE) and was predictive of the increase in blood glucose over this period. These observations suggest that the exaggerated early postprandial glucagon response is accounted for, at least in part, by accelerated GE in

well-controlled T2D, which supports the concept of using therapies that slow GE to reduce postprandial hyperglucagonaemia and hyperglycaemia in T2D.

Dietary and pharmacological interventions that have the capacity to modulate intestinal and pancreatic hormone secretion directly represent a logical and attractive strategy to restore metabolic balance. Of emerging interest are the discoveries of a range of bitter taste receptors (BTRs) expressed on enteroendocrine cells along the gut and their coupling with intestinal hormone release. Although a range of bitter substances has been shown to stimulate intestinal hormone release, including GLP-1, to suppress appetite and lower blood glucose concentrations in rodents and humans, the effect of bitter substances on the function of extra-gastrointestinal tissues was poorly defined. Observations made in **Chapter 6** showed that a bitter substance, denatonium benzoate (DB), was able to drive insulin secretion from rodent pancreatic β-cells, an effect mediated in part by the closure of K_{ATP} channels and the activation of BTRs, and that DB-evoked insulin secretion from isolated pancreatic islets also involved a paracrine action of intra-islet GLP-1 signalling. This work attests to the complex interaction of bitter substances with endocrine tissues beyond the gut, and calls for attention to the potential off-target effects of any bitter tasting medication that has systemic exposure.

Investigation of intestinal and pancreatic hormone secretion has been reliant on measurements of hormone levels from blood samples or supernatants of tissues under well-based static incubation. These conventional methodologies are both demanding and limited by the lack of capacity to characterise the dynamic secretory activity in response to stimulation. There is an increasing demand for innovative platforms to investigate the secretory function of endocrine tissues.

Chapters 7 and 8 reported two microfluidic 'organ-on-a-chip' platforms that are suitable for

studying hormone secretion from primary intestinal mucosa and isolated islets. The gut-on-a-chip (GOC) device described in **Chapter 7** enabled the delivery of luminal stimulation with monitoring of GLP-1 secretion on the serosal side with high temporal resolution (one assay every 2 minutes). The tissue viability on the chip was maintained for over 90 minutes, allowing multiple cycles of 'on' and 'off' stimulation. The multiplexed microfluidic platform devised in **Chapter 8** is capable of trapping microscale subjects (surrogates for pancreatic islets) in a biomimetic perfusion system, allowing simultaneous quantification of insulin concentration (15-150 mU/L) and Ca²⁺ (0.2-2 mM), an important regulator of insulin secretion that is co-released with insulin) from the effluents, via ELISA and light-induced fluorescence sensing respectively, with high temporal resolutions.

In summary, the studies outlined in this thesis utilised a combination of clinical and preclinical models to deepen the understanding of mechanisms involved in the regulation of intestinal and pancreatic hormone secretion in health and T2D. The 'organ-on-a-chip' platforms developed in this thesis will enable future mechanistic studies in relation to the regulation of intestinal and pancreatic hormone secretion, and high throughput screening of novel therapeutic compounds for the management of T2D.